PROCEEDINGS OF THE XXth ANNUAL MEETING OF THE SOCIEDADE ASTRONÔMICA BRASILEIRA

(AUGUST 1994)

EDITED BY B. BARBUY, N. V. LEISTER AND J. BRAGA

ISSN 0104-6071

PROCEEDINGS OF THE XXth MEETING OF THE BRAZILIAN ASTRONOMICAL SOCIETY

August 1 - 4, 1994
Campos do Jordão, SP, Brazil

S A B

Edited by

Beatriz Barbuy and Nelson V. Leister
Instituto Astronômico e Geofísico - USP
C. P. 9638, São Paulo, SP 01065-970, BRAZIL

João Braga
Instituto Nacional de Pesquisas Espaciais
C. P. 515, S. J. Campos, SP 12201-970, BRAZIL

Ficha Catalográfica:

Sociedade Astronômica Brasileira
Proceedings of the XX^{th} meeting of the Brazilian Astronomical Society
200 páginas

Contribuições de conferencistas. 1996.
I. Título: Proceedings of the XX^{th} meeting of the Brazilian Astronomical Society

ISSN: 0104-6071

Distribuição:

Instituto Astronômico e Geofísico - USP
Av. Miguel Stefano, 4200 - Parque do Estado
04301-902 - São Paulo - SP

XX REUNIÃO DA SAB
HOTEL OROTUR CAMPOS OO JORDÃO AGOSTO 1994

TABLE OF CONTENTS

Section 4: Extragalactic Astronomy

FOREWORD

This volume contains the proceedings of the XXth Meeting of the Brazilian Astronomical Society, held at Hotel Orotur in Campos do Jordão, state of SP, on August 1-4, 1994. This has been a special meeting given that in 1994 the Society celebrated its 20th anniversary. In this occasion we succeeded to gather most of our astronomers, including most of those who had founded the Society in 1974.

In this volume only the invited talks given at the conference are included, but a large number of posters were also presented, whose abstracts have been published in a special volume of the Bulletin of the Brazilian Astronomical Society.

The excellent conferences, and the large number of interesting results presented during the conference, have made this an important meeting, where the quality and strength of brazilian astronomy has been made evident.

We are very grateful to Fundação de Amparo à Pesquisa do Estado de São Paulo (FAPESP) and Conselho Nacional de Desenvolvimento Científico e Tecnológico (CNPq) for financial support.

Beatriz Barbuy
Nelson V. Leister
João Braga

Section 1:

SOLAR SYSTEM AND ASTROMETRY

DYNAMICS AND COSMOGONY OF ASTEROIDS IN RESONANCES

S.FERRAZ-MELLO

Universidade de São Paulo
Instituto Astronômico e Geofísico
sylvio @ vax.iagusp.usp.br

Abstract. – This paper is a short review of the dynamics of the main asteroidal resonances as currently determined from maps and simulations over $10^6 - 10^7$ years. Recent results concern the extensive exploration of the phase space to determine the occurrence of close approaches to the inner planets, the origin of the gaps in the asteroidal distribution, the topological dynamics of tbe planar Sun-Jupiter-asteroid problem and the differences amongst the 2/1 and 3/2 resonances able to explain the observed existence of a gap in the asteroidal belt at the 2/1 resonance and of a group of asteroids in the 3/2 resonance. Current results point to a confirmation of purely gravitational theories for the formation of the gaps by chaotic orbital diffusion and asteroid scattering by the inner planets.

1 Introduction

Several features in the distribution of the asteroids are associated with resonances. They are groups and gaps appearing in plots where the horizontal axis displays the semi-major axis or the mean motion. The gaps are located at positions corresponding to the 4/1, 3/1, 5/2, 7/3 and 2/1 commensurability between the orbital period of Jupiter and that of the asteroid, while the groups are located in the neighbourhood of the 3/2, 4/3 and 1/1 commensurabilities (fig.1). The gaps were discovered by Kirkwood, in 1867, and are known as Kirkwood gaps. The groups in the neighbourhood of the 3/2 and 4/3 resonances have, respectively, 58 and 2 members currently known (EMP 1995); their two paradigms – (153)Hilda and (279)Thule – were discovered by J.Palisa, an active asteroid discoverer that discovered 83 of the 323 asteroids known by 1891.

The asteroids moving in the neighbourhood of the 3/1, 2/1 and 3/2 commensurabilities are considered in this review. Throughout the 20^{th} century, several theories have been formulated to explain the Kirkwood gaps. One of them, the statistical theory, claims that the gaps are only apparent: asteroids near resonances oscillate about the exact resonance value and expend most of the time far from the commensurabilities. This motion, known as libration or σ-libration, is characterized by the oscillation, around a fixed value, of the angle

$$\sigma = (r+1)\lambda_{Jup} - r\lambda - \varpi$$

(λ and ϖ denote, respectively, the asteroid's mean longitude and longitude of the perihelion, r is a rational number and $(r+1)/r$ is the commensurability ratio). It was recognized since the early work of Poincaré and notwithstanding having, for some asteroids, a very large

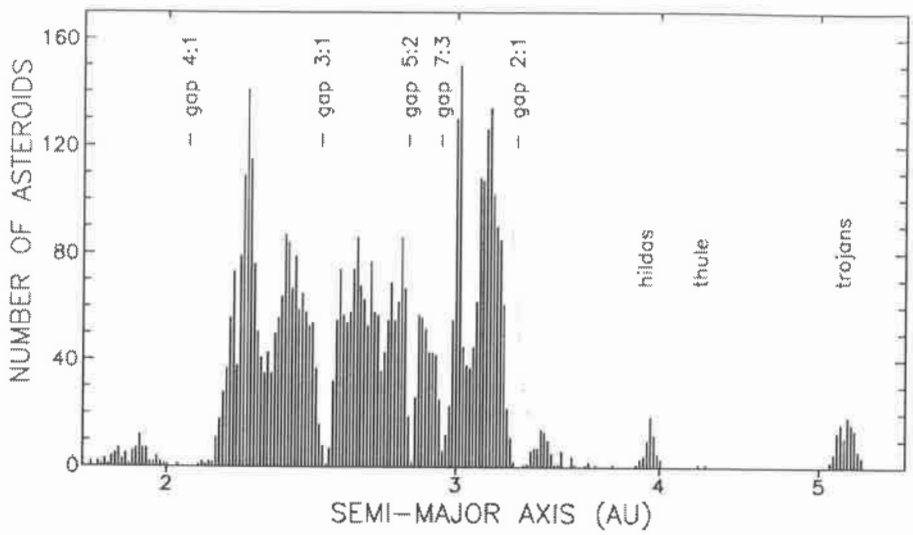

Figure 1: Histogram of the number of asteroids *vs.* semi-major axis showing the location of the main gaps and groups (from Ferraz-Mello, 1994a).

amplitude (up to 0.15 AU, see Ferraz-Mello, 1988), it is not large enough to originate a statistical gap as wide as those observed in the actual asteroidal distribution. Current numerical simulations over 10^7 years do not show any larger oscillation able to create such an effect. On the contrary, they show that in the observed gaps, asteroids librating about the resonance are exactly the ones that are missing. Fig.2 shows the distribution of nonresonant numbered asteroids around the 3/1 and 2/1 resonances as well as the curves indicating the boundaries of the libration regions.

All other theories assume that the gaps are real and either primordial or the result of the orbital evolution of the asteroids. Gravitational theories say that pure gravitational evolution is sufficient to explain the gaps. It is difficult to have a direct confirmation of these theories, even using numerical simulations, because of the large time interval elapsed since the origin of the asteroidal belt. However, they stand high in favor since Wisdom's work on the formation of the gap in the 3/1 resonance. Wisdom (1982, 1983) showed that the chaotic diffusion of these orbits is able to drive an asteroid to orbits approaching Mars closely in a very short time-scale ($10^5 - 10^6$ years). Later results using more complete models, pointed out that these asteroids can, in fact, be driven to orbits diving deep inside the inner Solar System and, even, coming close to the Sun.

Cosmogonic theories assume that the gaps were formed in the early stages of formation of the Solar System. They are generally made plausible by assembling assumptions on the processes at work during the formation of the Solar System and consist in finding some scenario able to produce gaps in the early asteroidal distribution. To the extent that the gravitational theory becomes widely accepted as a general explanation for the scattering of asteroids in resonances, cosmogonic hypotheses becomes less important. Indeed, if the efficiency of gravitational evolution mechanisms is as large as pointed out by some recent investigations, the present state of the asteroidal belt at resonances depends only weakly on its primordial state and can provide only a little cosmogonic information. Cosmogonic

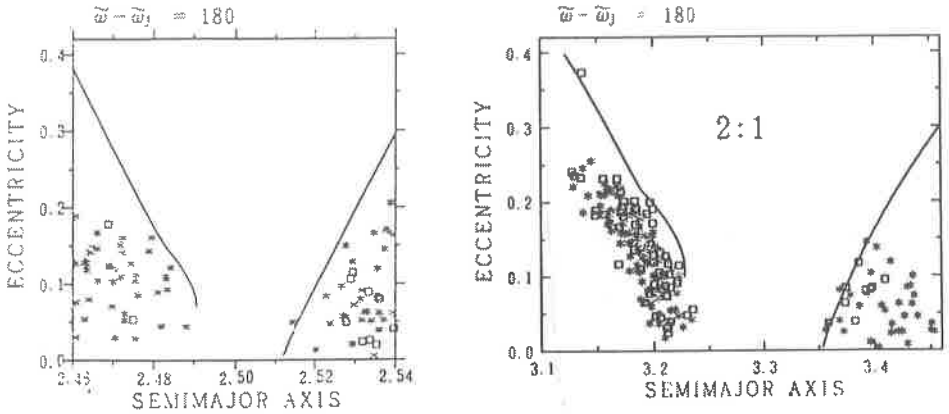

Figure 2: Distribution of the numbered asteroids around the 3/1 and 2/1 resonances and boundaries of these resonance regions in the planar case. In the right-side figure, the asteroids in the lower left region were omitted (asterisks: $i < 15°$; squares $i > 15°$) (after Yoshikawa, 1990, 1991).

theories are not considered in this review.

The crucial point concerning Kirkwood gaps and Palisa groups is that, in spite of their opposite distribution characteristics, they have very similar dynamics. For instance, the theoretical models of the 3/2 and 2/1 resonances are identical and differ only in the numerical value of one parameter (see, for instance, Henrard and Lemaître, 1987; Lemaître and Henrard, 1988). Thus, in order to be fully accepted, a theory must explain both the existence of gaps at the 4/1, 3/1, 5/2, 7/3 and 2/1 resonances and the existence of groups at the 3/2 and 4/3 resonances. It must also explain the particular features of the distribution in each resonance.

2 The 3/1 resonance

The first gap to receive an acceptable explanation was the 3/1 gap. Its depletion mechanism started to be unraveled with Wisdom's (1982, 1983, 1985) results showing the existence of two regimes of motion indicated by (a) and (b) in fig. 3. (a) is the ordinary low-eccentricity regime in whose most typical examples the perihelion retrogrades and the eccentricity has a small periodic variation (for very low eccentricities, the perihelion may oscillate about the position of Jupiter's peribelion); (b) is the mid-eccentricity regime – discovered by Wisdom – in which the asteroid's perihelion oscillates about the position of Jupiter's perihelion and the eccentricity has large oscillations approaching values as high as 0.4 which allows the asteroid orbit to cross the orbit of Mars. The chaotic dynamics of this resonance is such that an orbit may alternate between these two regimes in a short timescale (much less than 1 Myr). Wisdom's simulations have shown orbits having a seemingly regular low-eccentricity motion for long times and suddenly transiting to the mid-eccentricity regime and crossing Mars' orbit. In the mid-eccentricity regime, the asteroid can have a close approach to the planet. This behaviour is intermittent and the orbit may transit back to the low-eccentricity regime before a close approach to Mars happens. However, sooner or

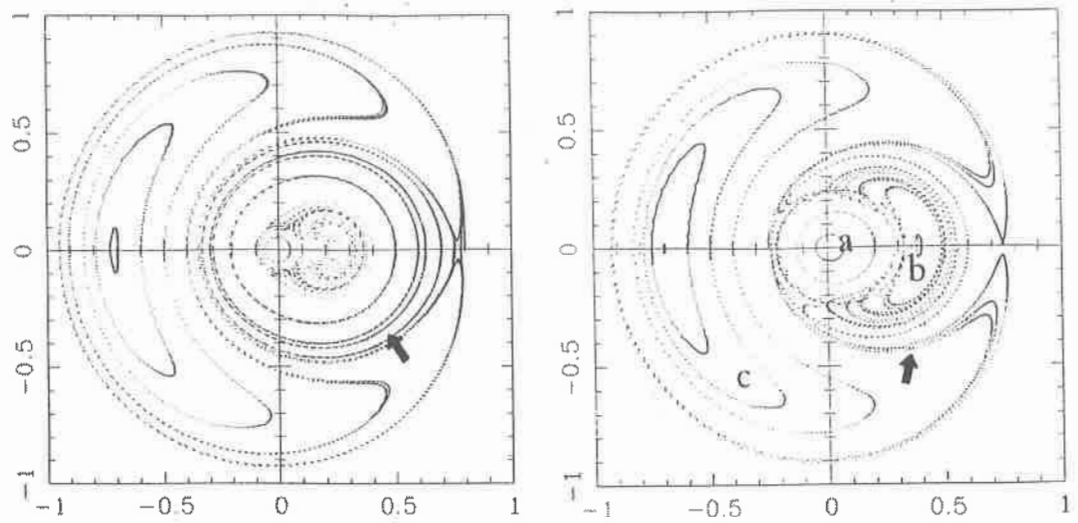

Figure 3: Poincaré maps ($\sigma = \pi/2$, $\dot{\sigma} < 0$) of the resonance 3/1 in the frame of the planar averaged Sun-Jupiter-asteroid problem at two different energy levels. Coordinates are $x = e.\cos(\varpi - \varpi_{Jup})$, $y = e.\sin(\varpi - \varpi_{Jup})$. On the left side, the chaotic domain found by Wisdom is seen in the inner part of the figure. It is confined by a bunch of almost regular motions (arrow). On the right side, these motions no more exist and a heteroclinic bridge (arrow) allows the transitions between (b) and (c) (after Ferraz-Mello and Klafke, 1991).

latter one close approach may occur and, as a consequence, the orbit suffers an important energy change and leaves the resonance. The occurrence of a phenomenon of this kind is consistent with the observed absence of permanent asteroids in the 3/1 resonance (in fact the few asteroids currently observed in this resonance are believed to have come from recent captures and are bound to close approaches with the inner planets; see Milani *et al.*, , 1989). The only doubts came from the fact that Mars is a small planet and we do not know if this scattering process would have been efficient enough to expel all asteroids expected to be there after the formation of the Solar System, 4.5 billion years ago.

Anyway, Wisdom's works set new paradigms in asteroidal dynamics and inspired all subsequent investigations which generalized his results in several directions. In what concerns the 3/1 asteroidal resonance, Ferraz-Mello and Klafke (1991) have used new models for the averaged potentials allowing to extend Wisdom's results to high eccentricities. They bave shown the existence of a very-high-eccentricity regime (c) where the eccentricity oscillates in a wide range reaching values close to 1 and the perihelion may perform a complete revolution before the eccentricity decreases again. In the energy range considered hy Ferraz-Mello and Klafke, this regime is almost always separated from the other ones hy some regular motions (fig.3 left) able to avoid transitions between them, at least in a timescale as short as the one observed in the transitions between the regimes (a) and (b). However, FM and Klafke have shown tbat, decreasing the energy, these seemingly regular orbits cease to exist and a heteroclinic bridge appears allowing the solutions to go from (b) to (c) (fig.2 right) and the eccentricity to grow to values close to 1. Decreasing the energy still more, the regimes (a) and (b) become parted and direct transitions between (a) and (c) become possible (see Klafke *et al.* 1991).

The intermittences associated with orbits going through (c) can drive the asteroidal eccentricity to values close to 1 and back. In this case, the asteroid will not only cross the orbit of Mars, but also those of the Earth and Venus, planets which are 10 times more massive than Mars, and even approach the Sun and become liable to be disrupted by solar tidal forces.

Orbits of fictitious asteroids going through heteroclinic bridges to high eccentricities were actually computed by Saha (1992) and Farinella *et al.* (1993). In fact, they are very common: the orbit of (4179) Toutatis lies in this region.

3 The 2/1 resonance

In the case of this resonance, the use of the existing expansions of the disturbing forces potential is limited to small domains by the small convergence radius of these expansions. Thus, techniques not involving expansions are mandatory.

One way of studying the dynamics of this resonance is to perform numerical integrations and to smooth the output by filtering out the high frequencies (Michtchenko, 1993; Michtchenko and Ferraz-Mello, 1993, 1995). When the model is the planar Sun-Jupiter-asteroid model, these smoothed integrations may be interpreted as solutions of an averaged dynamical system with 2 degrees of freedom and allow the construction of Poincaré maps (Ferraz-Mello, 1994b). Figure 4 shows some of these maps obtained from 1 Myr numerical integrations.

In the maps of fig.4, the motion regimes denoted (a) and (b) in the 3/1 resonance are almost absent; they are only seen in the last Poincaré map corresponding to orbits with very large libration amplitudes ($\Delta\sigma > 200°$). Generally, these regimes are substituted by a single chaotic low-eccentricity zone (Giffen, 1973; Froeschlé and Scholl, 1976, 1981; Murray, 1986; Wisdom, 1987).

Lemaître and Henrard (1990) have shown that the origin of this chaotic zone is the existence of resonances between the libration of the critical angle σ and the perihelion motion. There is, in fact, a succession of microregimes of motion associated with each of these secondary resonances and their overlapping allow an orbit to transit through them. This chaotic zone is confined to low-eccentricities by regular motions starting near $e = 0.2$; the maps of figure 4 show large regions of seemingly regular motions, even for eccentricities as large as 0.5.

The regime denoted (c) in the 3/1 resonance has now two counterparts: One on the left side (asteroid perihelion librating about Jupiter's aphelion) and another in the right side (asteroid perihelion librating about Jupiter's perihelion). The motion in these regimes are such that both the critical angle σ and the perihelion are librating. The motions in the right-side lobe are similar to the high-eccentricity regime of the 3/1 resonance: they grow up from the exact stable corotation existing at the maximum possible energy: an orbit where both the critical angle and the perihelion longitude are constant (see Ferraz-Mello 1989, Morbidelli and Giorgilli, 1990; Ferraz-Mello *et al.*, 1991). The motions in the left-side lobe are similar but they do not emanate from a stable corotation: in this regime

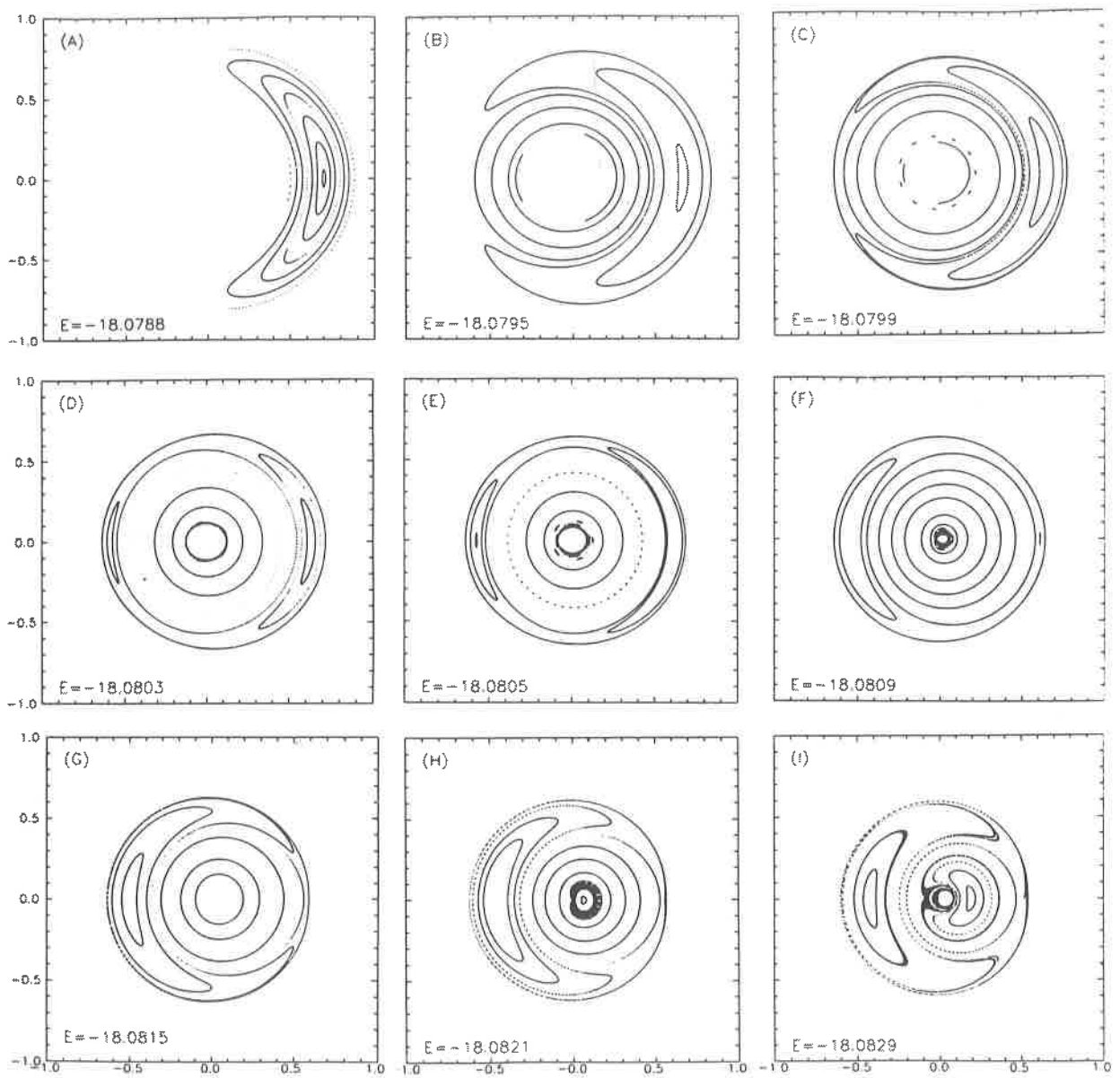

Figure 4: Poincaré maps ($\sigma = 0$, $\dot{\sigma} > 0$) of the resonance 2/1 in the frame of the planar averaged Sun-Jupiter-asteroid problem. Coordinates as in Fig. 3 (from Ferraz-Mello, 1994b).

there are no solutions where both the critical angle and the perihelion longitude are both constant. At higher energies, only the right-side lobe appears; as the energy decreases this lobe becomes less important up to completely disappear; on the otber hand, as the energy decreases, the left-side lobe appears, increases and becomes the main bigh-eccentricity feature of this motion.

Between the two lobes and the low-eccentricity chaotic zone there is always a wide bunch of regular orbits making tbeir communication impossible in the frame of the planar Sun-Jupiter-asteroid model. This separation persists even wben the long-period perturbations of the orbit of Jupiter are considered (Morbidelli and Moons, 1993) what led many authors to find impossible to explain the Kirkwood 2/1 gap by the same mechanisms explaining the 3/1 gap.

However, when Saturn is included in the model and inclined orbits are assumed ($i_0 = 5°$), all solutions become clearly chaotic (Ferraz-Mello, 1994b). Maximum Lyapunov exponents were estimated from some fifty 5–7 Myr integrations, for initial eccentricities in the interval $0.1 < e < 0.4$ and initial semi-major axes ranging from the middle to the border of the resonance region. The results are generally in the range $10^{-5} - 10^{-3.5}$ yr^{-1}, except for a few orbits starting from the very middle of the resonance (Ferraz-Mello, 1994b). These results show that Saturn triggers the destruction of tbe regular structures seen in fig. 4. Even if KAM tori may exist, they are not expected to be important; Jupiter's mass is much larger than the most optimistic evaluations of the small-parameter values of KAM and Nekhoroshev theories and, on the other hand, the number of degrees of freedom of the considered models is high. Thus, intermittences allowing orbits to transit between low and high eccentricities are expected to exist and were indeed observed in some numerical integrations. Current researches (Michtchenko, 1993; Henrard et al., 1995; Ferraz-Mello, in preparation) are devising intermittent mechanisms that may be responsible for large eccentricity changes and, thus, be able to deplete the resonance at a time rate consistent with the fact that only a few asteroids are observed librating about $\sigma = 0$ inside the 2/1 resonance.

4 The 3/2 resonance

The 3/2 resonance was studied using the same techniques used to study the 2/1 resonance. Figure 5 shows two Poincaré maps of this resonance. They differ from those of fig.4 in several aspects. For instance, we devise only two regimes of motion: (a) the inner domain of perihelion circulation and (b) the perihelion libration lobe on the left side. At variance with the 2/1 resonance, no apparent chaotic activity exists in the region of perihelion circulation (confirmed by Lyapunov exponents tending to zero in numerical integrations over 10 Myr); the analysis of these solutions shows the same kind of secondary resonances web responsible for the inner chaotic region in tbe 2/1 resonance, but the cbaotic regions associated witb every secondary resonance in the web seem to be very narrow and they do not overlap (Michtchenko 1993, Michtchenko and Ferraz-Mello, 1994). The only source of appreciable chaoticity is bifurcation between the two modes of oscillation of tbe perihelion. Strong chaos is visible spreading itself over a large part of the perihelion libration lobe

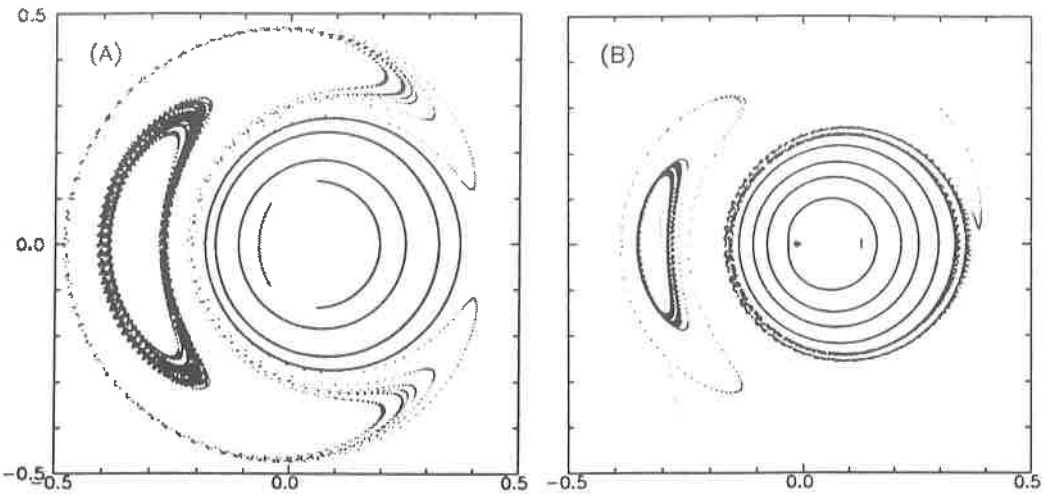

Figure 5: Poincaré maps ($\sigma = 0$, $\dot{\sigma} > 0$) of the resonance 3/2 in the frame of the planar averaged Sun-Jupiter-asteroid problem. Coordinates as in Fig. 3. Orbits in the perihelion libration lobe are highly chaotic and are bound to close approaches to Jupiter in short times. Orbits in the innermost part remains regular for long terms even when inclined orbits and the perturbations of Saturn are taken into account. The actual Hildas are in are in the inner region. (from Ferraz-Mello, 1994a)

and in the outer region around the two regimes. The non-existence of observed asteroids with mean orbital eccentricities larger than ~ 0.3 is due to the fact that the outer orbits are scattered by approaches to Jupiter itself. The inclusion of Saturn only accelerates this phenomenon allowing the orbits to be scattered in less than 1 Myr. The results of Morbidelli and Moons (1993) for this resonance also show an extended chaotic region surrounding seemingly regular motions with $e < 0.25$.

When the perturbations due to Saturn are taken into account and the asteroid is left to move in an inclined orbit, the maximum Lyapunov exponents of the inner regular orbits still tend to very small values. They are in the range $10^{-5.5} - 10^{-7}\mathrm{yr}^{-1}$. These values are very small and coherent with the observed existence of about 60 asteroids in this resonance.

5 Conclusion

We reviewed the main asteroidal mean-motion resonances. Whenever possible, we emphasized the results concerning the topological dynamics of these resonances. The collected results refer to current maps and simulations extending over $10^6 - 10^7$ years. They show that several conclusions, obtained in tbe past on the basis of simulations over $10^4 - 10^5$ years, were not correct. In the same way, we cannot assume the current conclusions as definitive. They are certainly an improvement on the previous scenario but we do not know what will be unraveled when our theories become able to show evolutions over as large as $10^8 - 10^9$ years.

The current results point to many similarities in the dynamics of the 2/1 and 3/2

resonances. In many respects, the 2/1-gap orbits appear as more regular than those of the 3/2 resonance, at variance with the observational result showing almost no asteroids in the libration zone of the 2/1 resonance and some 60 asteroids in that of resonance 3/2. The only instance in which the results go in the direction shown by the observed truth, is when maximum Lyapunov exponents are computed using the Sun-Jupiter-Saturn-asteroid model. The fact that the maximum Lyapunov exponents of the orbits in the 2/1 gap are 2 orders of magnitude larger than those in the 3/2 group is, likely, the reason for the observed distribution differences. But the values of the Lyapunov exponents found in the less stochastic regions show that we are dealing with very slow processes and the necessary timespan to unravel all dynamical mechanisms at work in these resonances is of the order of $10^8 - 10^9$ years (see Franklin *et al.*, 1993), or even larger, making yet impossible a complete exploration of the phase space by numerical integrations.

6 References

Efemeridi Malikh Planet na 1995 god (EMP 1995), Inst. Teoret. Astron., St. Peterburg, Russia (1994).

Farinella, P., Froeschlé, Ch. and Conczi, R.: 1993, "Meteorites from the asteroid 6 Hebe". *Celest. Mech. Dyn. Astron.* **56**, 287-305.

Ferraz-Mello, S.: 1988, "The high-eccentricity libration of the Hildas". *Astron. J.* **96**, 400-408.

Ferraz-Mello, S.: 1989, "A semi-numerical expansion of the averaged disturbing function for some very-high-eccentricity orbits". *Celest. Mech. Dyn. Astron.* **45**, 65-68.

Ferraz-Mello, S.: 1994a, "Kirkwood Gaps and Resonant Groups". In *Asteroids, Comets, Meteors 1993* (A.Milani *et al.*, eds.), Kluwer, Dordrecht, 175-188.

Ferraz-Mello, S.: 1994b, "Dynamics of the asteroidal 2/1 resonance" *Astron. J.* **108**, 2330-2338.

Ferraz-Mello, S. and Klafke, J.C.: 1991, "A model for the study of very-high-eccentricity asteroidal motion. The 3:1 resonance". In *Predictability, Stability and Chaos in N-Body Dynamical Systems* (A.E.Roy, ed.), Plenum Press, New York, 177-184.

Ferraz-Mello, S., Tsuchida, M. and Klafke, J.C.: 1992, "On symmetrical planetary corotations" *Celest. Mech. Dyn. Astron.* **55**, 25-46.

Franklin, F., Lecar, M. and Murison, M.: 1993, "Chaotic orbits and long-term stability: an example from asteroids of the Hilda group". *Astron. J.* **105**, 2336-2343.

Froeschlé, C. and Scholl, H.: 1976, "On the dynamical topology of the Kirkwood gaps". *Astron. Astrophys.* **48**, 389-393.

Froeschlé, C. and Scholl, H.: 1981, "The stochasticity of peculiar orbits in the 2/1 Kirkwood gap". *Astron. Astrophys.* **93**, 62-66.

Giffen, R.: 1973, "A study of commensurable motion in the asteroidal belt". *Astron. Astrophys.* **23**, 387-403.

Henrard, J.: 1988, "Resonances in the planar restricted elliptic problem". In *Long-term Dynamical Behaviour of Natural and Artificial N-Body Systems* (A.E.Roy, ed.), Plenum Press, New York, 405-425.

Henrard, J. and Lemaître, A.: 1987, "A perturbative treatment of the 2/1 Jovian resonance". *Icarus* **69**, 266-279.

Henrard, J., Watanabe, N. and Moons, M.: 1995, "A bridge between secondary and secular resonances inside the Hecuba gap" *Icarus* (in press).

Klafke, J.C., Ferraz-Mello, S. and Michtchenko, T.: 1992, "Very-high-eccentricity librations at some higher-order resonances". In *Chaos, Resonance and Collective Dynamical Phenomena in the Solar System* (S.Ferraz-Mello, ed.), Kluwer, Dordrecht, 153-158.

Lemaître, A. and Henrard, J.: 1988, "The 3/2 resonance". *Celest. Mech.* **43**, 91-98.

Lemaître, A. and Henrard, J.: 1990, "Origin of the chaotic behaviour in the 2/1 Kirkwood gap". *Icarus* **83**, 391-409.

Michtchenko, T.A.: 1993, *Dr. Thesis*, University of São Paulo.

Michtchenko, T.A. and Ferraz-Mello, S.: 1993, "The high-eccentricity libration of the Hildas. II. Synthetic-theory approach". *Celest. Mech. Dynam. Astron.* **56**, 121-129.

Michtchenko, T.A. and Ferraz-Mello, S.: 1995, "Comparative study of the asteroidal motion in the 3:2 and 2:1 resonances with Jupiter". *Astron. Astrophys.*(in press).

Milani, A., Carpino, M., Hahn, G. and Nobili, A.M.: 1989, "Project Spaceguard: Dynamics of planet-crossing asteroids. Classes of Orbital Behaviour". *Icarus* **78**, 212-269.

Morbidelli, A. and Giorgili, A.: 1990, "On the dynamics of the asteroids belt. Part II: Detailed study of the main resonances". *Celest. Mech. Dynam. Astron.* **47**, 173-204.

Morbidelli, A. and Moons, M.: 1993, "Secular resonances in mean-motion commensurabilities. The 2/1 and 3/2 cases". *Icarus* **102**, 316-332.

Murray, C.D.: 1986, "Structure of the 2:1 and 3:2 Jovian Resonances". *Icarus* **65**, 70-82.

Saha, P.: 1992, "Simulating the 3:1 Kirkwood gap". *Icarus*, **100**, 434-439.

Wisdom, J.: 1982, "The origin of Kirkwood gaps: A mapping for asteroidal motion near the 3/1 commensurability". *Astron. J.* **85**, 1122-1133.

Wisdom, J.: 1983, "Chaotic behaviour and the origin of the 3/1 Kirkwood gap". *Icarus* **56**, 51-74.

Wisdom, J.: 1985, "A perturbative treatment of motion near the 3/1 commensurability". *Icarus* **63**, 279-282.

Wisdom, J.: 1987, "Chaotic dynamics in the Solar System". *Icarus* **72**, 241-275.

Yoshikawa, M.: 1990, "Motions of asteroids at the Kirkwood gaps. I. On the 3:1 resonance with Jupiter". *Icarus* **87**, 78-102.

Yoshikawa, M.: 1991, "Motions of asteroids at the Kirkwood gaps. II. On the 5:2, 7:3 and 2: 1 resonances with Jupiter". *Icarus* **92**, 94-117.

NATURAL SATELLITES[1]

R. Vieira Martins[2] and C.H. Veiga[2,3]

[1]Based on observations made at Laboratório Nacional de Astrofísica/CNPq/Pico dos Dias/Brazil.
[2]Observatório Nacional, Rio de Janeiro, Brazil.
[3]Bureau des Longitudes, Paris, France.
E-mail: rvm@on.br, cave@on.br, cave@bdl.fr

ABSTRACT. General information on the discoveries, the physical properties and the classification of natural satellites are presented. Also some procedures related to the observations of astrometric positions of satellites and some results of our observations are presented.

1. DISCOVERIES AND SOME BACKGROUND

The discoveries of the natural satellites are closely related to technological developments like improvement in telescopes' optical quality and in spacecrafts and their detectors. Before the seventeenth century, the Moon was the only known satellite. With magnitude -12.7 for the full Moon, it is the only satellite seen with naked eye. In 1610, Galileo pointed his primitive telescope at Jupiter and discovered its four greater satellites: Io, Europa, Ganymede and Callisto with magnitudes 5.0, 5.3, 4.6 and 5.6 respectively, which are known as Galilean satellites. Later, on the second half of the seventeenth century, C. Huygens and J.D. Cassini sighted the five greatest satellites of Saturn: Titan, Iapetus, Rhea, Tethys and Dione with magnitudes 8.3, 11.0, 9.7, 10.2, and 10.4 respectively.

William Herschel discovered Uranus (mag. 5.5) in 1781 and after six years its outermost pair of satellites: Titania and Oberon with magnitudes 14.4 and 14.2. Two years later, he detected two satellites of Saturn: Mimas (mag. 11.7) and Enceladus (mag. 11.7). In the middle of the nineteenth century, Lassel found the Neptunian satellite Triton (mag. 13.6), the Saturnian satellite Hyperion (mag. 14.2) and two Uranian satellites, Ariel (mag. 14.4) and Umbriel (mag. 15.3). In 1877, Hall discovered the two known satellites of Mars: Phobos and Deimos with magnitudes 11.3 and 12.4. In 1892, Barnard detected a close Jupiter satellite,

Amathea (mag. 14.1) and in 1898, Pickering, the outermost Saturnian satellite Phoebe (mag. 16.5).

In this century, before 1979, the 8 outermost satellites of Jupiter were discovered: Himalia (mag. 15.0) and Elara (mag. 16.6) by Perrine in 1905; Pasiphae (mag. 16.9) by Mellote in 1908; Sinope (mag. 18.0), Lysithea (mag.18.2), Carme (mag. 17.9), Ananke (mag. 18.9) by Nicholson between 1914 and 1951; and finally, in 1974, Kowal found Leda (mag. 20.2). In 1948 and 1949 Kuiper detected the satellites Miranda (mag. 16.5) of Uranus and Nereid (mag. 18.7) of Neptune and in 1978 Christy found Charon, the close satellite of Pluto with visual magnitude 16.8.

In the beginning of the second half of the twentieth century, 30 satellites were known and today we know at least 60. After 1979, the five closest satellites of Saturn were discovered by ground-based observations. These Saturnian satellites were discovered in 1980 when the Saturn's rings were nearly edge-on to the Earth and so they scattered little sunlight. They are Janus (mag. 14.5) and Ephimetheus (mag. 15.7) which are co-orbitals, Helene (mag. 18.4) in the Lagrangian point of Dione, Telesco (mag. 18.7) and Calypso (mag. 19), in the Lagrangian points of Tethys. After 1979, Voyagers 1 and 2 detected 23 small satellites close to the outer planets. They are: Thebe, Adrastea and Metis for Jupiter; Pan, Atlas, Prometeus and Pandora for Saturn; Cordelia, Ophelia, Bianca, Cressida, Desdemona, Juliet, Portia, Rosalind, Belinda and Puck for Uranus; Naiad, Thalassa, Despina, Galatea, Larissa and Proteus for Neptune.

At this moment the distribution of satellites for the nine planets is: no satellite for Mercury and Venus, one for the Earth and Pluto, two for Mars, eight for Neptune, fifteen for Uranus, sixteen for Jupiter and eighteen for Saturn.

The sizes, mass and densities of the satellites go through a great range of magnitudes. The known radius of natural satellites vary from 2500 km for Ganymede to 8 km for Leda, both satellites of Jupiter. The mass of satellites related to their planet mass is 10^{-1} for Charon, 10^{-2} for the Moon, 10^{-3} for Triton, 10^{-4} to 10^{-5} for the Galilean satellites and the Saturnian satellite Titan and not greater than 10^{-6} for all other satellites. Almost all satellites have density about 1.5×10^{-3} kg/m^3. Titan, Ganymede and Callisto have density 2×10^{-3} kg/m^3 and the most dense

satellites are the Moon, Europe and Io with $3x10^{-3}$ kg/m^3, whereas the less dense satellite is Charon with $0.8x10^{-3}$ kg/m^3.

2. A CLASSIFICATION

Based on their orbits, sizes and perhaps on their origins the natural satellites can be classified in four classes: the regular satellites, the collisional shards, irregular satellites and the special satellites.

2.1. Regular Satellites

This class comprises virtually all the major satellites. They form miniature solar systems about their planets with circular and equatorial orbits. Their densities decrease with their distance from the planet like that of the planets from the Sun.

The regular satellites are thought to originate through processes that have caused the solar system itself. Like planets which are formed from the accretion of planetesimals' disk (in circular orbit around the proto-sun) which are originated from condensation of the dust from the primordial nebula, the regular satellites are formed from accretion of the planetesimals in circular orbit around their proto-planet.

The regular satellites are: the four Galilean satellites of Jupiter, the eight classical satellites of Saturn and the five classical satellites of Uranus.

2.2. Collisional Shards

They are the small satellites with circular orbits close to the planets . Most of these satellites have been discovered since 1979, chiefly by Voyagers 1 and 2. They presumably are the remanents of once-larger satellites, battered and ground down by the on going meteoroid flux.

The larger of these satellites, with radius smaller than 100 km, have sizes near the small regular satellites (Mimas with radius egual 197 km and Miranda with 242 km). These two satellites have comparatively the most irregular orbits amongst the regular satellites. They lie across the size transition where objects disrupted by the collisional flux do not accumulate into spheres.

Belonging to this group we place the small satellites close to the outer satellites and the Martian satellites Phobos and Deimos. These two satellites are too small (Phobos and Deimos mean radius are egual 11 and 6 km respectively) to be considered regular satellites and there are dynamical evidence that they have not been captured.

2.3. Irregular satellites

This satellites have elongated and highly inclined orbits (eccentricity larger than 0.1 and inclination larger than 27 degrees). Often their orbits are retrogrades (larger than 148 degrees). Their outer orbits are strongly perturbed by the Sun. These satellites are, perhaps, the collisional debris captured by the giant planets.

In this group we place the eight outer satellites of Jupiter and the satellites Phoebe of Saturn and Nereid of Neptune. The eight outer Jovian satellites can be distributed in two groups. For every group we collect four satellites with almost the same period and inclination. The first group has prograde orbit and the second retrograde orbit.

2.4. Special satellites

There are three special satellites. the Moon, Triton and Charon which do not satisfy the criteria for any the above three classes. They are the largest satellites relative to their planets being almost binary companions and those that have undergone extensive tidal evolution.

The Moon may have originated in a singular event: from a circumplanetary nebula that itself was produced out of the escaped ejecta of a nearly catastrophic terrestrial impact event. The great distance from the Earth is probably the result of tidal evolution.

Triton has a retrograde orbit around Neptune. This hints at an origin by capture but its large size means that such an origin would not have been accomplished.

Charon is better considered as a binary object together with its planet Pluto. Its origin was probably by a process similar to that which originated the Moon.

3. POSITION OBSERVATIONS OF NATURAL SATELLITES

As we mention above, the knowledge of the orbital evolution of natural satellites is very important for the determination of their origin. Moreover many important physical parameters of the planets and satellites, like the mass and its distribution, can be obtained from orbital motion.

Many physical parameters of planets and satellites were determined by the spacecrafts which explored the Solar System. These parameters are mainly the satellite masses, the rotation axes and period of planets and satellites and the osculating orbital elements. However, some parameter determinations are closely related to the distance and velocity of the spacecraft in the planet or satellite's closest approach and so, more accurate determination of many parameters must be done.

The spacecraft missions are very expensive and so infreguent. Therefore systematic and accurate observations of satellites must be accomplished by ground-based observations. There are two kinds of difficulties occurring for these observations of natural satellites. For the close satellites, they come from the great differential magnitude between planets and satellites. For the outer satellites they are related to their identification and also to the determination of their positions related to the planets.

The required accuracy in the reduction of satellite-planet relative positions must be better than 0".1. Indeed, for a semi-major axis egual to 10", if an error in the planet-satellite distance is larger than 0".1, then it corresponds to an error in the eccentricity larger than 0.01 or in the inclination larger than 0.5 degrees. These errors are unacceptable for satellite orbits because the eccentricities and the inclinations of the regular satellites are, in general, smaller than these values.

In 1982 we started a systematic program of astrometric observations of satellites of Jovian planets. This program was motivated by the present southern declination of these planets,

which allowed observations close to the zenith from our latitude ($\phi \approx -23^{\circ}$).

The observations were made at the Cassegrain focus of the 1.6 m Ritchey-Chretien reflector (Perkin-Elmer) of the Laboratório Nacional de Astrofísica, Brazil. This telescope has the focal distance for the Cassegrain combination egual to 15.8 m, which gives the scale of 13.0 at focal plane. From 1982 to 1988 all observations were made using photographic plates and since then CCD devices have been used.

The reduction of satellites images consists in the determination of the center of each satellite in an eguatorial reference system.

We used photometric methods to determine the center positions of our images. Therefore, all the images of planets, satellites and stars in photographic plates were digitized with the PDS 1010A of the Observatório Nacional at Rio de Janeiro.

Related to the determination of the center, the images of natural satellites present some particular features. Often, faint satellites are close to bright planets and therefore, their images are embedded in the planet's halo light. Moreover, the planetary motion during the observation can elongate the satellites' image.

It is difficult to overcome the light diffused from the planet. Sometimes it causes the destruction of the maximum density that points out of the center of a satellite image and thus prevents a good determination of its center when using traditional methods. Even when the maximum density survives, it can be affected by systematic errors generated by the addition of a non horizontal background to the satellite's two-dimensional Gaussian.

To remove the background gradient produced by the overexposed image of the planet, we assume that the planetary image is symmetric relative to one or two particular axes (both of which contain the planetary center). The background is removed through the subtraction of counts measured at a position which is symmetric relative to the satellite image. Thus, the result is the satellite's image without the background gradient. After this

procedure, the center of the image is found by a method referred bellow.

For satellites images without background gradient, the centers are found with a method presented in the literature for astrometric centering of stars. The choice of a particular method depends on the images characteristics. Applying these methods to our observations we concluded that the elliptic two-dimensional Gaussian model with constant background is better than the other models.

For satellites with background gradient, the elliptic two-dimensional Gaussian with a sky background represented by a polynomial surface of degree two gives results equivalent to the method described above.

The usual method to obtain the position of the natural satellites in an eguatorial reference system is the same which is used in astrometric reductions of faint objects. It consists in the construction of a secondary astrometric catalogue of faint stars in the neighborhood of the satellites using high quality astrometric plates taken with small focal distance telescopes. This procedure presents some problems such us the use of different instruments, the differences of magnitude and the catalogues errors which are responsible for the lesser guality of astrometric positions of many satellites.

However, the observations of satellites present some particular features:
- usually, many images repeat the same star field and for many satellites, the image of the planet appears in every frame;
- for every image, the position of the planet changes relative to the star field;
- the astrometric positions of planets are known with good accuracy.

Considering these features, we developed a method for the reduction of astrometric positions of natural satellites. This method consists in the construction of a mosaic containing the complete set of plates of every mission using the common stars presented on consecutive frames. Using the eguatorial positions of the planet (or a satellite) we find the direction of this system and a scale for the mosaic and then the eguatorial reference system for every frame.

4. SOME RESULTS

We observed the five greatest satellites of Uranus: Miranda, Ariel, Umbriel, Titania and Oberon. Comparing 701 positions of each satellite (641 for Miranda) with the ephemeris, we obtained 0".04 for the observed-calculated (o-c) standard deviation (0".07 for Miranda). The larger residuals for Miranda are caused by the difficulty in obtaining good measures of this satellite which is faint and close to the planet.

Many observations of the Neptunian satellites (Triton and Nereid) were also accomplished. The 322 observations of Triton have the (o-c) standard deviation equal to 0".07 and for the 48 positions of Nereid it is 0".23. The bad accuracy in Nereid observations is caused by the difficulty in the observation of this faint satellite (mag. 18.7) and the small number of published positions (less than 80).

For the Saturnian system, a special attention was given to the faint satellites Helene, Calypso and Telesco. Almost 30 positions of the satellites are obtained. These satellites are very difficult to observe and their orbits are not well established. Our internal error for these observations is about 1".

During 1995-96, as in every sixteen years, the Earth and the Sun will pass through Saturn's ringplane reducing the light diffused by the rings. Therefore we make an effort to observe the faint satellites and also the mutual events between the other satellites (occultations and eclipses). With these observations we expect to have more information about the family of the close satellites (collisional shards) and the regular satellites of Saturn.

5. SOME REFERENCES

For an overview about natural satellites we recommend the book "Satellites" edited by J.A. Burns and M.S. Mathews, The University of Arizona Press, Tucson, 1986.

The general results from Voyagers 1 and 2 are presented in the reports in Science: **204**, 945-1006, 1979; **206**, 925-995, 1979; **212**,

159-243, 1981; **215**, 499-594,1982; **233**, 39-109, 1986 and **246**, 1417-1501, 1989.

Our results are presented in Astronomy and Astrophysics Supplement Series: **70**, 325-334, 1897; **107**, 551-558, 1994; **107**, 559-561, 1994 and other three papers accepted and to be published in 1995.

The results of the astrometric observational program of the Sun

Nelson Vani Leister
Instituto Astronômico e Geofísico da USP
Caixa Postal 9638
01065-970 - São Paulo
Brazil[1]

Abstract. The astronomical results contained in this publication represent a continuation of the fundamental programme of the observation of the Sun with prismatic astrolabe begun in 1974 at the Abrahão de Moraes Observatory (Brazil) and Calern Observatory (France). The main purpose of this program is to determine the orientation of the reference frame as well as the correction of the orbital elements of the Earth. The observational programmes include the FK5 and FK5 Supp's stars and some planets of the solar system. However, the successive observation of the transits of both limbs through the same altitude circle yields the solar diameter well. I discuss here the results of the determinations of corrections to the FK5 equinox and equetor, the correction of the Earth's orbital elements and the possible variations of the solar radius, which are of interest because of their astrophysical significance and because their potential relation to the terrestrial climete.

[1]Invited talk on the XX Brazilian Astronomical Society Annual Assembly, Campos do Jordão, SP.

Introduction. The studies of the celestial bodies motion as a function of position and time, requires the adoption of the reference coordinate system that represents the best empirical realization of an inertial system. The Fourth Fundamental Catalogue (FK4), giving the positions and proper motions of 1535 fundamental stars represented the reference coordinate system adopted for international use till 1984. The fundamental stars are brighter limited at the magnitude 7.5, and they are uniformly distribution over the sky. It was adopted the Newcomb's value of the general precession in longitude for to compute the mean place of date that defined the position of the fundamental plane of the coordinate system, the equator, and of the zero-point of right ascensions, the catalogue equinox (Fricke 1978).

Soon after the completion of the FK4, progress was made in disclosing various deficiencies of this fundamental catalogue. A significant error in Newcomb's precession was confirmed and its origin traced by Fricke (Fricke 1967). As a consequence of this error, observetions of the Sun, Moon and planets carried out with respect to the FK4 should yield and equinox correction E(T) that is a function of time. In 1976 the International Astronomical Union (IAU) adopted a new system of astronomical constants, and concerning the FK5 the recommendations included the time-scales and a new standard epoch.

The Fifth Fundamental Cetalogue (FK5) replaced the FK4 system, and since 1984 the IAU adopted the FK5 for international use as fundamental system as close as possible to dynamical reference freme. Particularly, observations of the Sun with transit circle have been used to help stabiles the orientation of the fundamental reference systems. The observationel program with modified prismatic astrolebe, permit to compare this results with different observational techincs usually used.

On the other side, the accuracy of the results obtained with prismatic astrolabe has led us to investigate whether this type of observation could contribute to determine the value of the Sun's diameter. The diameter value is obtained from the difference between the zenith distance of the solar centers corresponding to the instants of successive limb crossings by the same almucantar. This kind of observations hes the advantage that these measurements are not affected by effects caused by direct refraction (Ribes et all 1991).

Observational basis of determinations of the Equinox and Equator. The reference system defined by fundamental catalogues is that the earth's equator as the fundamental plane from which declinations are reckoned, and the vernal equinox as zero-point of right ascensions. Observations of the Sun and other members of the planetary system have been used to determine both equinox and equator. For this purpose the meridian circle have been used for a long time. The principle of the determination may be explained by considering observations of the Sun and the stars through the meridian and zenith distances are measured over a period of several years. The positions of the stars may either be assumed to be

known in the system adopted or determined independently within the program. In both cases the observations of the Sun yield differences between the observed positions of the Sun, and the position computed from an ephemeris. Their analysis yields corrections to the elements of the earth's orbit used constructing solar ephemeris, a correction ΔE to all right ascensions and a correction ΔA to the observed declinations. The same results it is possible to obtain with prismatic astrolabe by analysis direct of the zenith distance (Leister 1992, Leister and Poppe 1994)

In case of the meridian observations, the equations of condition are

$$\Delta\alpha = -\Delta E + f_1(\Delta L,\Delta\varepsilon,\Delta h,\Delta k) \text{ and } \Delta\delta = -\Delta A + f_2(\Delta L,\Delta\varepsilon,\Delta h,\Delta k),$$

where

$$f_1 = \cos\varepsilon \sec^2\delta\, \Delta L - \cos\alpha \tan\delta\, \Delta\varepsilon + 2\sin\alpha \sec\delta\, \Delta h - 2\cos\varepsilon \cos\alpha \sec\delta\, \Delta k$$

$$f_2 = \sin\varepsilon \cos\alpha\, \Delta L + \sin\alpha\, \Delta\varepsilon + 2\cos\alpha \sin\delta\, \Delta h - 2\sin\varepsilon \cos^2\alpha \cos\delta\, \Delta k,$$

and

$$\Delta h \cos\varpi + \Delta k \sin\varpi = \Delta e$$
$$-\Delta h \sin\varpi + \Delta k \cos\varpi = e\Delta\varpi.$$

The unknowns are the corrections

$\Delta E, \Delta A$, to the RA and equatorial DEC of the FK4/5, respectively,
ΔL to the mean longitude of the Sun,
$\Delta\varepsilon$ to the obliquity of the ecliptic,
$\Delta\varpi$ to the longitude of perigee of the apparent solar orbit,
Δe, to the eccentricity of the orbit.

Hence, we are dealing with six unknowns whose determination requires a sufficiently large number of observations within one program. Such determinations were made not only from observations of the Sun, but also from Mercury, Venus, Mars, a number of minor planets, and Moon.

In analysis of the observations of a planet the number of unknowns is increased at least by the corrections to the orbit of the planet. If such observations can only be made near opposition, as in the case of Mars and of minor planets, correlations between some of the unknowns must be expected which make a determination of corrections to the coordinate system unreliable (Branham 1992).

In Figure 1 the raw determination of the equinox correction is given which has to be analyzed for the calculation of the equinox of the FK5. Plotted are corrections ΔE to

the FK4 equinox either as given directly by the observers or reduced to the FK4. The standard deviation of each point is about 0.15". In some cases the relation of the observer's instrumental system to the FK4 has still to be examined. Included in Figure 1 are results from observations of the Sun (◆), planets (●), minor planets (■), lunar occultation (x) and observations of the Sun with prismatic astrolabe (*) at the "Abrahão de Moraes" Observatory.

In particular, the analysis of the Sun's observations made with a prismatic astrolabe, could to be made from directly by mean the equation of the condition:

$\Delta z = g_1(\Delta E, \Delta A) + g_2(\Delta L, \Delta\varepsilon, \Delta h, \Delta k)$, where

$g_1 = \cos\phi \sin Z \Delta E + \cos Z \Delta A$

$g_2 = (\cos S \sin\varepsilon \cos\alpha + \sin S \cos\varepsilon \sec\delta)\Delta L + (\cos S \sin\alpha - \sin S \cos\alpha \sin\delta)\Delta\varepsilon +$
$+2(\sin\delta \cos S \cos\alpha + \sin S \sin\alpha)\Delta h - 2(\cos S \sin\varepsilon \cos\delta \cos^2\alpha + \sin S \cos\varepsilon \cos\alpha)\Delta k);$

where S is the paralactic angle and Z is the azimuth of the observation.

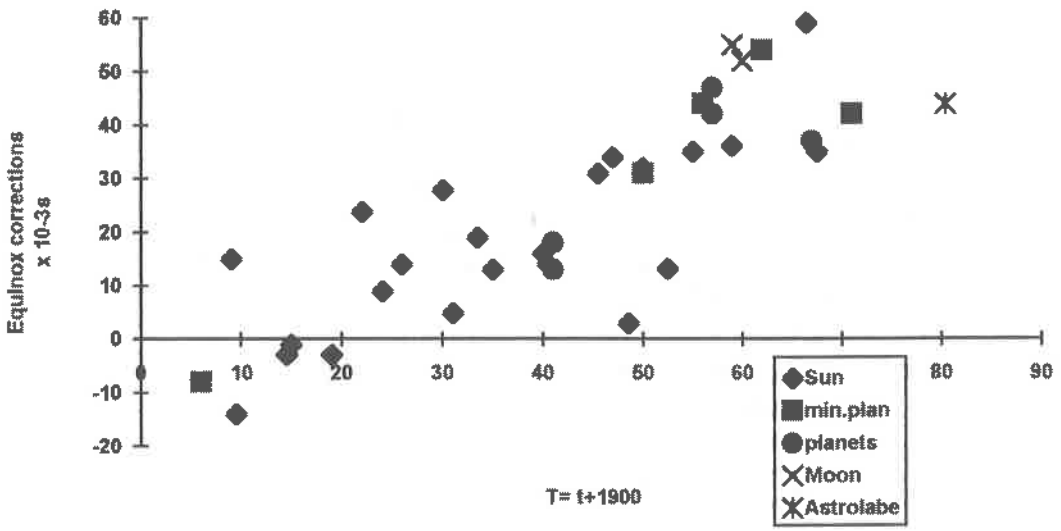

Figure 1. The equinox corrections

The equator's corrections of the FK4 is represented in Figure 2. The equator was determined with an accuracy of +0.03" m.e., from fundamental observations in which the Sun, Moon, planets, minor planets and asteroids were included. The values obtained before 1950 refered to the FK3 was yours values modified in agree with the expression:

$$\Delta A_{FK4} = \Delta A_{FK3} - (0.038 \pm 0.030)".$$

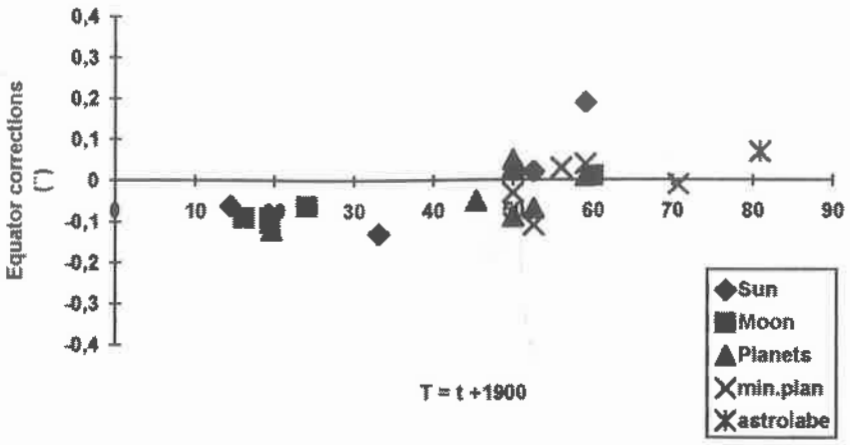

Figure 2. The equator corrections

Observational program with prismatic astrolabe. The results of the analysis of the observations made with prismatic astrolabe depend both, the prism angles that is used during the observation and the latitude of the site (Leister 1989, Poppe 1994).

From 1982 onwards, in Brazilian Observatory, two prisms reflecting cervit prisms, of 120° and 135° aperture, were substituted for the transmitting equilateral prism. With the news prisms it is possible to observe at 30° and 45° zenith distance. The use of two different prisms increased the interval of occurrence of transits from 8 months a year, at 30° zenith distance to 10 months at 45°. The same kind of instruments situated at the "Calern" Observatory in France works with 11 zenith distance and permitting increase the observational period of about 10 months for year too.

For to eliminate the correlations between the unknowns, the zenith distances of 2,610 transits of the solar limbs, obtained in two centers, are analyzed. The observations as a whole cover 5 yr. time span from 1988 to 1992, with a mean epoch of 1989.8 (JD 2,447,740.87). The distribution of the observations by zenith distances and by Observatory are in Figure 3 and 4, respectively.

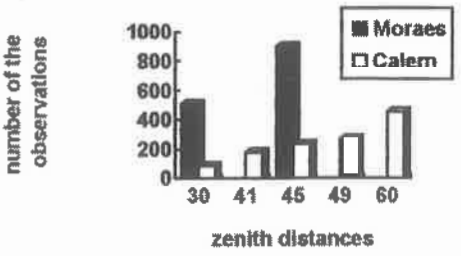

Figure 3. Distribution of the observations by zenith distances.

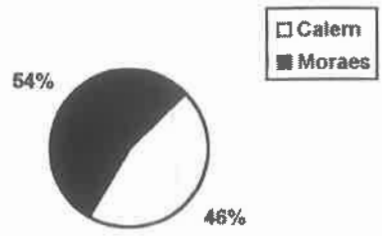

Figure 4. Distribution of the observations by Observatory.

The solution, together with the standard errors, were calculated in the usual way from the variance-covariance matrix, are display in Table 1. The variance of the solution is 0.53", giving a standard error of 0.73" for an observation of unit weight. The values of latitude and the clock correction, that we utilized here, was provided from of the International Earth Rotation Service (IERS). The mean values of the latitude and longitude were refered to the FK5 reference system, obtained for the stars observations.

	Solution(")
ΔE	$+0.09 \pm 0.05$
ΔA	$+0.08 \pm 0.07$
ΔL	-0.37 ± 0.04
$\Delta \varepsilon$	-0.47 ± 0.08
Δe	-0.03 ± 0.02
$e\Delta\pi$	-0.36 ± 0.10
dispersion	0.73
N	2610

Table 1. General solution from the observations of the Sun.

Concerning the determination of the equator and equinox corrections the solution obtained by least square method reveal the corrections $0.09" \pm 0.05"$ and $0.08" \pm 0.07"$ to equinox and the equator, respectively, at the mean epoch of observations 1989.8. The precision obtained was 0.73" revealing a good quality of this set and shows that the equator and equinox of the FK5 do not support a significant correction.

Solar diameter variations. The possibility of variations in the solar radius or luminosity are important for understanding any Sun-Earth climate connection. Considerable effort has been devote to the observation of the solar radius over the past three centuries. Reviews describing the methods and assessing their limitations are available by Gilliland (1981), Brown (1987), Delache (1988) and

Ribes (1989). The solar radius has been measured with an accuracy of a few parts in 10^{-4}. Since the radius can be measured so precisely, it is natural to ask whether this precision can be used to tell us something useful about the processes at work within the Sun. The radius measurements present a large dispersion and there are several reasons for this. Observations should refer to a standard definition of the radius, for example the radius of a shell on which the tangential depth is unity. In most cases, the limb is defined by a visual contact between an image and a wire, or an edge, or a reversed image of the same limb, and does not conform to the standard definition of the radius. The real motivation for observing the solar radius is the suspicion that it might be variable, and the role of the results is to guide theory, not to verify it.

Furthermore, the timing of the contact depends very much upon the observer. Some new techniques have been developed to approach this ideal. However, all measurements are sensitive to various distortions (instrumental and/or atmospheric), thus making the interpretation of the apparent radius change difficult. This chapter is devoted to discussions of the long visual time-series obtained with prismatic astrolabe at the "Abrahão de Moraes" Observatory. A discussion of long-term variability is also possible. Comparison between independent observation it is possible for confirmation some of the reported periodic signal.

The solar diameter problem is therefore one of the oldest problems in astrophysics and the importance of any detectable change cannot be overemphasized. A change in size would be indicative of a change in potential energy which could be driven by such process as a change in the efficiency or precise location of the convective process or the strength and configuration of the magnetic field. Thus a detail knowledge of changes in the solar size and luminosity would have a profound influence our current understanding of the solar interior.

The limb of the Sun does not appear as a sudden step but it has a well defined limb-darkening function. All of the methods used up to the present have been unable to define exactly where on this curve they have defined the edge. This made inter comparison difficult and has led to the introduction of arbitrary correction factors such as the correction for irradiation.

When discussing changes in either the solar semi-diameter or irradiance we are most careful to distinguish a secular change, meaning a long-term, irreversible change always having the same sign or going in the same direction (e.g. the expansion due to main sequence evolution) from a variation which changes sign regularly (i.e. periodically) or irregularly. If this latter case is sampled for less than a complete cycle or sampled erratically the a pseudo-secular change can be derived due to insufficient sampling.

It is also important to identify the possible source of systematic error in each technique, some of which may not be immediately obvious. For example, observers

all have a personal equation which involves such things as reaction times, experiences in recognizing the phenomena under study, familiarity with the apparatus etc.

All of the methods used up to the present use some variety of marker to indicate points on opposite sides of the disk. Such pointers are a wire in the eyepiece of a telescope or astrolabe, the moon, which acts as an oversize occulting disk, or the planets Mercury on the rare occasions when it traverses the solar disk.

Methods for measuring the soler diameter. There are basically two approaches for measuring of the solar diameter. One consists in measuring directly an angle (or a distance on an image) between two opposite limbs. The other methods consist in timing the duration between successive contacts of opposite limbs with fiducial lines on the sky. The case of a vertical meridian line yields the horizontal transit time meridian values, whereas a horizontal line (almucantar) defined by a mercury bath and a constant prism angle corresponds to astrolabe transit times.

The type of observations available since the application of the lens to astronomical research are essentially based on timings of the trensit of the solar image. A long debate has been going on, to decide whether or not meridian visual timings are sufficiently accurate to be used for the purpose of radius determination. As we have already pointed out, meridian observations are subject to defects which are difficult to control, such variability of the focal length, the reference system, end personal bias.

During the nineteenth century, observers focused their interest on the size of the solar envelope as well as the solar disc shape. The variability of the apparent radius (both vertical and horizontal) has been made to link the variebility with solar activity.

More recently, we have measured the apparent solar radius by means of an prismatic estrolabe, to determine the Earth orbit parameters as we describe previously. Though the measurements are still visual, the instrument is well adapted for metrology measurements.

For the solar work, the astrolabe was fitted with an objective filter, consisting of a fused silica parallel plate, whose external surface is coated. The single equilateral prism has been replaced by a series of vitro-ceramic prisms allowing observations at various zenith distances, and hence better coverage of the apparent orbit of the Sun.

The procedure consists of timing the point at which a directly received image coincides with one that is reflected off a level mercury surface (Figure 5), when the upper (or inner) edge of the Sun crosses the almucantar fixed by the prism angle (Figure 6).

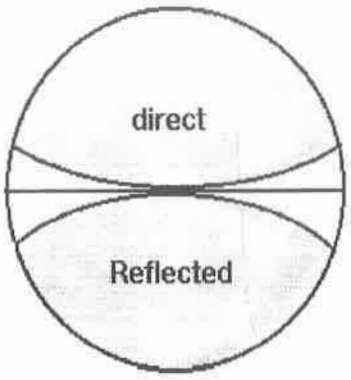

Figure 5. Contact of two images at the astrolabe.

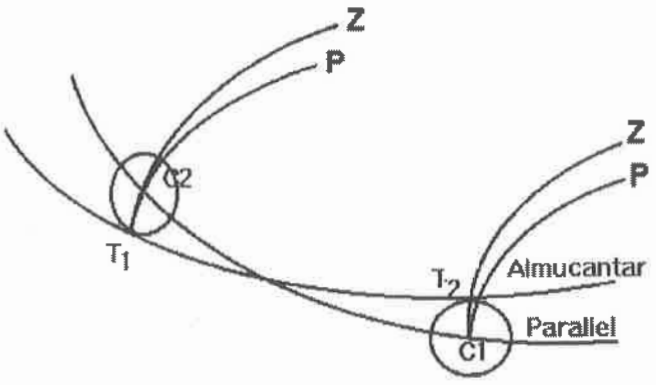

Figure 6. The semi-diameter is derived from the timings of the two contacts.

Let Δt_O be the observed time interval between the lower and upper limb transits. Let Δt_C be the interval computed from the solar ephemeris for the given latitude and zenith distance. Let C denote the sum of measured corrections arising from small refraction variations and geometrical effects. The correction D' for apparent solar diemeter can be written $D' = 15 \cos\phi \sin Z(\Delta t_O - \Delta t_C) + C \pm 2\Delta F$, where ΔF is the unknown plate prismatic error, its sign depending on the initial plate position.

The above equation was solved for the unknowns D' and ΔF at monthly intervals, with en average of 20 transits each. The results for the period 1980.7 to 1992.9 are displayed in Figure 7 (Leister et Benevides-Soares 1990, Leister 1990).

The standard deviation of monthly means is about 0.3".A harmonic enalysis reveals a significant term of period $1{,}000 \pm 20$ days and amplitude $0.21" \pm 0.04"$. The average observed solar semi-diameter turned out to be $959.41 \pm 0.03"$, which is in agreement with Laclare's results $959.37 \pm 0.02"$ (Laclare 1983).

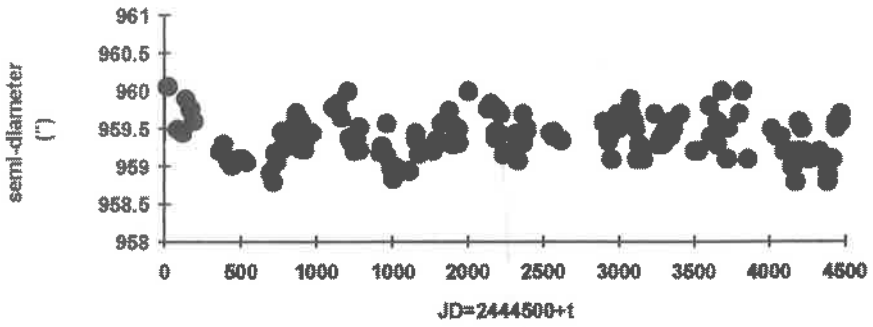

Figure 7. Monthly means of the semi-diameter obtained at the "Abrahão de Moraes Observatory.

Remarks: Visual observations are subjected to various systematic errors, and modern instruments tend to use electronic detectors that a two-dimensional digital data offers advantages in the case of the Sun because their large angular sizes. The observations of the Sun consists of observing a small region, and their limb consists a fitting a parabola to the distribution of edge points at the time of the observation. A better physical definition of the solar limb will permit comparison of the results with those obtained with other instruments, whether they are similar or different principle of the observations (Stone 1990).

Acknowledgments: This research was partially supported by FAPESP (grants no. 92/3672-0).

Reference

Branham, L.R. 1992, The FK5 equator and equinox from observations of minor planets. Astron.J. 103(6), 2099.

Brown, T.M. 1987, Grown-based observations relating to the global state of the Sun. In Solar Radiative Output Radiation, ed. P. Foukal, 176-188.

Delache, Ph. 1988, Variability of the solar diameter. Adv. Space Res. 8: 119-128.

Fricke, W. 1967, Astron.J., 72,1368.

Fricke, W. 1978, Methods of Compiling a Fundamental Reference Systems. Colloquium on European Satellite Astrometry. Padova, 175-184.

Gilliland, R.L., 1981, Solar radius variations over the past 265 years. Astrophys. J., 248, 1144-1155.

Laclare, F., 1983, Astron. Astrophys. 125, 200.

Leister, N.V., 1989, Orientação do sistema fundamental de referência: observações do Sol com o astrolábio de Valinhos. Tese de Doutoramento, IAGUSP.

Leister, N.V. and Benevides-Soares, P. 1990, Variations du diamètre solaire. C.R.Acad. Sci. Paris, t.311, Série II, p.399-404.

Leister, N.V. 1990, Solar Diameter Measurements. Rev. Mexicana Astron. Astrof., 21,567.

Leister, N.V. 1992, Determinations des elements orbitaux de la Terre a partir des observations du Soleil a l'Observatoire de São Paulo. Journées 1992 Systèmes de Référence spatio-temporels (Département d'Astronomie Fondamentale-Observatoire de Paris).

Leister, N.V. and Poppe, P.C.R. 1994, Orientation of the frame system: Observations of the Sun with the prismatic astrolabe. Journées 1994 Systèmes de Référence spatio-temporels (Département d'Astronomie Fondamentale-Observatoire de Paris).

Poppe P.C.R. 1994 , Análise das observações do Sol obtidas com o astrolábio solar no período de 1988-1992. Dissertação de Mestrado, IAGUSP.

Ribes, E. 1989, Astronomical determination of the solar variability. Phil. Trans. Roy. Soc. London, 330, 487-497.

Ribes, E., B. Beardsley, T.M.Brown, Ph. Delache, F. Laclare, J.R.Kuhn and N.V. Leister, The variability of the solar diameter in The Sun in Time. C.P.Sonett, M.S.Giampapa and M.S.Matthews. University of the Arizona Press.

Stone, R.C. 1990, Digital centering algorithms for the Sun, Moon and planets. Astron.J. 99(1), 424.

SUBMM AND FAR-IR EMISSIONS FROM SOLAR FLARES

P. Kaufmann

CRAAE - Centro de Rádio-Astronomia e Aplicações Espaciais (USP, INPE, Mackenzie, UNICAMP) e Universidade Estadual de Campinas - UNICAMP/ NUCATE.

ABSTRACT

Very few measurements of solar emissions were done in the submm and far IR continuum. Attempts to measure flare emissions were inconclusive. It is now recognized that the missing observational information in that wavelength range can bring essential contributions for the understanding of physical processes in the Sun (quiet, quiescent and explosive phenomena). Certain bursts exhibit spectra with flux rising for shorter mm wavelengths, suggesting maxima in the submm/IR range. At the other spectral end, nothing is known about white light flare emission trends into the IR. Very fast time scales in bursts, shorter than 1 second, may become more pronounced in the submm/IR range, bringing serious difficulties for conventional interpretations. One explanation assumes inverse Compton action of relativistic electrons on photons from compact synchrotron sources, shortening the emission duration in the submm/IR range, and producing rapid concurrent X-ray pulses. One unique project of a solar submm-wave telescope (SST project) was proposed four years ago to study these problems at two frequencies, with good sensitivity and high time resolution, using multiple beams for dynamic imaging of solar flares. The project is now in final phase of evaluation by FAPESP, and will receive collaboration from the solar groups of University of Bern, Switzerland, and of IAFE, Argentina, for installation at El Leoncito Observatory, CASLEO, in the Argentinean Andes.

The solar emissions in the continuum remain nearly unexplored in the submm/IR wavelength band (about 3000 to 20 microns). Some far-IR observations of the quiet Sun and of quiescent regions were reported, on solar center brightness temperature (Eddy *et al.*, 1969; Gezari *et al.*, 1973); on limb brightening, emission above sunspots and proeminences (Lindsey *et al.*, 1981; Lindsey, 1994); and on solar active centers (Degiacomi *et al.*, 1984).

Attempts to measure solar bursts in the submm/IR were few and inconclusive. Exploratory observations were done by Hudson (1975) in the atmospheric "windows" centered at 350 and 20 microns. The sensitivity was poor and the time integration large. Few observations were not enough to indicate upper limits for fluxes. Perhaps the first indication of a solar flare emission in continuum was reported by Clark and Park (1968), who noted significant variability in an active region at 1200 microns, which was interpreted as being non-thermal (Beckman, 1968).

There are several evidences indicating that burst emissions may be significant in the submm/IR and, in certain cases, more intense than at microwaves, as shown in Figure 1. The event observed by Kaufmann *et al.* (1985), with high sensitivity and time resolution, was more intense at mm-waves compared to microwaves. Shimabukuro (1970) has shown a similar spectrum for a solar burst. Composite emission spectra, with possible independent component at mm/submm, were obtained by several authors. Spectra which are flat in the microwave to mm-wave range are not uncommon. From a sample of bursts spectral indices between 19 and 35 GHz observed by the University of Bern, it was found that 75% are flat or exhibiting intensity increasing with the frequency (Correia *et al.*, 1994).

Figure 2 shows a simplified diagram for the whole electromagnetic spectrum for a "typical" solar burst continuum emission (after Kaufmann, 1988). Various thermal and non-thermal models can fit to the observed spectral features, at frequencies lower or higher than the submm/IR range. Their study depends critically on the knowledge of the continuum emissions in that interval of frequencies.

The most critical boundary condition is set by the time scales observed in continuum emissions. The event observed at mm-waves only, shown in Figure 1 (Kaufmann *et al.*, 1985), exhibited multiple pulses, very fast (lasting less than 100ms), and well correlated to time structures observed at hard X-rays (Figure 3).

Such time scales (<<1sec) are too short to be explained by synchrotron losses (at the mm-submm range) or by bremsstrahlung (X-rays). One possible interpretation assumes that the bursts are initially made of compact synchrotron sources, with emission spectrum peaking in the IR, with a lifetime reduced by an efficient inverse-Compton action, producing concurrent fast pulses at hard X-rays (Kaufmann *et al.*, 1986). Indeed, recent observations of solar bursts at hard X-rays, obtained with higher sensitivity and time resolution by BATSE experiment on board of GRO satellite (Machado *et al.*, 1993; Emslie *et al.*, 1994), and by PHEBUS experiment on board of GRANAT satellite (Vilmer *et al.*, 1994), have shown that subsecond time structures are common to most of the impulsive events.

The synchrotron/inverse-Compton model may be reconciled to current interpretations of solar burst emissions by assuming a "pre-impulsive" phase for the event (Figure 4(a)). In this phase, the primordial compact synchrotron source lifetime is shortened to less than 100ms by the inverse-Compton action on the synchrotron photons, reducing the energy of the relativistic electrons to mildly relativistic levels producing, as a byproduct, beams which produce the well known manifestations, such as the gyrosynchrotron radio emissions and the X-rays by bremsstrahlung in the denser levels of the solar corona and chromosphere (Figure 4((b)).

When spectra are derived in large time scales, compared to the typical lifetime of the "pre-impulsive" bursting sources, they may exhibit the two components, at submm/IR and at microwaves. The simplified resulting spectral composition is shown in Figure 5. Such composite spectra are in fact suggested by various examples of bursts measured in the past, in the range microwaves/mm, shown in Figure 1. In addition to the striking examples shown by Kaufmann *et al.* (1985) and Shimabukuro (1972), we draw the attention to the examples

shown by Hachenberg and Wallis (1961); Shimabukuro (1972); Croom (1970) and Cogdell (1972); Akabane *et al.* (1973); Zirin and Tanaka (1973) and White *et al.* (1992).

One new and unique project for a solar submm-w telescope (SST) was conceived, to operate at two frequencies, 210 GHz and 405 GHz (Figure 6). It is in final phase of evaluation by FAPESP and receives support of co-participating solar groups from University of Bern, Switzerland, and the Institute of Astronomy and Space Physics, IAFE, Argentina, to be installed and operated at the El Leoncito Astronomical Complex, CASLEO, in the Argentinean Andes, where the atmospheric conditions are exceptionally good for submm transmission, along nearly 300 clear days per year.

REFERENCES

Akabane, K., Nakajima, H., Ohki, K., Moriyama, F., Miyaji, T.: 1973, *Solar Phys.*, **33**, 431.

Beckman, J.E.: 1968, *Nature*, **220**, 52.

Benz, A.O.: 1994, *Space Sci. Rev.*, **68**, 135.

Clark, C.D., and Park, W.M.: 1968, *Nature*, **219**, 922.

Cogdell, J.R.: 1972, *Solar Phys.*, **22**, 147.

Correia, E., Kaufmann, P., and Magun, A.: 1994, in "Infrared Solar Physics" (ed. by D.M. Rabin, J.T. Jefferies and C. Lindsey), Kluwer Acad. Publ., Dordrecht, NL, 125.

Costa, J.E.R., and Kaufmann, P.: 1986, *Solar Phys.*, **104**, 253.

Croom, D.L.: 1990, *Solar Phys.*, **15**, 414.

Degiacomi, K., Kneubühl, F.K., Huguenin, D., and Müller, E.A.: 1984, Int. J. Infrared and MM-Waves, **5**, 643.

Eddy, J.A., Léna, P.J., and MacQueen, R.M.: 1969, *Solar Phys.*, **10**, 330.

Emslie, A.G., Mehta, S., and Machado, M.E.: 1994, *AGU, EOS Trans.*, **75**, 295.

Gezari, D.Y., Joyce, R.R., and Simon, M.: 1973, *Astron. Astrophys.*, **26**, 409.

Hachenberg, O., and Wallis, G.: 1961, *Zs.f.Ap.*, **52**, 42.

Hudson, H.S.: 1975, *Solar Phys.*, **45**, 69.

Hudson, H.S., and Lindsey, C.: 1974, *Astrophys. J.*, **187**, L35.

Kaufmann, P., Correia, E., Costa, J.E.R., Zodi Vaz, A.M., and Dennis, B.R.: 1985, *Nature*, **313**, 380.

Kaufmann, P., Correia, E., Costa, J.E.R., and Zodi Vaz, A.M.: 1986, *Astron. Astrophys.*, **157**, 11.

Kaufmann, P.: 1988, *Adv. Space Res.*, **8**(11), 39.

Lee, J.W., Gary, D.E., and Zirin, H.: 1994, *Solar Phys.*, in press.

Lindsey, C., Hildebrand, R.H., Keene, J., and Whitecomb, S.E.: 1981, *Astrophys. J.*, **248**, 830.

Lindsey, C.: 1994, in "Infrared Solar Physics" (ed. by D.M. Rabin, J.T. Jefferies and C. Lindsey), Kluwer Acad. Publ., Dordrecht, NL, 85.

Machado, M.E., Ong, K.K., Emslie, A.G., Fishman, G.J., Meegan, C., Wilson, R., and Paciesas, W.S.: 1993, *Adv. Space Res..*, **13**, 9/175.

Ramaty, R., Schwartz, R.A., Enome, S., and Nakajima, H.: 1994, *Astrophys. J.*, in press.

Shimabukuro, F.I.: 1970, *Solar Phys.*, **15**, 424.

Shimabukuro, F.I., 1972, *Solar Phys.*, **23**, 169.

Vilmer, N., Trottet, G., Barat, C., Dezalay, J.P., Talon, R., Sunyaev, R., Terekhov, O., and Kuznetsov, A.: 1994, *Space Sci. Rev.*, **68**, 233.

White, S.M., Kundu, M.R., Bastian, T.S., Gary, D.E., Hurford, G.J., Kucera, T., and Bieging, J.H.: 1992, *Astrophys. J.*, **384**, 656.

Zirin, H., and Tanaka, K.: 1973, *Solar Phys.*, **32**, 173.

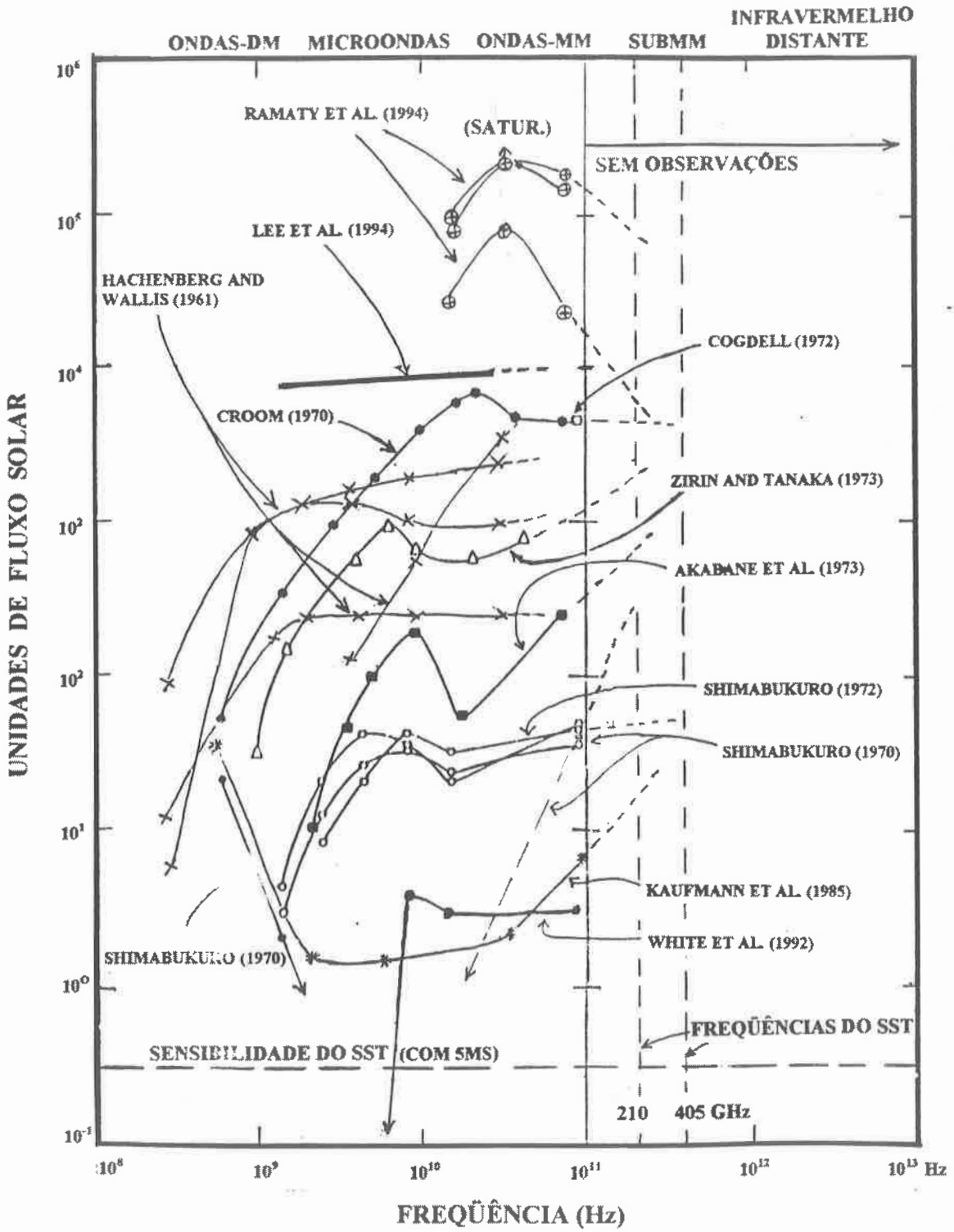

Figure 1 - Examples of solar bursts emission spectra indicating the importance of the contribution into the submm-w range. There are indications of the frequencies and sensitivity considered for the new solar submm-w telescope project.

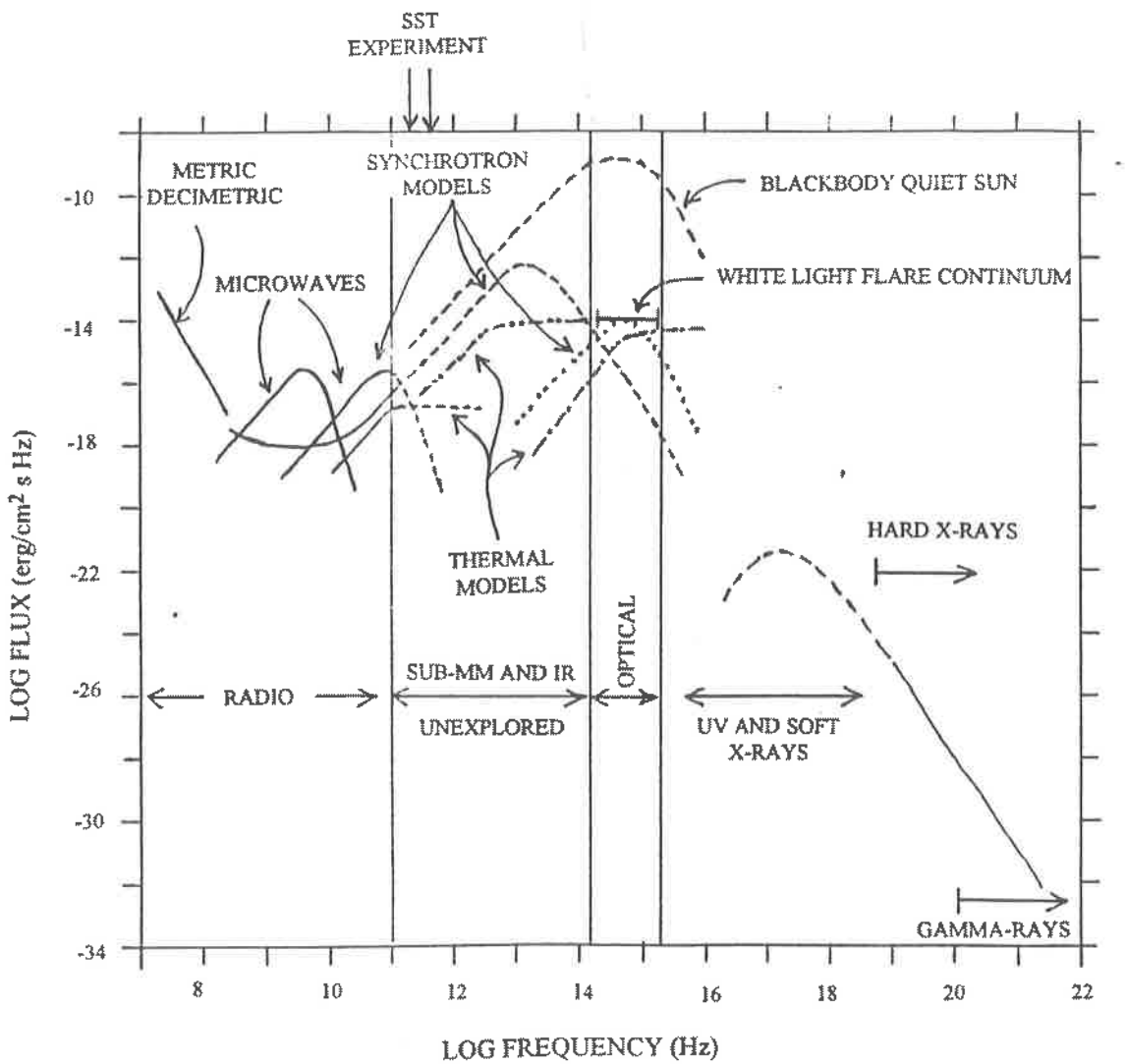

Figure 2 - The whole electromagnetic spectrum for continuum emissions produced by a "typical" solar burst.

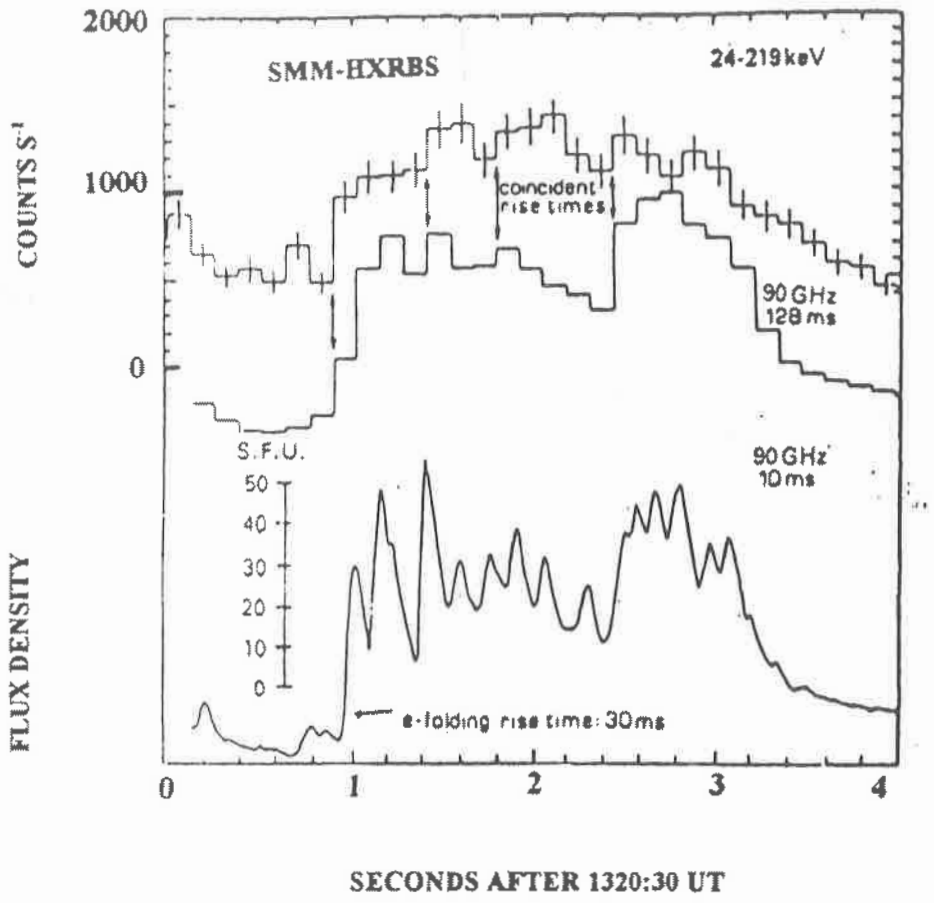

Figure 3 - The main time structure of the solar burst of 21 May 1984, obtained at 90 GHz (Itapetinga Radio Observatory), and at hard X-rays, obtained by the HXRBS experiment on board of SMM satellite (Kaufmann *et al.*, 1985). The 90 GHz output was simulated with the same time resolution of the hard X-ray detector (128ms), showing a time coincidence better than 100ms (Costa and Kaufmann, 1986).

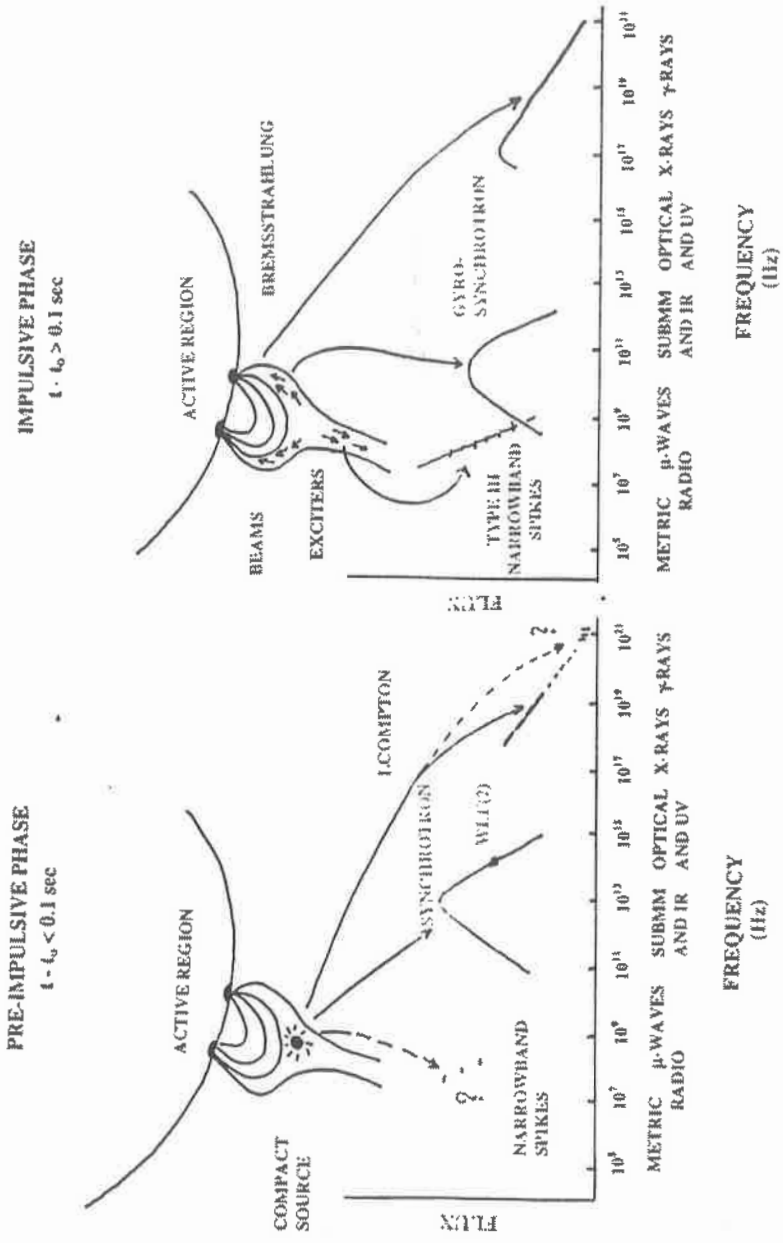

Figure 4 - Sequence of burst phases suggested by the model for a simple impulsive event. In the pre-impulsive phase (a) a compact synchrotron source produces a continuum spectrum maximizing in the submm/IR. The inverse-Compton effect in that source reduces the electrons' energy in less than 100ms, producing a corresponding pulse at X-rays. Maybe in this phase there are also produced some of the gamma radiation, metric and decimetric pulses (Benz, 1994), and white light emission. The electrons' energy is immediately reduced to mildly relativistic levels, producing the impulsive phase (b), which physical description is well known.

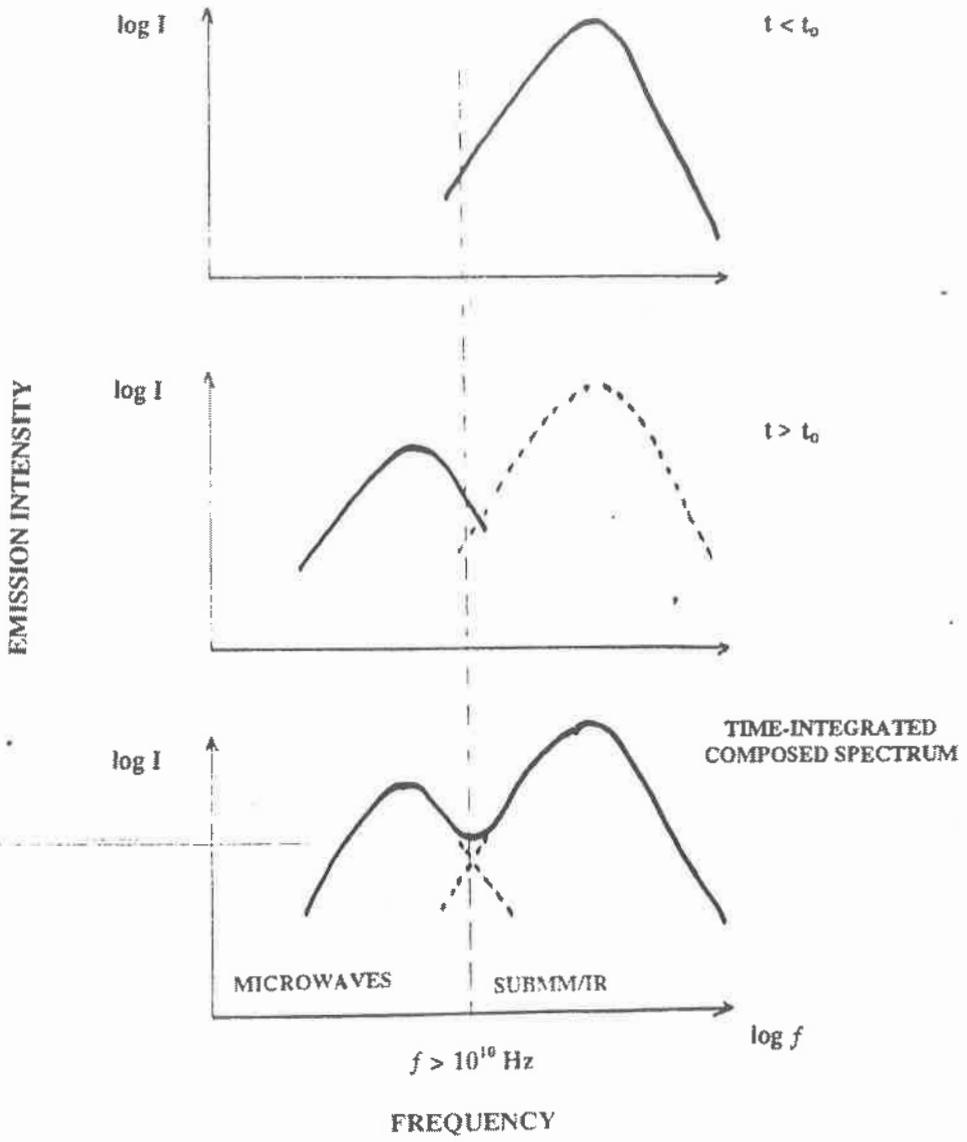

Figure 5 - A simplified sequence of spectral composition, which initiates at the pre-impulsive phase ($t<t_o$), before the instant which defines the impulsive phase ($t>t_o$). The first one builds up the IR spectral component, due to the compact synchrotron sources made by ultrarelativistic (> tens of MeV). The second one is due to the same electrons with energies turned down to tens of keV by the inverse-Compton action, and is well known. For larger durations, the composite spectra have contributions from the two phases of the event.

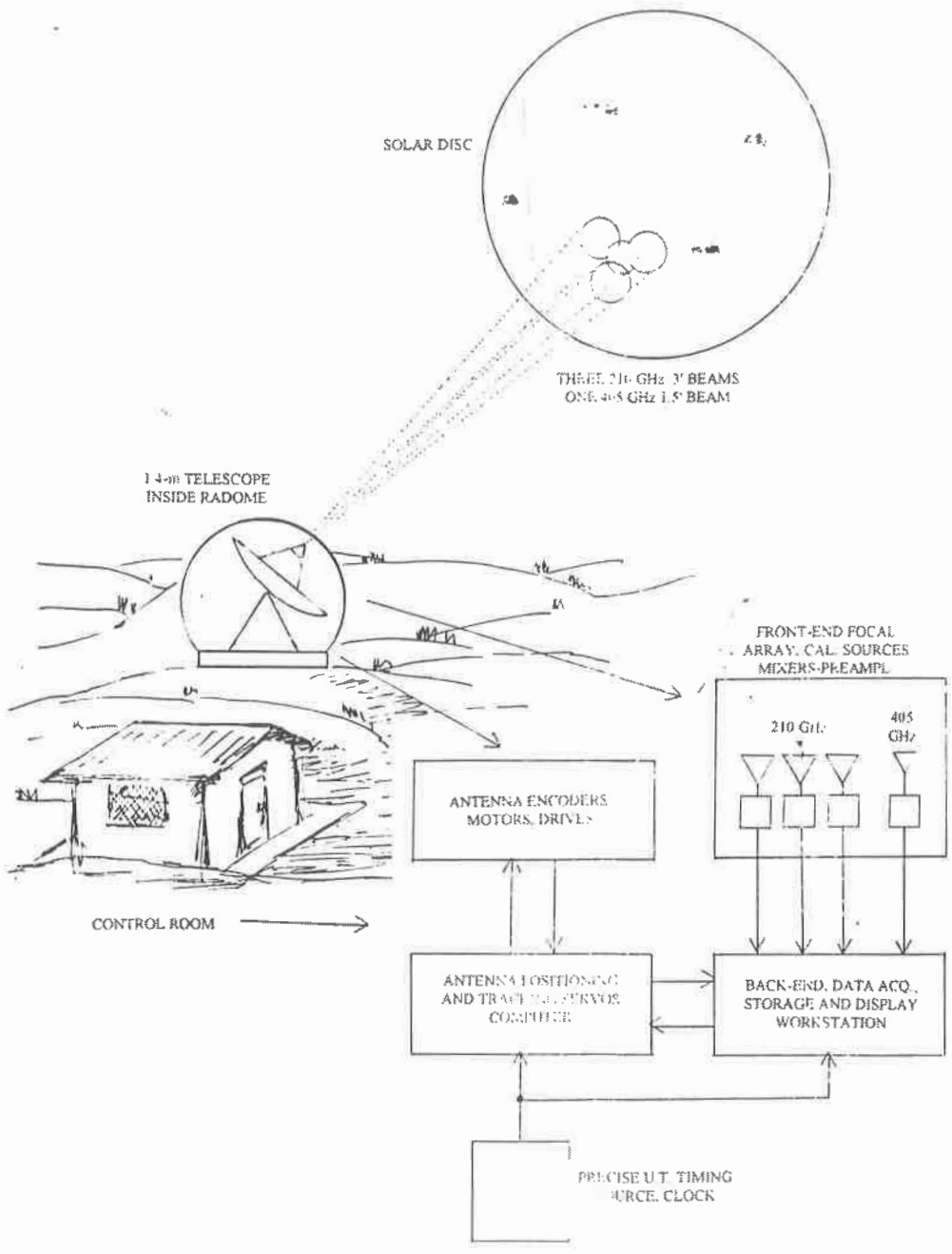

Figure 6 - Simplified block diagram of the new solar submm-w telescope (SST). Its unique conception proposes the spectral diagnostics at two frequencies in the atmospheric "windows" centered at 210 GHz and 405 GHz, and dynamic imaging of bursts using the multiple beams technique.

CURRENT RESEARCHES IN SOLAR ECLIPSES

Oscar T. Matsuura
Instituto Astronômico e Geofísico, Universidade de São Paulo,
Caixa Postal 9638, São Paulo, SP, Brasil, CEP 01065-970

ODUCTION

to the ever changing scientific motivations and technological innovations, different types of ırch have been carried out during solar eclipses in different periods of the scientific history. Soon Newton's *Principia*, the value of eclipses was mainly regarded as affording information on the ement of the Moon (Dyson and Woolley, 1937). Examining records of historic eclipses, Halley)vered the secolar acceleration of the mean motion of the Moon, ultimately traced to a lengthening e day due to the tidal friction.

tradition of scientific expeditions to observe solar eclipses began in 1842. The first astronomical ograph, a daguerreotype, was obtained by Barkowski in the eclipse of 1851 July 28, in Königsberg. / in 1880, doubts were dissipeted on whether the red prominences and white corona were mere cal effects due to the Moon, or real appendages of the Sun. That year the radial polarization of the ınetic vector of the coronal white light was put in evidence by the first time.

spectrum of prominences with the red and blue lines of hydrogen, and a yellow line of unknown in at that time, was first obtained in the eclipse of 1868 August 18, observed in India and Malaya. In following day, Janssen in Meudon Observatory succeeded in observing prominences out of an pse. The yellow line was correctly interpreted as due to helium in 1895.

e coronal spectrum with continuum plus the green emission line was observed in the eclipse of 1869 gust 07, in USA; and with the dark Fraunhofer lines, in 1871. The eclipse of 1870 December 22, served in Mediterranean, disclosed the chromospheric flash spectrum. The statistical theory of ization developed by Meg Nad Saha in 1920 was crucial for its interpretation and further studies on structure of the chromosphere.

ter the obtention of good coronal pictures in the eclipse of 1871 December 12, in the South of India, e variation of the shape of the corona along the solar cycle was suggested by Ranyard in 1881, and nfirmed by Hansky in 1887. The radiel distribution of the coronal brightness has been investigated nce 1878. Schuster (1879) computed the polarization of the white-light corona by Thomson attering, and applied the results for the observations of 1871.

ortable coelostats are common light feeders in eclipses. The first one was constructed in 1896.

he announcement by Einstein of the deflection of light by the Sun's gravitational field in 1911 in the amework of Newtonian dynamics, and twice its value in 1915, according to the General Theory of elativity, raised up along the following years a series of expeditions attempting to confirm such a rediction. One successful observation was performed in Brasil (Sobral, CE) by Davidson and Crommelin in the eclipse of 1919 May 29.

n the subsequent eclipses, measurements were made on the variation of the influx of solar neutrons nd cosmic rays, and geophysicists were interested in changes occurring in the Earth's ionosphere and nagnetosphere.

Since the end of the World War II, when radio astronomers published the first detection of solar radio waves, a new interest was raised by the realization that eclipses could provide a way of improving the poor spatial resolution reached hitherto in measuring the distribution of radio-brightness over the Sun, especially on active regions.
With today's CCDs, time series of two-dimensional white-light or monochromatic observations can be obtained. The image acquisition time is still long and constrains the time resolution. Also the smallness

of the chip of most CCDs available nowadays is another inconvenience. But the increasingly widespread digital treatment of images offers new possibilities for the analysis of time evolution of diverse phenomena occurring in structures of smaller scales in the solar atmosphere.

The imperative for the coming yaars is to decipher the structure and the activity at all levels of the solar atmosphere down to 100 km (0.1 arc sec) resolution (Moore, 1990). This requires space-borne, as well as ground-based telescopes observing simultaneously. In the visible light, the telescope has to be of aperture of a meter or more, and endowed with adaptive optics. A sensible guide for guessing now the action of the magnetic field in the smaller structures, is to well resolve with current state-of-art instrumentation during eclipses, the action of the field in larger and magnetically stronger regions.

Following the current trend of astrophysical researches in eclipses, this review will mainly focus onto the studies of the varied coronal structures of magnetized plasmas. But a discussion on the zodiacal dust in the neighborhood of the Sun, and on the controversial secular variation of the solar photospheric diameter will complement the next section.

CURRENT RESEARCHES

1. White-light observations. Structure and structural changes of the solar atmosphere

The low-beta plasma of K corona is a good tracer of the lines of force of magnetic fields. Space-borne coronographs do not show the inner corona where the most dynamic processes take place. However, the aclipse pictures show the K plus F corona superimposed on the sky background and the coronal aureola. The last one is due to the atmospheric single scattering and optics. It can be represented as A(r), a function of the heliocentric distance only. Koutchmy and Koutchmy (1974) proposed a model for its calcolation. Measurements of the solar aureola under similar conditions are necessary for deriving empirical scattering functions. For the aclipse of 1981 July 31, Lebecq *at al.* (1985) used a Bailey bead. Under good observing conditions, the coronal aureola almost does not affect the F-corona everywhere, tha latter one being brighter than the faint K-corona at heliocentric distances > 2.5 $R_\odot$ naar the minimum of solar activity. Under unfavorable conditions (small eclipse magnitude, high K-corona brightness at maximum of activity) the aureola may compete with the F-corona intensity. Over the Moon's disc, the coronal aureola A is superimposed on the earthshine **E**, and the sky background S. Usually it is assumed that $\mathbf{E} = 2.5 \times 10^{-10} \langle B_\odot \rangle$ ($\langle B_\odot \rangle$: mean intensity of the solar disc) at 540 nm (Koutchmy and Laffineur, 1970).

The sky background is polarized and due to the atmospheric multiple scattering. It can be represented by S(z) where z is the zenith distance, and measured through wide-field pictures neglecting A(r) for heliocentric distances r > 3 $R_\odot$,

Subtracting A(r) and S(z), the total intensity of (K + F) corona is left. The K-corona can be separated by assuming that only K-corona is polarized and splittable into the tangential and radial components, while the F-corona is not polarized for r < 5 $R_\odot$. An assumption should be made for the polarization of the K-corona as function of the radial distance in different azimuthal directions, based on models of K-corona (Saito, 1972; Koutchmy *et al.*,1978). An alternative procadura is to subtract the F-corona, computed e.g. from the axisymmetric model proposed by Koutchmy and Lamy (1984).

Since long it is known that the global shape of the K-corona undergoes variations along the solar cycle. In general, overlying the coronal holes the magnetic field lines are open. Conversely, near the sunspots, active regions and filaments, the magnetic structure is closed in arches or loops which eventually disrupt, giving placa to coronal mass ejections. The global morphological behavior along the solar cycle suggests a corona more dependent on the evolution of large-scale magnetic fields, than on the local thermodynamical parametars assumed for a quasi-static magnetic field. According to Loucif and Koutchmy (1989), the sectorial extent of the polar regions free of streamers, and the deviation of the streamers from the radial direction, both follow the solar cycle getting larger at the minimum of sunspot activity, the time behavior of the last one being skew. The Ludendorf's (1934) flattening indax (at equatorial radius = 2 $R_\odot$) also follows the solar cycle, but its maximum and minimum occur about one year before the minimum and the maximum of the cycle, respectively. The integrated brightness of the K-corona seems to follow the solar cycle of sunspot activity in phase (Lebecq *et al.*, 1985).

Revisiting such questions is still valuable, as new features of the solar cycle have been established (overlapping cycles, ectivity cycle of polar regions, torsional oscillations of the Sun, cycle of ephemeral regions, etc), new features of the solar dynamo and of the solar global field are being predicted, and new insights on the rotating corona can be inferred from helioseismology and solar-terrestrial relations through the M-regions. The coronal structures are well observed with coronographs in the green coronal line of Fe XIV. They show asymmetry between the N and S hemispheres and double-peaked maximum. All these discoveries should be taken into account along the future analyses of the corona's global shape.

The amount of free electrons along the line of signt can be derived from the white-light intensity of the K-corona, since both are linearly related. Assuming a gaussian profile for several stars present on the same coronal picture, with known magnitudes and with spectral class not too different from that of the Sun, the half-width of each star image can be determined together with the relative peak Intensity. Then a pseudo-magnitude can be determined for each star. Of course, the transmission of the neutral radial filter, if used, has to be taken into account. The pseudo-magnitude of the Sun can also be expressed in terms of the mean intensity of the solar disc, $<B_{\odot}>$, and of its radius. Then, by a single constant, the pseudo-magnitudes can be converted into standerd magnitudes of the sters and the Sun and, finally, the coronal brightness can be expressed in units of $<B_{\odot}>$ (Koutchmy *et al.*, 1978).

Up to r = 3 - 4 $R_{\odot}$, the observetional data agree with an isothermal model in hydrostatic equllibrium (Badalyen and Livshits, 1989) with T = 1.6x10^6 K and electron density of 10^9 cm^{-3} at r = 1 $R_{\odot}$, The observed densities within the streamers drop faster with distance than the hydrostatic model predicts. So, for r > 5 $R_{\odot}$ a Parker-type outflow is assumed in a slowly diverging structure with a critical point located at 7.6 $R_{\odot}$. Analyzing a streamer observed in the eclipse of 1970 March 07, Koutchmy (1972a) found a neck (a kind of Laval nozzle) in the cross section of the streamer at r ≈ 3 - 3.5 $R_{\odot}$. The density dropped outwards elmost monotonically but, according to the conservation of mass, the velocity which increased quickly to 100 km/s until raaching the neck, increased afterwards much slowly. The absence of a curvature in the streamer beyond r ≈ 3 $R_{\odot}$ meens that the radial forces of magnetic origin were still acting there, so that the plasma wes not flowing freely (Koutchmy, 1992).

Independent observations of the eclipse of 1970 March 07 agree in evidencing a new type of coronal structure (or component) designated diffuse extemal reinforcement (Koutchmy, 1972b). It appears along the solar equator at r > 4 $R_{\odot}$, and seems to be correlated with active regions underneath. It is distinct from the K-corona since it is not polarized. At leest its polarization does not raach the degree expected from Thomson scattering. It is also distinct from the circularly symmetrical F-corona which looses such a symmetry only at larger elongations, where the interplanetary dust is observed as the zodiacal light in a belt. This component has not been confirmed so far, and the physical process giving rise to the light coming from the diffuse extemal reinforcements still remains unknown.

The most important disadvantages of color films for general astronomical applications are the latent image decay with feilure of reciprocity, and the interimage effect. The first one can be reduced by cooling, but in different amouts for different emulsion layers, so producing false colors. The interimage effect in a filtered image can be expressed through coefficients of linear combinations giving account of the influence of the other colors. Koutchmy (1978) found that such effect is considerably reduced if the study is limited to the blue and the red filters. In solar eclipses the main advantage of color films is the possibility of displaying the two-dimensional color distributions obtained simultaneously, over fields larger than the present size of CCD chips. This advantage is most appreciated when objects are studied which change in time. Color pictures allow easy colorimetric discrimination of cool prominence-like emissions, from coronal emissions recorded simultaneously (Koutchmy and Stellmacher, 1978). The cool component of the solar plasma produces large color effects due to the line emission of low excitation states. Also the blue sky background which dominates in the outer corona, produces a large color effect. The original picturas with the calibration wedge marks and field stars, should be suitably illumineted and filtered through broad band conventional filters, in order to render proper images for colorimetric analysis.

In the eclipse of 1973 June 30, Koutchmy and Stellmacher (1976) observed the corona near the solar South pole. In polar regions the characteristic features are the chromospheric spicoles associated with polar plumes, both related to the chromospheric network. Koutchmy and Stellmacher (1976) disclosed coronal spikes with half widths of only 1.67" and electron densities of 10^{10} cm^{-3}. The true size was darived by deconvolving the raw data with different peint spread functions for different filtars, to take into account the chromatic aberration. A coronal temperature was inferred from the color-index, which diffarad from that of chromospheric structures. Subtracting the emission of D_3 helium line, and neglecting the continuum in the red filter, the Hα emission of the chromospheric structures can be expressed in terms of $<B_{\odot}>$ through the red filter. Then the Hβ emission can be related to the Hα emission, and expressed in terms of $<B_{\odot}>$ through the green filter. Taking into account the other prominence lines falling in the bandpass of the green filter, and the different attenuation of the filters, the continuum in the green filter can be estimated for the detarmination of the electron density. This was found to be 10^9 cm^{-3}. A spectrum of the same region takan simultaneously shows the Fe XIV green line with broad asymmetric profile, implying an outward velocity of $\approx$ 200 km/s, contrasting with the behavior of the chromospheric Hβ line. This result afforded an insight on the source of the high speed solar wind. Such a thin stream suggests a non-orthodox view of the corona filled with fina striations (< 1") in density, valocity and magnetic fiald. The analyzed pelar region corresponded to a disappearing coronal hole. It was also suggested that in polar regions, perhaps in tha coronal holes, the chromospheric macrospicules, the coronal spikes and the polar plumes are associated, and that spicules, in soma unknown way, play a key role in the acceleration of tha solar wind.

Structural changes in the corona comprise proper motions of clouds, morphological changes of structures, variations of brightness and oscillations. Total eclipses allow observations of the inner corona at distances much closer to the solar limb than achievabla by space-bome coronographs (Koutchmy, 1988), not to mention the shadowing and vignetting in artificial eclipses. A neutral filtar with density decaying radially outwards allows the entire corona to be recordad photographically up to about $r \approx 5\ R_{\odot}$ without ovarexposure. Sevaral idantical instrumants installed along the path of totality, and oparated identically, allow to follow the time evolution of structural changes. Using such a method, the solar activity can ba covared ovar a time span longer than 03 hours. In some past attampts the coordinated effort failedmainly because of unfavorable waather, although individual axperiments have succeaded. Such was the obsarvation of the aclipse of 1981 July 31, by Stellmacher *et al.* (1966). At the South polar limb a helmet-like streamer overtaid a prominance from tha polar crown. Bright knots from an eruptive prominence rose with velocities up to 160 km/s. From the amount of Thomson scattered light, an alectron dansity of $2x10^9$ cm^{-3} was obtained for the bright knots, and of $6x10^8$ cm^{-3} for the associated leg of the coronal helmet. As usual, the helmet appeared topped with a straight and thin coronal ray, perhaps undergoing magnetic field reconnection and annihilation (Cliver and Kahler, 1991). The eclipse of 1990, July 22, was observed from the ground, and aboard a Falcon jet aircraft (Koutchmy *et al.*, 1992). The airbome experiments were partially hindared because frozen water coverad most of tha optical window. Besides the absolute photometry and the determination of the flattening index, the comparison of the whita-light images with the synoptic data of the graen coronal line from tha National Solar Observatory/Sacramento Peak Observatory showed correlation when the prominence amissions are excluded from the white-light pictures. Long coronal rays were seen up to $r = 6\ R_{\odot}$ and, intarastingly, several of them appeared to begin at a significant radial distance. Also above faint prominences in the Eastarn limb, several dark voids were saan revealing deficit of electron density. They are not the cavities observed undar tha helmet streamars and their natura still remains mysterious.

A partially successful coordinated observation was performed in the eclipse of 1991 July 11, within the Multi-station Intemational Coronal Experimant (MICE), with observing stations in Hawaii (Mauna Kea and Kona), Mexico (La Paz and Baja Califomia) and Brasil (Tefé and Manicoré) (Zirker *et al.*, 1992). The standard apparatus of MICE was described by Lebecq *et al.* (1985). A spatial resolution of 3.5" was astimated from the FWHM of star images. From visual inspection, the following interesting rasults were obtained: a) untwisting and alignmant of coronal rays; b) straamers at unusually high solar latitude; c) displacement of straamers along the eclipse by $\approx 0.5^{\circ}$, possibly due to tha global coronal rotation; d) no evidence of nanoflares (Parker, 1988) for an exposure time of 20 s. Tha digital analysis of the data was parformed by Matsuura *et al.* (1993a), including an analysis of the color-indices of the

global corona as well as of its structures, through conventional B, V and R filters. The rather unusual morphology of the global corona (large streams at high heliogrephic latitudes) was interpreted in terms of the orientation of the magnetoheliospheric neutral sheet, in the framework of the model of Saito and Akasofu (1987) proposing the rotation of the solar dipole magnetic field within the Sun along the solar cycle. The color-indices showed to be much valuable for tracing hot coronal structures mingled with the cool chromospheric gas. Further analysis of the existing data with finer spatial resolution is in progress, and the preliminary results show subtle changes in the clumped material within the magnetic loops of helmet streamers (Matsuura *et al.*, 1993b). The morphological analysis of subtle and small scale gredients can be better performed in image procassing and visualization seftwara anvironments offered, *e. g.* by the Khoros system (Rasure *et al.*, 1990) than by astronomical packages devoted to specific brenches of astronomy.

Matsuura *et al.* (1993a) also contributed for better characterizing the coronal rays as fine coronal structures, and distinguishing them observationally from the polar plumes. Briefly, the designation coronal rays referring usually and loosely to any type of coronal structure, was restricted (as here) to the straight, thin, very long and almost radial very fine structures occurring over chromospharic active regions. Measuring the electron density and estimating the cross section of the rays, a flow velocity of 50 to 400 km/s was derived assuming conservation of mass (Koutchmy, 1992). Some reys appear to begin at a significent radial distance from the Sun. Are they neutral shaets in the top of invisible and expanding helmets? Koutchmy *et al.* (1992) do not believe all reys have circular cross-section. The sharp edge may correspond to a tangantial discontinuity of the magnetic field.

Another interesting achievement of MICE experiment was the demonstration that the three-dimensional (stereoscopic) structure of the solar corona can be derived from its images (Koutchmy and Molodensky, 1992). The motivation for such work was the realization that large coronal structures associated with the polar regions and the equatorial belt of magnetic activity, are direct counterparts of the heliomagnetospheric sheet, mora than the small-scale sunspots, prominences and filaments. The attempts to use coronal imagas obtained by space-borne coronographs during a solar rotation failed because of several reasons: lack of spatial resolution; vignatting effect; coronal changes along the collection of the data; and lack of informations at $r < 2\ R_{\odot}$. Tha images from MICE can be considered of a quasi-rigid corona. The rotational stereoscopic shift was applied to 7 structures in order to determine their true positions.

2. Observations in monochromatic light

2.1. Two-dimensional determination of lina profiles

2.1.1. Residual depression of Fraunhofer linas in K-coronal spectrum

Observational information concerning the thermal structure of the lower corona is important both, for confirming theories of coronal heating and for use in solar wind computations. For example, the location of the temperature maximum in the corona has important implications for the coronal heating mechanisms.

Tha temperature structure of the low corona (where the K-corona dominates the F-corona) can be mapped by taking advantage of the high sensitivity of current CCD detectors, and using the hitharto unused theoretical calculations of the Doppler-broadening of Fraunhofer linas due to three-dimensional Thomson scattering by the electrons from tha corona (Cram, 1976). The electron temperature is determined from the residual depression of absorption lines from the K-coronal spectrum. These calculations show that accurate measurements of the intensities at e selected set of wavelengths can lead to the determination of coronal electron temperature independent of prior methods. Since the corona is not in equilibrium, the determination of the coronal tempereture by different methods is important for understanding the coronal excitation and structure. By determining the ratio of the intensities to an accuracy of 1%, the corona temperature can be determined within an accuracy of 200,000 K. The ratio for tha hottest and the coldast temperature is maximum at 3900 Å and 4100 Å respectively. An additional measurement at 4000 Å can provide the normalization and measurements of polerization necessary for separating K- from F-corona. The filters to be used must avoid the coronal emission lines, especially Fe XI (3987 Å), Ca XII (4086 Å) and Ni XII (4231 Å). The potential

results will be comparable to coronal electron temperatures deduced from space observations of Lyman-α broadening (Withbroe *et al.*, 1982) and from X-ray observations with a normal-incidence telescope.

2.1.2. Fabry-Pérot interferometry

Besides the information on Doppler shifts, this method can provide high resolution profiles of the forbidden emission lines from the corona. From these profiles the line equivalent width and the thermal broadening can be deduced. The Fabry-Pérot interferometer is especially suitable in observations involving low intensity source and requiring reasonably high spectral resolution. A disadvantage of the single étalon Fabry-Pérot spectrometer for general astronomical use is the small free spectral range, *i. e.*, the upper limit of the spectral breadth acceptable without confusion between orders. This disadvantage is more serious when observing a continuum spectrum or absorption lines. If, as in the solar E-corona, the source consists of one or two isolated emission lines, the addition of a narrow bend interference filter as pre-filter, allows unambiguous measurements to be made.

Jarrett and von Klüber (1955) described a successful ettempt to photograph interference fringes with a Fabry-Pérot interferometer from the green coronal line in the eclipse of 1954 June 30, near the minimum of solar activity, in Sweden. They established the feasibility of investigating the corona in eclipses with this method. The fringe half-widths decreased with increasing distance r between 1.05 and 1.3 $R_\odot$. This was interpreted in terms of kinetic temperatures that ranged from $5x10^6$ to $2.2x10^6$ K, with most velues near $2.5x10^6$ K. The same kind of observation was made again by the same authors (Jarrett and Klüber, 1961) in the green and red coronal lines, in the eclipse of 1956 October 12, in the coral atoll Atafu, South Pacific. The observations reached up to 0.8 $R_\odot$ above the limb. The mean temperature for the green line was $3.2x10^6$ K, and for the red line $3.5x10^6$ K, with an error of 10% in each case. This eclipse came near to the maximum of solar activity.

Hirschberg *et al.* (1971) used a photographic Fabry-Pérot interferometer to measure the widths and shifts of the green coronal line during the eclipse of 1970 Merch 07, in Mexico. The instrumental half-ihtensity width was 0.2 Å.Observations attempted on the CaXV (5694 Å) coronal line failed beceuse the line proved to be much weaker than expected. The center of the fringe system was set at r = 1.1 $R_\odot$ in the NW limb, near a large helmet streamer associated with a prominence and a filament. Microdensitometer tracings were first reduced to intensities using a step-wedge calibration, then corrected for the background continuum by assuming an exponential law. The Doppler shifts in the neighborhood of the axis of the streamer suggested a vortex-like structure in the corona with a velocity of 6 km/s at r = 1.5 $R_\odot$. Doppler temperatures were $6.0x10^6$ K in the core of the vortex, and $2.5x10^6$ K in the periphery.

Profiles of the green and red coronal lines were observed by Marshall and Henderson (1973) at different positions in corona, using a photoelectric scanning Fabry-Pérot interferometer during the same eclipse in Mexico. The photoelectric detection allowed observetions further out from the limb than possible with photogrephic multi-slit method. But radiation from only one spatial element is detected at any one time. This means thet the corona must be scanned spatially in order to obtein profiles from different regions. The instrumental width was 0.2 Å. In order to scan over one free spectral range, the optical path between the plates was varied by a half-wavelength. In order to scan quickly, the spacing was changed utilizing the piezoelectric effect. Useful profiles were obtained at r = 1.05 and 1.1 $R_\odot$. Other profiles were also obtained with the coronograph at Pic-du-Midi during October 1970 and September 1971, in some instances from as far es r = 1.5 $R_\odot$. The domineht noise was shot noise of the signal and background (continuum from K- and F-corona plus scattered sunlight), not from the receiver or varying atmospheric transparency. The type of noise being white noise, DC and AC detection systems gave approximately the same result. The true line profiles were obtained by meens of a least square technique, fitting synthetic gaussian profiles convolved to the instrumental profile. Observations with the coronograph provided temperatures from $1.12x10^6$ and $6.32x10^6$ K (overall mean value: $3.7x10^6$ K) in the green line, end from $1.76x10^6$ and $4x10^6$ K (overall mean value: $2.8x10^6$ K) in red line. No systematic temperature variation was found, but possible fluctuations were seen in the width of the lines within time intervals of 10 min. No large scale line of sight velocity

components were detected, as the maan value of 1.18 km/s had a standard deviation 3 times larger. The temperature from the green line profiles in the eclipse was about 4x10^6 K, and from the red line profiles, about 3.5x10^6 K. The eclipse results were the first ones obtained by a ground based photoelectric scanning interferometer. The temperatures obtained by Marshall and Henderson (1973) are slightly higher in comparison to those obtained by other authors. This may be due to the observations being made close to the maximum of the solar cycle. Assuming thet the excess of broadening in the lines is due to a turbulent velocity, such a velocity would exceed 20 km/s. But then, large scale Doppler shifts should be observed, what was not the case.

Interferograms of coronal HeI D_3 (5878 Å), green and red lines were obtained in the eclipse of 1972 July 10, in Russian Paclfic coast (Kim and Nikolsky, 1975). The HeI D_3 line was overexposed in the chromosphere, but did not appear in corona. Detalled photometry with 3% accuracy was mada for the green line with an instrumental width of 0.31 Å. For r between 1.2 and 1.7 $R_\odot$, no Doppler-shift velocities exceeding 10 km/s were found. The half-width increased with height in almost all regions, except in quiet regions. The excess broadening was attributed to turbulent velocities of 24 km/s at r = 1.2 $R_\odot$, increasing up to 34 km/s at r = 1.7 $R_\odot$. A constant equivalent width found for almost all regions was interpreted as due to the dominance of the radiative excitation of the line. In quiet regions, where the equivalent width decreased with the distance from the Sun, the collisional excitation wes assumed to be dominant.

With an instrumental resolution of 0.23 Å, photographic Fabry-Pérot interferometry was done by Dasai and Chandrasakhar (1983) up to r = 1.5 $R_\odot$, during the eclipse of 1980 February 16, in the green line. The accuracy of line-width measurements was limited by the grain noise of the film, what corresponded to an accuracy of ±10% In the tamperature. A least square enalysis indicated a tentative temperature maximum near r = 1.2 $R_\odot$. The ratio of the line Intensity (proportional to the square of electron density for a collisionally excited line) to the square of the continuum intensity (the continuum is proportional to the electron density) appeared to ba inversely correlated to the temperature, instead of being constant. This anticorrelation may indicate a real change in the ionization temperature. Using this ratio to evaluate the Ionization temperature, the observed line-widths showed peak turbulent velocities of about 10 km/s. The radial distribution of turbulent velocities did not show any systematlc trend.

Both, green and red coronal lines were observed simultaneously by Chandrasekhar *et al.* (1984) in the interferometric Fabry-Pérot experiment during the eclipse of 1983 June 11, in Indonesia. The instrumental width was 0.33 Å for the green line, and 0,21 Å for the red line. Line-width temperatures derived from the green line up to r = 1.3 $R_\odot$ were appreciably lower than temperatures determined similarly during the solar maximum eclipse of 1980. They conjectured that excess broadening caused by turbulence may have been much less in the 1983 eclipse.

Analising Fabry-Pérot intarferometric observations in the green and the red coronal lines with spatial resolution of a few arc seconds from fiva eclipses (1965 May 30, 1968 September 22, 1970 March 07, 1972 July 10, 1981 July 31), Delona *et al.* (1988) found that the half width of the profiles increases with the radial distance from the limb. They interpreted es features moving in the radial direction. One exception occurred above an active region with very closed configuration in the eclipsa of 1965. Many of the line profiles have complicated shapes (mora complicated in red than in graen line), what wes interpreted as evidence of many small moving features in the corona. The velocity ranged from 30 to 150 km/s. Such features have sizes between 10" and 30", end ere more abundant in red than in green line. However, care must be exercized as complex profiles might also be ceused by brightness inhomogeneities of E- and K-corona. Line-shifts were elso datected. They correspond to ascent of matter at up to 60-70 km/s (±10 km/s). But other 15 observations do not show evidence of moving elements, what may be due to insufficient spatial resolution.

2.2. Periodic and non-periodic motions and intensity fluctuations

The chromospheric acoustic flux is insufficient for heating corona. If however acoustic waves develop shock fronts in the chromosphere and transition region, very little energy reaches the corona. On the other hand, ordiney Alfvén waves have a limited influence in heating corona because they are

reflected back in the chromosphere and do not dissipate efficiently in the corona. Short period (< 10 s) fast magnetoacoustic, and surface Alfvén, waves may play an important role in the haating process.

A tiny but explosive process of dissipating magnetic into thermal energy, designated nanoflares, was proposed by Parker (1988) as an alternative process for heating the corona. Instead of a continuous process of heating by hydromagnetic waves or DC currents, nanoflares should occur as discrete spark-like realeases of magnetic energy, short-lived and small-scale phenomena in a magnatically turbulent plasma.

Koutchmy *et al.* (1983) performed a specific experiment out of an eclipse, in 1975 October 19, at Sacramento Paak Observatory, looking for short period coronal waves. They obtained time series of intensity fluctuations and Doppler velocity oscillations of the green line with time resolution of 5 s, with a slit 40" above a faint facular area and small changing chromospheric features. The sky aureola fluctuations were subtracted. The power spectre showed evidence of Doppler velocity oscillations with periods near 300, 80 and especially 43 s, but no discernible intensity fluctuations.

At the eclipse of 1980 February 18, in India, Pasachoff and Landman (1984) searched photoelectrically for high-frequency (0.1-2 Hz) fluctuations in the intensity of the green line in saveral portions of coronal loops limited up to few arc seconds. The purpose was testing the theory of coronal heating via magnetohydrodynamic waves. Power excess in the Fourier transform at 1-2% level of tha total incident power was detected between 0.5 and 2 Hz. Such fluctuations were attributed to Alfvén waves trapped in loops a faw thousand kilomaters long, or to fast mode waves trapped in loops with a few thousand kilometers in diamater. Tha power axcess was detected again in the eclipse of 1983 June 15, in Indonesia, with an instrument improved with a second channel for the continuum, to monitor atmospheric and instrumental affects. The results, howaver, should be more indicative of fast magnetoacoustic waves than Alfvén waves which produce no density (line intensity) fluctuations to first order.

Frequent brightnenings of SiIV and OIV ultraviolet lines, with amplitude between 20 and 100% and lasting 40-60 s, were racorded aboard Solar Maximum Mission Satellite in active regions with spatial resolution of 3"x 3" and 0.08 s sampling in time (Porter *et al.*, 1984). This observation indicated an intermittant heating of modest amplitude and suggested a stochastic heating mechanism produced by magnetic reconnections. More recently the high resolution images of the Soft X-Ray Telescope, taken in a quick succession on board the Japanese satellite Yohkoh, allowed to search for the nanoflares. By recording the frequency of microflares (the faintest flashes and sparks), it is possible to extrapolata downward for estimating the nanoflare frequency. The conclusion was reached that the transient energy releases in active regions should not be a significent contribution to the heating (Shimizu, 1994). This poses a serious problem for the nanoflare concept, howevar a door is left open by considering that the diffuse background might consist of nanoflares that run together because they happen so often. Tha Normal Incidence X-Ray Telescope flown still more recently on sounding rockets took only snapshots, but with a higher spatial resolution. The images suggest that strong electric currents forced by magnetic activity near the surface play the relevant role in heating the corona. The magnetic bundles are slim and tubular, what requires an electric currant to generate azimuthal magnatic fields that would wrap the bundles, preventing their bulging. Tha images reveal hot gases outlining the bundles divided into fine threads (Glanz, 1994).

Monochromatic images of coronal loop structures overlying an active region at r = 10^5 km were obtained photogrephicelly in green and red coronal lines during the eclipse of 1980 February 18, in Kenya, with resolution of 3" (Hanaoka and Kurokawa, 1988). Combined with images in the neighbor spectral continuum, the temperatures and densities of the loops were derived. The matter at $2x10^6$ K (green line) is dominant in tha active region corona forming diffuse loop structures. The cooler matter at $1x10^6$ K (red line) forms sharp and slender loops constituting the core of the hot loops. The diameter estimated for a single cool loop is about 1000 km or less, so that they may consist on many unresolvabla fine threads with a small filling factor. It is conjectured that a cool loop is formed by the rediative cooling when the heating is blocked in the core of the loop. The cool loops are at least 5 times denser than the hot ones, and extend much higher than the expectad pressure height scale, so they

cannot be in hydrostatic equilibrium. The density in the interloop region is half that in the hot loops. Similar observations were made in the eclipse of 1991 July 11, in Mexico, in coronal green, red and CaXV (5694 Å) lines, chromospheric Hα and continuum near 6100 Å. The instruments and the observational procedure were described by Kurokawa *et al.* (1992). Experiments able to collect a time series of such monochromatic images can be helpful for the detection of intensity fluctuations and proper motions associated to oscillations as well as to dynamic processes in the loops. Moreover such experiments are suitable for testing the hypothesis of nanoflares.

The 1991 July 11 eclipse afforded the unique opportunity of using a modern and large telescope like the 3.6m Canadian-French-Hawaiian Telescope (CFHT) in Mauna Kea, Hawaii. It was used to obtain time sequences of small coronal fields reaching the finest structures so far attained (Koutchmy, 1992; 1993; 1994). It was found that the fina structures in emission lines formed at $T > 1.5x10^6$ K do not show obvious correlation with fine structures with lower temperatures. There are therefore small-scale inhomogeneities in temperature. Since the correlation with white-light images is better noticed in Fe XIV pictures (red line), it is concluded that the most probable coronal temperature outside active center is $2x10^6$ K. Since the kinetic pressure changes much slowly, the inhomogeneities of temperature are compensated for by local variations of density. Thin loops with cross-section of 1 to 2" show blobs at sub-arcsec, as well as irregularities along the loop, suggesting that some kind of heating is going on along it. Coronal threads with sub-arc second cross section (0.4") after correction for smearing effects were detected with lifetimes < 100 s. Threads with larger cross sections have longer lifetimes. They show proper motions, but fade-out on an ever changing background. A particular plasmoid with initial size of 3" split several times producing ephemeral thread-like structures and disappeared after 200 s. The conventional cavity-like structure above a prominence channel could be resolved into dark loops of large scale where matter was missing.

3. Polarization

3.1. Polarization of white light

Measurements of white-light polarization provides important complementary informations to the measurements of the coronal brightness. First of all, as mentioned before, they allow to separata the K-corona from the F-corona under the assumption that the latter one is unpolarized. Moreovar, they provide information in the coordinate of depth about the spatial distribution of the coronal density, as they are sensitive to the extent of the structures along the line of sight. The measurements however are difficult because the observed polarization refers to the total intensity which, beyond $r = 2\ R_\odot$ can be dominated by the light of the F-corona, the atmospheric and instrumental scattered light.

The pioneering work modelling and calculating the polarization of white-lignt corona was performed by Schuster (1879) considering a generic type of scatterer. Accepting the suggestion by Schwarzschild in 1905 that the polarization was produced by the Thomson scattering of frae electrons, and assuming a simple power-law for the radial distribution of electrons, Minnaert (1930) derived an exact expression for the scattered light and its polarization, taking into account the solar limb darkening. van de Hulst (1950) computed his modal corona based on several measurements of brightness and polarization of white-light corona. He separated F- from K-corona assuming that Fraunhofer lines maintain their full strength in the F-corona, but are completely obliterated in the K-corona. Hata and Saito (1966) compiled observational data for flattening, integrated brightness, brightness distribution and polarization of the white-light corona, in an attempt to define the most reliable description of the corona. But along this discussion they did not separate F- from K-corona. Concerning the polarization, they derived typical polarization values for the corona at minimum and maximum of solar activity.

An eclipse photoelectric polarimeter designed and built by Ney *et al.* (1960) operated successfully in the eclipse of 1959 October 02, in two stations installed in Sahara Desert (Ney *et al.*, 1961). The polarization was measured simultaneously in 4750 and 8300 Å once every 30 s out to $r = 2.5\ R_\odot$ in 1000 raster points. Rejecting the hydrostatic corona model, Ney and Kellogg (1959) suggested that part of coronal light could arise from synchrotron radiation of electrons trapped in Van Allen-like belts within the solar magnetic field with energies of several GeV. Such high energy electrons should be injected into the corona more likely at sunspot maximum, and the eclipse of 1959 was only shortly after the maximum. For synchrotron mechanism, the visible light would be polarized with the magnetic vector

parallel to the solar magnetic field, so being able to produce deviations from the diraction of polarization expocted from Thomson scattering. Indeed, four of five previous experiments had failed in confirming the prediction of radial polarization of the magnetic vector (Ney and Kellogg, 1959). One exporiment by von Klüber (1956) was the only exception, confirming radial polarization within 10^{o}. Measurements of the polarization in magnitude and direction, and of the absolute intensity of the light from the solar corona, were obtained by Ney *et al.* (1960). The spatial resolution was of 3'. Ironically the direction of the polarization of the magnetic vactor was found to be radial within ± 1^{o}, what precluded tha presence of synchrotron radiation in the top of the magnetic loops. The absolute values of the intensities were good to ± 5%, and of the polarization, to ±1%. Also, no change in the corona was observed within the time span of approximately 1/2 h separating the observations in two stations. In addition, a small infrared excess was found in the F-corona, larger in the polar than in the equatorial direction (see Section 4). Such excess however was much smaller than those previously obtained by Allen (1946) and Blackwell (1952).

Nikol'skii and Sazanov (1971) made photographic polarimetry from 5000 to 7000 Å during the eclipse of 1968 September 22 in Southern Urals. The polarization varied from 30 up to 60% (± 10%) at coronal distances r < 1.25 $R_{\odot}$. Sazanov (1973) made similar observations in the eclipse of 1970 March 07, in Mexico, and measured polarizatlons as large as 67% at 1.1 < r <1.5 $R_{\odot}$. Such a value ls 1.3-1.5 times larger than the maximum value expected from Thomson scattering.

Badalyan *et al.* (1993) analysed polarimetric data obtained in the actipse of 1980 February 16, in India. The data consisted on six sets of three photographs obtained in three positions of the polaroid differing by 120^{o}. The solar cycle was then at its maximum, and the polarization of K+F corona reached 55 (±5) % near r = 1.7 $R_{\odot}$, not only in well defined streamers, but also in the overlapping faint and small streamers. Assuming Thomson scattering and spherically-symmetric corona in hydrostatic equilibrium, the maximum degrea of polarization can be calculated for the K-corona. Than, assuming a model for the F-corona, the theoretical upper limit for the polarization of K+F corona can be calculated. The maximum does not exceed 45%. A higher polarization would be possible assuming a higher electron density, but then, the corresponding brightness in white light would exceed the observed values. To explain the discrepancy within the framework of Thomson scattering, they suggested that isolated coronal structures may produce the observad high degrees of polarization, not implying exceedingly high densities. The hydrostatic equilibrium applies well in quiet regions, but not above r = 2.5 $R_{\odot}$. Arguing that the observed degree of polarization was not too far above the maximum allowed by Thomson scattering, Badalyan *et al.* (1993) concluded that there was no reason enough to reject this mechanism to explain the white-light corona.

Arnquist and Menzel (1970) made photographic maasurements of the polarization in the eclipse of 1966 November 12, in Peru, with an improved resolution of 1'. In general the polarization and the intensity, both increased and decreased together, but some exceptions were found. They reported polarizations near the limb above and below the values predicted by the Thomson scattering with the van de Hulst's model of corona, and suggested that the electron density could be much more inhomogeneous than conceived so far. Pepin (1970) observed photographically the brightness and the polarization of the white-light corona (r = 3.5 to 13 $R_{\odot}$) during a flight over Atlantic Ocean near Brazil, in the eclipse of 1966 November 12. He reported anomalous polarization directions at r > 3 $R_{\odot}$ in certain position angles. The same paper reported another directional anomaly of the polarization observed in the eclipse of 1965 May 30, in the Northern solar sector during a flight over South Pacific. Beyond r = 5 $R_{\odot}$, the polarization was seen to increase above 5% in sectors where the low corona displayed streamers and plumes. Such a polarization, unseen before at such great a distance from the Sun, was ascribed to the alectrons from the solar wind. Koutchmy and Schatten (1971) made photographic measurements of the polarization up to r = 6 $R_{\odot}$ in the eclipse of 1970 March 07, in Mexico. They used neutral density radial filter and reported polarizations of magnetic vector in radial direction as high as 60% and 90% at r = 2 $R_{\odot}$. Polarizations > 60% are anomalous because their degrees ara higher than the maximum allowed by Thomson scattering considering electrons at rest. The anomalies occur in radial filamentary structures, but not in discontinuities. Also one case of high polarization of the magnetic vector in the tangential direction was found. Kulidzanishvili *et al.* (1993)

obtained photoelactric measurements of polarization of white-light corona in the eclipsa of 1991 July 11, in Mexico. The corona was scanned in 10 concentric rings up to r = 4 $R_\odot$. In each ring, measurements were made on 90 position angles separated by 4^o each other. In the innermost ring the spatial resolution was 1'. It deteriorates outwards, reaching 3' in the outermost ring. Tha polaroid was rotated to 16 different position angles. The polarization measured with 1% accuracy, first increased radially outwards up to about 25% at r = 2.8 $R_\odot$ in average, then decreased. Where the brightness is larger, the maximum value of the polarization occurs farther from tha limb, and vice-versa. The polarization plane, determined with precision batter than 1^o, is mainly radial for the magnetic component, with small but real deviations reaching $\pm 9^o$.

Tha deviation of the magnetic vector from the radial direction is unexplainable in terms of pure Thomson scattering. Plasma oscillations or Cerenkov radiation are much below the optical frequencies and also cannot explain the anomaly. Synchrotron radiation would requlre unconcaivable 10 GeV elactrons (they should be, but are not seen at 1 AU). Molodensky (1973) proposed that electrons with energies of $\approx$ 5 keV may produca directional daviations of the polarization plane by about $\pm 10^o$, because the scatterars moving perpendicularly to the radial direction see the incoming light with aberration. On the other hand, the elactrons moving radially see a larger solar angular diameter if they move toward tha Sun, and vica-versa. So the dilution factor dapends on the motion of the electrons and, accordingly, the degree of polarization. He argued that such suprathermal electrons can exist, bacause tha lifetime for synchrotron and bremsstrahlung radiation, and for collisional tharmalization with particles or photons, are all long. If this suggestion proves to be right, the resaarch of anomalies can give important information on the accelaration processes in tha Sun. The anomalies of polarization may be associated to the high coronal flares proposad by Clivar and Kahlar (1991). A class of impulsive events of low-energy (2-10 keV) solar electrons obsarved near the Earth by satallites is not associated to Hα flares, neither to metric/decametric type III radio bursts, but to interplanetary kilometric type III bursts. Indeed it constitutes the most common type of impulsive solar energetic particles. The acceleration must ocour high in corona at r $\approx$ 1.5 $R_\odot$, where the transient temperature of about 10^7 K is inferred from the high charge states of high-Z (Z > 6) ions. The high coronal flares have not been observed directly, but have been conceived to explain the impulsive acceleration of the electrons (and ^{3}He ions) at places beyond r = 1.5 $R_\odot$. They may occur as a result of reconnection in the open magnetic structure of neutral current sheets of coronal streamers.

3.2. Polarization of emission lines

Such a polarization results from tha anisotropic excitation of coronal ions. The direction of polarization is aithar in the direction of, or normal to, the projection of the coronal magnetic field onto the plane of the sky. The thaoretical maximum amount of polarization is determined by the Zeeman pattem of tha upper and lower levels involved in the transition. There are howaver savaral depolarizing processes operating in the corona, and it is not easy to establish thair identity. If the direction and the magnituda of polarization are measured simultaneously in many emission lines at the same location, it is possible to gain information on: the magnatic field orientation (but not strength); the Zeeman patterns of the ions producing the lines (providing a new criterion for line idantification); tha tamperature and density through the effects on the radiative and collisional excitation ratas; and the fine structure of the corona. But the measuraments are difficult to accomplish bacausa the intensity and the polarization vary in opposite fashion with distance from the solar limb. Also the polarization of the K-corona must be carefully eliminated.

The 10747 Å emission line of Fe XIII is the brightest feature of the coronal spectrum in the photographic infrared. Its transition configuration is ideal for the resonance polarization, since for pure scattaring the apparent polarization of tha incident radiation field in the corona is preserved in the reemittad line. Hyder (1965) pointed out that this line could display a maximum linear polarization of 100% at asymptotic distances above the limb, in absence of collisions and coronal magnetic field depolarization. The depolarization by the magnetic fiald is due to the precession of the scattering ion in the magnetic fiald during the lifetime of tha excited state. So the amount of polarization in this line may compete with that of K-corona, although different in direction by 90^o. House (1972) made a numerical calculation of the polarization. Not far from the limb, the magnetic vector of resonance-polarized line emission lies in the tangential direction. Photoelectric measuremants of polarization in this line were

first made in the 1965 May 30 eclipse, in Society Islands, by Eddy and Malville (1967). Polarization with magnetic vector in tangential direction, between 6 and 30%, were obtained with low spatial resolution at $1.2 < r < 1.72\ R_\odot$. Eddy *et al.* (1973) repeated the observation in the eclipse of 1966 November 12, during a jet aircraft flight from Brazil to Uruguay intercepting the totality path. A complete description of the polarization could be derived from three images obtained through an interference filter, with a polaroid analyser rotated 60^o between exposures. After the subtraction of undesirable polarizations, the instrumental one and from the continuum, it was found that line polarization ranged from about zero at $r = 1.08\ R_\odot$ to 80% at $r = 1.6\ R_\odot$, with the magnetic vector tangent to the solar limb in most of cases. The average polarization was largest outside the streamer regions, and beyond $r = 1.2\ R_\odot$, where pure radiative excitation of the line is expected. The depression of the polarization in the streamers can be interpreted as depolarization by collisional excitation of the line. Directional departures occurred in non-radial magnetic fields of helmet streamers, where the magnetic vector has a tendency to lie porpendicularly to the field lines. The effect of the magnetic field on the amount of polarization seemed to be a second-order effect.

Mogilevsky *et al.* (1960) reported a very high degree of polarization, both in green and red coronal lines, below $r = 1.6\ R_\odot$. This result from the eclipse of 1954 June 30, was not confirmed in several subsequent observations. They recorded photogrephically the spectra of the lines split into orthogonal polarizations by means of a Wollaston prism. In the green line the polarization increased monotonically from 22 to 53% as r increased from 1.1 to $1.6\ R_\odot$. In the red line the polarization increased from 50 to 80% from r = 1.1 to $1.3\ R_\odot$, but decreased afterwards to 47% at $r = 1.45\ R_\odot$. The direction of the polarization is not mentioned. Charvin (1985) made a thorough theoretical study on the polarization of the green coronal line, and concluded that the polarization increases for larger distances from the Sun, but anyhow is weak. Hyder *et al.* (1968) observed the polarization of green and red lines in the eclipse of 1965 May 23. The green line was observed during a flight over the South Central Pacific, and the red line, from the ground in Bolivia. The polarization of the green line below $r = 1.5\ R_\odot$ was > 2% but < 25%, and its direction was tangential to the Sun for the magnetic vector. All these results are in agreement with the theoretical predictions. The red line presented a polarization smaller than its error, i. e., null according to the predictions.The polarization in red and green coronal lines was measured again during the eclipse of 1970 March 07 by Mogllevsky *et al.* (1973) in Mexico. The data consisted on spectra obtained simultaneously with two mutually perpendicular directions of the polarization. Two spectrographs were used and both gave similar results. A polarization in the green line of about 30% was found at $r = 1.06\ R_\odot$, while in the red line it was close to the errors of the measurements and did not exceed 6%. By means of a photographic polarimeter, Beckers and Wagner (1971) observed all emission lines between 3400 and 9000 Å in the inner corona ($1.034 < r < 1,065\ R_\odot$) in the same eclipse, in Mexico. They did not find any polarization > 1% in the green line, and > 1.8% in the red line all over the limb. Other 17 lines did not show any polarization > 5%. The results of Mogilevsky *et al.* (1960, 1973) are in variance with the results of almost all other observers.

4. Circumsolar dust ring

The spectrum of F-corona displays the Fraunhofer lines. No flattening and no color effect is found in the inner part ($r < 2.5\ R_\odot$) of the F-corona (Koutchmy *et al.*, 1976). The interplanetary particles producing the spherically symmetric F-corona are located between the Sun and the Earth. Most of such particles being far from the Sun, the sunlight is rather diffrected than scattered by them. As a consequence, the F-corona is almost unpolarized. If the white-light corona were due entirely to Thomson scattering, the polarization should continue to increase at larger distances from the Sun, and approach some relatively high asymptotic value. But the unpolarized light of the F-corona dilutes the total polarization of the corona beyond several radii from the Sun.

Attempting to link the measurements of the zodiacal light, observed only when the Sun is about 20^o or more below the horizon, with those of the inner F-corona, the brightness of which equals the scattered sky light at $\approx 2^o$ from the Sun, Ney (1963) made observations with balloon-borne cameras during the eclipse of 1962 February 4-5. The Sun was 12^o below the horizon and, in spite of the eclipse, the atmosphere was still bright, so that the zodiacal light could be photographed no closer to the Sun than 19^o. He planned another experiment to measure the inner solar corona during an eclipse from a high altitude, where the sky was free of light scattered by the atmosphere. This experiment was performed

in the 1963 July 20 eclipse. Ground-based equipments consisted on TV scanning telescopes. They were installed in two sites: Canada (Quebec) and USA (Maine). The data from Maine, where the experiment was successful, confirmed the radial nature of the polarization. The crew there also launched baloon telescopes prepared to observe the zodiacal light. The corona out to $r \approx 35\ R_\odot$ was brighter than the background, and displayed a lemon shape with symmetry axis oriented along the ecliptic. This suggested that outer corona is most F-corona, closely related to the zodiacal light. Also very long and straight streamers reached the edge of the pictures, seemingly connected with active regions in the inner corona. Atter this experiment, a gap at elongations between 10^o and 20^o from the Sun still persisted.

There are several claims that infrared color measurements disclosed a reddening at $r > 2\ R_\odot$, stronger that could be expected from the thermal emission of warm grains of zodiacel dust heated by the Sun (Blackwell, 1952; Peterson, 1963 and 1969). The dust particles spiral towards the Sun due to the Poynting-Robertson effect but, at a critical distance which depends on their composition, they start to sublimate. Belton (1966) suggested that, as the heliocentric distance decreases, the radiation pressure acts more efficiently than the gravity, so that the inward spiraling can be slowed down, stopped, and possibly reversed. Some grains can fly away in hyperbolic orbits, but most could oscillate in a narrow circumsolar dust ring. The grains accumulated in the postulated ring could reach temperatures of 1000 to 1300 K, and emit thermal radiation peaking in near infrared wavelengths. Many attempts to confirm the existence of such a ring led to conflicting results. The few positive results are not convincing beceuse they rise serious conceptual difficulties. For example, Peterson (1967) and MacQueen (1968) detacted a so narrow ring with enhanced density of dust at $r \approx 4\ R_\odot$, that the explanation in terms of dynamics and composition falls in difficulties. Moreover, a peak in the visible should be observed that never was seen. Peterson (1967) found also a secondary diffuse emission zone inside the narrow ring which he ascribed to dust in elliptical orbits undergoing less rapid vaporization. MacQueen (1968) found rings apparently concentrated at $r = 4.0$, 8.7 and 9.2 $R_\odot$ in the ecliptic plane.

Grains from the elusive dust ring should be close to the Sun, and scatter the sunlight at nearly 90^o producing a highly polarized component of the F-corona. The availability of large infrared HgCdTe array detectors provided an unprecedented opportunity of mapping the brightness and the polarization of the dust ring in J, H and K bands. Tha experiment was conducted on Mauna Kea, Hawaii, during the eclipse of 1991 July 11 (Lamy *et al.*, 1992). In spite of the bad weather prevailing along the observations, the H- and K-band surface brightnesses showed the infrared light scattered by the electrons of the streamers from tha K-corona, as well as patches farther from the Sun of infrared light scattered by the dust particles of F-corona. However there was no evidence of dust ring out to $r = 15\ R_\odot$. Also no anomalous polarization ring was evidenced there. Similar results were reported also by Hodapp *at al.* (1992).

Isobe and Kumar (1993) collected the results of 23 observations aimed at detecting the dust ring since 1988 until 1991. Most observations are in infrared, but some are in visible wavelengths attempting the datection of anomalous polarization, or of radial velocity in Fraunhofer lines scattered by the grains. Isobe and Kumar (1993) found that the detection and non-detection of the ring occurred at the minimum and at the maximum of the solar cycle, respectively. They interpreted that Lorentz force acting on charged dust particles sweep them out near the maximum of the solar cycle, when the grains acquire a higher positive potential and the magnetic field at low solar latitudes is stronger. The dust ring may be a transient feature modulated also by the injection of dust into near-solar space by a Sun-grazing comet (Hodapp *at al.*, 1992).

5. Timing of contacts

Analyzing measurements obtained with a meridian circle from the Royal Qbservatory at Greenwich since 1853 until 1953, a decrease of the solar angular diameter 2"/century was reported by Eddy and Booroazian (1979). In order to check the validity of such a result, Dunham *at. al.* (1980) analysed the duration of the totality near the edges of the umbral path in the eclipses of 1715, 1976 and 1979, and concluded that the solar diameter is shrinking by ≈ 0.26"/century. Shapiro (1980) analysed the time of contact of 23 transits of Mercury in front of the solar disk occurred between 1738 and 1973, and did find no indication of any significent change in the solar diameter. Parkinson *at al.* (1980) reconsidered

the observations anelyzed by Eddy and Boomazian (1979), and argued that they are unsuitabla for investigating possible changes in the solar diameter, especially because of the personal bias of the observers. They examined over 2,000 timings of 30 transits of Mercury spread over the past 250 years, and durations of 7 total solar eclipses between 1715 and 1925, all with a precision of 1 s, but they did not detect the secular change claimed by Eddy and Boomazian (1979). On the other hand, in the spectrum derived from the transits of Mercury, a significant peak appeared with a period of 80 years. The daily full-disk megnetograms of Mount Wilson obtained since 1974 were analised by LeBonte and Howard (1981), searching for socular variations of the solar diameter. Affer correcting the raw measures for all axpected effects, it was found that the residuals have not e random, but a systemetic distribution: a clumping with 40 days period and an annuel pattarn in the spring. The couses of such a distribution are still unknown. But any soculer trend is within the 1/4"standard deviation of a singla residual. Sofia *et al.* (1983) argued that the determination of the solar diameter from observations meda near the edges of the path of totality in aclipses are affectad by timing errors less than observations made near the path conter. So they analysed numerous reports on the duration of the totality of the eclipses on 1925 Jenuary 24, and 1979 February 26, determined from different locations. Thay found that the solar radius at the earlier date was 0.5" largar than at tha later date, aven taking into account the systematic inaccuracies in the knowledga of the lunar figure. They concluded that solar radius changes are not seculerly monotonic.

The second and third contacts of a total aclipse can be easily video-recorded nowadays with accurate time signals. The second contact can be dafined as the disappearance of tha last Bally's bead or of the diamond ring, and the third contact, as the first visibility of the post-totality diamond ring. The uncertainty in timing is $\pm$ 0.2 s. Pasachoff end Nelson (1987) made one such measurement. On the other hand, the best predictions of contacts take into account empirical corrections to the Moon's ephemeris and figure. A discrepancy $\approx$ 0.5 s was found by Pesechoff and Nalson (1987), what corresponds to 0.25" in the Sun. Dunham *et al.* (1980) reported thet the Sun contracted secularly, and Sofia *et al.* (1983), within decades, in amounts comparable to such e discrepancy. More abundant eclipse measurements that can be obtained in coordinated campaigns with a standardized method and with the accuracy attainable today even with modest resources, may help to clarify this open question.

CONCLUSIONS

There are global properties end processes affecting the large-scale corona, that still require careful and deteiled ground-based observations during eclipses for thair full characterization. Such are the large-scala morphology, the North-South hamispherical symmetry and tha colors of tha K- and F-corona, the observational unfilled gap between the zodiacal lignt and F-corona, the rotation end the three-dimensional structure of the K-corona, and the relationships with the solar cycla of activity. The knowledge of global propertias are of key importance for tha understending of the dipole component of tha general magnetic field of the Sun. Two-dimensionel observations in the near infrared mey help to disentangle unambiguosly the K- from F-corona, for a better characterization of each one.

Connected to the global structures, there are some unconfirmed appendages needing further verification, like the excess of infrared radiation claimed by several authors and ascribed to a dust ring, the anomelies of polarization in white-light end emission lines of the corona, the dark voids overlying faint prominences, but distinct from the covities surrounding filement channels inside the helmet streamers, and the ellusive equatorial diffuse extemal reinforcements. Coordinated observations bringing complementary informations about the same object, may shed new light on such obscure and uncartain observetional problems.

There are also local properties and processes affecting only small-scale structures or fine structures of tha corona and chromosphare, thet deserve further observations. The potential field approximation is suitable for extrapolating the coronal magnetic fiald from photospheric measurements, but this is satisfactory only for low-order harmonic components of the photospheric field. The solar corona is filled with very small-scale structures requiring non-potential magnetic components of corresponding scale in order to balance the lateral gas pressure. Accordingly, tha determinatlon of densitias gives simply an average where the correction by a filling factor is always uncertain. Actual dansities should be much larger then usually assumed. Tangentiel discontinuities elso are drematically strong. The fine structures

can interact producing reconnection phenomena over volumes with small-scale. No account of the inhomogeneities in the corona has been made in theories of coronal heating and acceleration of the solar wind. Theoretical works are essentially based on time and space averages. In this concern, it seems more natural that the observational efforts should precede the theoretical ones.

Although limited by the diumal seeing of ≈ 3", it is clear that so far no full advantaga has been taken of the possibilities made available by the astronomical CCDs and packages for digital treatment of images with high spatial and temporal resolution. With currently available techniques, much more can be leamed about tha clumpiness of matter in small knots and threads, the tharmal structure of the corona, the localized populations of suprathermal electrons, the equivalent widths, Doppler shifts and turbulent broadening of emission lines, the oscillation of structures, the propar motion and splitting of plasmoids, the occurrenca of the postulated nanoflares, the hlgh coronal flares, etc. Because the small-scale structures have shorter lifetimes and time scales, their observations should be made with high temporal resolution and involve several obsarving stations along the totality path, in order to be worthwile scientifically. Looking still farther to the futura, one could think of observations with spatial resolution of ≈ 100 km over tha Sun with resources of adaptive optics with last generation coronographs with large and curved mirrors (Moore, 1990). Regions of magnetic neutral sheets and sheared field lines ara predictably prone to turbulent reconnection or DC Joule dissipation, causing the heating and the acceleration of coronal matter. They constitute the locations to be observed and followed in eclipse experiments devoted to the study of small scala structures.

One particular type of coronal structure that deserves more attention are the coronal rays. Due to their simple geometry of plane sheets or cylinders, their flow, stability and hydromagnetic oscillations can be predicted theoretically with relative aasiness (Matsuura, 1994; Matsuura *et al.*, 1994). A systematic search of rays recorded in images of past eclipses is just starting. Rays rooted in condensations suspended in the solar corona should be examined carefully in the future.

Obvious motions of matter can be seen within expanding loop systems of helmet-like streamers (Matsuura *et al.*, 1993b). A simple, but realistic one-dimensional model, has been proposed by Stepanova and Kosovichev (1992) that can be applied for such existing data. The model considars that a magnetic loop loses the hydrostatic equilibrium because a flare heats the plasma inside, or because the magnetic field under the loop is increased by a coronal transient. The axpanding magnetic loop acts as a piston and produces a shock in the surrounding plasma. The shock waves can be computed in the two-fluid approximation, taking into account the turbulant viscosity. If the expansion is strong, the magnetic forces are dominant and the expansion is monotonic. If not, the magnetic forces can be counteracted by the gravity, producing multiple shocks.

Current researches in eclipses will acquire a renewed scientific reach if, instead of being carried out independently, should be coordinated in such a way to guarantee, besides the individual analysis of the data of each experiment, a global analysis crossing the complementary data obtained in the same eclipse by different experiments and different methods, from ground and space. The ground based observations should involve several stations along the eclipse totality path, as well as the solar observatories performing routine patrol of the solar activity.

REFERENCES

Allen, C. W.: *Mon. Not. Royal Astron. Soc.*, 106, 137 (1946)
Arnquist, W. N. and Menzel, D. H.: *Soler Physics*, 11, 82 (1970)
Badalyan, O. G. and Livshits, M. A.: *Sov. Astron.*, 33 (4), 432 (1989)
Badalyan, O. G.; Livshits, M. A. and Sýkora, J.: *Soler Physics*, 145, 279 (1993)
Beckers, J. M. and Wagner, W. J.: *Solar Physics*, 21, 439 (1971)
Belton, M. J. S.: *Science*, 151, 35 (1966)
Blackwell, D. E.: *Mon. Not. Royel Astron. Soc.*, 112, 852 (1952)
Chandrasekhar, T.; Ashok, N. M.; Desai, J. N.; Pasachoff, J. M. and Sivaraman, K. R.: *Applied Optics*, 23, 508 (1984)
Charvin, P.: *Ann. d'Astrophys.*, 28, 877 (1985)
Cliver, E. and Kahler S.: *Astrophys. J. Letters*, 366, L91 (1991)

Cram, L. E.: *Solar Phys.*, 48, 3 (1976)
Delone, A. B.; Makarova, E. A. and Yakunina, G. V.: *J. Astrophys. Astr.*, 9, 41 (1988)
Desai, J. N. and Chandrasekhar, T.: *J. Astrophys. Astr.*, 4, 65 (1983)
Dunham, D. W.; Sofia, S.; Fiala, A. D.; Herald, D. and Muller, P. M.: *Science*, 210, 1243 (1980)
Dyson, F. and Woolley, R. v. d. R.: Eclipses of the Sun and Moon, Clarendon Prass, Oxford (1937)
Eddy, J. A. and Malville, J. M.: *Astrophys. J.*, 150, 289 (1967)
Eddy, J. A.: *Solar Physics*, 30, 385 (1973)
Eddy, J. A.; Lee, R. H. and Emerson, J. P.: *Solar Physics*, 30, 351 (1973)
Eddy, J. A. and Boornazian, A. A.: *Bull. Am. Astr. Soc.*, 11, 437 (1979)
Glanz, J.: *Science*, 283, 758 (1994)
Hanaoka, Y. and Kurokawa, H.: *Publ. Astron. Soc. Japan*, 40, 369 (1988)
Hata, S. and Saito, K.: *Ann. Tokyo Astron. Observ.*, 10, 18 (1966)
Hirschberg, J. G.; Wouters, A. and Hazalton Jr., L.: *Solar Physics*, 21, 448 (1971)
Hodapp, K-W.; MacQueen, R. M. and Hall, D. N. B.: *Nature*, 355, 707 (1992)
House, L. L.: *Solar Phys.*, 23, 103 (1972)
Hulst, H. C. van de: *Bull. Astron. Inst. Netherlands*, 11, 135 (1950)
Hyder, C. L.: *Astrophys. J.*, 141, 1382 (1965)
Hyder, C. L; Montar, H. A. and Shutt, R. L.: *Astrophys. J.*, 154, 1039 (1968)
Isobe, S. and Kumar, A. S.: *Astrophys. Spa. Sci.*, 205, 297 (1993)
Jarrett, A. H. and Klüber, H. von: *Mon. Not. Roy. Astron.* Soc.,115, 343 (1955)
Jarrett, A. H. and Klüber, H. von: *Mon. Not. Roy. Astron.* Soc.,122, 223 (1961)
Kim, I. S. and Nikolsky, G. M.: *Solar Physics*, 43, 351 (1975)
Klüber, H. von: *Mon. Not. Roy. Astron. Soc.*, 118, 201 (1958)
Koutchmy, S. and Laffineur, M.: *Nature*, 226, 5241, 1141 (1970)
Koutchmy, *S.* and Schatten, K. H.: *Solar Phys.*, 17, 117 (1971)
Koutchmy, S.: *Solar Physics*, 24, 374 (1972a)
Koutchmy, S.: *Astron. Astrophys.*, 16, 103 (1972b)
Koutchmy, O. and Koutchmy, S.: *Astron. Astrophys. Suppl.*, 13, 295 (1974)
Koutchmy, S. and Stellmacher, G.: *Solar Physics*, 49, 253 (1976)
Koutchmy, S.: "Practical work on color amulsions using filtered duplicates", *in* Modern Techniques in Astronomical Photography, *ESO Proceedings*, Eds.: R. M. West and J. L. Heudier, 225 (1978)
Koutchmy, S.; Lamy, P.; Stallmacher, G.; Koutchmy, O.; Dzubenko, N. I.; Ivenchuk, V. I.; Popov, O. S.; Rubo, G. A., and Vsekhsvjatsky, *S.* K.: *Astron. Astrophys.*, 69, 35 (1978)
Koutchmy, S.; Zugzda, Y. D. and Locans, V.: *Astron. Astrophys.*, 120, 185 (1983)
Koutchmy, S. and Lamy, P. L.: "The F-corona and the circum-solar dust: evidences and propertias" *in* Properties and interaction of interplanetary dust, *Proc. IAU Colloq. No.* 85, Marsailla 9-12 July 1984, D. Reidel Publishing Company, Dordrecth, 63 (1984)
Koutchmy, S.: *Spa. Sci. Reviews*, 47 (1988)
Koutchmy, S.: "Streamer eclipse observations" *in* Proceedings of the First SOHO Workshop, Annapolis, Maryland, USA, 25-28 August 1992, *ESA SP-348*, 73 (1992)
Koutchmy, S.; Altrock, R. c.; Darvann, T. A.; Dzubenko, N. I.; Henry, T. W.; Kim, I.; Koutchmy, O.; Martinez, P.; Nitschalm, C.; Rubo, A. A. end Vial, J.: *Astron. Astrophys. Suppl. Ser.*, 98, 189 (1992)
Koutchmy, S. and Molodensky, M.: *Nature*, 360, 6408, 717 (1992)
Koutchmy, S.: *Solar Phys.*, 148, 169 (1993)
Koutchmy, S.: *Astron. Astrophys.*, 281, 249 (1994)
Koutchmy, S.; Balmahdi, M.; Coulter, R. L.; Démoulin, P.; Galzauskas, V.; MacQueen, R. M.; Monnet, G.; Mouette, J.; Noäns, J. C.; November, L. J.; Noyas, R. W.; Sime, D. G.; Smartt, R. N.; Sovka, J.; Vial, J. C.; Zimmermann, J. P. and Zirker, J. B.: *Astron. Astrophys.*, 281, 249 (1994)
Kulidzanishvili, V.; Mayer, A.; Mayer, V.; Danik, S.: *private communication* (1993)
Kurokawe, H.; Kitai, R. and Ishiura, K.: "The Observation of the Inner Corona at the 1991 Total Solar Eclipse" *in* Observations of Solar Corona at the Mexico Total Solar Eclipse of July 11, 1991, Kwasan and Hida Observatories, Kyoto University, Japan, 10 (1992)
LaBonte, B. J. and Howard, R.: *Science*, 214, 907 (1981)
Lamy, P.; Kuhn, J. R.; Lin, H.; Koutchmy, S. and Smartt, R. N.: *Science*, 257, 1377 (1992)
Lebecq, C.; Koutchmy, S. and Stellmacher, G.: *Astron. Astrophys.*, 152, 157 (1985)

Loucif, M. L. and Koutchmy, S.: *Astron. Astrophys. Suppl. Ser.*, 77, 45 (1989)
Ludendorf, H.: *Sitzber. Preuss. Akad. Wiss.*, 18, 200 (1934)
MacQuaen, R. M.: *Astrophys. J.*, 154, 1059 (1968)
Marshall, P. M. and Henderson, G.: *Solar Physics*, 33, 153 (1973)
Matsuura, O. T.; Picazzio, E. and Campos, R. P.: *Solar Physics*, 144, 89 (1993a)
Matsuura, O. T.; Fogliano, F. L. and Campos, R. P.: *Bolatim SAB*, 13, 2, 23 (1993b)
Matsuura, O. T.: "Non-Steady, Plane, One-Dimensional, Isothermal Flows" *in* Solar Coronal Structures, Proceedings of IAU Colloquium No. 144, Tatranská Lomnica, Slovakia (1994)
Matsuura, O. T.; Shigueoka, H.; Azevedo, C. A. and Lavras, W. O.: "MHD Spectrum of Coronal Rays" *in* Solar Coronal Structures, Proceedings of IAU Colloquium No. 144, Tatranská Lomnica, Slovakia (1994)
Minnaert, M.: *Zeitschnift für Astrophysik*, 1, 209 (1930)
Mogilavsky, E. I.; Nikolsky, G. M. and Nikolskaya, K. L.: *Soviet Astron.*, 4, 225 (1960)
Mogilevsky, E.; Ioshpa, B. and Obridko, V.: *Solar Physics*, 33, 169 (1973)
Molodensky, M. M.: *Solar Physics*, 28, 465 (1973)
Moore, R. L.: *Mem. S. A. It.*, 61, 2, 317 (1990)
Ney, E. P. and Kellogg, P. J.: *Nature*, 183, 1297 (1959)
Ney, E. P.; Huch, W. F.; Maas, R. W. and Thomess, R. B.: *Astrophys. J.*, 132, 812 (1960)
Ney, E. P.; Huch, W. F.; Kallogg, P. J.; Stein, W. and Gillett, F.: *Astrophys. J.*, 133, 618 (1961)
Ney, E. P. *Sky & Telescope*, November, 251 (1963)
Nikol'skii, G. M. and Sazanov, A. A.: *Sov. Astron.*, 14, 831 (1971)
Parker, E. N.: *Astrophys. J.*, 330, 474 (1988)
Parkinson, J. H.; Morrison, L. V. and Stephenson, F. R.: *Nature*, 288, 548 (1980)
Pasachoff, J. M. and Landman, D. A.: *Solar Physics*, 90, 325 (1984)
Pasachoff, J. M. and Ladd, E. F.: *Solar Physics*, 109, 365 (1987)
Pasachoff, J. M. and Nelson, B. O.: *Solar Physics*, 108, 191 (1987)
Pepin, T. J.: *Astrophys. J.*, 159, 1067 (1970)
Petarson, A. W.: *Astrophys. J.*, 138, 1218 (1963)
Peterson, A. W.: *Astrophys. J. Leffers*, 146, L37 (1967)
Patarson, A. W.: *Astrophys. J.*, 155, 1009 (1969)
Porter, J. G.; Toomre, J. and Gabble, K. B.: *Astrophys. J.*, 283, 879 (1984)
Rasura, J.; Argiro, D.; Sauer, T. and Williams, C.: *Intern. J. of Imaging Systams and Tachnology*, 2, 183 (1990)
Saito, K.: *Annals of the Tokyo Astron. Obs.*, 12, 2, 53 (1972)
Saito, T. and Akasofu, S.-I.: *J. Geophys. Ras.*, 92, 1255 (1987)
Sazanov, A. A.: *Sov. Astron.*, 16, 674 (1973)
Schuster, A.: *Mon. Not. Roy. Astron. Soc.*,40, 35 (1879)
Shapiro, I. I.: *Science*, 208, 51 (1980)
Shimizu, T.: "Actice-region transient brightnenings and tha heating of the active region corona", *in* Proceedings of Symposium on New Look at tha Sun with Emphasis on Advanced Observations of Coronal Dynamics and Flares, National Astronomical Observatory of Japan, September 8-10, 1993, Kofu, Japan, in press (1994)
Sofia, S.; Dunham, D. W.; Dunham, J. B. and Fiala, A. D.: *Nature*, 304, 522 (1983)
Stellmacher, G.; Koutchmy, S.; Lebecq, C.: *Astron. Astrophys.*, 162, 307 (1986)
Stapanova, T. V. and Kosovichav, A. G.: "A numerical model of interaction of coronal transients with tha solar wind", *in* Proceedings of the First SOHO Workshop, Annapolis, Maryland, USA 25-28 August 1992, *ESA SP-348*, 209 (1992)
Withbroe, G. L.; Kohl, J. L; Weiser, H. and Munro, R. H.: *Spa. Sci. Rav.*, 33. 17 (1982)
Zirker, J. B.; Koutchmy, S.; Nitschelm, C.; Stellmacher, G.; Zimmermann, J. P.; Martinaz, P.; Kim, I.; Dzubenko, N.; Kurochka, L.; Makarov, V.; Fatianov, M.; Rusin, V.; Klocok, L. and Matsuura, O. T.: *Astron. Astrophys.*, 258, L1 (1992)

Section 2:

INTERSTELLAR MEDIUM

CHEMICAL COMPOSITION OF COMETS

P.D.Singh

Instituto Astronomico e Geofisico

Universidade de Sao Paulo

Av. Miguel Stefano 4200

Agua Funda, Cep. 04301-904, Sao Paulo, Brasil

ABSTRACT

The chemical composition of comets is reviewed from observations made by in situ and remote measurements. The cometary gas is mostly composed of H_2O followed by CO, H_2CO, CO_2, CH_4, and NH_3. N_2 is a minor species in comets. The elemental composition of Halley's dust consists of an inorganic (mineral) fraction, which appears to be essentially type 1 carbonaceous (CI) chondrites, and an organic fraction consisting essentially of highly unsaturated hydrocarbon. The inorganic fraction forms a core which is embedded in essentially organic material. The density of pure organic grains, called CHON particles, is near 0.3 g/cm^3 and is believed to be the origin of the distributed source of CO, H_2CO, CN, and C_2 found in the coma of Comet Halley. In general, the isotope ratios of N, O, and S in comets agree with solar system values. The D/H ratio in Comet Halley is comparable to the corresponding D/H ratios found in other solar system objects poor in hydrogen, but distinctly different from the protosolar nebula and objects that accreted hydrogen gas. The ratio $^{12}C/^{13}C < 89$ (bulk solar system) found in the CN radical of Comet Halley indicates the presence of unaltered interstellar material likely preserved in the dust

grains; however, if the ratio $^{12}C/^{13}C > 89$, found in some dust particles by in situ measurements is real, then carbon from different nucleosynthesis sites has been incorporated in the nucleus of Comet Halley.

INTRODUCTION

About 10^{11} small bodies (cometary nuclei) reside in the Oort cloud - a cloud which surrounds the planetary system and extends to about 50000 AU from the Sun (Lust, 1981; Oort, 1950). Their small sizes, usually less than 20 km, and generally large distance from the Sun, place them amongst the most primitive objects remaining in our solar system. These objects are loosely bound by gravity to the Sun. The albedo of cometary nuclei is very small ($\leq$ 4%); making them amongst the darkest objects of the solar system (Keller, 1990). The mean density and tensile strength of the material of these nuclei are estimated to be < 0.5 g/cm^3 (Rickman and Huebner, 1990) and $1x10^3$ dynes/cm^2 (Newburn, 1994) respectively. Close passages of stars, which occur in average intervals of a few million years, result in a few nuclei perturbed to move towards the planetary system (Lust, 1981). These small bodies can then be captured by the massive planet Jupiter, causing them to move into the inner solar system (Marsden et al., 1978). When a cometary nucleus comes close enough to the Sun, the outer layers are heated. Material vaporizes by the sublimation process with a speed greater than the escape velocity at the nucleus (Singh, 1991), and is released into space. Fresh material on the nuclear surface is then exposed to solar radiation. The sublimated ices (volatile gas

component - see below) streaming away from the nucleus carry along fine solid particles, called dust (dust component - see below), and together they form the familiar coma atmosphere and tails. Dust, representative of non-volatile material of the nucleus, is also a source of cometary gas in the coma (see below). During one apparition, a comet looses a very small fraction of its total mass in the form of gas and dust (Singh et al., 1992; Singh, 1991) which stays in the interplanetary medium.

Comets with periods less than 200 years are classified as "short period" comets; and those with period more than 200 years are in the category of "long period" comets. Comets, which come from the Oort cloud for the first time to the planetary system, are called "new", and those which have made many apparitions, are termed "old" comets (Lust, 1981). The spectra of comets have been studied from ultraviolet to radio wavelengths, and spectral analyses of comae and tails have yielded, to a greater extent, the chemical composition of cometary nuclei (Wilkening, 1982; Newburn et al., 1991; Huebner, 1990). The most complete compositional study of cometary nuclei comes from fly-by missions to comets Halley (Astron. Astrophys., **187**, Nov. 1987; Newburn et al., 1991), Giacobini-Zinner (von Rosenvinge et al., 1986), and Grigg-Skejellerup (Astron. Astrophys., **268**,L5-L13).

A) GAS COMPONENT:- Photodissociation lifetimes of molecules at 0.89 AU distance from the Sun are of the order of 10^3 to 10^5 s. With cometary gas expansion speed of 0.8 km/s (Lammerzahl et al., 1987; Neubauer, 1987) the Giotto spacecraft came close enough (600 km) to

the nucleus of Comet Halley to record a fairly unaltered mixture of "parent molecules" by its Neutral Mass Spectrometer NMS (Krankowsky et al., 1986). The NMS, having good resolution and capability of distinguishing differences in ionization potential, has not been successful in the identification of some parent molecules and radicals because of the overlap of molecular weight in specific mass bins (CO and N_2, or NH_3 and OH). This problem has been resolved by comparison with optical observations, and by studying the radial evolution of neutral and ionized fragments. The contact surface of Comet Halley, formed by the balance between the pressure of outstreaming gas, coupled with dust particles, from the nucleus and the magnetic field pressure and ion-neutral friction of the incoming solar wind from the Sun, was encountered by Giotto at a distance of 4660 km from the nucleus (Neubauer, 1987). The volume inside the contact surface containing the nucleus, called the ionosphere, is characterized by very low temperatures ($\leq$ 200 K) of molecules and ions, and a hydrodynamic, supersonic outflow of partially ionized gas (Geiss, 1987; Lammerzahl et al., 1987). Some suprathermal ions are found in the outer ranges of the ionosphere which probably cross the contact surface by the double charge exchange mechanism proposed by Goldstein et al. (1987), and probably have no great influence on the chemistry of the ionosphere. With a gas speed of 0.8 km/s, cometary species cross the ionosphere in less than two hours. The dominant processes yielding the neutral gas component in the ionosphere are evaporation, which is fast from ices and delayed from grains, and

photodissociation in the gas phase that perhaps also occurs inside grains. In the ionosphere, electron densities and energies are very low to contribute significantly to ionization (Reme et al., 1986). In table 1 we list effects of these dominant processes on relative abundances of cometary species.

Table 1: Effects of Dominant Processes on Relative Abundances (see text):

Small molecules:	Only a limited fraction is destroyed
Radicals:	Radial build-up
Ions:	Total ion content determined by photoionization and dissociative recombination
	Composition largely determined by ion-molecule reactions

The ionized component of the gas in the ionosphere is determined by photoionization, ion-molecule reactions, and dissociative electron recombination processes and can be modelled quite well (Huebner and Giguere, 1980; Mitchell et al., 1981, Biermann et al., 1982). It was expected that Particulate Impact Analyzer (PIA) data would be useful for identifying cometary molecules. The data obtained in the vicinity of Halley's Comet confirm that NMS results and data on the ion composition give additional information on the inventory of molecular species. In table 2 we list a summary of the molecular abundances determined by in-situ measurements and earth-based observations. In the ion mass

spectra obtained by Giotto, evidence is found for the existence of molecules more complex and heavier than those listed in table 2; however, it is premature to draw definite conclusions about their parents from which they have been formed. Table 2 shows that H_2O is the most abundant parent species of the nucleus whose density in the coma of Comet Halley obeys very accurately a R^{-2} power law (R = distance from the nucleus in the coma) for R lying between 1500 km and 10000 km (Krankowsky et al., 1986). This indicates that H_2O evaporation takes place inside R < 1500 km or very near to the nucleus (point source). However, other constituents appear to come, at least in part, from an extended source in the coma (10^4 km beyond). There is evidence that some evaporation from solids takes place even several hours after their release from the nucleus. Klavetter and A'Hearn (1994) and Singh et al. (1994) conclude that dust grains are responsible for increases in abundances of CN and C_2 in the coma of Comet Halley. Simpson et al. (1987), Vaisberg et al. (1986), and Combi (1994) have argued for disintegration of conglomerate of grains in the coma which may be explained by the loss of glue that held them together. Eberhardt et al. (1987) have noticed a spatial distribution of CO enhanced over a R^{-2} power law for R < 20000 km and have argued the increase of CO as due to an extended source (small grains) in the inner coma of Comet Halley. At heliocentric distance (r) = 0.9 AU, small cometary grains assume temperatures up to a few hundred degrees celsius (Hanner, 1982), and hence it is most unlikely that CO, whose sublimation temperature is about 25° K, is retained as a parent in the grains

for hours after their release from the nucleus. Formaldehyde, whose photodissociation lifetime at 0.9 AU from the Sun is 3000 s, has recently been identified to come from an extended source (Meier et al., 1993) in comet Halley's coma and accounts for 2/3 of the measured CO density within the ionosphere. Formaldehyde polymers, coating dust grains and evaporating as monomers provide the most likely explanation for the extended H_2CO source. In table 2 we have listed the sum of H_2CO and CO abundances.

Methane and ammonia abundances in the coma of Comet Halley have been derived from Giotto Ion Mass Spectrometer (IMS) data by Allen et al. (1987) using an Eulerian model of chemical and physical processes inside the contact surface. The IMS data can be best fitted if NH_3 and CH_4 abundances, relative to H_2O, are $\leq$1.5 and 2, respectively. The J=1-0 rotational transition at 3.4 mm of HCN has been observed between Nov. 1985 and May 1986 in Comet Halley by Schloerb et al. (1987). The HCN abundance, relative to H_2O, is 0.1 and is a major parent molecule of CN but probably not the sole parent. The upper limit for N_2 in Halley's coma, determined from $N_2/CO < 0.1$ (Balsiger et al., 1986) by Allen et al. (1987), is less than 2% of H_2O, and hence $N_2/NH_3 < 1$ (Table 2). Solar UV radiation field breaks up the original molecules into smaller radicals, atoms and ions until all components are dissected into atomic ions that can easily be picked-up and identified by instruments of fly-by missions. Hence, extended radial profiles to distances of $R \approx 3 \times 10^5$ km helps to obtain elemental composition in the volatile component of a comet. First estimates of elemental

abundances in the gas phase were made by Balsiger et al. (1986) who found C/O, N/O, and S/O ratios = 0.33, ≤0.01, and 0.03, respectively, for Comet Halley. The C/O ratio is about half the solar value, the N/O ratio is much below the solar value, and the S/O ratio is close to the solar value (Anders and Ebihara, 1982). A considerable fraction of nitrogen in the volatile component of a comet could be present in the form of N_2 (Table 2).

Table 2: Gas Coma of Halley's Comet (Point source + Extended Source R < 15000 km) - see text.

Species	Abundance	Species	Abundance
H_2O	100	CH_4	2 (Refs: 9,10)
CO_2	2.5 (Refs: 1-4)	NH_3	≤1.5 (Ref: 9)
CO	15 (Refs: 5-8,2)	HCN	0.1 (Refs: 11,12)
H_2CO		N_2	< 2 (Refs: 13,9)

Refs: 1- Krankowsky et al. (1986); 2 - Combes et al. (1988); 3 - Crovisier et al. (1987); 4 - Encrenaz et al. (1988); 5 - Meier et al. (1993); 6 - Eberhardt et al. (1987); 7 - Woods et al. (1986); 8 - Festou et al. (1986); 9 - Allen et al. (1987); 10 - Drapatz et al. (1987); 11 - Bockelee-Morvan et al. (1986); 12 - Schloerb et al. (1987); 13 - Krankowsky and Eberhardt (1990).

The problem of missing carbon in the volatile (gas) component of comets has long been a mystery (Delsemme, 1985); however, it has

recently been shown by in situ measurements that the missing carbon is in the dust (see below).

B) DUST COMPONENT:- The gas, streaming out from the cometary nucleus, carries along fine solid particles (grains) of mass distribution down to 10^{-17} g (McDonnell et al., 1987), and indications are of even finer grains. The composition of a large number of dust particles of Comet Halley has been investigated in the dust mass spectra obtained by VEGA and Giott spacecraft (Jessberger et al., 1988; 1991) whose encounter velocities with Halley had been 70 to 80 km/s (Grard et al., 1987). The impact energies of several hundred eV per atom resulted in grains disintegrating to a large extent into atomic (ionic) species. The dust mass spectra show high yields of ions, and a strong variability in composition of dust particles whose masses are as low as 10^{-15} g. The elemental composition of Comet Halley's dust consists of an inorganic (mineral) fraction, which appears to be type 1 carbonaceous (CI) chondrites, and an organic fraction consisting of highly unsaturated hydrocarbons. The inorganic fraction forms a core which is embedded in essentially organic material (Greenberg,1982). The density of pure organic grains, called CHON particles (composed of almost entirely of volatile materials, presumably in polymerized form), is near 0.3 g/cm^3 and is believed to be the origin of the distributed source of CO, H_2CO, CN, and C_2 found in the coma of Comet Halley. In table 3 we list average elemental abundances in Comet Halley's dust where we compare them with the corresponding abundances of type 1

carbonaceous (CI) chondrites (Anders and Ebihara,1982), which are the least metamorphosed rocks from the early solar system. The abundances of the condensible elements (Na to Ni in table 3) in CI chondrites represent, to an approximation, the abundances in the solar photosphere and hence provide the basis for the "cosmic" abundance of the elements. From Na to Ni, the elemental abundances in Comet Halley's dust and CI are the same within a factor of 2, which coincides with the uncertainty of the ion yields (Table 3) in the mass spectra of in situ measurements. The light volatile elements H, C, N, and O are enriched in Comet Halley's dust relative to corresponding abundances in CI (Table 3), and are almost as abundant as in the solar photosphere (Palme et al., 1981).

Table 3: Average Abundances of the Elements in Halley's Dust and Type 1 Carbonaceous (CI) Chondrites.

Element	Halley's Dust[a]	CI[b]	Halley/CI
H	2025	492	4.1
C	815	70.5	11.6
N	42	5.6	7.5
O	890	712	1.3
Na	10	5.3	1.9
Mg	=100	=100	1.0

Contd.

Table 3 Contd.

Al	6.8	7.9	0.9
Si	185	93.0	2.0
S	72	47.9	1.5
K	0.2	0.35	0.5
Ca	6.3	5.68	1.2
Ti	0.4	0.22	1.9
Cr	0.9	1.25	0.7
Mn	0.5	0.88	0.6
Fe	52	83.7	0.6
Co	0.3	0.21	1.2
Ni	4.1	4.59	0.9

[a]The data on cometary dust are from 79,mode 0, high-quality mass spectra from PUMA-1 (Jessberger et al., 1988).

[b]Data from Anders and Ebihara (1982).

C) THE BULK COMPOSITION OF COMET HALLEY'S NUCLEUS:- Ideally the determination of the average chemical composition of a cometary nucleus would be to sample different sites and different depths of the nucleus and then unfold the composition of samples with the internal structure. This objective has been achieved to some extent by the analyses of in situ measurements of many grains which come from the nucleus from different sites and possibly from different depths below the immediate surface, especially when they are released in the form of jets (McDonnell et al., 1987). The gas-to-

dust mass ratio in the nucleus of Comet Halley can be estimated from the derived composition of gas (Table 2) and dust (Table 3) assuming that the primordial C/Mg ratio of 1126/100 (Anders and Ebihara, 1982) is preserved for the whole (gas and dust) comet. For cometary material in the solid phase we have 815 carbon atoms for every 100 atoms of Mg (Table 3). If the primordial C/Mg ratio is conserved, then for any 100 atoms of Mg in the dust, there are 311 carbon atoms in the gas phase. From table 2, these 311 C atoms are accompanied by about 3849 H atoms, 1904 O atoms, and 89 N atoms in the gas phase. Thus a fraction of nuclear material of Comet Halley contains, for every 100 Mg atoms, total of 35559 amu in the gas phase (Table 2) and 42442 amu in the solid phase (Table 3) resulting in a gas/dust ratio ≈ 0.9. This is consistent with the range 6.3 to 0.63 determined by McDonnell et al. (1987) using different arguments.

Table 4 :- Abundances of C, H, O, and N Atoms Relative to Mg of the Material (Gas and Dust) Released by Comet Halley.

Element	Abundance	Geiss(1987)	Solar System[b]	CI[b]
H/Mg	32.6	39	25200	4.9
C/Mg	11.3	12	11.3	0.71
N/Mg	0.7	0.4-0.8	2.3	0.06
O/Mg	15	22.3	18.5	7.1
N/C	0.06	0.03-0.07	0.2	0.08
O/C	1.3	1.9	1.6	10.0

[b]The abundances in the primordial solar system and in CI chondrites are from Anders and Ebihara (1982).

The total composition (gas plus dust) of cometary nuclear material containing C, H, O, and N elements, relative to Mg, can be obtained from tables 2 and 3, and these are listed in table 4 together with the result of a study by Geiss (1987) which is based on different lines of arguments. The abundances of non-CHON particles are listed in Table 3. Table 4 shows that the light volatile elements (H, C, N, and O) are strongly enriched in the cometary material relative to CI chondrites and are similarly abundant to the primordial solar nebula.

D) ISOTOPES:- Ratios of stable isotopes of the elements hydrogen, carbon, oxygen, nitrogen, magnesium, sulphur, and iron found in many comets are presented in table 5 where we compare them with corresponding ratios found in the local interstellar medium and the solar system. The D/H ratio derived in situ from HDO/H_2O in Comet Halley by Eberhardt et al. (1987a) is in the range of $0.6x10^{-4}$ to $4.8x10^{-4}$ and the average of these values does not differ significantly from that found for the Titan atmosphere and outer planets (Smith et al., 1989). It is almost the same as that in the standard mean ocean water. The enhancement of the D/H in comets and outer planets is real.

Emission lines of $^{13}C^{14}N$, resolved for the first time, in the ground-based spectra have been used to estimate the $^{12}C/^{13}C$ abundance ratio in Comet Halley (Wyckoff et al., 1989). This ratio

is 65±9 (2.7σ lower than the solar system value 89) and is evidence for an enhancement in the ^{13}C abundance (Table 5). There is strong evidence that a sizeable fraction of cometary CN comes from CHON particles (Klavetter and A'Hearn, 1994). If only 2% by number of the CN originated from CHON particles with $^{12}C/^{13}C \approx 4$, corresponding to the equilibrium value for CNO burning in stars (Iben, 1975), then the $^{12}C/^{13}C$ ratio of CN is lowered from 89 to 66 (Krankowsky, 1991). The $^{12}C/^{13}C$ ratio obtained from PIA ranges from 1 to 5000 (Jessberger and Kissel, 1991). Values smaller than 89 suffer contamination with ^{12}CH, and $^{12}C/^{13}C$ ratios greater than 89 are real in Comet Halley. Higher $^{12}C/^{13}C$ ratios have also been found in other objects - for example, $^{12}C/^{13}C = 159$ has been found in a silicon carbide aggregate from the Murchison carbonaceous chondrite (Ming et al., 1989; Zinner et al., 1989), and the ratio reaches a value of 4500 in graphite grains from the Murchison meteorite (Zinner and Wopenka, 1990). Abundances of the stable isotopes of elements heavier than carbon, including oxygen and sulphur in the gas phase and in the dust of comets, appear to be identical with the isotopic ratios in the solar system. This conclusion can be extended to Mg, Si, Ca, and Fe in solids of comets.

The D/H data in Comet Halley neither rule out nor confirm an interstellar origin of Comet Halley's H_2O. The ^{13}C enrichment ($^{12}C/^{13}C < 89$) discovered through CN lines (Wyckoff et al., 1989) indicates the presence of unaltered interstellar material likely preserved in the dust grains. If the ratios $^{12}C/^{13}C > 89$ found in

some dust particles are real, then carbon from different nucleosynthesis sites has been incorporated to Comet Halley's nucleus.

Table 5:- Ratios of Stable Isotopes Found in Comets

Species	Solar System[a]	Local ISM[b]	Comets
D/H	2×10^{-5}	1.5×10^{-5} [c]	$(0.6 \text{ to } 4.8)\times10^{-4}$ [d]
D/H	-	$(1\text{-}100)\times10^{-4}$ [e]	-
$^{12}C/^{13}C$	89	43 ± 4 [f]	65 ± 9 [g]
$^{12}C/^{13}C$	-	65 ± 20 [h]	70 to 130 [i]
$^{12}C/^{13}C$	-	12 to 110 [e]	< 100 [j]
$^{14}N/^{15}N$	250	≈ 400 [h]	> 200? [g]
$^{18}O/^{16}O$	0.002	≈ 0.0025 [h]	0.0023 ± 0.0006 [d]
$^{24}Mg/^{25}Mg$	7.8	-	variable [j]
$^{25}Mg/^{26}Mg$	0.9	-	< 2 [j]
$^{34}S/^{32}S$	0.044 ± 0.010	-	0.045 ± 0.010 [j]
$^{56}Fe/^{54}Fe$	15.8	-	15

[a] -Encrenaz (1984), [b] -ISM stands for interstellar medium, [c]Ferlet (1992), [d] - data for Comet Halley by Eberhardt et al. (1987a), [e] - range of observed values for dense interstellar clouds, [f] - Hawkins and Jura (1988), [g] - for Halley by Wyckoff et al. (1989), and Krankowsky (1991), [h] - Combes (1980), Penzias (1983), Gerin et al. (1984), and Bastien et al. (1984); [i] - For several comets (Danks et al., 1974; Vanysek and Rahe, 1978; Lambert and Danks, 1983);

j - Kronkowsky et al. (1986); Jessberger et al. (1988).

CONCLUSIONS

Analyses of in situ and remote measurements on cometary dust and gas show that: 1) abundances for rock-forming elements in comets are within a factor of two relative to the solar system abundances (Table 3), 2) hydrogen in comets is strongly depleted relative to the solar system (Table 4), 3) oxygen and carbon in comets are in solar proportion (Table 4), and 4) nitrogen in comets is depleted relative to the solar system (Table 4). The isotopic D/H data observed in Comet Halley probably suggest an interstellar origin of Comet Halley's water. The $^{12}C/^{13}C < 89$ discovered in CN (Wyckoff et al., 1989) indicates the presence of original interstellar material likely preserved in the dust grains; however, the ratios $^{12}C/^{13}C >> 89$ found in some dust particles (Jessberger and Kissel, 1991) indicate incorporation of carbon from different nucleosynthesis sites in the nucleus of Comet Halley (Table 5).

ACKNOWLEDGEMENTS

I am thankful to Dr. Daniel C. Boice of Southwest Research Institute, San Antonio, Texas, USA for making valuable comments. This work was supported by CNPq under grant 304076/77.

REFERENCES

Allen, M., Delitsky, M., Huntress, W.T., Yung, Y., Ip,W.-H., Schwenn, R., Rosenbauer,H., Shelly, E., Balsiger,H., and Geiss,J.: 1987, Astron. Astrophys., **187**, 502.

Anders,E., and Ebihara,M.:1982,Geochim. Cosmochim.Acta,**46**,2363.

Balsiger, H., Altwegg, K., Buhler, F., Geiss, J., Ghielmetti,

A.G., Golstein, B.E., Goldstein, R.,Huntress, W.T.,Ip, W.-H., Lazarus, A.J., Meier, A., Neugebauer, M., Rettenmund,U., Rosenbauer, H., Schwenn, R.,Sharp, R.D., Shelley, E.G., Ungstrup, E., Young, D.T.: 1986, Nature, **321**, 330.

Bastien, P., Bartla,W., Henkel,C., Paulus,T., Walmsley,C.M., and Wilson, T.L.: 1984, Astron. Astrophys., **149**, 86.

Biermann, L., Giguere, P.T., and Huebner, W.F.: 1982, Astron. Astrophys., **108**, 221.

Bockelee-Morvan,D., Crovisier,J., Despois,D., Forveille,T., Gerard, E., Schraml, J., Thum, C.: 1986, Proc. 20th ESLAB Symposium on the Exploration of Halley's Comet. Heidelberg, 27-31,October 1986, ESA SP-250, Vol.I, 365.

Combes, M., Moroz, V.I., Crovisier, J., Encrenaz, T., Bibring, J.P., Griggoriev, A.V., Sanho, N.F., Coron, N., Crifo, J.F., Gispert, R., Bockelee-Morvan, D., Nikolsky, Yu.V., Krasnopolsky, V.A., Owen, T., Emerich, C., Lamarre, J.M., and Rocard, F.: 1988, Icarus, **76**, 404.

Combes, F., Falgarone, E.,Guibert, J., and Nguyen-Q-Rieu :1980, Astron. Astrophys., **90**, 88.

Combi, M.R.: 1994, Astron. J., **108**, 304.

Crovisier, J., Moroz,V.I., Encrenaz, T., Combes, M., Grigoriev, A.V., Sanko, N.F., Crifo, J.F., Bibring, J.P., Coron, N., Bockelee-Morvan, D., Gispert, R., Emerich, C., Lamarre, J.M., Rocard,F., Krasnopolsky, V.A., Owen, T.: 1987, Proc. Symposium on the Diversity & Similarity of Comets, Brussels, 6-9 April, 1987, ESA SP-278, 157.

Danks,A.C.,Lambert, D.L.,Arpigny,C.: 1974, Astrophys.J., **194**,745.

Delsemme, A.H.: 1985, Publ. Astron. Soc. Pac., **97**, 861.

Drapatz, S., Larson, H.P., Davis, D.S.: 1987, Astron. Astrophys., **187**, 497.

Eberhardt, P., Krankowsky, D., Schulte, W., Dolder, U., Lammerzahl, P., Berthelier, J.J., Woweries,J., Stubbemann, U., Hodges,R.R., Hoffman,J.H., and Illiano, J.M.: 1987, Astron. Astrophys., **187**,481.

Eberhardt, P., Krankowsky, D., Schulte, W., Dolder, U., Lammerzahl, P., Berthelier, J.J., Woweries,J., Stubbemann, U., Hodges, R.R., Hoffman, J.H., and Illiano, J.M.: 1987a, Astron. Astrophys., **187**,435.

Encrenaz, T.: 1984, in 'Isotopic Ratio in the Solar System', Cepadeus-Edition, Toulouse, pp. 173.

Encrenaz, T., d'Hendecourt, L., and Puget, J.L.: 1988, Astron. Astrophys., **207**, 162.

Ferlet, R.:1992, in 'IAU Symposium # 150 - Astrochemistry of Cosmic Phenomena',P.D.Singh (editor), Kluwer Academic Publishers, Dordrecht, The Netherlands, pp. 85.

Festou, M.C., Feldman, P.D., A'Hearn, M.F., Arpigny, C., Cosmovici, C.B., Danks, A.C., McFadden, L.A., Gilmozzi, R., Patriarchi,P., Tozzi, G.P., Wallis, M.K., Weaver, H.A.: 1986, Nature, **321**, 361.

Geiss, J.: 1987, Astron. Astrophys., **187**, 859.

Goldstein, R., Young, D.T.,,Balsiger, H., Buhler, F., Goldstein, B.E., Neugebauer,M., Rosenbauer,H., Schwenn,R., Shelly,

E.G.: 1987, Astron. Astrophys., **187**, 220.

Grard, R.J.L., McDonnell, J.A.M., Grun, E., and Gringauz, K.I.: 1987, Astron. Astrophys., **187**, 785.

Gerin, J., Combez, F.,Encrenaz, P., Linke, R., Destombes, J.L., and Demuynck,C. :1984, Astron. Astrophys., **136**, L17.

Greenberg, J.M.: 1982, in 'Comets', L.L.Wilkening (editor), The University of Arizona Press, Tucson,Az. 131.

Hanner, M.S.: 1982, in 'Cometary Exploration II, T.I.Gambosi (editor), Hungarian Acad. of Sciences, 1.

Hawkins, I., and Jura, M.: 1987, Astrophys. J. **317**, 926.

Huebner, W.F., and Giguere, P.T.: 1980, Astrophys. J., **238**, 753.

Huebner,W.F.: 1990, 'Physics and Chemistry of Comets', Springer-Verlag, Berlin. 1-367.

Iben,I.,Jr.: 1975, Astrophys. J., **196**, 525.

Jessberger, E.K., and Kissel, J.: 1991, in 'Comets in the Post-Halley Era', R.L.Newburn,Jr., M.Neugebauer, and J.Rahe (Editors), Vol **II**, pp. 1075.

Jessberger, E.K., Kissel, J., and Rahe, J.: 1988, in 'Origin and Evolution of Planetary and Satellite Atmospheres', S.K. Atrya, J.B.Pollack, Mathews (Editors), The University of Arizona Press, Tucson, Az. 167.

Keller, H.U.:1990, in 'Physics and Chemistry of Comets', Walter F.Huebner (editor), Springer-Verlag, Berlin,13.

Klavetter, J.J., and A'Hearn, M.F.:1994, Icarus, **107**, 322.

Krankowsky,D.: 1991, in 'Comets in the Post-Halley Era',Newburn, Jr. ,R.L., Neugebauer, M., and Rahe,H. (Editors) Kluwer

Academic Publishers, Vol. II, Dordrecht, The Netherlands.pp. 855.

Krankowsky, D., and Eberhardt, P.: 1990, in Comet Halley - Investigations, Results, and Interpretations, J.Mason (Editor), Ellis Horwood Ltd., Chichester, England.

Krankowsky, D., Lammerzahl, P., Herrwerth, I., Woweries, J., Eberhardt, P., Dolder,U., Herrmann,U., Schulte,W., Berthelier, J.J., Illiano,J.M., Hodges,R.R., and Hoffman, J.H.: 1986, Nature, **321**, 326.

Lambert, D.L., and Danks, A.C.: 1983, Astrophys.J.: **268**, 428.

Lammerzahl,P., Krankowsky,D., Hodges,R.R., Stubbemann,U., Woweries, J., Herrwerth,I., Berthelier, J.J., Illiano,J.M., Eberhardt,P., Dolder,U., Schulte,W., and Hoffman,J.H.:1987, Astron. Astrophys., **187**, 169.

Lust, R.: 1981, in 'Topics in Current Chemistry', M.J.S.Dewar, J.D.Dunitz, K.Hafner, Heilbronner,E., Ito,S., J.-M.Lehn, K. Niedenzu, K.N.Raymond, C.W.Rees, K.Schafer, G.Witting (eds), Springer-Verlag,Berlin Heidelberg, 73.

Marsden, B.G., Sekanina, Z.,Everhardt,E.: 1978, Astron.J.,**83**, 64.

McDonnell, J.A.M.,Alexander,W.M., Burton,W.M., Bussoletti, Evans, G.C., Evans, S.T., Firth,J.G., Grard,R.J.L., Green, S.F., Grun,E., Hanner,M.S., Hughes,D.W., Igenbergs,E., Kissel,J., Kuczera,H., Lindblad,B.A.,Langevin,Y.,Mandeville,J.-C., Nappo,S.,Pankiewicz, G.S.A.,Perry,C.H.,Schwehm,G.H., Sekanina, Z.,Stevensen,T.J., Turner,R.F.,Weishaupt, U., Wallis,M.K., and Zarnecki,J.C.: 1987, Astron. Astrophys.**187**,719.

Meier, R.,Eberhardt, P.,Krankowsky,D., and Hodges,R.R.: 1993, Astron. Astrophys., **277**, 677.

Ming,T., Anders,E., Hoppe,P.,and Zinner,E.: 1989, Nature,**339**,351.

Mitchell,G.F., Prasad,S.S., and Huntress,W.T.: 1981, Astrophys. J., **244**, 1087.

Neubauer,F.M. : 1987, Astron. Astrophys., **187**, 73.

Newburn,Jr.,R.L.: 1994, "Periodic Comet Shoemaker-Levy 9 Collides with Jupitor", NASA JPL 400-520 Publication , page 5.

Newburn,Jr.,R.L., Neugebauer, M., and Rahe,H.: 1991,'Comets in the Post-Halley Era', Kluwer Academic Publishers, Vol. I and II, Dordrecht, The Netherlands.

Oort, J.H.: 1950, Bull. Astr. Inst. Netherlands, **11**, 91.

Palme, H.,Suess,H.E., and Zeh,H.D.: 1981, in Landolt-Bornstein Vol. 2, Astron. Astrophys.,K.Schaifers, and H.H.Voight, Springer-Verlag,Berlin, pp. 257.

Penzias,A.A.: 1983, in 'Interstellar Molecules', B.H.Andrews (editor),D.Reidel Co.,Dordrecht, pp. 397.

Reme,H., Sauvaud,J.A.,d'Uston,C.,Cros,A.,Anderson,K.A., Carlson, C.W.,Curtis,D.W.,Lin,R.P.,Korth,A.,Richter,A.K., Mendis,D.A. : 1986, Proc. 20th ESLAB Symposium on the Exploration of Halley's Comet,Heidelberg, 27-31 October,1986, ESA-SP-250, Vol. I,29.

Rickman,H., and Huebner, W.F.:1990, in 'Physics and Chemistry of Comets',Walter F.Huebner(editor),Springer-Verlag,Berlin,245.

Schloerb,F.P., Kinzel,W.M., Swade,D.A., Irvine,W.M.: 1987,Astron. Astrophys., **187**, 475.

Simpson,J.A.,Rabinowitz,D.,Tuzzolino,A.J.,Ksanfomality, and Sagdeev, R.Z.: 1987,Astron. Astrophys., **187**, 742.

Singh, P.D., de Almeida,A.A., and Huebner, W.F.: 1992, Astron.J., **104**, 848.

Singh, P.D.,Huebner, W.F., Costa, R.D.D., Landaberry, S.J.C., and de Freitas Pacheco, J.A.: 1994, Astrophys. J.(Comm.)

Singh, P.D.:1991, Thesis ,Liv-Doc, University of Sao Paulo,SP.

Smith, H.W., Schempp,W.V., and Baines,K.H.: 1989, Astrophys.J., **336**, 976.

Vaisberg, O., Smirnov, V., and Omelchenko, A.: 1986, Proc. 20th ESLAB Symposium on the Exploration of Halley's Dust, ESA SP-250, Vol. II, 17.

Vanysek, V. and Rahe,J.:1978, Moon & Plan., **18**, 441.

Von Rosenvinge, T.T., Brandt,J.C.,Farquhar,R.W.: 1986, Science, **232**, 353.

Wilkening, L.L.: 1982, 'Comets', The University of Arizona Press, Tucson, Az.

Woods,T.N., Feldman,P.D., Dymond,K.F., Sahnow,D.J.: 1986, Nature, **324**, 436.

Wyckoff, S.,Lindholm, E.,Wehinger, P.A., Peterson, B.A., Zucconi, J.M., and Festou, M.C.: 1989, Astrophys. J., **339**, 488.

Zinner,E., Tang,M., and Anders, E.: 1989, Geochim. Cosmochim. Acta, 53, 3273.

Zinner,E., and Wopenka,B.: 1990, Lunar and Planet.Sci., XXI (Houston: Lunar and Planetary Institute), 1379.

Section 3:

STELLAR ASTROPHYSICS

The Use of Stellar Thorium Lines to Determine the Age of the Galaxy *

Licio da Silva and Ramiro de la Reza

CNPq-Observatório Nacional

Rio de Janeiro, Brazil

1. Introduction

The use of "Radioactive Chronology" is one of the most powerful instruments to obtain ages of stellar systems. Although its use is very difficult, its principle is very simple: knowing the abundance of a chemical element in a body when it was created and as it changes with time, by measuring its present abundance we can determine the age of the body. If the element is destroyed by radioactive decay, its abundance a is given by $a = a_0 e^{-\alpha t}$, where a_0 is the initial abundance and α is a constant characteristic of the considered element, being the time $\tau = 1/\alpha$ the half-life of that element. To have a sensitive clock, τ must be of the order of the age that we want to measure.

Inversely, by measuring the present meteoritic abundance of a radioactive element, we can obtain its abundance when the solar system was formed, 4.6 Gyr ago. Knowing this value, we can estimate, by means of models, how that abundance changed with the evolution of the Galaxy, then it is possible to determine when the process of creation of that element began. If we suppose that it began when the Galaxy was formed, we can determine the age of the Galaxy. Several authors have used the meteoritic relative abundances of the actinides, that is, the element of the Uranium groupe, ^{238}U, ^{235}U, ^{322}Th, among others, to date the beginning of nucleosynthesis in the Galaxy. Various authors have also pointed out how model depending those estimates are (see Pagel (1993) and references therein). To have the abundance of a given element in a time t^0 we must dispose of its production rate and

* Observations collected at the European Southern Observatory, ESO, Chile

the ejection rate from each possible star, the initial mass function and the net rate of star formation for every time $t < t^0$. Therefore, even supposing that the Galaxy is isolated (no infall or outflow), to determine its age from those measured abundances is not a simple task.

The situation is less complicated if we compare two radioactive element abundances formed by the r (rapid) nucleosynthetic processus, as is the case of the elements above. A complete analysis of this problem (which is out of the purpose of the present article) can be seen in the nice article of Cowan, Thielemann and Truran (1991). It is interesting also to note that, using data from Fowler (1987), Pagel (1993) find that, according to the chosen Galactic evolution model, the age of the Galaxy ranges from 6.5 Ga to 21 Ga, but even a infinity age is possible. The smaller value is based in the "pure initial-spike" model, wich has been defended by Butcher (1988) but has not however a general acceptance. By this model, a single nucleosynthetical initial explosion would have formed all the heavy elements of the Galaxy.

2- The Use of Stellar Th Abundances to Determine the age of the Galaxy

The importance of using ^{232}Th as cosmochronometer came from the fact that its half-life of $\sim$14 X 10^9 years is of the same order of the oldest stars of our Galaxy.

The first convincing indentification of thorium lines, at λ4019 and λ4086, was made by Holweger(1980). Somewhat contrary to what we think today, he declared: "The primary significance of identifying thorium in stars of different age and metallicity does not arise from its rôle as a cosmochonometer, the 14 X 10^9 year half-life of Th 232 probably precluding adequate time resolution..."

It was Butcher(1987) who introduced the idea of using the *stellar* Th abundances to check the evolutive ages and, in this way, to attempt to establish an independent radioactive time scale and age for the Galaxy. In his work he used the line of the ionized long lived isotope ^{232}Th at 4019.129 $\AA$ together with the nearby line of the heavy element Nd II at 4018.823 $\AA$, taken as a reference. Measuring 18 dwarf and 3 giants stars of different low metallicities corresponding to different stellar evolutionary lives, he detected no variation of the Th/Nd ratio with the stellar ages, suggesting a short lifetime for the Galaxy (9.6 Gy) or, what is similar, that the evolutionary ages of stars are in error. Among the positive aspects of Butcher (1987)'s analysis we can

point out:

- Very good observational material, obtained with a Reticon detector at the CES on the CAT of ESO, with a resolving power = 100,000 and high signal to noise ratio.
- Very careful image treatment.
- The two Th and Nd analysed lines are very close.
- There are two "enough good"continuum windows of the stellar spectrum near those lines.

But there are also some negative aspects:

- Nd (formed half by s and half by r-process) and Th (a pure r-process element) have different nucleosynthetic histories. (This is the main negative aspect that brought us to use Th/Eu ratio as chronometer for the Galaxy.) Mathews & Schramm (1988) also pointed out this problem in Butcher's analysis.
- The stellar models used are too simples (just one shell).
- The stellar abundances of Th and Nd were not strictly measured, just the equivalent widths.
- He didn't take into account the CoI line at λ4019.133 that is very close to the Th line at λ4019.136.

Using a "excessively naive model of Galactic chemical evolution" (Pagel 1990), Butcher(1987) obtained an upper for the Galaxy age of 9.6 Gyr. This result is in complete disagreement with the stellar ages of the globular clusters ($\sim$ 15 *Gyr*).

In their critical analysis of Butcher's work, Mathews and Schramm (1988) argue that his age result is model-dependent and find a possible range of galactic ages that can reach even 20 Gyr.

Another fact that can be considered wben using the Th clock is the possibility of Th destruction by photofission in the stellar interiors. Malaney et al (1989) estimated this effect and concluded that ages must be increased by nearly 30

Lawler et al (1990) deduced a new value for the Co line at λ4019.126 and corrected the gf value of Simonsen et al (1988) for the Th line λ4019. Their values differ a little from those used by us in our previous analysis (see below). Using the equivalent widths given by Butcher (1987) and the gf values deduced by them, Lawler et al (1990) found Th/Nd results that are in good agreement with Arnould & Takahashi (1990)'s Galactic chemical evolution models for galactic ages of 15–20 Gyr.

Morell, Kallander & Butcher (1992) revised carefully the previous work about Th/Nd ratio, with the best possible available spectroscopic data. They also used the Uppsala Model Atmosphere Code developed by Gustafsson and collaborators. To improve the fitting between the observed and the synthetic spectra they introduced some "fake lines" to substitute unknown lines (Fig. 1). Of course, it is very difficult to determine fake lines that work well for each star in the studied range of spectral type and in general, the fitting between both spectra is not perfect. But those fake lines are not that necessary to determine the thorium abundance because they are not very close to the Th line. Their influence on the Nd abundance determination are more important, at least for the coolest stars. According to these authors, the major trend previously found by Butcher (1987) is confirmed, but no conclusion concerning the age of the Galaxy was possible due to the scatter produced by the probable presence of an unknown line at 4019.10 $\AA$.

3-The Use of Th/Eu Ratio to Estimate the Age of the Galaxy

In 1988 we began a study aiming to introduce a new clock based on the ratio Th/Eu, determining the Th and Eu abundances of about twenty stars, dwarfs and subdwarfs, of the Galactic Disk. The first results (of four stars) were presented in the symposium "Astrophysical Ages and Dating Methods" (da Silva, de la Reza & Magalhães 1990).

The main positive aspect of this analyses is that Eu is known as being formed mainly (at least 90%) by the r-process. Then it is a much better reference element for Th, which is a pure r-process element. The observational data used are as good or better than that of Butcher(1987). They were obtained with a CCD detector at the long camera of the Coudé Echelle Spectrograph of the ESO Coudé Auxilary Telescope. The resulting resolving power is 100.000 and the signal/noise is always better than 200. The data were reduced by using a code especially developed by our group of Observatório Nacional (Magalhães & da Silva, 1990). Tests made recently showed that this code gives, for data from ESO-CAT-CES, the same results as the IRAF code. All the lines listed in Kurucz & Peytremann (1975) were considered in the synthetic spectrum calculation. This was made using a LTE code kindly provided by M. Spite and the model atmosphere developed by Gustafsson and collaborators (Gustafsson et al 1975 and ref. therein). In general (see below), the gf values used for

the very weak lines were taken in Kurucz and Peytremann, but for the lines strong enough to be visible on the stellar spectra, the gf were determined from the solar spectrum, observed in the same conditions as the stars.

The results presented in da Silva et al. (1990) were deduced taking into account the influence of the almost coincident Co I line at 4019.126 $\AA$ mentioned above, using the gf value given by Holweger (1980). But for the final analyses, which will be published soon, we have used the hyperfine structures determined recently for that line and for tbe close Co line at λ 4019.29 by Pickering & Semeniuk (1995). These autors determined also the gf value of the V line λ 4019.13. This line being the main candidate which presence can explain the scatter found by Morell et al (1992) for their abundances of Th and also for the fact that the Th abundance derived for the solar spectrum is 40 % larger than the meteoritic abundance (Grevesse & Noels 1993). Pickering & Semeniuk found that this line has a gf value five times larger than the value calculated by Kurucz (1989) but it is equal to the value given by Kurucz & Peytremann (1975), which was used by da Silva et al. (1990).

François, Spite & Spite (1993) also measured the Th/Eu ratios but specially for stars of very low metallicities. Their results show an increase of the Th/Eu ratio for these very low metallicities. If this behaviour is true, it will be more difficult, but not impossible (Pagel & Tautsaisiene 1995), to use of the Th/Eu clock. However, other careful analyses are necessary to confirm these results, taking into account that they were obtained for giant stars and not for dwarfs and the data have a smaller resolving power than those, mentioned above, used for the dwarfs.

The data of da Silva et al. (1990), Morell et al. (1992), Lawler et al. (1990) and Francois et al. (1993) were collected and used with simple galactic models by Pagel (1993). He found that the Th/Eu clock, at least for moderate low metallicities disk stars, produces a galactic age compatible with that of globular clusters.

4. The Use of the Thorium Line at λ4086

All thorium analyses mentioned above were made using only the Th II line at λ4019.126. It would be interesting to look for another Th line that would be less blended. For this reason we are trying since 1990 to use another Th II line at 4086.52$\AA$, also detected in the sun and a few stars by Holweger (1980). Our analysis of this line is based on observations made with CCD+CES+CAT of ESO, made in

the same conditions as those for λ4019 described above. The λ4086 Th line is known to be much weaker than the λ4019 line but it is placed in a less contaminated region. For solar stars this line is well-defined enough (Fig. 2), but even for the moderately deficient stars it is very weak and its measurement is very delicate. For HR 3018, for ex., changing the continuum by 1% is enough to make the line to disappear (Fig. 3). Its equivalent width is only $\sim$ 1 m$\AA$.

There was another problem increasing the difficulty of measuring that line: the hyperfine structure of the line CoI λ4086.3, near the Th one, was not known. For our preliminary results, as for the synthetic spectrum presents on Fig. 3, we simulated their hyperfine structure by fitting the observed solar spectrum with the calculated one. But to mesure the λ4086 Th line with confidence, it is necessary to know well all the neighbouring lines, wich was not the case. Happily, as an answer to our claim made in a workshop realized in Brussels in 1994 (da Silva & de la Reza 1995), the hyperfine structure of the line CoI λ4086.3 was recently measured by Pickering & Semeniuk (1995). Now it will be possible to measure this very weak line of Th, at least for some solar type stars, to have a second value for the thorium abundance determination.

5. Conclusions and Recommendations

The nucleochronological determination of the age of the Galaxy based on stellar ratios of Th/Nd and, specially, Th/Eu can give very important and interesting results. Therefore, since the stellar Th lines are very weak and are in two crowed spectral regions, it is a technically difficult research. But as radioactive chronology produces an independent scale of time, this gives us an independent way of determining the age of the Galaxy and to compare with the constraints established by Solar System data, it is worth the effort.

In da Silva & de la Reza (1995) are listed some "technical problems" to be resulted for getting a correct solution for this question. The aim was to call attention to the "spectroscopic community" which solutions will be most helpful for solving this problem. That claim receive an important help (Pickering & Semeniuk 1995), but there are some remainder points not yet resolved:

Identification or missing lines problems

- Morell et al. (1992) and Grevesse and Noels (1993) suspect the presence of

an unknown line at about 4019.10$\AA$. The V I line measured by (Pickering & Semeniuk 1995) is not strong enough to resolve this problem because it is smaller than the value (log gf=-1.30) used by Morell et al. (1992).

- Butcher (1987) mentions the possibility of a Tb II contamination at 4019.14$\AA$. Grevesse (privated communication) says that this line is too weak to change the synthetic spectrum.
- What are the real lines replaced, by some authors, by fake ones?

Hyperfine structure

It is very important to know accurately the hyperfine structure of the following lines:

- Eu II at 4129.72$\AA$ and Ba II at 4130.66$\AA$, to determine accurately the stellar abundances of those elements.

Other Lines

- Are molecular lines involved?

References

Arnould, M. & Takahashi, K.: 1990, in*Astrophysical Ages and Dating Methodes*, Editions Frontières, eds. E. Vangioni-Flam et al., p. 325

Butcher, H.R.: 1987, Nature, 328, 127

Cowan, J.J., Thielemann, F.K. & Truran, J.W.: 1991, Physics Reports 4 & 5, 267

da Silva, L., de la Reza, R. & Magalhães, S.D. : 1990, in *Astrophysical Ages and Dating Methodes*, Editions Frontières, eds. E. Vangioni-Flam et al., p. 419

Fowler, W.A.: 1987, Quart. J. R. Astr. Soc, 28, 87

François, P., Spite, M. & Spite, F.: 1993, A&A 274, 821

Gilroy, K.K, Sneden, C., Pilachowski, C.A., Cowan, J.J.: 1988, Ap J, 327, 298

Grevesse, N. & Noels, A.: 1993, Phys. Scr., 47, 133

Gustafsson, B., Bell, R.A., Eriksson, K., Nordlund, A.: 1975, A&A, 42, 407

Holweger, H.: 1980, The Observer, 100, 155

Kurucz, R.L. & Peytremann, E.: 1975, S.A.O. Special Report nº 362

Kurucz, R.L.: 1989, in Transactions IAU, Vol. XXB, ed D. McNally, Kluwer, Dordrecht

Lawler, J.E., Whaling, W., Grevesse, N.: 1990, Nature 346, 635

Morell, O., Kallander, D. & Butcher, H.R.: 1992, A&A 259, 543

Magalhães, S.D. & da Silva, L.: 1990, Rev. Mex. de Astro. y Astrof. 21, 751

Pagel, B.E.J.: 1989, in *Evolutionnary Phenomena in Galaxies* , Cambridge University Press, p. 201

Pagel, B.E.J.: 1990, in *Astrophysisical Ages and Datting Methodes* , Editions Frontiéres, eds. E. Vangioni-Flam et al, p. 493

Pagel, B.E.J.: 1993, in *Origin and Evolution of the Elements*, Cambridge University Press, p. 496

Pagel, B.E.J. & Tautvaisieni, G.: 1995, to bo published in Mon. Not. R. Astrn. Soc

Pickering, J.C. & Semeniuk, J.I.: 1995, Mon. Not. R. Astrn. Soc. 274, L37

Simonsen, H., Worm, T., Jessen, P. & Poulsen, O.: 1988, Phys. Scr., 38, 370

FIGURE CAPTIONS

Figure 1 - Observed spectrum of α Cen A together with the synthetic spectra calculated with the same atomic data (element, excitation potential and gf) of Morell et al. and da Silva et al. The difference of the calculated spectrum with that one of Morell et al. can be due to the use of different LTE codes or values of C_H, vsini, etc. Our main goal here is to show that even using the fake lines of Morell et al., the fitting is not perfect even in an almost solar star as α Cen A.

Figure 2 - Fitting of the observed and the synthetic spectra of α Cen A, for the λ4086 region.

Calculations: a) without the Th line; b) with the Th line.

(observed spectrum: solid line; synthetic spectrum: dotted line)

Figure 3 - Fitting of the observed and the synthetic spectra of HR 3018, for the λ4086 region.

a) With the best fitting of the continuum. b) Changing the continuum by 1%.

Figure 1

Th4019 alfa Cen A

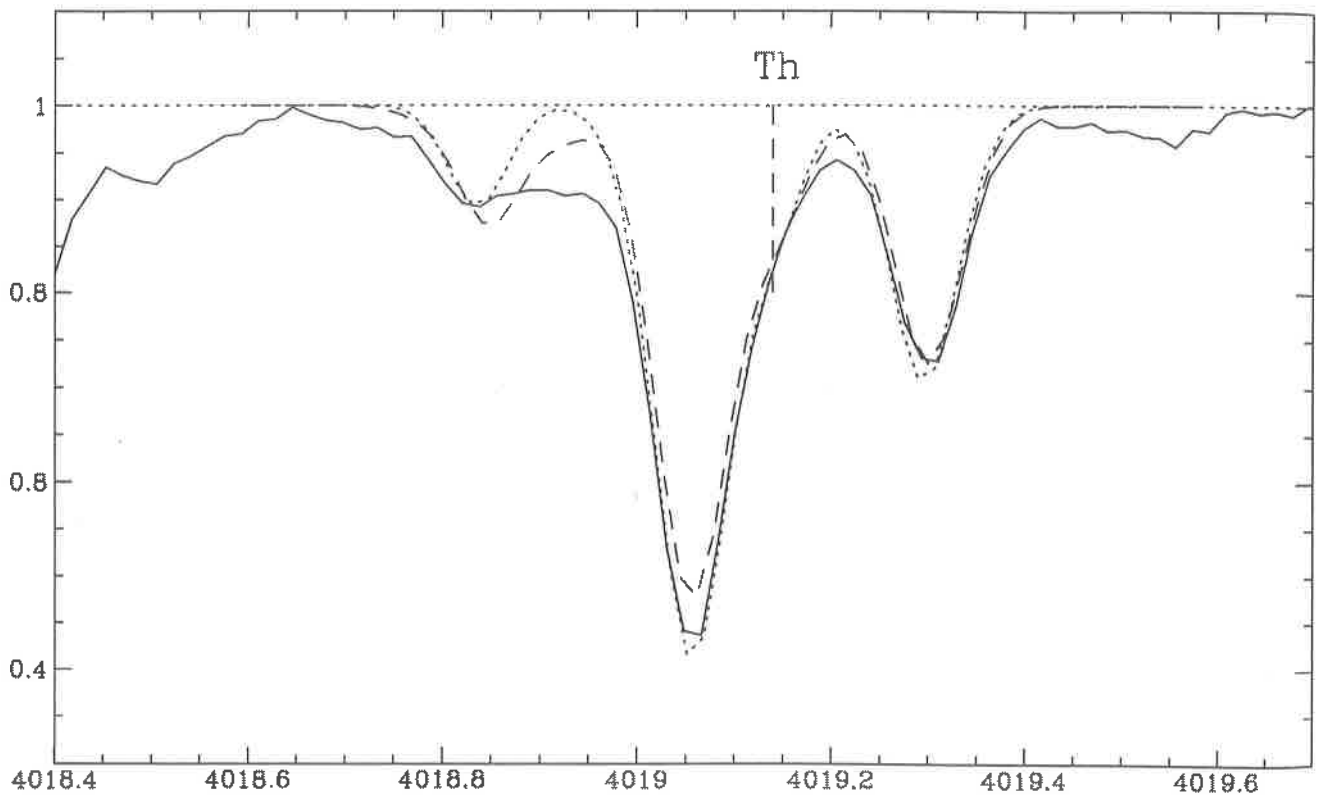

Atomic data from Morell et al _ _ _ _ _ _

Atomic data from da Silva et al .....

Figure 2

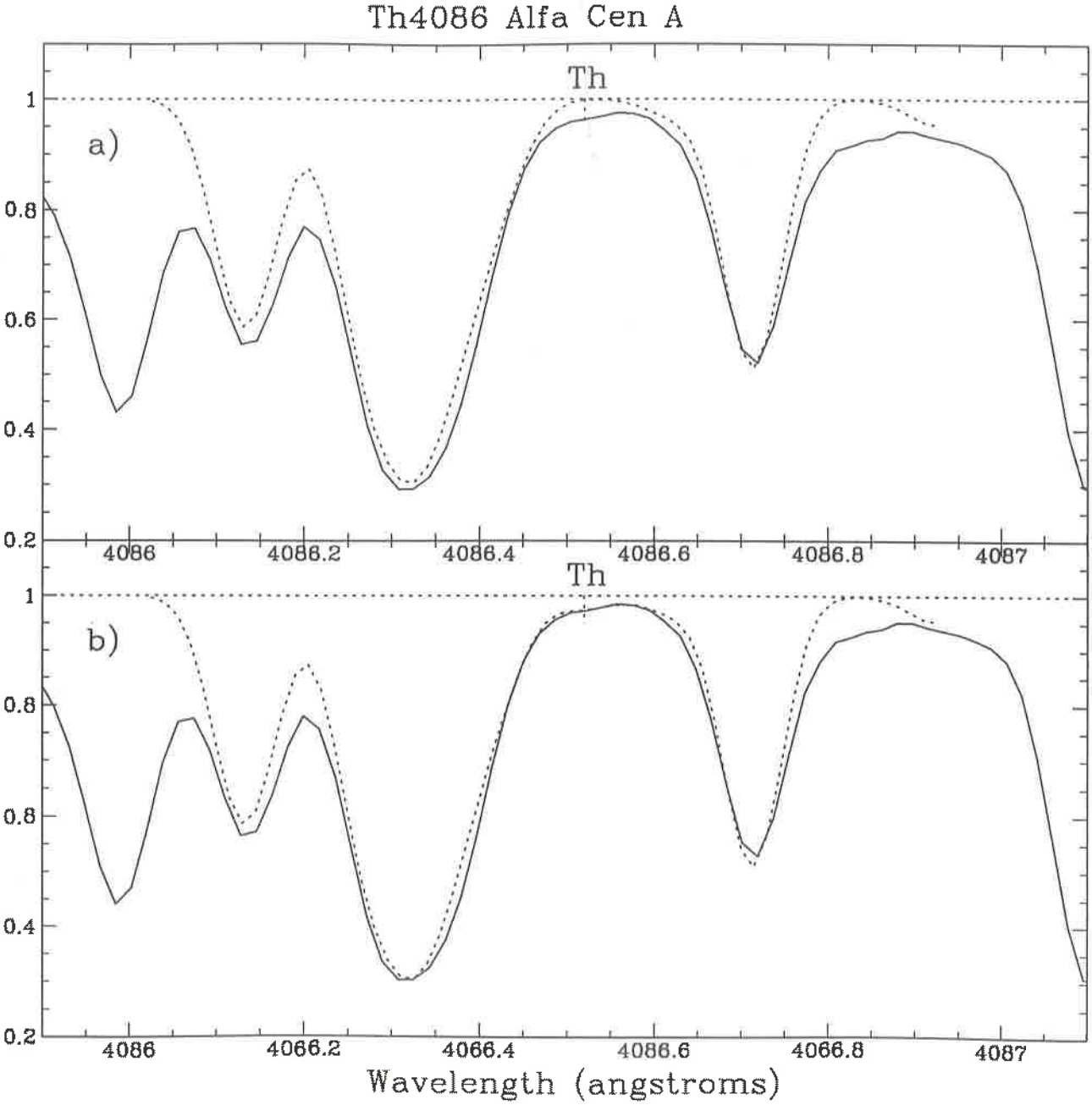
Th4086 Alfa Cen A
Th
a)
Th
b)
1
0.8
0.6
0.4
0.2
4086
4086.2
4086.4
4086.6
4086.8
4087
4066.2
4066.4
4066.6
4066.8
Wavelength (angstroms)

Figure 3

Th4086 HR 3018

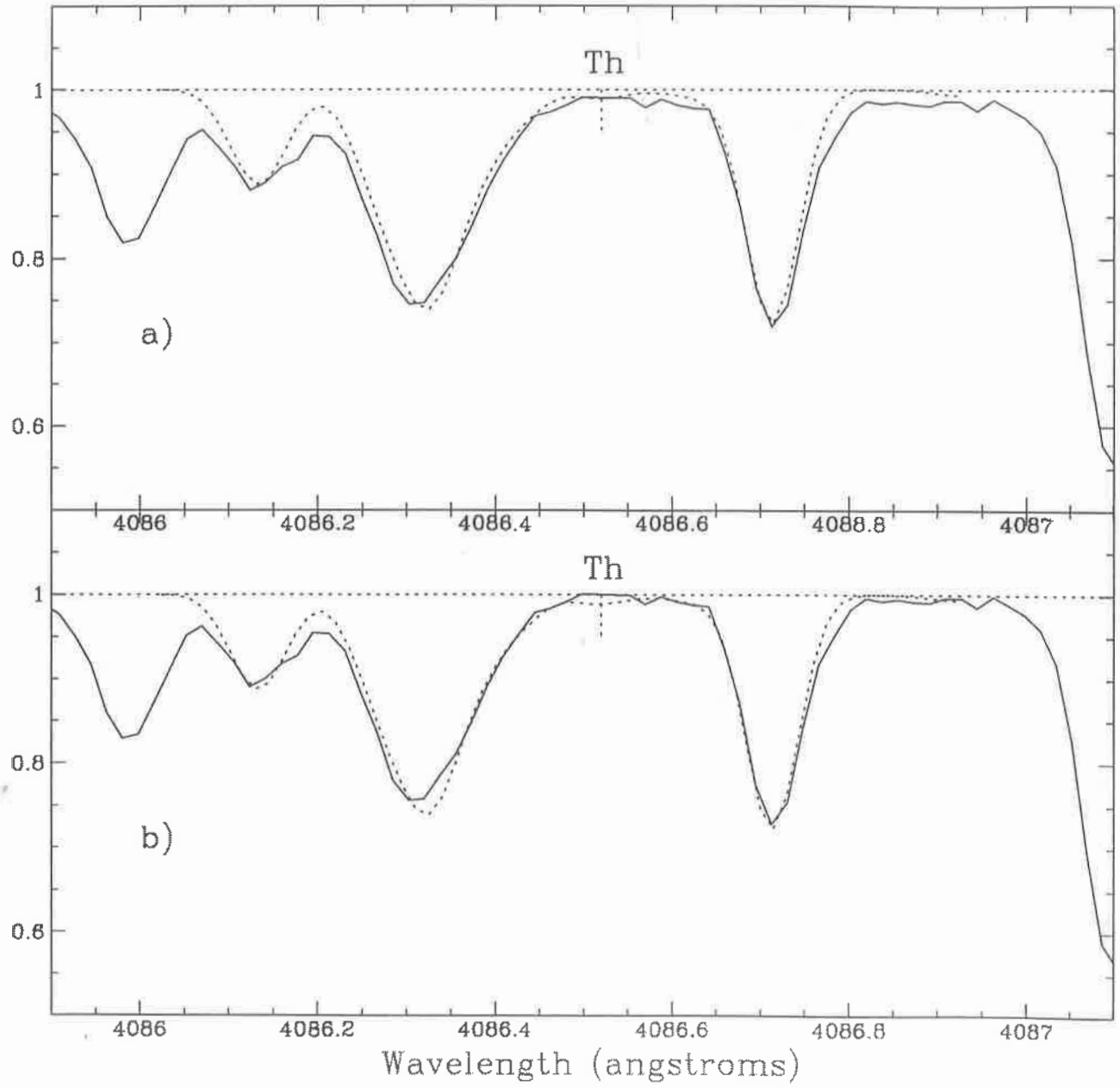

Figure 3

Th4086 HR 3018

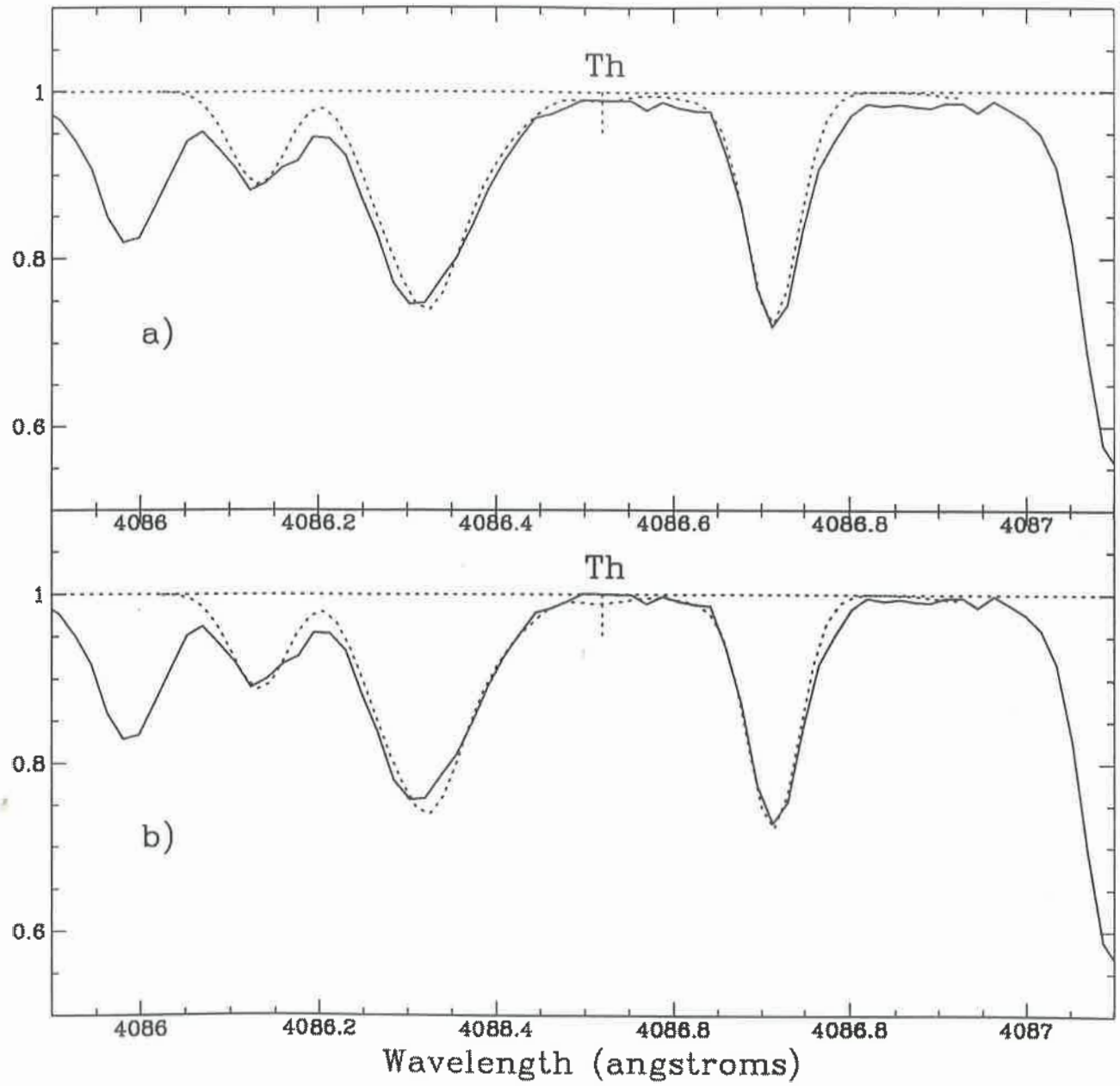

Star Formation by Impact of High-Velocity Clouds on the Galactic Disk

Jacques R.D.Lepine, IAG-USP

Introduction

Many groups of OB stars in the Galaxy seem to belong to aligned structures extending over scale-sizes of a hundred parsec or more. Typical examples are found in Orion and ρ Oph. In the last 20 years, the generally accepted interpretation was a mechanism known as **sequential** star-formation (Blaauw, 1964, 1991, Elmegreen and Lada, 1977). According to that model, when a first group of OB stars forms at one extremity of an interstellar cloud, an H II region is formed which expands and produces a shock wave in the surrounding medium. Compression of gas in a layer between the shock front and the ionization front triggers gravitational collapse and gives rise to the birth of a new group of OB stars. This cycle repeats itself, resulting in a sequence of OB clusters. This process was compared by Hubert Reeves to a fire propagating in a forest, until it is completely consumed.

In spite of the great appeal of this model, and of its acceptance, mostly due to the lack of an alternative, a detailed analysis shows that it is wrong. The model is qualitative, and in the cases which were considered as obvious cases of sequential star-formation, it does not explain striking aspects of the morphology, such as the displacement of a large mass of gas with respect to the middle of the galactic plane, and the existence of filaments connecting the main clouds to the plane. A series of questions are left without answers. What triggers the formation of the first OB group? If there is a different mechanism for the first group, why would not it also be responsible for the other groups? Why the first group does not appear in the middle of the star-forming clouds, and propagates in different directions? According to Wynn-Williams, infrared observations show that groups of massive protostars can be found in regions far enough from the nearest OB cluster, that there would have been no time for the propagation of a shock wave. On the other hand, clusters of small mass (T Tauri) stars of are found in some molecular clouds, with geometry similar to OB clusters. However, T Tauri stars are unable to dissipate molecular clouds nor to induce star formation.

The oldest open clusters belonging to aligned sequences of clusters have ages of the order of 20 million years. Such ages are comparable to the half-period of oscillation of a star perpendicular to the plane, under the action of the gravitational field of the disk, which is about 35 million years in the solar neighborhood. The displacement of a cluster which was born at 100 or 200 pc from the plane is not negligible in such a time interval. The forces which act on stars and on gas are not the same, since stars are not sensitive to pressure gradients or to shock waves. As a consequence, stars are gradually removed from the gas from which they formed. It is expected that old stars should be farther from their birth-place than younger ones. Aligned groups of stars

form naturally in a sequence of ages, without need for one group to trigger the birth of the other.

A new model: the effect of high-velocity clouds

High-velocity clouds have been observed in many directions and cannot be ignored. Complete maps of their spatial distribution are presented by Bajaja et al.(1985) and by Hulsboch & Wakker (1988). We are interested in the effect of their collisions with the gelactic disc, without worrying whether they are of extragalactic origin or they are produced locally in a process like corrugation waves of the gas of the disk, or any other. We performed hydrodynamic simulations of such collisions, taking into account the gravity of the disk (Lepine and Duvert, 1993). The model predicts the formation of structures which are very similar to those observed in the solar neighborhood, examples of which are shown in Figure 1. This similarity stimulated us to adjuste the parameters of the model in order to fit more precisely these structures.

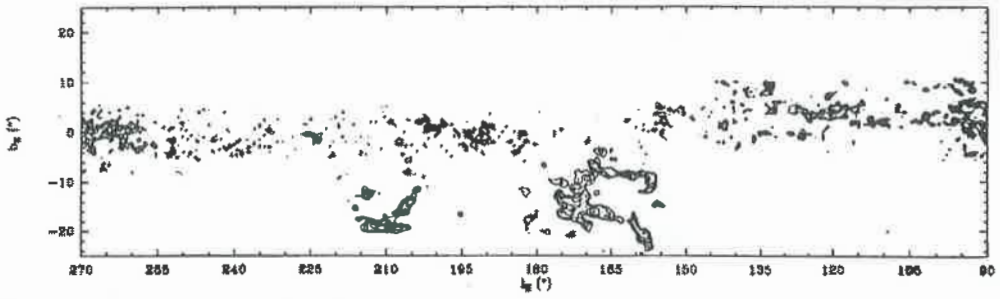

Figure 1. *Large-scale distribution of CO emission in the galactic plane, adapted from Bloemen et al. (1990). The Orion and Taurus molecular cloud complexes can be seen.*

An hydrodynamic model of a HVC collision:

We consider a simplified model of a spherical cloud of constant density falling on the gas of the galactic disk, represented by a Gaussian distribution of density; the thickness of the disk is about 100 pc and the maximum density 1 cm^{-3}. In the frame of the galactic gas, the cloud presents both parallel end perpendicular components of velocity. Typical velocities are a few hundred km s^{-1}.

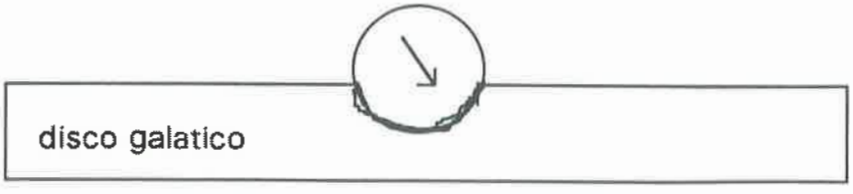

Figure 2 : Schematic HVC collision

We studied the evolution of the accretion layer or shock layer, which is being fed on one side by the HVC gas and on the other side by the gas of the disk. The main hypotheses are:

1) conservation of mass and of momentum. The velocity of the layer is obtained as a function of time by integrating the momentum per unit area of the gas that accreted the layer from both sides, and dividing by the integrated mass.

2) isothermal shock: the cooling mechanism is considered to be very efficient in the shocked layer, due to rotational and vibrational transitions of molecules. Since the cooling function increases with the square of density, the layer almost does not expand although its density increases by orders of magnitudes as it sweeps the galactic disk.

3) stars begin forming when the density in the layer reach a critical value, given by Jean's criterion. The new stars have initial velocity equal to the velocity of the layer at the position and instant of formation.

4) gas and stars move in the gravitational field $G(z)$ of the disk. For small z , $G(z) = az$ with $a = -2.6\ 10^{-16}$ km s^{-2} pc^{-1} . For stars, this gravity law produces an oscillation across the galactic plane, with a period of 70 million years. The velocity component parallel to the plane is not affected by the z component of the disk gravity; as a consequence, the trajectory of stars look like a sine function, in a simplified treatment in which rotation around the galactic center is ignored. This approximation is valid if the time interval spanned by the experiment is small compared to the rotation period.

Results

An example of a good fit that we obtained is the molecular cloud complex of Orion, that we shall discuss in detail. All the important parameters are known (the distance of the complex, its size, its morphology, the distance to the galactic plane, the position and age of the associated clusters of OB stars). A good fit of the overall morphology of the complex is obtained by the following choice of parameters:

radius 62 pc
ρ (HVC)/ ρ (gal) = 1/10
z *init* = 600 pc
Vz *init* = -150 km s^{-1}
Vy *init* = 40 km s^{-1}
present time, since the instant of crossing the plane: 33 My
threshold density for star formation attained when 70% of the column density of the disk is swept.

It should be stressed that almost all the parameters are determined by observations. For instance, the radius of the HVC is fixed by the two parallel strings of small clouds observed in CO, which are left after the passage of the shock (Figure 1). If we consider a spherical infalling cloud, the column density of HVC gas that is mixed with gas of the disk is smaller on edges of the HVC. Due to conservation of momentum, a cylindrical wall of low-velocity gas is left behind, forming the observed strings. The angle of the strings with respect to the disk tells us the ratio of the velocity components V_y and V_z. The height reached by the shocked layer before falling back towards the plane tells us the initial momentum in the z direction.

Since the parameters that describe the HVC are fixed by fitting the morphology of the cloud complex, there are no arbitrary parameters left to fit the relative positions of OB clusters with respect to the gas, nor the direction of the age gradient of the OB stars. The prediction that the OB groups should be in a sequence almost parallel to the plane, as observed, was a grateful surprise and a confirmation of the self-consistency of the model. This situation corresponds to a very precise instant, since for instance in 5 million years the direction of alignment of the OB groups will be very different from now. The observed and predicted ages of the OB groups are found to be in agreement. The time elapsed since the beginning of the collision which explains the morphology of the complex is the same which produces the observed direction of alignment of the OB groups. Furthermore, the observed mass of the Orion cloud complex is the same that we would obtain by sweeping a cylindrical hole with 62 pc diameter across the disk.

Applying the same model to the Ophiuchis complex we obtained equally good results. The morphology of the Ophiuchis clouds, with the relative positions of the Scorpius and Centaurus open clusters, considered by Blaauw as a typical case of sequential star formation, are well reproduced by our model. The predicted proper motions of the stars of these clusters are also in perfect agreement with observations. We conclude from the simulations that the Ophiuchis complex correspond to a more evolved stage than that of the Orion complex. In roughly 10 million years the OB clusters of Orion will present a spatial distribution with respect to the galactic plane similar to those of Ophiuchis today.

The **Taurus-Auriga-Perseus** molecular cloud complex is also explained. The Pleiades are a galactic cluster 70 million years old, situated almost on the same axis perpendicular to the galactic plane of the cloud complex, but at larger distance from the plane. Both the cloud complex and the Pleiades are estimated to be 130 pc distant from the Sun; the proper motion of the Pleiades is directed towards the plane. The present situation is the result of the infall of an HVC which reached the galactic plane from the southern galactic hemisphere. This HVC crossed the plane a first time, forming the Pleiades, and both the Pleiades and the molecular cloud formed by this first collision crossed the plane a second time, reaching back the southern hemisphere. New T Tauri stars, presently observed in the complex, were formed in the second collision.

Conclusions

The impact of HVCs is able to induce star formation. since it is a process which squeezes the gas until it reaches self-gravity. It also explains the morphology of a number of prominent cloud complexes, and predicts the direction of aligned OB groups and their age sequence. This is already much more than the sequential star formation model was able to do. This model is rich in consequences and also in possibilities of observational confirmations.

It is surprising that all the main star formation regions which lie within a radius of about 500 pc of the Sun, like Orion, ρ Oph , Taurus and Chamaeleon, can be fitted by the HVC collision model. We have not yet attempted to explain the morphology of other clouds of the solar neighborhood like those in Lupus, Norma, etc. These clouds bear meny similarities with the sample that we studied, like filamentary structures or cometary aspect. The rate of mass accretion to the disk that we derive for the solar neighborhood, if extrapolated to the whole galactic disk, is about 0.5 solar mass/year. This is the same rate estimated by F. Mirabel from the 21 cm observations of HVCs.

We shall now discuss some of the prospective possibilities of this model. It could explain "anomalous" scale-heights of stars. One anomaly is the presence of a small quantity of young stars of spectral type A or B at large distances (1kpc or more) from the galactic plane; another one is the existence of many open clusters outside the normal scale-height of the gas distribution. The open clusters formed by HVCs spring into existence with a non-negligible velocity component perpendicular to the galactic plane. It is usually believed that stars start their life with a very small scale-height, and that scattering processes like collisions between stars and molecular clouds increase the scale-height as a function of time. However, such collisions would tend to disrupt open clusters. Star formation by HVC offer a new way of understanding the normal scale-height distribution of stellar populations. If we suppose that the quantity of gas in the disk has been increasing as a function of time (in a billion years time scale), then the scale-height must have decreased as a function of time. The reason is conservation of momentum. HVCs have collided with increasing column density of gas, resulting in decreasing velocity in the z direction and decreesing scale-height.

As another kind of prospective consequence, we cen imagine that most molecular clouds are thin sheets, because they are the result of a sweeping process like the one that we described. All kinds of shocks produce thin sheets, and spiral arms are another possible source of shock waves. In this hypothesis, molecular clouds would only survive due to shock pressure, and dissipate when they reach a velocity close to zero with respect to the surrounding interstellar medium. In a sense, molecular clouds would be a transient phenomenon. They are accreting mass on the side that is sweeping the medium, and this is the process that gives them stability due to excess external pressure, and also produces turbulence. Other authors already reached the conclusion that molecular clouds are geometrically thin, by comparing observed column densities, for instance in the CO lines, with theoretical densities required for the

excitation of energy levels. It is possible that all those who are thinking in terms of almost spherical molecular clouds are mistaken.

Finally, we predict that the first stars formed in the collision process are the most massive ones. According to the simulations, the parts of the shocked layer which reach the largest velocity are those which originate from the central regions of the projected area of the HVC, which have large column densities. These parts of the layer are those which travel a larger distance across the galactic disk and sweep more matter before slowing down. A slow velocity is a condition to reach Jean's instability. This prediction seems to be supported observationally; for instance in ρ Oph only T Tauri stars are being formed at present, but the first groups formed contained OB stars. These considerations are certainly important to understand the initial mass function.

References

Bajaja, E., Cappa de Nicolau ,C.E., Cersosimo J.C., et al., ApJS 58, 143
Blaauw, A., 1964, ARA&A 2, 13
Bloemen, J.B.J.M., Deul E.R., Thaddeus P., 1990, A&A 233, 437
Elmegreen, B.G., Lada, C.J., 1977, ApJ 214, 725
Hulbosch, A.N.M., Wakker, P.B., 1988, A&A 75, 191
Lepine, J.R.D., Duvert,G., 1994, A&A 286, 60
Mirabel, I.F., 1989, in Structure and Dynamics of the Interstellar Medium, IAU Colloquium 120, ed Tenorio-Tagle G., Springer-Verlag, p.396
Reeves, H., 1978, in Protostars and Planets, ed. T. Gehrels (Tucson: Univ. Arizona Press), 399
Wynn-Williams, C.G., 1982, Annu. Rev. Astron. Astrophys. 20, 597

The discovery of Krypton, Xenon, and other heavy elements in the planetary nebula NGC 7027

D. Péquignot

Laboratoire d'Astrophysique Extragalactique et de Cosmologie
DAEC, Observatoire de Paris–Meudon
F–92195 Meudon Principal Cédex, France

An important aim of nebular spectroscopy is the identification of new elements. Since the pioneering work of Bowen (1928), who identified the "nebulium" lines with forbidden lines of abundant elements, most elements in nebulae have been discovered thanks to forbidden lines. The number of elements known in nebulae grew from 5 to approximately 15 between 1927 and 1939. By 1960, forbidden lines from 28 ions of 13 elements (N, O, F, Ne, Na, Mg, S, Cl, Ar, K, Ca, Mn, and Fe) were known in HII regions and planetary nebulae (Bowen, 1960). A dozen more ions of H, He, C, N, O, Si, and perhaps Ne were also known from permitted lines only, leading to a total of 17 elements.

Subsequent detections in classical nebulae included Cu and Ni in Orion (Thackeray, 1975) and P in NGC 7027 (Kaler et al., 1976).

Meanwhile, objects such as the slow nova RR Telescopii, in which refractory elements were presumably not much depleted, provided many lines from iron-peak elements, adding about 10 ions of Fe, Cr, Co, Ni, and Cu (Thackeray, 1977).

Thus, despite extraordinary improvements of equipment, the identification of new elements in the optical spectrum of nebulae, especially classical nebulae, did not significantly progress for one third of a century, that is since the end of Bowen's scientific activity. The last new detection goes back two decades. Altogether no more than 22 elements are presently detected, the heavier one being Copper (Z=29).

Apparently a serious search for elements beyond the Iron peak – $Z > 30$, hereafter "heavy elements" – has not heen undertaken in nebulae. One possible explanation is that solar-system ahundances of heavy elements look discouragingly low (no more than $\sim 10^{-9}$ and 10^{-10} by number relative to H on the fourth and fifth rows of the Periodic Table respectively), when compared to iron-peak elements ($\sim 10^{-5}$ to $\sim 10^{-7}$) which already proved difficult to detect.

Understandably a forseeahle difficulty of trying to detect heavy elements in nebulae is in distinguishing a weak forbidden line from any "anonymous" permitted line of an abundant element. The fact very few new elements were discovered in classical nebulae since the 60's may be paralleled with a general stagnation of the process of line identification. The lists of lines – identified or not – currently available for the optical spectra of classical nebulae differ very little from those established until the mid-60's. Considering for example the optical spectral survey performed by Aller et al. (1955, 1963) for the reference planetary nebula NGC 7027, the next surveys by Kaler et al. (1976) and Keyes et al. (1990) are mere updates of line intensities.

Nonetheless iron-peak elements are often hard to detect in galactic nebulae because they are partly locked into dust grains. Certainly not all heavy elements are refractory. Also the strongest forbidden lines are generally produced by np^k rather than $3d^k$ ions. In fact $4p^k$ and $5p^k$ ions of elements Z ~36 and ~54 provide a wealth of forbidden and fine-structure lines in the optical range.

More importantly, it was suspected for several decades (Burbidge et al., 1957), and it is now well established, on both theoretical (e.g., Iben, 1991) and observational (e.g., Lambert, 1991) grounds, that low- and intermediate-mass stars ($M \leq 8M_{\odot}$) are important sites of heavy-element synthesis by slow neutron captures on ^{56}Fe seeds, during the Asymptotic Giant Branch (AGB) and post-AGB phases. Free neutrons would be mainly released by reactions $^{22}Ne(\alpha, n)^{25}Mg$ and $^{13}C(\alpha, n)^{16}O$. The ^{22}Ne source is activated at high temperatures ($T \geq 3x10^8$), generally more apropriate to relatively massive stars, while the ^{13}C source is activated at temperatures achievable in low-mass stars ($M < 3M_{\odot}$). ^{22}Ne is a by-product of the destruction of ^{14}N in the He-burning zone. Production of ^{13}C involves the injection of small amounts of protons in the ^{12}C-rich zone built up by incomplete helium burning.

Low-mass stars ascending the AGB eventually evolve into carbon stars which end as carbon-rich planetary nebulae after expelling their envelope. In these stars, freshly synthesized carbon is brought to the surface by the so-called "third dredge up", which is an accepted consequence of thermal pulses occuring in the helium-burning shell along the AGB (e.g., Iben, 1991). According to present views, these pulses may provide favourable conditions for the operation of the so-called "main s-process" of neutron capture via ^{13}C (Lambert, 1991; Busso et al., 1992, 1993), corresponding to the synthesis of s-nuclides with atomic mass $A \geq 85$, that is Krypton and beyond (Käppeler et al., 1989).

The enrichment of typical s-elements observed in AGB stars can reach a factor of 10 or more (Lambert, 1991) and perhaps as much as 30 in carbon stars (Utsumi, 1985). Hence the search for heavy elements in planetary nebulae does not seem as hopeless as often believed since even more extreme enrichments may be expected in a more advanced stage of evolution.

In this context, the bright carbon-rich planetary nebula NGC 7027 appears as a good target.

Deep spectra of NGC 7027 were secured in the range 400.0–1050.0 nm at a resolution of .10 or .05 nm/px, using the CARELEC spectrometer attached to the 193 cm telescope of Observatoire de Haute-Provence (Péquignot & Baluteau, 1988; Baluteau et al., 1995; Péquignot et al., 1995, in peparation). Hundreds of new lines were recorded and identified, particularly in the near infrared, superseding the intensity limit *and* the identification rate achieved even in classical optical surveys. Most identifications correspond to permitted lines from abundant elements, notably lines arising from large angular momentum levels, not recorded by means of laboratory spectroscopy.

This effort towards full identification of permitted lines was a prerequisit to establish with some confidence that many of the lines left unidentified were not due to common elements.

A systematic search for new forbidden and fine-structure lines was undertaken, leading to many new convincing identifications. As a result the number of elements detected in

nebulae was brought up from ~22 to ~30.

In particular, elements with atomic number Z > 30 were detected for the first time in a nebula (Péquignot & Baluteau, 1994, PB94). Based on a total of 20 undoubtful emission lines, 14 ions belonging to 8 different elements are considered as certainly or probably detected: [XeVI], [PbII] in p^1, [SeIII], [KrV] (2 lines) in p^2, [BrIII], [KrIV] (3 lines), [XeIV] (2 lines), [BaV] in p^3, [KrIII], [RbIV], [XeIII] (2 lines) in p^4, [SrIV], [BaIV] in p^5, and a permitted multiplet of the 6s ion BaII (2 lines). In this list, the identifications of [BaV] and [PbII] are the most fragil.

Half a dozen more weak lines affected by large uncertainties may provide identifications for [BrIV] in p^2, again [BrIII], [RbV], [SrVI] in p^3, [YV] in p^5, and again BaII. A dozen more features quoted by PB94 should be regarded as interesting targets for future studies rather than genuine identifications.

It is concluded that elements Krypton, Xenon, Bromine, Selenium, Rubidium, and Barium are certainly or probably detected in NGC 7027. Strontium is quite probably detected, while Lead and Yttrium are suspected.

The strength of the newly identified lines almost certainly implies that these elements are at least ten times more abundant in NGC 7027 than in the solar system, confirming that the capture of neutrons onto iron-peak seed nuclei is very effective in progenitor stars of planetary nebulae and showing directly that the by-products of this nucleosynthesis are injected into the interstellar medium.

At first view, the nature of the elements detected is paradoxical in that:
1/ Xenon, predominantly an r–element, was copiously synthesized in a low-mass star,
2/ Krypton and Xenon, predominantly synthesized in very different sites, are enhanced in similar proportions,
3/ Elements typical of the so-called "main s-process component" (Sr, Y, Zr, Ba) are not selectively enhanced in NGC 7027: Rubidium for example seems to show up more than Strontium.

However, these results can be reconciled with current ideas about the slow capture of neutrons in stars after noticing that, by some strange coincidence, all of the a priori most enhanced elements are likely to be selectively locked into refractory dust grains. Then the enrichment of NGC 7027 in pure s-nuclides of the main component may approach a factor of a hundred.

It is foreseen that the study of heavy elements in planetary nebulae will provide new important insights into final stages of stellar evolution and chemical evolution of galaxies since several kee elements (particularly Kr and Xe), undetectable in stars, are easily observed in nebulae.

Acknowledgments

I am pleased to acknowledge the kind invitation of the SAB at the conference celebrating its 20th anniversary.

References

Aller L.H., Bowen I.S., Minkowski R., 1955, ApJ 122, 62
Aller L.H., Bowen I.S., Wilson O.C., 1963, ApJ 138, 1013
Baluteau J.-P., Zavagno A., Morisset C., Péquignot D., 1995, A&A in press
Bowen I.S., 1928, ApJ 67, 1
Bowen I.S., 1960, ApJ 132, 1
Burbidge E.M., Burbidge G.R., Fowler W.A., Hoyle F., 1957, Rev. Mod. Phys. 29, 547
Busso M., Beglio L., Gallino R., Lambert D.L., Raiteri C.M., Smith V.V., 1993, in *Nuclei in the Cosmos*, ed. F. Käppeler and K. Wisshak, IOP, p. 515
Busso M., Gallino R., Lambert D.L., Raiteri C.M., Smith V.V., 1992, ApJ 399, 218
Iben I., Jr., 1991, in *Evolution of stars: the photospheric abundance connection*, ed. G. Michaud and A. Tutukov, Kluwer, Dordrecht, p. 257
Kaler J.B., Aller L.H., Czyzak S.J., Epps H.W., 1976, ApJS 31, 163
Käppeler F., Beer H., Wisshak K., 1989, Rep. Prog. Phys. 52, 945
Keyes C.D., Aller L.H., Feibelman W.A., 1990, PASP 102, 59
Lambert D.L., 1991, in *Evolution of stars: the photospheric abundance connection*, ed. G. Michaud and A. Tutukov, Kluwer, Dordrecht, p. 299
Péquignot D., Baluteau J.-P., 1988, A&A 206, 298
Péquignot D., Baluteau J.-P., 1994, A&A 283, 593
Thackeray A.D., 1975, MNRAS 172, 49P
Thackeray A.D., 1977, Mem. Roy. Astron. Soc. 83, 1
Utsumi K., 1985, in *Cool stars with excesses of heavy elements*, ed. H. Jaschek and P.C. Keenan, Dordrecht, Reidel, p.243

RADIAL ABUNDANCE GRADIENTS IN THE GALACTIC DISK: OBSERVATIONS AND THEORY

W. J. Maciel
Instituto Astronômico e Geofísico da USP
Av. Miguel Stefano 4200, 04301-904 São Paulo SP
e-mail: maciel@iag.usp.ansp.br

Abstract

The radial abundance gradients observed in the disks of the Galaxy and other spiral galaxies are reviewed, in the context of the chemical evolution of these galaxies. A detailed account is given of the main observational evidences for the gradients, both in the Galaxy and other galaxies, on the basis of observations of HII regions, planetary nebulae, and stars. The origin of the gradients is discussed according to the main physical processes proposed so far. The so-called "simple model" is invoked in order to obtain some physical insight on the origin of the gradients.

1 Introduction

Radial abundance gradients in the disks of spiral galaxies are made evident from observations of photoionized nebulae (HII regions and planetary nebulae) and stars in the Galaxy and in other neighbouring galaxies. They have been observed for several chemical elements, and their presence can be considered as an established fact, despite some inconsistencies and incompleteness of the results. Therefore, these gradients have become an additional constraint to models of the chemical evolution of galaxies, in the same sense as the age-metallicity relation or the metallicity distribution of the G-dwarfs.

In this paper, we stress on the importance of abundance gradients in the framework of the chemical evolution of the Galaxy and galactic evolution in general (section 2). The main observational evidences for radial gradients are reviewed in section 3. The models proposed to explain the gradients are briefly discussed in section 4, especially the so-called "simple" model in its original form and including later developments, in order to stress the physical insight that follows from its application.

Previous reviews on abundance gradients include Peimbert (1979), Pagel and Edmunds (1981), Shaver et al. (1983), Güsten and Mezger (1983), Díaz (1989), Dinerstein (1990) and Pagel (1992). Recent work on chemical evolution models both for the Galaxy and spiral galaxies in general are discussed and referenced by Audouze and Tinsley (1976), Pagel (1979, 1987, 1991), Tinsley (1980), Twarog (1985), Güsten (1986), and Rana (1991).

2 Abundance gradients and chemical evolution

Galactic evolution generally comprises the *dynamical evolution*, the *chemical evolution*, and the *evolution of the photometric properties* (cf. Tinsley 1980). Although frequently considered separately, these aspects basically refer to the same phenomenon - galaxy evolution - so that the usual treatment is largely a matter of convenience. The interplay of dynamical and chemical processes is made clear for example by the well known two phase evolution of the Galaxy, which gave origin to the spheroidal and disk components, respectively. Or, as confirmed by recent models, by the influence of infall from the halo and radial flows within the disk.

The structure of chemical evolution models includes a series of characteristics sometimes called "ingredients" (cf. Pagel 1979, 1987, 1991, 1992). In the following we will consider the most important of these ingredients, emphasizing the application to the solar neighbourhood and the galactic disk, where radial abundance gradients are observed.

(a) Initial conditions

These refer to the pregalactic - often primordial - abundances. The main species considered are D, ^{3}He, ^{4}He, and ^{7}Li, and the observed abundances must be interpreted in terms of galactic evolution effects in order to determine primordial values, thus providing a link with theoretical models. Of particular importance is the ^{4}He pregalactic abundance, which is claimed to be known to the third decimal place (Pagel et al. 1992; Pagel and Kazlauskas 1992; Chiappini and Maciel 1994). Recent determinations, based both on helium vs. oxygen and helium vs. nitrogen correlations in galactic and extragalactic HII regions and planetary nebulae, indicate that the He pregalactic abundance by mass is $Yp = 0.233 \pm 0.003$ (Chiappini and Maciel 1994). A related parameter is the helium to metals enrichment ratio, $\Delta Y/\Delta Z = 5.2 \pm 1.1$, according to the same source. It is interesting to note that this ratio does not seem to be very sensitive to the evolutionary stage of the data, implied by a metallicity range from the metal poor blue compact galaxies to the type IIb planetary nebulae. This is an indication that these objects (and host galaxies) have undergone similar evolutionary processes (cf. Maciel 1988; Chiappini and Maciel 1994).

The heavy element abundance by mass is originally small, $Z \approx 0$, but very often evolution models include some kind of initial enrichment, which brings the metal abundances to values up to [Fe/H] $\approx$ -2 to -3, where [Fe/H] is the logarithmic difference of the iron abundance by number of atoms relative to the solar abundance.

(b) The initial mass function (IMF)

From the pioneering work of Salpeter (1955) to the extensive study by Scalo (1986), this is a relatively well known function of the stellar mass, derived from present-day luminosity function and a mass-luminosity relation. However, there is a long standing controversy on whether *time* and *space* variations are important. Results from HII regions, HII galaxies, and stellar clusters are consistent with some mild variations of this function. On the other hand, a dip in the luminosity function can be interpreted as an evidence for a bimodal IMF.

(c) The star formation rate (SFR)

This is a rather complex function, which is still largely unknown, basically because the physical processes involved in stochastic star formation are not adequately known (cf. Larson 1977). Therefore, different approximations are frequently used. From the work of Schmidt (1959), a dependence with some power n of the surface gas density of interstellar material is often assumed, SFR $\propto g^n$. Current work include self-regulating, bimodal and non-monotonic time dependence of the SFR, which is supported by growing evidence on starburst galaxies and in the solar neighbourhood itself.

(d) Nucleosynthesis yields

A basic ingredient of chemical evolution models is the stellar yield, or the fraction of processed material returned to the interstellar medium relative to that stored in stars and remnants. The determination of the yields requires detailed nucleosynthetic calculations involving stars in the mass range $M \simeq 0.1-100 M_{\odot}$. Basically, low mass stars ($M < 1 M_{\odot}$) live longer than the age of the Galaxy, and do not return a significant amount of mass to the interstellar medium. Intermediate mass stars ($1 M_{\odot} < M < 10 M_{\odot}$) eject planetary nebula material that has had some secondary processing, which implies some enrichment in He, N and C, but not of oxygen and other heavy metals. The massive ($M > 10 M_{\odot}$) stars eject the primary nucleosynthesis products, built from H and He during stellar evolution. Elements such as O, Ne and Ar are produced this way.

The basic equations are given by Tinsley (1980), and recent results have been obtained by Henry (1990) and Köppen and Arimoto (1991). These results depend strongly on the adopted mass limits, the IMF/SFR functions, and also on physical processes and parameters of nuclear reaction rates, opacities, mass loss, convection, etc., apart from the adopted chemical composition.

(e) Contamination processes

These may include *infall* of largely unenriched gas from the halo, as well as *radial flows* into the concentrical cylindrical zones in the disk itself. The inclusion of these processes may account for most of the constraints (see below), but generally introduces several parameters such as the metallicity of the infalling gas or the velocity of the gas flows, which are difficult to determine observationally, so that the problem of uniqueness of solutions still remains (cf. Tosi 1988).

(f) Constraints

• *Stellar populations:* These include stars and gas observed in the galactic halo, thick disk, thin disk, and bulge, as defined by their chemical composition, space distribution, and kinematics. As a consequence, important relationships such as the metallicity distribution are often different for each of these populations. For example, the average scale height from the galactic plane increases according to the sequence of HII regions and planetary nebulae of types I (population I old), II (population I old), III (population II intermediate) and IV (population II extreme), indicating the population differences of these objects (cf. Maciel and Dutra 1992).

• *Metallicity distribution:* This is the main constraint to the chemical evolution models, which originated the (in)famous G-dwarf problem, namely, the lack of low metallicity stars as compared to the predictions of the simple model (cf. Pagel 1991). Recent work is able to solve this problem, at least partially, with widely differing processes, such as infall, radial flows, presence of remnants, as well as modifications of the structure of the simple model ("bells and whistles"). Also, the observational data itself is subject to some controversy, as the adoption of a expansion law for the stars in the z-direction can alter the number of stars in a given metallicity bin, so that the general metallicity distribution is modified.

• *The age-metallicity relation:* The "metallicity index" [Fe/H] is often a convenient way to measure stellar abundances other than H and He, in contrast with the oxygen abundances (log O/H + 12) better determined for gaseous nebulae. Adopting [Fe/H] as representative of the stellar metallicity at a given time, several age-metallicity relations have been proposed for the disk, all of which include a relatively steep initial metallicity increase followed by a slower, nearly constant plateau (cf. Twarog 1980; Nissen et al. 1985).

• *The [O/Fe] vs. [Fe/H] relation:* As discussed by several papers (cf. Pagel 1991), some heavy elements display variations with the [Fe/H] ratio, which places important constraints on chemical evolution models. The ratio [O/Fe] vs. [Fe/H] is particularly important in this respect, and a different behaviour is observed for older, subsolar objects, and high metallicity, younger stars (cf. Nissen 1992).

• *Radial gradients:* Radial gradients are the most important large scale trend in the galactic disk, and are probably related to the distribution of gas and stars in the Galaxy. In the following section, a detailed account of the observational evidences will be given, followed by a brief discussion of the main theoretical models.

3 Observational evidence of abundance gradients

(a) Spiral galaxies

Radial abundance gradients in spiral galaxies are well established, at least for the ratios O/H, N/H and S/H (cf. Villa-Costas and Edmunds 1992, 1993). The first study on the systematic variations in the spectra of HII regions located near or far from the galaxy centre was that by Aller (1942), who have considered 18 HII regions in M33. It was noted that the ratio [OIII]/Hβ increased with the distance ρ to the centre. A more detailed study was made later by Searle (1971) on several galaxies like M33, M51, M101, etc., where the excitation gradient was further observed. Among the possibilities to explain the gradient, Searle (1971) assumed that the cooling rates were higher in the inner regions, so that the electron temperature was lower there, and the oxygen abundance was higher. This would explain the higher excitation seen in the outer HII regions, and predict an electron temperature gradient in the same direction as the excitation gradient. Later

work developed and extended these ideas (Shields 1974; Shields and Searle 1978), and gradients of O/H, and N/H were determined, remaining some doubts on a S/O gradient. A temperature gradient of the order of 500 K/kpc was quoted in the last reference.

The past five years have witnessed an increase in the amount and quality of the data, especially with the advent of CCD detectors. Not only the number of HII regions observed in a given galaxy increased (cf. Vilchez et al. 1988). but also the spectral range, which produced new data on elements such as Ne, Ar and S. Coupled with HII region model or empirical calculations, these investigations led to well defined abundance gradients, which also include some data from supernova remnants, apart from HII regions. Newly determined O/H gradients have been given recently by Kennicutt et al. (1993) and Zaritsky et al. (1994), with average slopes of -0.10 dex/kpc. It seems that all galaxy types can have rather steep gradients *except* pure barred spirals, which seem to show small or no gradients at all. A recent work on environmental effects on abundance gradients in galaxies in the Virgo cluster has produced some very interesting results, as shown in figure 1 for O/H (Henry et al. 1992, 1994), to which we will return later. Here we have used in the abscissa the quantity ρ_{eff}, the effective galaxy radius, that is, the radius at which half of the optical emission is contained.

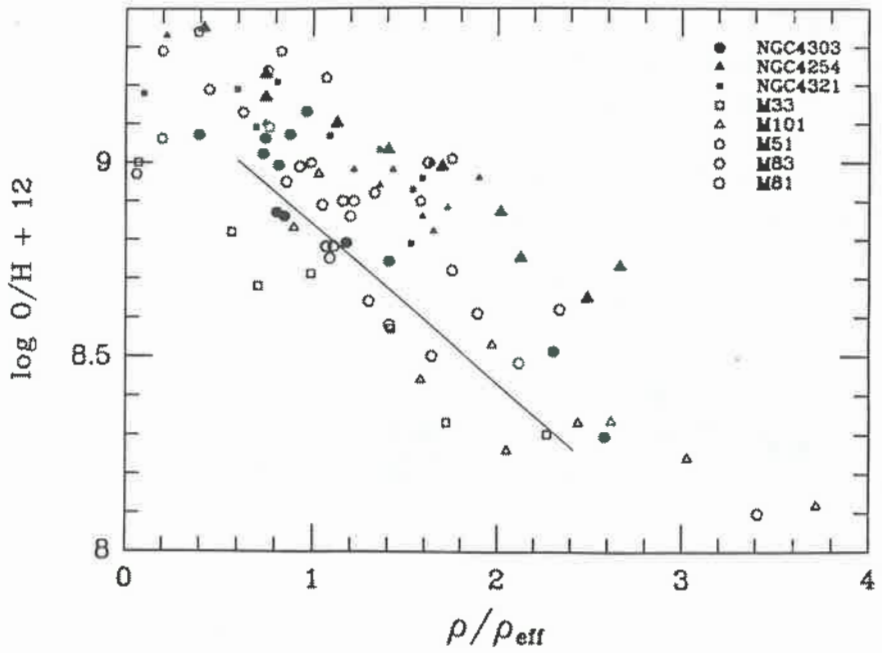

Figure 1 - O/H gradients for spiral galaxies (Henry et al. 1994). The PN galactic gradient is also plotted (straight line).

The S/H and S/O ratios have been subject to some controversy, especially regarding the existence of a S/O gradient in spiral galaxies. An anticorrelation of this ratio with O/H has been reported (cf. Díaz et al. 1991), which can be seen for the 5 HII regions studied in the high metallicity spiral M51. In principle, several HII regions should be selected at different distances from the centre, but in practice those close to the nucleus

are difficult to measure, either due to the nuclear contamination, or to the fact that the abundances are higher, so that the electron temperature and the excitation of the nebulae are too low. As shown by Díaz et al. (1991), this anticorrelation is apparent in the merged plot including the Galaxy, M33, M101 and M51. However, this does not necessarily mean that S/O decreases as ρ increases, since the individual galaxies have different metallicities. On the other hand, the evidence for an S/H gradient in external galaxies is becoming more clear, as shown by Vilchez et al. (1988). This can be associated with the negative results for an S/O gradient, suggesting that the S/H gradient is similar to the O/H one (see also Díaz 1989).

The shape of the gradients is still subject to discussion. Some flattening in the outer regions of the spiral disks has been proposed (Díaz 1989; Vilchez et al. 1988), but recent work seems to indicate an exponential gradient with constant slope (Henry and Howard 1994).

(b) The Galaxy: HII regions

As it is often the case, evidences for large scale trends in the Galaxy are more difficult to understand than for nearby, face on spirals. The basic evidence for abundance gradients in the Galaxy comes from direct oxygen data and indirect electron temperature gradient determinations in galactic HII regions. The basic reference is Shaver et al. (1983), where reasonable gradients for the O/H, He/H and N/H ratios were established, amounting to about - 0.06 dex/kpc. More recent work on the oxygen gradient from HII regions are given by Edmunds (1992), and the derived gradient is of the order of -0.07 dex/kpc (figure 2, squares).

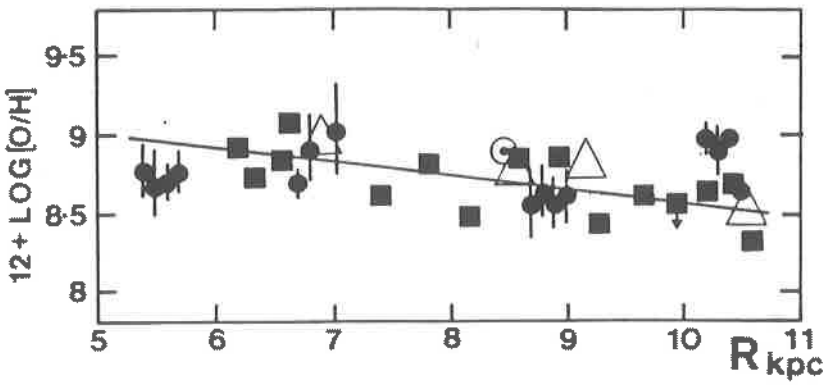

Figure 2 - The galactic O/H gradient from HII regions and stars (Edmunds 1992).

Galactic HII regions also show evidences for an electron temperature gradient, observed from radio recombination lines (Churchwell and Walmsey 1975). Although other processes may affect the nebular temperatures, such as the stellar effective temperatures, both HII and planetary data suggest similar gradients, which are further consistent with the abundance gradients.

(c) The Galaxy: planetary nebulae

Evidences of abundance gradients from planetary nebulae have been hampered in the past basically due to (i) the existence of a mixed population of planetary nebulae in the Galaxy, and (ii) the lack of a reliable distance scale that could be applied to a statistically large number of nebulae. Earlier work include D'Odorico et al. (1976) and Aller (1976) and references therein. The first detailed determination of abundance gradients of the main chemical elements in galactic planetary nebulae was given by Faúndez-Abans and Maciel (1986, 1987), where it was established that O, S, Ne and Ar had gradients similar to the HII region gradient. These results were confirmed by the determination of an electron temperature gradient of the order of 600 K/kpc, from the same data, which was interpreted as a mirror image of the abundance gradients (Maciel and Faúndez-Abans 1985). This work has been completely revised and expanded to include a larger sample of nebulae and chemical elements (Maciel and Köppen 1994; Maciel and Chiappini 1994). The main results have been recently reviewed (Maciel 1994), and can be summarized as follows: all disk nebula, which comprise Peimbert types I, II and III, display measurable gradients of the order of -0.04 to -0.07 dex/kpc. The small differences in the gradients have been interpreted in terms of a chemical evolution model, for the elements that are *not* produced by the progenitors of the central stars, namely O, S, Ne, Ar, and Cl (figure 3, from Maciel and Köppen 1994). In other words, the gradients have become steeper with time, so that type I planetary nebulae have generally steeper gradients than type II, and these relative to type III. Therefore, the planetary nebula gradients that best resemble those of HII regions are those derived from type I and II objects. This can be seen in figure 4, where we plot the O/H gradient for type II objects using two different distance scales. The first panel uses basically the distance scale developed by Maciel (1984), while the second uses the new Cahn et al. (1992) distance scale. The gradients are essentially the same, namely - 0.06 dex/kpc, and should be compared to the HII region gradient of figure 2. A similar conclusion can be observed in figure 1, where we have included the type II nebulae (straight line) from Maciel and Köppen (1994) with the galaxies studied by Henry et al. (1994). We have used $\rho_{eff} = 5.98$ kpc for the Galaxy (Henry et al. 1992, de Vaucouleurs and Pearce 1978). An idea of the intrinsic dispersion of these plots can be obtained by studying a ratio such as Ne/O. This ratio is expected to be constant in planetary nebulae, so that a comparison with the O/H, etc. gradients shows clearly that the gradients are real.

Another confirmation of the gradients can be observed in figure 5, where we have plotted the electron temperatures of type II planetary nebulae in the sample of Maciel and Köppen (1994). The derived gradient is now of the order of 500 K/kpc, somewhat lower than the original result by Maciel and Faúndez-Abans (1985), and closer to the HII region value.

Regarding the elements that *are* produced during the evolution of the progenitor stars, namely, He, N and C, the situation is less clear (Maciel and Chiappini 1994). "Raw" abundances for N and C seem to suggest similar gradients as for O/H, etc., but detailed calculations must take into account the contamination of the nebular gas by the central star (cf. Chiappini and Maciel 1994).

Finally, although independent analysis have confirmed the existence of radial gradients from planetary nebulae (cf. Acker et al. 1992; Köppen et al. 1991), the separation of the PN classes still produces some inconsistencies (cf. Pasquali and Perinotto 1993), as well as the use of different classification systems, which are sometimes difficult to compare (cf. Amnuel 1993).

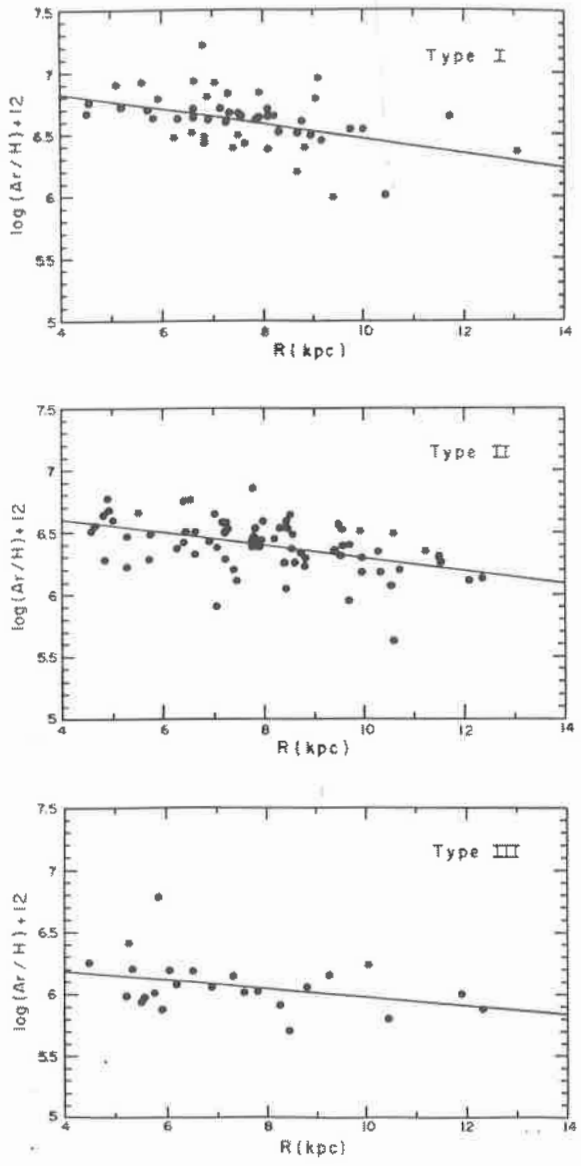

Figure 3 - The Ar/H gradient from galactic PN (Maciel and Köppen 1994)

(d) The Galaxy: stars

Other indicators than photoionized nebulae also give some information on galactic abundance gradients, such as *cepheid variables*, *supergiants* (cf. Pagel 1985, 1992), and *open cluster stars* (cf. figure 2, triangles). Some discrepancies are apparent from deep

surveys of *red giants* (Neese and Yoss 1988; Lewis and Freeman 1989), and *B stars* in young associations (Fitzsimmons et al. 1990; cf. figure 2, dots). which seem to indicate small or no measurable gradients. Some of these results may be explained by other causes such as the time evolution of the gradients (see section 4), so that the general conclusion on the existence of the gradients remain positive.

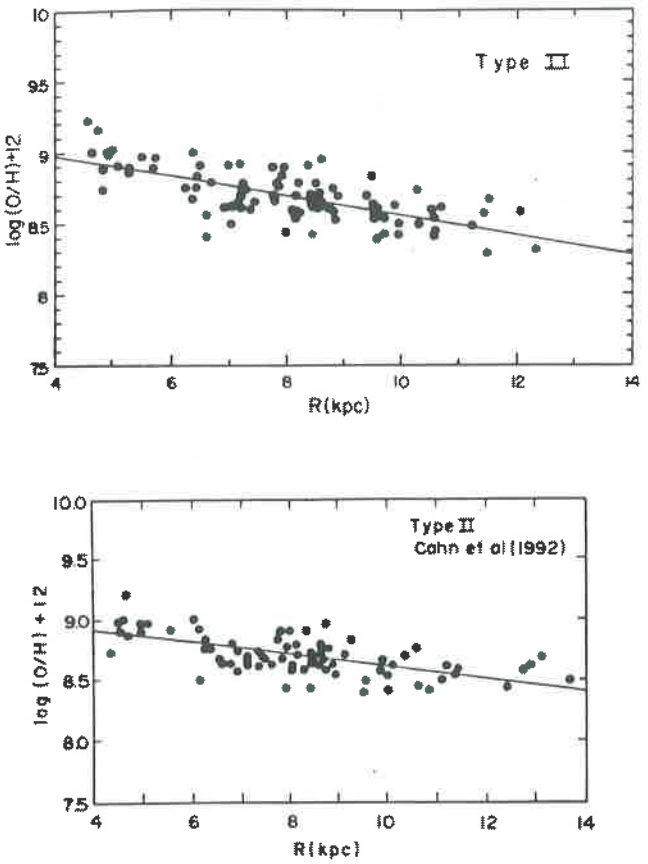

Figure 4 - The O/H gradient for type II PN with two distance scales (Maciel and Köppen 1994).

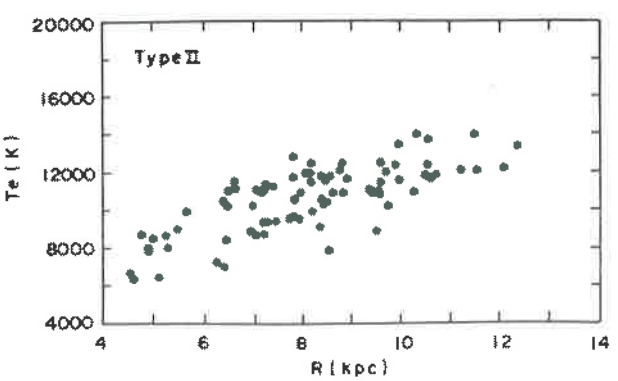

Figure 5 - The electron temperature gradient from type II PN.

4 Theory of abundance gradients

(a) Causes of abundance gradients

The connection of the abundance gradients with the chemical evolution of the host galaxy was recognized from the earliest studies (cf. Shields 1974). However, the physical processes causing the abundance variations are not well determined, despite the large number of possibilities in the literature. According to recent reviews (cf. Pagel 1992), about half a dozen possibilities can be considered, which in practice can be increased, as some of the hypotheses involved can be interchanged:

- Variations in the gas distribution in isolated concentric zones;
- Variations in the distribution of the ratio gas/stars
- Variable or bimodal IMF
- Infall of unprocessed material
- Ejection of processed material in galactic winds, etc.
- Variable yields
- Variable or self regulated star formation

In view of the multiplicity of models and associated parameters used to explain the abundance gradients, it is perhaps more instructive to investigate some consequences of the simple model of chemical evolution (cf. Searle and Sargent 1972: Tinsley 1980).

(b) An application of the simple model

In the framework of the simple model, we will assume an interstellar medium of uniform composition, no infall and the instant recycling approximation (IRA). Calling y the metal yield, the heavy element abundance Z is given as a simple function of the gas fraction $\mu = M_g/M$ (cf. Tinsley 1980; Maciel 1992), where M_g is the total surface gas mass and M is the total (gas + stars) mass:

$$Z = y \ln\mu^{-1} = y \ln(1 + \frac{M_s}{M_g}) \tag{1}$$

where M_s is the mass in stars. Therefore, we can write

$$\frac{dZ}{dR} = \frac{d}{dR}[y \ln(1 + \frac{M_s}{M_g})] \tag{2}$$

so that a convenient radial dependence of the yield or the gas to star mass ratio could produce abundance gradients similar to the observations. Both have been proposed in the literature, but let us assume for a while that the yield is constant. According to Pagel (1979), a larger fraction of the gas has turned into stars in the inner regions of

the Galaxy as compared to the outer regions, which implies abundance variations in the right direction. From the calibration of Maciel (1992), we have

$$1 + \frac{M_s}{M_g} \simeq C \exp(-\alpha R) \tag{3}$$

where ln $C \simeq 4.6$ and $\alpha \simeq 0.3$. Adopting $Z = 26$ O/H for type II planetary nebulae (cf. Maciel 1992; Chiappini and Maciel 1994), we can calculate from (1) the oxygen abundances as a function of R for a given yield, as shown in figure 6 (Maciel 1992). The curves are labelled 1 to 6 according to the yield, from $y = 0.002$ to $y = 0.012$. It can be seen that the agreement is better for $0.004 < y < 0.010$, and some variation of the yield itself is implied from the data points, unless some flattening occurs, as proposed for some galaxies (cf. Díaz 1989). These yield values are close to the "canonical" value of 0.01, and agree with recent determinations of the oxygen yield for reasonable IMFs (Köppen and Arimoto 1991).

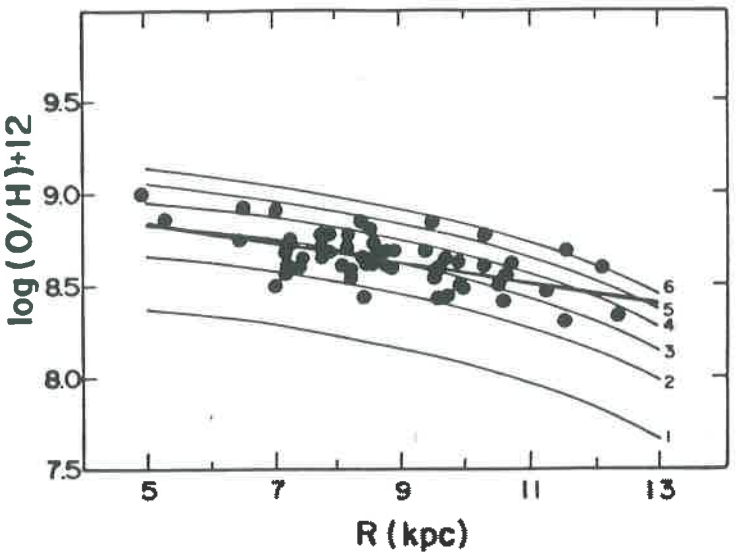

Figure 6 - Results from the simple model applied to the O/H gradient (Maciel 1992).

How can we he sure about the gas/stars variations implied by equation (3)? this is a difficult question, which is confirmed by some recent work both on the Galaxy and in other galaxies. Although the gas surface density cannot be considered constant throughout the disk (it decreases as R increases), the stellar mass decreases *faster*, so that, at least qualitatively, equation (3) holds. This can be seen from the recent calculations by Henry et al. (1992) for NGC 4303. As can be seen from figure 7, the HI gas density does not change appreciably in the inner parts of the galaxy, while the H_2 density steadily decreases, so that the total gas density also decreases. From the total disk mass variation given, the *stellar* mass can be obtained, which shows that the ratio M_s/M_g decreases as ρ increases. From the data on this galaxy, we can determine the ratio $1/\mu = M/M_g$, which is also plotted against ρ/ρ_{eff} in the figure (broken line). Also, we can calculate $1/\mu$ for the simple model from equation (3), adopting again $\rho_{eff} = 5.98$ kpc for the

Galaxy. The results are also plotted (solid line), showing that a steady decrease in the ratio $1/\mu$ is observed, although not as strong as implied by our exponential relation for the inner disk.

Apart from the yield values and implicit radial variations. other conclusions can be drawn from the application of the simple model to the observed gradients, namely, some information on the stellar mass above which black hole formation takes place, and possible variations of the IMF.

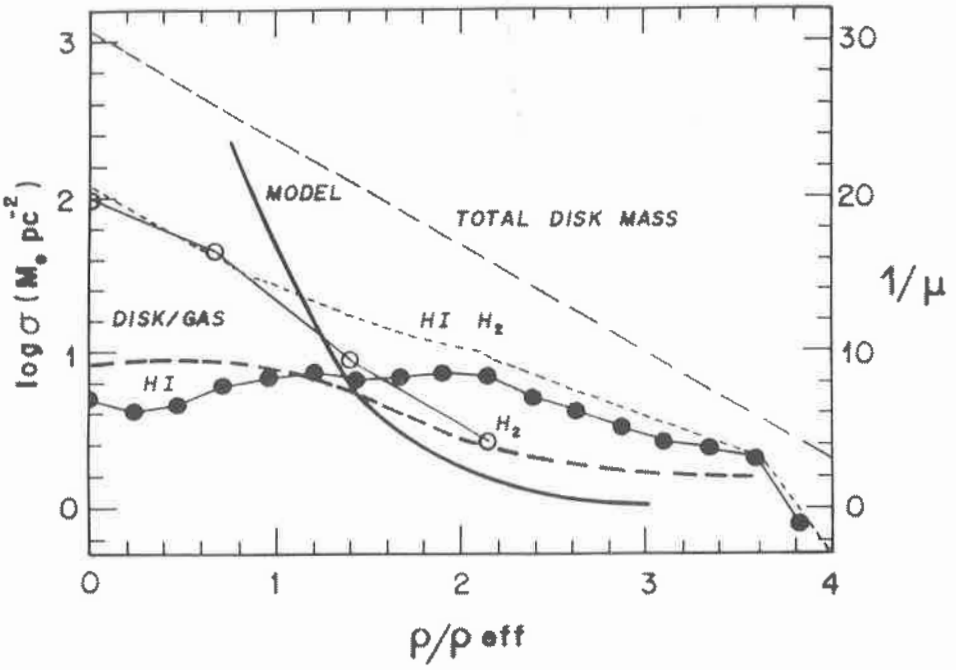

Figure 7 - Disk surface density as a function of the distance to the centre for NGC 4303 (Henry et al. 1992). Results from the simple model as applied to the Galaxy are also included.

(c) Time variations of the gradients

Some recent models have been calculated for the chemical evolution of the Galaxy, which include the effects of infall, radial flows and different gas density dependences of the star formation rate (Götz and Köppen 1992; Köppen 1994). According to these models, the existence of the radial gradients can be predicted, and also their temporal variations. Recent models by Köppen (1994) show that the initial gradient is determined by radial variations of the metal yield and the star formation timescale, and the dependence of the SFR on the gas density. Later on, this gradient can be modified by radial gas flows, depending on the infall timescale. For convenient values of the radial flow velocities (~ 1 km/s), the gradients are expected to steepen with time. This can be seen in figure 8 (Maciel and Köppen 1994), and places some important restrictions on the SFR, in the sense that the index n of the density dependence should be $1.5 > n > 1.0$. Some similar results have been obtained with the chemical evolution models reported by Mollá et al.

(1990). Their results indicate a definite increase of the O/H gradient in the last few Gyr, from calculations of three galactic rings located at different distances from the centre.

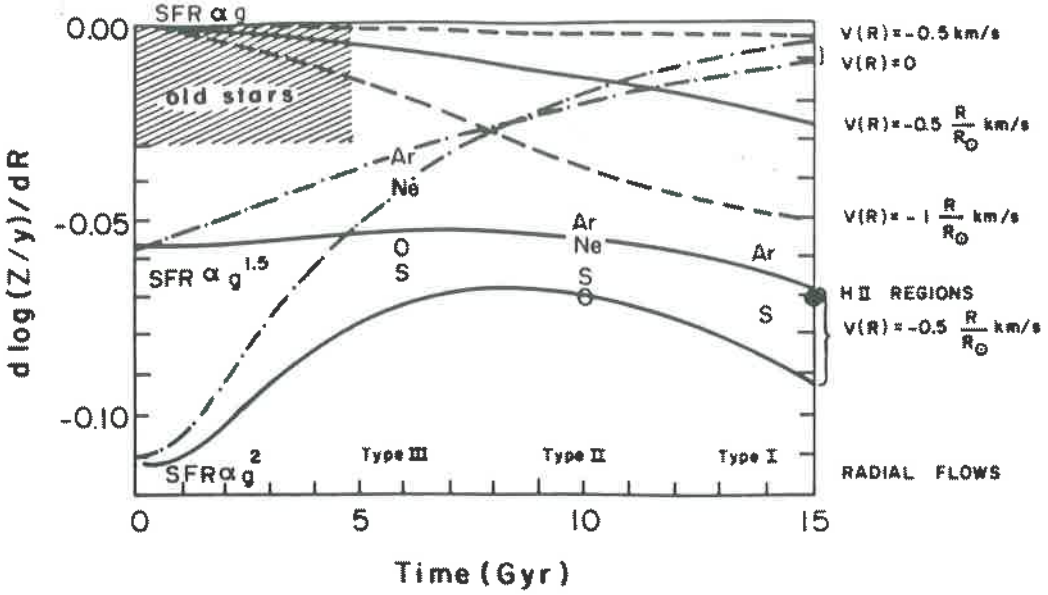

Figure 8 - Time variations of the abundance gradients (Maciel and Köppen 1994).

Acknowledgements

This work was partially supported by CNPq, FAPESP, and SAB.

References

Acker, A., Köppen, J., Stenholm, B., Jasniewicz, G.: 1992, *IAU Symposium 149*, ed. B. Barbuy, A. Renzini, Kluwer, Dordrecht, p. 383

Aller, L.H.: 1942, *Astrophys. J.* **95**, 52

Aller, L.H.: 1976, *Publ. Astron. Soc. Pacific* **88**, 574

Amnuel, P.R.: 1993, *Monthly Not. Roy. Astron. Soc.* **261**, 263

Audouze, J., Tinsley, B.M.: 1976, *Ann. Rev. Astron. Astrophys.* **14**, 43

Cahn, J.H., Kaler, J.B., Stanghellini, L.: 1992, *Astron. Astrophys. Suppl.* **94**, 399

Chiappini, C.M.L., Maciel, W.J.: 1994, *Astron. Astrophys.* (in press)

Churchwell, E., Walmsley, C.M.: 1975, *Astron. Astrophys.* **38**, 451

De Vaucouleurs, G., Pearce, W.D.: 1978, *Astron. J.* **83**, 1163

Díaz, A.I.: 1989, in *Evolutionary phenomena in galaxies*, ed. J.E. Beckman, B.E.J. Pagel, Cambridge, p. 377

Díaz, A.I., Terlevich, E., Vilchez, J.M., Pagel, B.E.J., Edmunds, M.G.: 1991, *Monthly Not. Roy. Astron. Soc.* **253**, 245

Dinerstein, H.L.: 1990, in *The interstellar medium in galaxies*, ed. H.A. Thronson, J.M. Shull, Kluwer, Dordrecht, p. 257

D'Odorico, S., Peimbert, M., Sabbadin, F.: 1976, *Astron. Astrophys.* **47**, 341
Edmunds, M.G.: 1992, in *Elements and the cosmos*, ed. M.G. Edmunds, R.J. Terlevich, Cambridge, p. 289
Faúndez-Abans, M., Maciel, W.J.: 1986, *Astron. Astrophys.* **158**, 228
Faúndez-Abans, M., Maciel, W.J.: 1987, *Astrophys. Space Sci.* **129**, 353
Fitzsimmons, A., Brown, P.T.F., Dufton, P.L., Lennon, D.J.: 1990, *Astron. Astrophys.* **232**, 437
Götz, M., Köppen, J.: 1992, *Astron. Astrophys.* **262**, 455
Güsten, R.: 1986, in *Spectral evolution of galaxies*, ed. C. Chiosi, A. Renzini, Reidel, Dordrecht, p. 449
Güsten, R., Mezger, P.G.: 1983, *Vistas Astron.* **26**, 159
Henry, R.B.C.: 1990, *Astrophys. J.* **356**, 229
Henry, R.B.C., Pagel, B.E.J., Lassiter, D.F., Chincarini, G.L.: 1992, *Monthly Not. Roy. Astron. Soc.* **258**, 321
Henry, R.B.C., Pagel, B.E.J., Chincarini, G.L.: 1994, *Monthly Not. Roy. Astron. Soc.* **266**, 421
Henry, R.B.C., Howard, J.W.: 1994, *Astrophys. J.* (in press)
Kennicutt, R.C., Oey, M.S., Zaritsky, D., Huchra, J.P.: 1993, *Rev. Mex. Astron. Astrophys.* **27**, 21
Köppen, J.: 1994, *Astron. Astrophys.* **281**, 26
Köppen, J., Acker, A., Stenholm, B.: 1991, *Astron. Astrophys.* **248**, 197
Köppen, J., Arimoto, N.: 1991, *Astron. Astrophys. Suppl.* **87**, 109 (erratum: **89**, 420)
Larson, R.: 1977, in *The evolution of galaxies and stellar populations*, ed. B.M. Tinsley, R.B. Larson, Yale, p. 97
Lewis, J.R., Freeman, K.C.: 1989, *Astron. J.* **97**, 139
Maciel, W.J.: 1984, *Astron. Astrophys. Suppl.* **55**, 253
Maciel, W.J.: 1988, *Astron. Astrophys.* **200**, 178
Maciel, W.J.: 1992, *Astrophys. Space Sci.* **196**, 23
Maciel, W.J.: 1994, *VII Escola Avançada de Astrofísica*, IAG/USP
Maciel, W.J., Chiappini, C.M.L.: 1994, *Astrophys. Space Sci.* (in press)
Maciel, W.J., Dutra, C.M.: 1992, *Astron. Astrophys.* **262**, 271
Maciel, W.J., Faúndez-Abans, M.: 1985, *Astron. Astrophys.* **149**, 365
Maciel, W.J., Köppen, J.: 1994, *Astron. Astrophys.* **282**, 436
Mollá, M., Díaz, A.I., Tosi, M.: 1990, in *Chemical and dynamical evolution of galaxies*, ed. F. Ferrini, J. Franco, F. Matteucci, ETS Editrice, Pisa, p. 577
Neese, C.L., Yoss, K.M.: 1988, *Astron. J.* **95**, 463
Nissen, P.E.: 1992, in *Elements and the cosmos*, ed. M.G. Edmunds, R.J. Terlevich, Cambridge, p. 110
Nissen, P.E., Edvardsson, B., Gustafsson, B.: 1985, in *Production and distribution of the CNO elements*, ed. I.J. Danziger, F. Matteucci, K. Kjär, ESO, Garching, p. 131
Pagel, B.E.J.: 1979, in *Stars and star systems*, ed. B.E. Westerlund, Reidel, Dordrecht, p. 17
Pagel, B.E.J.: 1985, in *Production and distribution of the CNO elements*, ed. I.J. Danziger, F. Matteucci, K. Kjär, ESO, Garching, p. 155

Pagel, B.E.J.: 1987, in *The Galaxy*, ed. G. Gilmore, B. Carswell. Reidel, Dordrecht, p. 341
Pagel, B.E.J.: 1991, in *IUPAP conference on primordial nucleosynthesis and evolution of early universe*, ed. K. Sato, Kluwer
Pagel, B.E.J.: 1992, *IAU Symp. 149*, ed. B. Barbuy, A. Renzini. Kluwer, Dordrecht, p. 133
Pagel, B.E.J., Edmunds, M.G.: 1981, *Ann. Rev. Astron. Astrophys.* **19**, 77
Pagel, B.E.J., Kazlauskas, 1992, *Monthly Not. Roy. Astron. Soc.* **256**, 49p
Pagel, B.E.J., Simonson, E.A., Terlevich, R.J, Edmunds, M.G.: 1992, *Monthly Not. Roy. Astron. Soc.* **255**, 325
Pasquali, A., Perinotto, M.: 1993, *Astron. Astrophys.* **280**, 581
Peimbert, M.: 1979, *IAU Symp. 84*, ed. W.B. Burton, Reidel, Dordrecht, p. 307
Rana, N.C.: 1991, *Ann. Rev. Astron. Astrophys.* **29**, 129
Salpeter, E.E.: 1955, *Astrophys. J.* **121**, 161
Scalo, J.M.: 1986, *Fund. Cosm. Phys.* **11**, 1
Schmidt, M.: 1959, *Astrophys. J.* **129**, 243
Searle, L.: 1971, *Astrophys. J.* **168**, 32
Searle, L., Sargent, W.L.W.: 1972, *Astrophys. J.* **173**, 25
Shaver, P.A., McGee, R.X., Newton, L.M., Danks, A.C., Pottasch. S.R.: 1983, *Monthly Not. Roy. Astron. Soc.* **204**, 53
Shields, G.A.: 1974, *Astrophys. J.* **193**, 335
Shields, G.A., Searle, L.: 1978, *Astrophys. J.* **222**, 821
Tinsley, B.M.: 1980, *Fund. Cosm. Phys.* **5**, 287
Tosi, M.: 1988, *Astron. Astrophys.* **197**, 33
Twarog, B.A.: 1980, *Astrophys. J.* **242**, 242
Twarog, B.A.: 1985, *IAU Symp. 106*, ed. H. van Woerden, R.J. Allen, Reidel, Dordrecht, p. 587
Vilchez, J.M., Pagel, B.E.J., Díaz, A.I., Terlevich, E., Edmunds. M.G.: 1988, *Monthly Not. Roy. Astron. Soc.* **235**, 633
Villa-Costas, M.B., Edmunds, M.G.: 1992, *Monthly Not. Roy. Astron. Soc.* **259**, 121
Villa-Costas, M.B., Edmunds, M.G.: 1993, *Monthly Not. Roy. Astron. Soc.* **266**, 199
Zaritsky, D., Kennicutt, R.C., Huchra, J.P.: 1994, *Astrophys. J.* **420**, 87

ANISOTROPY IN ASTROPHYSICS

N.O.Santos
Observatório Nacional CNPq
Departamento de Astrofísica
rua General José Cristino 77
20921 Rio de Janeiro, Brazil

Abstract

Some physical processes ranging from primordial gas to supermassive systems where local anisotropies can develop are presented. The influence of anisotropy in analytical models, dynamical instability, Jeans' mass and cracking of self-gravitating systems with astrophysical importance are discussed. We show that anisotropy can change dramatically the evolution of self-gravitating objects compared to systems where only isotropic processes are allowed.

Introduction

Local isotropy, meaning local equal principal stresses, is a common assumption in astrophysics for studying the evolution of self-gravitating objects. However strong theoretical evidence suggests that for certain density ranges different kinds of physical phenomena may take place, giving rise to local anisotropy. We shall discuss now some of these processes that intervene in astrophysical scenarios.

The pioneering work on these processes was done by Jeans (1922) where he considered local anisotropies originated by anisotropic velocity distribution in spherical galaxies. More recent results for these same processes were obtained by Binney (1982). Other low density astrophysical scenarios producing local anisotropies have been studied in collisionless systems by Michie (1963), Gliddon (1966), Kent & Gunn (1982), Mellot (1983), Binney & Tremaine (1987) and Guddeford (1991). Anisotropies appearing in galactic halos of fermionic dark matter have been considered by Madsen & Epstein (1985), Ralston (1989) and Ralston & Smith (1991).

For highly dense systems locally anisotropic configurations can occur for exotic phase transitions during gravitational collapse as studied by Itoh (1970), Migdal (1971), Sawyer (1972), Collins & Perry (1975) and Sokolov (1980). Particularly noticeable are the transitions to a pion condensed state producing anisotropies, which softens the equation of state, considered by Hartle, Sawyer & Scalapino (1975), providing an enormous release of energy, Sawyer & Soni (1977), which have important implications in the evolution of collapsing configuration. Sawyer & Scalapino (1973) pointed out that, because of the geometry of the π^- modes, anisotropic distributions of pressure could be considered to describe a pion condensed phase configuration. The anisotropic part of the stress tensor associated with the flux lines in a type II superconductor, and its relevance for a neutron star configuration has been discussed by Jones (1975) and Easson & Pethick (1977).

Anisotropic matter representing these and others interesting physical situations, e.g., the existence of solid core considered by Ruderman (1972) and Cameron & Canuto (1973), the presence of type P superfluid, the use of two fluid model for non interacting perfect fluids, as considered by Letelier (1980), or boson stars, studied by Ruffini & Bonazzola (1969) and Gleiser (1988), is now thought to be the constituent of more realistic compact objects.

Since we restrict ourselves to review anisotropies in astrophysics, we just mention, for historical reasons, that Lemaître (1933) was the first to consider the influence of anisotropy in cosmology.

After the pioneering work of Bowers & Liang (1974), tbe influence of local anisotropy in general relativity has been extensively studied. Analytical static solutions were considered by Bayin (1982), Cosenza et al. (1981), Heintzmann & Hillebrandt (1975), Herrera & Ponce de Leon (1987), Florides (1994), Aherkar & Asgekar (1990,1991), Maartens & Maharaj (1990) and Bondi (1992). Anisotropic stresses in charged configurations were considered by Bonnor (1960) and more recently by Herrera & Ponce de Leon (1985c) and Herrera & Varela (1994). The problem of stability of anisotropic matter has been considered by Hillebrandt & Steinmet (1976), Herrera et al. (1979) and Chan et al. (1993a,b). The evolution of anisotropic fluids under different conditions was studied by Cosenza et al. (1982), Esculpi & Herrera (1986), Ibanez (1984) and Bayin (1982). Ibanez & Miralles (1985) pointed out the influence of anisotropy upon white dwarfs collapse.

Some geometrical aspects of spacetime with local anisotropy and its hydrodynamical implications were presented by Duggal (1987), Duggal & Sharma

(1986), Herrera et al. (1984) and Maartens, Mason & Tsamparlis (1986). The role played by anisotropy in the context of other gravitational theories was treated by Ram & Pandey (1986). The propagation of discontinuities in a composite sphere with different anisotropic phases has been modelled by Herrera & Nunez (1989). Energy conditions for anisotropic fluids were considered by Kolassis et al. (1988), and further aspects of anisotropic matter was studied by Magli & Kijowski (1992) and Magli (1993). Finally the relevance of local anisotropy in the occurrence of cracking in compact objects was recently pointed out by Herrera (1992).

Now we review the main theoretical results concerning tbe equilibrium, stability and evolution of anisotropic self-gravitating systems.

Analytical models

The first analytic model for superdense static anisotropic matter was studied by Bowers & Liang (1974). They demonstrated that tbe condition for hydrostatic equilibrium for a spherically symmetric distribution of anisotropic fluid witb P_r the radial pressure, $P_\perp$ the pressure orthogonal to the radius, μ the energy density, $m(r)$ tbe total mass inside the radius r is

$$\frac{dP_r}{dr} = -\mu^* \frac{m + 4\pi P_r r^3}{r(r-2m)} + 2\frac{\Psi}{r}, \tag{1}$$

where $\Psi = P_\perp - P_r$ and $\mu^* = \mu + P_r$ is the effective energy density. The Newtonian limit of equation (1) is

$$\frac{dP_r}{dr} = -\mu \frac{m}{r^2} + 2\frac{\Psi}{r}. \tag{2}$$

From equation (2) the anisotropy term in (1) is thus of Newtonian origin. This fact justifies that the effective relativistic energy μ^* is increased only by P_r, and not by $P_\perp$. Furthermore, this fact suggests that anisotropy can be important in the behaviour of self-gravitating systems.

For different equations of state some properties have been obtained for anisotropic spherically symmetric hydrostatic systems. If $\Psi > 0$ the critical mass of the sphere, when P_r becomes infinite at $r = 0$, can be up to 20% bigger than the corresponding isotropic system. However if $\Psi < 0$ the critical mass becomes smaller than the corresponding isotropic value. The redshift at the surface of the sphere increases witb increasing $\Psi > 0$ independently of the equation of state. It can be bigger than 2, which is the maximum redshift value for tbe critical isotropic

mass distribution. One can say that redshifts larger than 2 may be of anisotropic origin and may explain certain large redshifts of quasars. For some equations of state it has been proved that for small perturbations when $\Psi > 0$ the system is more unstable than for the corresponding isotropic configuration, while for $\Psi < 0$ the fluid becomes less unstable for the same perturbations.

Dynamical instability for anisotropic collapse

In order to study the dynamical stability of an anisotropic spherically symmetric fluid the equilibrium equation (1) is perturbed and we look for the range of values of the ratio of specific heats Γ, where the perturbations grow exponentially. After long calculations, we obtain that up to the post Newtonian order the unstable range of Γ is

$$\Gamma < \frac{4}{3} + \left[\frac{8\pi}{3} \frac{\mu P_r}{|P_r'|} + \frac{4}{3} \frac{\Psi}{|P_r'|} \frac{1}{r} \right]_{max}, \tag{3}$$

where the prime denotes the r derivative and the expression inside the brackets has its maximal value.

The inequality (3) tells us the following. The first term on the right is the typical Newtonian term of an isotropic perfect fluid (for radiating fluid see Bonnor et al. (1989)). Thus for all values of Γ smaller than 4/3, the Newtonian isotropic perfect fluid will collapse, since the increase of pressure after a small compression will not be enough to withhold the gravitational force.

The second term on the right contains the relativistic correction to the Newtonian perfect fluid. Being a positive quantity, it increases the unstable range of Γ, leading to more unstable configurations than the corresponding Newtonian ones. It arises because the effective energy density μ^* of the system is increased by the pressure from the relativistic point of view.

The third term gives the Newtonian contribution due to local anisotropy. Surprisingly there is no post Newtonian correction due to the anisotropy. This fact arises because only P_r, and not $P_\perp$, contributes to μ^*.

An important consequence emerging from equation (3) is related with the possibility of Ψ to change sign within the sphere. Of course, this possibility will ultimately depend on the specific origin of local anisotropy in an astrophysical body. Let us assume, as an example, that Ψ changes from positive to negative values as r varies from 0 to its value at the surface. This would imply that the

inner core, with $\Psi > 0$, becomes more unstable, whereas the stability of outer regions, $\Psi < 0$, increases. In order to visualize the consequences derived from this situation, let us assume that Ψ vanishes at $r = 0$ as r^n, $1 < n < 2$. In this case, the innermost layers, $r \approx 0$, are *absolutely* unstable which means that the unstable range of Γ for those layers is $\Gamma < \infty$. These layers will collapse if $\Psi > 0$, wbereas tbe fate of the outer layers will depend on the profile of Ψ. In particular, if Ψ becomes negative, these regions may bounce, leading to a fragmentation of tbe spbere.

Another fragmentation scenario may result if Ψ changes from negative, in the inner region, to positive, in the outer regions.

All these results, concerning the effects of local anisotropy on the stability of the sphere, are in good agreement with those presented in the analytical models. However our conclusions here are almost completely model-independent.

There are proposed mechanisms to explain the ejection of the outer mantle in the supernova event (Arnett 1987; Bethe et al. 1978; Betbe & Wilson 1985; Burrows 1987; Colgate & Jobnson 1960; Wilson 1985). For instance, after tbe gravitational collapse of the core of a highly evolved, massive star, a shock wave will be formed which propagates outward. At the same time, neutrinos from the inner core are absorbed by the outerlayers producing their ejection. We can expect then tbat in the scenario described above, $\Psi > 0$ at the inner core and $\Psi < 0$ at the outer layers, the ejection of the outer mantle in the supernova event, would certainly be enbanced.

Jeans' mass for anisotropic matter

We saw that local anisotropy can drastically change the stability of matter. Motivated by this result we extended the instability criterion of Jeans to interstellar gas that can produce anisotropies during its evolution. First we consider the Jeans' criterion for isotropic gas and then we compare to the anisotropic case.

Isotropic Jeans' mass

To obtain the instability condition for an isotropic interstellar gas, $P_r = P_\perp = P$, we consider an isothermal sphere of finite radius R imbedded in a medium of pressure $P^* > 0$. The structure of the sphere can be assumed to be an isothermal polytrope. Since this sphere is in equilibrium with the exterior medium then

$P(R) = P^*$. From the balance of energy of this system we obtain

$$P(R) = -\frac{\alpha_g}{R^4} + \frac{\alpha_i}{R^3}. \tag{4}$$

The first term in the right hand side of equation (4), with $\alpha_g > 0$, is the pressure due to the selfgravity of the sphere trying to contract it. The second term, with $\alpha_i > 0$, is the internal gas pressure trying to expand the sphere. We have $P < 0$ for small R and $P > 0$ by increasing R. At $R = R_m$ the pressure has its maximum value and then diminishes approaching zero from positive values for $R \to \infty$.

Suppose now that the sphere is in equilibrium with the surroundings. In this case $P(R) = P^*$. For $R < R_m$ the surface pressure $P(R)$ *decreases* with decreasing R. Therefore after a slight compression $P(R) < P^*$, the sphere will be compressed even more, being *unstable*. On the other hand, for $R > R_m$ the pressure $P(R)$ *increases* during compression, $P(R) > P^*$, and the sphere will expand back to equilibrium, being *stable*.

Considering the temperature $10^2 K$ and mass density $10^{-24} g\, cm^{-3}$, which are typical conditions in interstellar clouds of neutral hydrogen, we obtain for Jeans' mass M_J

$$M_J \approx 10^5 M_\odot, \tag{5}$$

where $M_\odot$ is the solar mass. Clouds $M \geq M_J$ start collapsing and since this process is isothermal, it can be proved that $M_J \sim \mu^{-\frac{1}{2}}$. Thus the Jeans' mass decreases with the cloud mass density μ. It results that while the cloud falls together, fragments of it become unstable and collapse faster than the cloud as a whole. This process is called *fragmentation* and it proceeds until the thermal adjustement of the cloud is of the order of free fall time of the particles, when the smaller fragments are formed. For the interstellar gas considered in (5) the fragmentation stops when

$$M_J \approx M_\odot. \tag{6}$$

Thus fragmentation terminates if the fragments are of the order of the solar mass, *not* of the order of planetary masses or a whole star cluster mass.

Anisotropic Jeans' mass

Considering now that local anisotropies can appear in the evolution of interstellar gas, from the balance of energy, instead of equation (4), we obtain for a sphere of gas of radius R,

$$P_r(R) = -\frac{\alpha_g}{R^4} + \frac{\alpha_i}{R^3} + \frac{2}{R^3}\int_0^R \Psi r^2 dr. \tag{7}$$

The third term in the right hand side of (7) with $\Psi = P_\perp - P_r$, due to the anisotropy of the system, tries to expand or contract the sphere if the net constribution of Ψ is positive or negative.

Considering, as an example, the anisotropy of the cloud arising from a slow rotation, then we have

$$\Psi = \frac{1}{3}\mu\omega^2 r^2, \tag{8}$$

where ω is the angular velocity. Substituting (8) into (7) we obtain

$$P_r(R) = -\frac{\alpha_g}{R^4} + \frac{\alpha_i}{R^3} + \frac{2}{15}\mu\omega^2 R^2. \tag{9}$$

From equation (9) we have $P_r < 0$ for small R and becomes $P_r > 0$ by increasing R and arrives to a maximum at $R = R_{max}$. Then, for still increasing values of R, P_r diminishes to a positive minimum at $R = R_{min}$. For bigger $R > R_{min}$, P_r steadily increases for increasing values of R.

Suppose that the sphere of gas is in equilibrium with the surroundings, then $P_r(R) = P^*$. For $R < R_{max}$ the surface pressure $P_r(R)$ *decreases* with decreasing R. Therefore after a slight compression $P_r(R) < P^*$, and the sphere will be compressed even more, being *unstable*. However, for $R_{max} < R < R_{min}$ the pressure $P_r(R)$ *increases*, $P_r(R) > P^*$, during compression and the sphere will expand back to equilibrium, being *stable* for that range of values of R. But for $R > R_{min}$ the surface pressure $P_r(R)$ *decreases* with decreasing R, consequently after a slight compression $P_r(R) < P^*$, the sphere will be compressed even more. Hence anisotropy has built a new *unstable* range for the radii.

If we assume the interstellar gas of neutral hydrogen rigidly rotating and basically homogeneous, then we obtain that the anisotropy introduced by the slow rotation is of the same type as the one considered in our example. Using the same values for the physical quantities as given in the isotropic scenario and the angular velocity of the cloud of the order of magnitude of the sun around the center of our galaxy, $w \approx 10^{-15} s^{-1}$, the fragmentation terminates with fragments of the order

$$M_J \approx 10^{-\frac{9}{2}} M_\odot. \tag{10}$$

But these fragments are of the order of planetary mass, or in any case, much smaller than $0.08 M_\odot$, which is the minimum mass required to start the ignition of hydrogen. Thus the collapse of interstellar gas with anisotropy may, in principle,

lead to fragments with masses even smaller than the typical value for brown dwarfs, $1M_{\odot} > M > 10^{-3}M_{\odot}$ (Daly & MacLaughlin 1992).

Cracking of self-gravitating compact objets

Anisotropy can deviate, in a very peculiar way, some fluids configurations from equilibrium or slow evolution once perturbations are introduced in the system. This arises because it can appear non vanishing total radial forces with different signs in different regions of the fluid configuration. We say that there is *cracking* whenever this radial force is directed inward in the inner part of the sphere for all values of the radial coordinate r between the center and some value, say $r = \tilde{r}$, beyond which the force reverses direction.

One of these situations refers to an anisotropic fluid (AF) which is either static or slowly evolving and the other kind of situation is a slowly contracting and radiating perfect fluid (RF). Although physically very different, both situations share the common feature that the principal stresses are unequal. It is not surprising since the superposition of a perfect fluid plus null fluid is formally represented by an anisotropic fluid. By slow contraction we mean that terms of the order of the square of the velocity of contraction of the system can be neglected.

For both fluids AF and RF, static and slowly contracting, we have

$$S \equiv \frac{dP_r}{dr} + \mu^* \frac{m + 4\pi P_r r^3}{r(r-2m)} + 2\frac{\Psi}{r}, \tag{11}$$

where $\Psi = P_{\perp} - P_r$ for AF and $\Psi = \epsilon$, ϵ being the radiation density travelling in the radial direction and $P_r = P_{\perp}$ for RF.

For integrating (11) we assume an equation of state as used for studying the dynamical stability of neutron stars (Misner & Zapolsky 1964),

$$\mu = \frac{K}{r^2}, \tag{12}$$

where K is a constant or a function of time depending which case we consider, static or slowly evolving. Introducing a positive perturbation in the density,

$$\tilde{K} = K + k, \tag{13}$$

where $1 \gg k > 0$. Thus our system will depart from equilibrium or slow evolution, a fact which is originated by the appearence of a total, non vanishing, radial force on every fluid element.

Integrating (11) by using (12) and (13) we obtain the following interesting results.

For a perfect fluid, $\Psi = 0$, $\tilde{S}$ does not change sign inside the fluid, meaning that all parts of the fluid will collapse. However, for AF and RF cases, assuming perturbed test functions, unlike the perfect fluid case where can occur cracking, the inner part collapses while the outer part of the system expands. The characteristics will depend upon the specific magnitudes of the perturbations. Thus let us suppose for example, that the inner core in the collapse of a supermassive star reaches a configuration like the one just considered. In this case the inner core becomes anisotropic or, alternatively, the inner core radiates in slow contraction. Then perturbations of this configuration produced by the fall-in of outer regions of the star onto the core, might lead to its cracking. The inner part will tend to collapse while the outer part will tend to expand. Under these circumstances it is clear that any of the proposed mechanisms to explain the ejection of the outer mantle in a supernova event could be considerably enhanced.

Conclusion

We presented some astrophysical processes ranging from primordial gas to supermassive systems where local anisotropies can develop. These processes suggest that anisotropy may be important in the equilibrium, stability and evolution of self-gravitating astrophysical systems. We reviewed the main theoretical results on the influence of anisotropy concerning analytical models, dynamical instability, Jeans' mass and cracking of compact systems. The theoretical results show that even small traces of anisotropy can drastically modify the picture described by isotropic systems. Further, anisotropic systems opens a wide field of open theoretical problems. Thermodynamics of anisotropic systems is practically unknown; the Cauchy problem and the consequent wave propagation study for anisotropic mediums has not been solved. These are just some examples of open fields of research with fundamental importance for the study of astrophysical scenarios.

References

Aherkar, S., & Asgekar, G. 1991 Inter.J.Theor.Phys. **30** 547; 1990 Il Nuovo Cimento **B105** 639.

Arnett, W. 1987 Ap.J. **319** 136.

Bayin, S. 1982 Phys.Rev.D **26** 1262.

Bethe, H., Brown, G., Applegate, J., & Lattimer, J. 1978 Nucl.Phys.A **324** 487.

Bethe, H., & Wilson, J. 1985 Ap.J. **295** 14.

Binney, J. 1982 Ann.Rev.Astron.Astrophys. **20** 399.

Binney, J., & Tremaine, S. 1987 Galactic Dynamics (Princeton: Princeton University Press).

Bondi, H. 1992 MNRAS **259** 365.

Bonnor, W.B. 1960 Z.Phys. **160** 727.

Bonnor, W.B., de Oliveira, A.K.G., & Santos, N.O. 1989 Phys.Rep. **181** 269.

Bowers, R., & Liang, E. 1974 Ap.J. **188** 657.

Burrows, A. 1987 Ap.J. **318** 157.

Cameron, A.G.W., & Canuto, V. 1973 Neutron Stars: General Review, Proc. Solvay Conference on Astrophysics and Gravitation (Brussels).

Chan, R., Herrera, L., & Santos, N.O. 1992 Class.Quantum Grav. **9** L135; 1993 MNRAS **265** 533.

Colgate, S., & Johnson, H. 1960 Phys.Rev.Lett. **5** 235.

Collins, J.C., & Peery, M.J. 1975 Phys.Rev.Letters **34** 1353.

Cosenza, M., Herrera, L., Esculpi, M., & Witten, L. 1982 J.Math.Phys. **22** 118.

Cuddeford, P. 1991 MNRAS **253** 414.

Daly, R., & MavLaughlin, G. 1982 Ap.J. **390** 423.

Easson, I., & Pethick, C.J. 1977 Phys.Rev.D **16** 275.

Florides, P. 1974 Proc.Roy.Soc.London A **337** 529.

Gleiser, M. 1988 Phys.Rev.D **38** 2376.

Gliddon, J.E.C. 1966 Ap.J. **145** 583.

Gokhroo, M., & Mehra, A. 1994 Gen.Rel.Grav. **26** 75.

Hartle, J.B., Sawyer, R., & Scalapino, D. 1975 Ap.J. **199** 471.

Heintzmann, H., & Hillebrandt, W. 1975 Astr.Ap. **38** 51.

Herrera, L., & Ponce de Leon, J. 1985a J.Math.Phys. 26 2018; 1985b J.Math.Phys. **26** 2847; 1985c J.Math.Phys. **26** 2302.

Herrera, L., & Varela, V. 1994 Phys.Lett.A **189** 11.

Herrera, L., Ruggeri, G., & Witten, L. 1979 Ap.J. **234** 1094.

Hillebrandt, W., & Steinmetz, K. 1976 Astr.Ap. **53** 283.

Itoh, N. 1970 Progr.Theoret.Phys. **44** 291.

Jeans, J.H. 1922 MNRAS **82** 122.

Jones, P.B. 1975 Astrophys.Space Sci. **33** 215.

Kent, S., & Gunn, J. 1982 Astron.J. **87** 945.

Krori, K., Borgohain, P., & Devi, R. 1984 Canadian J.Phys. **62** 239.

Lemaitre, G. 1933 Ann.Soc.Sci.Bruxelles A **53** 97.

Letelier, P. 1980 Phys.Rev.D **22** 807.

Maartens, R., & Maharaj, M. 1990 J.Math.Phys. **31** 151.

Madsen, J., & Epstein, R. 1985 Phys.Rev.Letters **54** 2720.

Mellot, A. 1983 Ap.J. **264** 59.

Michie, R. 1962 MNRAS **125** 127.

Migdal, A.B. 1971 Soviet Phys.JETP **34** 1184.

Misner, C., & Zapolsky, H. 1964 Phys.Rev.Letters **12** 635.

Ponce de Leon, J. 1987 J.Math.Phys. **28** 1114.

Ralston, J. 1989 Phys.Rev.Letters **63** 1038.

Ralston, J., & Smith, L. 1991 Ap.J. **367** 54.

Ruderman, M. 1972 Ann.Rev.Astr.Ap. **10** 427.

Ruffini, R., & Bonazzola, S. 1969 Phys.Rev. **187** 1767.

Sawyer, R.F. 1972 Phys.Rev.Letters **29** 382.

Sawyer, R., & Scalapino, D. 1973 Phys.Rev.D **7** 953.

Sawyer, R., & Soni, A. 1977 Ap.J. **216** 73.

Singh, K., & Bhamra, K. 1990 Int.J.Theor.Phys. **29** 1015.

Singh, T., Singh, G., & Srivastava, R. 1992 Int.J.Theor.Phys. **31** 545.

Sokolov, A.I. 1980 Soviet Phys.JETP **52** 575.

Wilson, J. 1985 Numerical Relativity, ed. J.Le Blanc & R.Bowers (Boston: Jones and Barlett).

CHEMICAL EVOLUTION OF THE GALAXY

J. A. de Freitas Pacheco*
Observatoire de la Côte d'Azur
B.P. 229-06304 Nice, Cedex 04 France

Abstract. We review some aspects of the chemical evolution of the Galaxy. In particular, we discuss the production of light elements in the early Galaxy and the metallicity distribution in the halo and in the bulge. The temporal evolution of the metallicity in the halo suggests that the onset of type Ia supernovae is about 2.7 Gyr. The chemical evolution of C, O, S and Ar in the galactic disk is modelled and compared with available data.

1. Introduction

The Galaxy is a huge and complex stellar system. For our present purposes, we recognize three main sub-systems: the halo, the bulge and the disk. Both the halo and bulge are constituted by old stellar populations (ages between 13-15 Gyr), with the latter being substantially more metal-rich than the former. The disk, on the average is younger, with stellar population ages ranging from 0.1-1.0 Myr up to 10-12 Gyr.

In order to discuss the halo metallicity distribution, we should make clear possible differences between data gathered from field stars and clusters. First, it is important to point out that halo subdwarfs and clusters with galactocentric distances $R_{GC} > 6kpc$ have similar kinematic properties (Norris & Ryan 1989; Carney, Latham & Laird 1990). The analysis of Laird et al. (1988), who compared the metallicity distribution of those halo subdwarfs with globular clusters, suggests that both have nearly the same mean value, namely, [Fe/H]=-1.6. Notwithstanding, one should have in mind the claim by Carney (1993), who argues about the presence of chemical substructures in the halo. On the other hand, clusters with $R_{GC} < 6kpc$ have kinematics and metallicities comparable with those of the thick disk stellar population (Armandroff 1989). These similarities are consistent with dissipation having played a role in the formation of structures at distances $R_{GC} < 40kpc$.

* On leave of absence from Instituto Astronomico e Geofísico, Universidade de São Paulo, Departamento de Astronomia, Av. Miguel Stefano 4200, 04301-904 São Paulo, Brazil

The metallicity distribution of the bulge was studied, among others, by Rich (1988) from a sample of 88 K giants in the Baade's window. The abundances range from [Fe/H]=-1.0 to 0.8 with a mean of twice solar. Some disk population clusters are found inside the bulge volume with metallicities comparable to the solar value (Ortolani et al. 1990, 1993), but presently it is by no means clear if they can be classified as a true bulge population.

In the following sections we will discuss some simple models, aiming to explain some major characteristics of the chemical evolution of the above mentioned galactic stellar systems.

2. The Chemical Evolution of the Halo

2.a Model Parameters and Iron Enrichment

The star formation in the halo reflects the activity of the early Galaxy. The modelling of such a system must be able to satisfy at least tbree observational constraints: 1.) the observed metallicity distribution; 2.) the age dispersion among clusters and stars $\sigma_{age} \approx 2Gyr$ and 3.) the nearly constant O/Fe ratio.

The first constraint refers simply to the observed metallicity distribution of halo stars (Ryan & Norris 1991). The second, the age dispersion (not to be confounded with the age spread), is a consequence that analyses of isochrone fitting to colour-magnitude diagrams (CMD's) of globulars indicate that significant differences in theirs ages may exist. Similar age scatter, of the order of 2 Gyr is also present in halo field star samples (Schuster & Nissen 1989). Chemical analyses of halo stars indicate that for metallicities $[Fe/H] < -1.0$, the oxygen-to-iron ratio remains nearly constant, [O/Fe]$\approx$+0.35 (Barbuy 1988; Kraf et al. 1992). This suggests that the medium was enriched by the yield of massive stars, imposing also a further constraint related with the time scale of the onset of type Ia supernovae. As we shall see, this time scale is of the order of 3 Gyr.

In our model, the total gas consumption is regulated by the rate at which the gas is converted into stars and by the rate of gas transfer into the disk ("infall"). We assume that both rates are proportional to the available gas mass, but with different time scales. Under these conditions, it is easy to show that the age dispersion is given by

$$\sigma_{age} = \frac{\sqrt{3}}{\alpha}$$

where α is defined by the equation

$$\alpha = \frac{1}{\tau_{dyn}} + \frac{(1-R)}{\tau_*}$$

In the above equation, τ_{dyn} is the "infall" characteristic time scale, R is the mass fraction returned to the interstellar medium by evolved stars and τ_* is the star formation time scale.

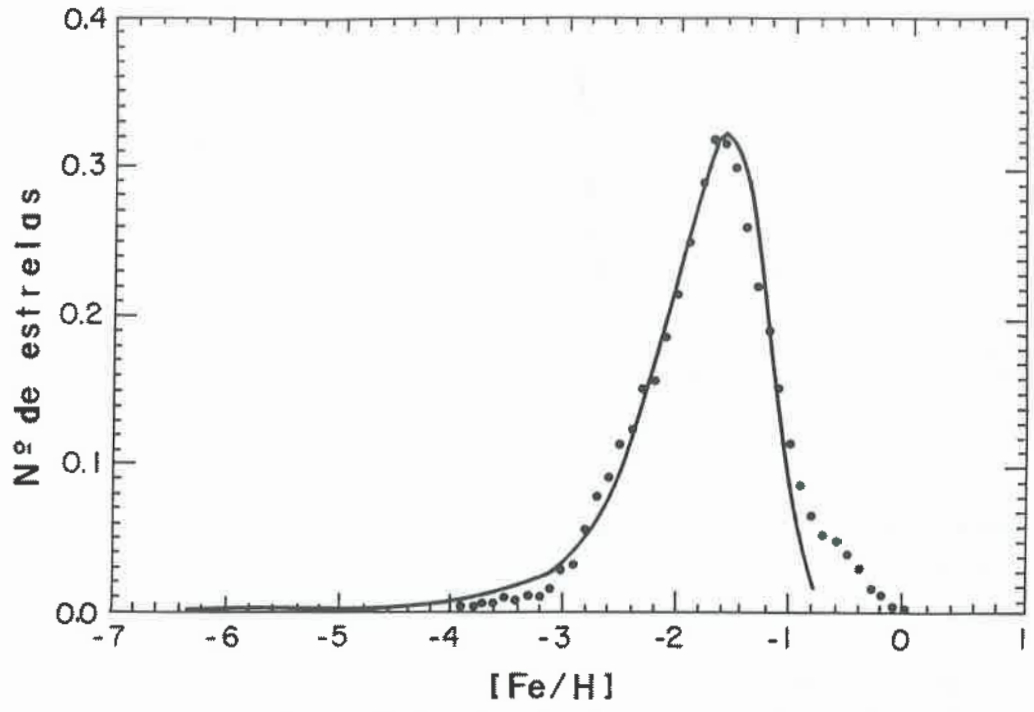

Figure 1 - Theoretical metallicity distribution computed by Idiart for the halo model discussed in the text. Data points are from Ryan & Norris (1991)

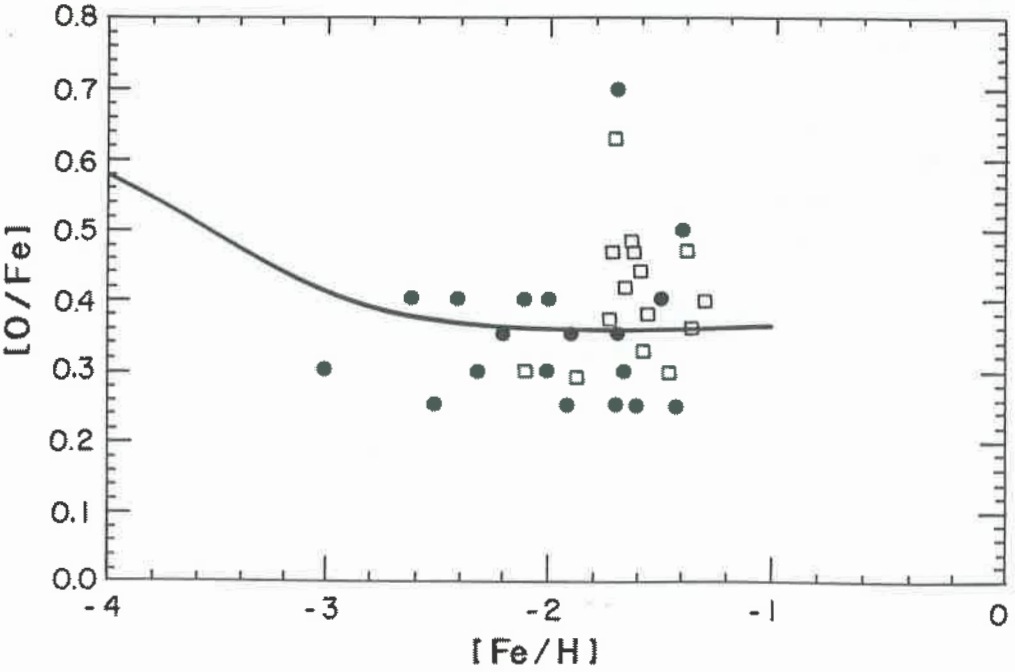

Figure 2 - Theoretical (O/Fe) ratio as a function of metallicity for the halo. Data points are from Barbuy (1988) and Kraft et al. (1992)

Numerical calculations of the chemical evolution of the system were performed by Idiart (1994). She computed chemical yields from Arnett's (1990) tables and solved the equations without the so-called "instantaneous recycling approxima-

tion".

In fact, different pairs of (τ_*, τ_{dyn}) are able to explain tbe observed metallicity distribution. The age dispersion fixes the pair of parameters as: $\tau_* \approx 6.39$ Gyr and $\tau_{dyn} \approx 1.19$ Gyr. Figure 1 shows the computed metallicity distribution compared with the actual distribution. We note the quite good agreement between both distributions, excepting for the "high-metallicity" tail, where the data seems to indicate a small fraction of metal-rich halo stars, not present in Idiart's calculations. We cannot exclude the possibility tbat these stars are real halo objects and not disk stars which contaminate the sample. In this case, type Ia supernova are required to enrich the halo. Idiart's computations require that the onset of type Ia supernovae is about 2.7 Gyr, if they contribute to the yield for $[Fe/H] > -1.2$. Figure 2 shows the ratio [O/Fe] vs. [Fe/H]. We observe that for $[Fe/H] < -3.0$, the oxygen-to-iron ratio increases as a consequence of the contribution by short-lived oxygen rich stars. This is an important theoretical prediction although difficult to verify due to the scarcity of very metal-poor stars and the faintness of the absorption features.

2.b The Light Elements

The most common light elements, ^2H, ^3He, ^4He, and ^7Li bave relative abundances determined by primordial nucleosynthesis. Their observed values are in adequate agreement with the predictions of the standard model (Walker et al. 1991).

Beryllium and boron are produced in observable amounts only in inbomogeneous Big-Bang models (Kajino & Boyd 1990), although recent calculations by Teresawa & Sato (1990), taking into account effects of back-diffusion of neutrons into proton-rich regions, indicate that the enhancement in those elements is not so important.

The uniformity of the lithium abundances in metal-poor halo stars with $T_{eff} \geq 5500K$ (Spite & Spite 1982) supports a cosmological origin for most of the observed lithium. On the other hand, recent data on the beryllium abundance in metal-poor stars (Gilmore et al. 1992; Boesgard & King 1993) show a clear correlation with metallicity, suggesting enrichment by processes that occurred in the early Galaxy. The same trend is verified for boron in three halo stars studied by Duncan, Lambert & Lemke (1992).

These results imply that on the average Be/Fe = 1.4 x 10^{-6} in halo stars and B/Be $\approx$ 10. Another important observational constraint is the isotopic lithium ratio recently measured in some halo stars (Smith, Lambert & Nissen 1993; Hobbs & Thorburn 1994). Upper limits and detections are consistent with a ratio $^6Li/^7Li \approx 0.05$ independent of metallicity. Since the beryllium abundance is nearly proportional to metallicity, a cosmological origin is excluded and its production is probably related with the activity of the early Galaxy. On the other hand, the observed isotopic lithium ratio suggests that "alpha-alpha" reactions played an

important role in their production.

Li, Be and B may be produced by cosmic rays (CR) interacting with the ambient interstellar medium (ISM). In fact, the observed abundances of those elements in population I stars, ISM and in the solar system may entirely be accounted by spallation reactions (Reeves, Fowler & Hoyle 1970; Meneguzzi, Audouze & Reeves 1971). The production of light elements by spallation of CNO nuclei by diffusing CR in the early Galaxy has been explored by many authors in the last few years (Vangioni-Flam et al. 1990; Steigman & Walker 1992; Fields, Schramm & Truram 1992; Freitas Pacheco & Barbuy 1993). The modelling of CR propagation in the early Galaxy is a matter of debate and different assumptions can be made concerning their production rate and confining time scale in the collapsing halo. However, the resulting Li/Be ratio in this model is quite high (≈ 2000). The reason is that the lithium production is dominated by the "alpha-alpha" reactions while most of beryllium is produced in a dilute CNO medium. As a consequence, the predicted Be and B abundances are quite small. Another possibility is to consider that the light elements are mostly produced in or near the supernova ejecta, during the very early evolutionary phases of the remnant. This scenario has also some difficulties, since it predicts $3 \leq (^6Li/^9Be) \leq 8$, quite less than the required ratio necessary to explain both the Be abundance and the Li isotopic ratio.

Here we explore a hybrid scenario where the light elements are produced by spallations in the ISM and "in situ".

Our basic assumptions are: a) CR have a power law spectrum in **total energy**; b) lithium isotopes are produced in the ISM (mostly) and "in situ"; c) Be and B have negligible production in the ISM. The parameters of the model are fixed by the observed $(^9Be/Fe)$ and $(^6Li/^7Li)$ ratios. If the exposure time in the remnant is of the order of 100 yr (required to avoid dilution of the oxygen-rich ejecta with the ISM material), then the average cosmic ray energy per event is about 3 x 10^{50} erg. This value is comparable to the power requirement per SN to mantain the present CR density in the disk. On the other hand, the average cosmic ray energy density during the halo evolution is about $5eV.cm^{-3}$, a few times higher than the present value observed in the galactic disk. Our theoretical predictions based on these assumptions are:

$(^7Li/^6Li)_{CR} \approx 1.6$; $(^6Li/^9Be)_{CR} \approx 46$; $(^{11}B/^{10}B)_{CR} \approx 2.3$ and $B/Be \approx 11.6$

This hybrid model explains the near linear correlation between Be and B abundances with metallicity, the observed B/Be ratio and the required isotopic lithium ratio in metal-poor stars.

Other possibilities are certainly possible. Deliyannis & Malaney (1994) revived an old idea concerning the production by active stars. They found from roughly computations tbat low-metallicity dwarfs and subgiants may produce observable amounts of ^6Li by flare activity. Further theoretical and observational work are still necessary, face to the consequences for the history of the early Galaxy and cosmology.

2.c The Structure of the Halo

We feel interesting to say, in this section, a few words about the halo structure and the nature of dark matter.

The study of the globular cluster kinematics (Borges & Freitas Pacheco 1989 and references therein) indicate a halo mass of 4 x $10^{11} M_{\odot}$ within a radius of 33 kpc. This mass is considerably higher than that under the form of stars. Moreover, recent "gravitational scintilation" experiments of LMC stars (Alcock et al. 1993; Aubourg et al. 1993), suggest that objects with masses consistent with those of brown dwarfs may be the major constituent of the halo.

During the early activity period in the halo, single stars and globular clusters were simultaneously formed (in fact, this is actually observed in the LMC). The idea that only complex structures ($10^5 to 10^8 M_{\odot}$) were initially present and partial or totally evaporated, originating "single" stars, seems to lack of observational support. Excepting for six stars in direction of the north galactic pole (Majewski, Munn & Hawley 1994), which apparently constitute part of a halo moving group, no other bona fide structures that could be derived from evaporation of stellar aggregates, have been found. On the other hand, computations by Hut & Djorgovsky (1992) indicate that the present GC population is being destroyed at a rate of about 3% per Gyr. If these calculations are realistic, then the present number of GC's represents a significant fraction of the original population, and the view that all halo stars came from desintegrated clusters can be ruled out (van den Bergh 1994).

Face to these facts, we assume that during the early activity of the Galaxy, objects in the mass range $0.01 \leq M/M_{\odot} \leq 80$ were formed. All objects with masses less than 0.1 $M_{\odot}$ will constitute our (baryonic) dark halo. We assume also that the initial mass function in the halo is slightly steeper than Salpeter's law, i.e.,

$$\xi(m) = \frac{A}{m^3}$$

From our model, it is easy to show that the mass M_* of alive stars is

$$M_* = \frac{\lambda_1 M_0 (1 - R)}{\alpha \tau_*}$$

where M_0 is the total initial halo mass, λ_1 is the mass fraction of alive stars (those in the mass interval 0.1 - 0.8 $M_{\odot}$), and the other symbols were already defined. Under these conditions, one obtains $\frac{M_*}{M_0} \approx 0.013$. If we take for the initial halo mass the value derived dynamically, one gets $M_* \approx 5.3 x 10^9 M_{\odot}$. The estimated mass of the GC population is about $4 x 10^7 M_{\odot}$. The field stars are estimated to have a total mass of about 100-150 times higher than the cluster population, namely, $(4 - 6) x 10^9 M_{\odot}$, which is quite comparable to our naive estimate.

3. The Chemical Evolution of the Bulge

The central region of our Galaxy is characterized by a diversity of stellar populations: late M giants, RR Lyr and faint carbon stars are found in the same volume. The discovery of long period variables in the bulge (Harmon & Gilmore 1988) raised the speculation that a relatively young metal rich population may be present in the bulge. On the other hand, Lee (1992) based on the HB morphology of "bulge" globulars compared with those in the halo, sustains that the bulge is older than the halo. His interpretation of the morphology vs. metallicity diagram was questioned by Catelan & Freitas Pacheco (1993), who showed that age is not necessarily the (second) parameter fixing the HB morphology. More recently, Paczynsky et al. (1994), from the ratio of the HB clump to RGB stars in the bulge, argued that a population younger than 10-12 Gyr must be present. However, such a ratio may be interpreted in terms of a high He abundance (0.30-0.35) as suggested by Renzini (1994). Therefore, the age distribution in the bulge is still rather uncertain.

The chemical composition of bulge giants (McWilliam & Rich 1994) suggests enrichment by massive stars. A simple model able to reproduce the observed star metallicity distribution ($< Fe/H > \approx 2 < Fe/H >_{\odot}$) and an age dispersion of ≈ 2 Gyr requires a returned gas mass fraction of about 23.6%, and a charateristic star formation time scale of 0.88 Gyr. This implies an efficiency of forming stars about 7 times higher than in the halo. Figure 3 shows the He abundance vs. metallicity. We remark that stars of solar metallicity have He mass fraction of about 0.36, required to explain the ratio of HB to RGB stars without invoking the presence of stars younger than 10 Gyr.

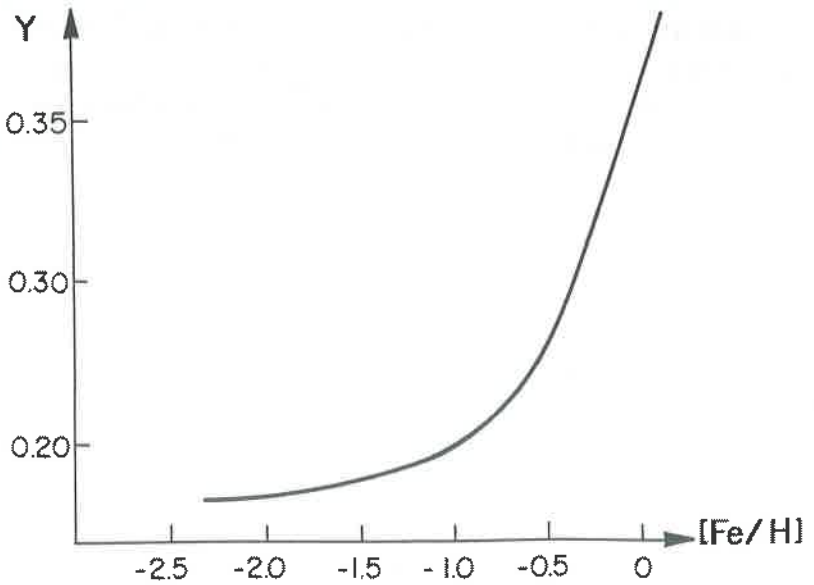

Figure 3 - Helium vs. metallicity for the bulge model discussed in the text

Ratag (1992 and references therein) performed a detailed study of a sample of

about 100 planetary nebulae in the direction of the galactic bulge. The abundance distribution of these objects poses some problems if indeed these planetaries are members of the bulge population. Some questions to be answered are:

1. the average metallicity deduced from K giants is about twice solar. If **only** massive stars contributed to the enrichment, then we would expect that the average oxygen abundance will be $\varepsilon(O) \approx 9.6$. However the observed value is one order of magnitude smaller, comparable to the disk value.

2. If we select only planetaries with $\varepsilon(O) \geq 9.0$, their He abundances are, in fact, compatible with the evolutionary predictions, but their high N/O ratios imply self-enrichment.

3. Neon, sulphur, and argon have distributions **similar to the disk**, which had a different evolutionary history.

Face to these facts, the membership of these objects to the bulge population may be questioned. Are those nebula an "intrusion of the disk" into the outer bulge ? Has the bulge an outer metallicity gradient ? In this case, the time scale to form the outer parts is larger (the central regions collapsed faster), the star formation rate is reduced and type Ia supernovae may also contribute to the enrichment. This could be a plausible scenario to explain the PN data, although no definitive conclusion can presently be draw.

4. The Chemical Evolution of the Disk

Models developed to explain the metallicity distribution of the disk were always plagued by the "G-dwarf problem", namely, the paucity of metal-poor dwarfs in the solar vicinity. Different solutions were proposed to solve this problem and some "infall" models are able to account for such a failure in detecting those stars.

Another constraint should now be added to the "G-dwarf problem". There are presently different set of data on stars and nebulae which seem to support an underabundance of oxygen in the ISM, with respect to the solar value. These evidences are:

1.) The analysis of the oxygen abundance in intermediate mass F-K supergiants having main sequence B stars as progenitors, indicate an average value $\varepsilon(O) \approx 8.70$ (Luck & Lambert 1985)

2.) B stars in associations and young clusters were studied by Fitzsimmons et al. (1990) and their results imply $\varepsilon(O) \approx 8.75$, suggesting an average deficiency of about 0.17 dex with respect to the sun.

3.) Unevolved B stars were also analyzed by Gies & Lambert (1992), who obtained similar results. They found an average value $\varepsilon(O) \approx 8.68$, pointing to a similar oxygen underabundance.

4.) Cunha & Lambert (1992;1994) studied the oxygen abundance in unevolved B stars in the Orion nebula, concluding that their average value is compatible with that of the associated HII region. This result says that, in fact, oxygen is underabundant in the ISM and it is not "condensed" into dust.

5.) The average oxygen abundance in HII regions is $\varepsilon(O)$ ≈8.76 (Shaver et al. 1983), compatible with the results derived from young stars.
6.) Oxygen abundances in planetary nebulae are less sensitive to model parameters as those required to model stellar atmospheres. The analysis od type I planetaries, which are originated from progenitors with masses higher than 2.5 $M_{\odot}$ and belonging to the young disk population, have an average oxygen abundance $\varepsilon(O) \approx 8.72$ (Freitas Pacheco 1993), entirely compatible with the former results.

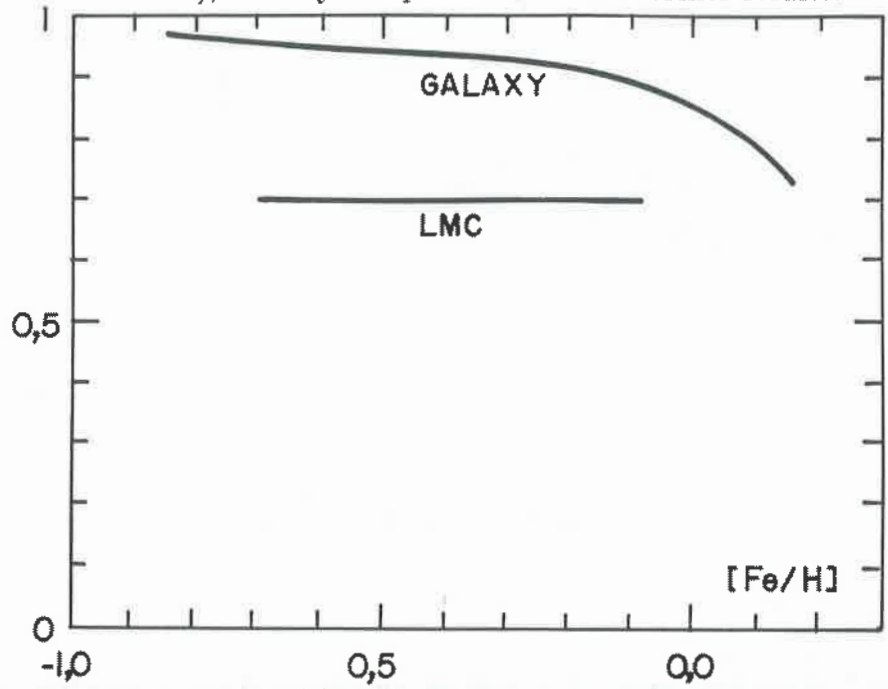

Figure 4 - Relative number of SN Ia and SN II vs. metallicity in the galactic disk and LMC

If the behaviour of the (O/Fe) ratio with metallicity for disk stars can be interpreted in terms of a relative contribution variation of both SN's Ia and II, then the evolution of other elements can be computed (Freitas Pacheco 1993). Figure 4 shows the relative contribution of type II SNe to the chemical yields, derived from the (O/Fe) ratio vs. metallicity measured for disk stars (Barbuy & Erdelyi-Mendes 1989). For comparison, the same curve for the LMC derived by Barbuy, Freitas Pacheco & Castro (1994). In these computations, we used the theoretical yields of Arnett (1990) for type II SN, averaged by a Salpeter's initial mass function, and the yields by Nomoto, Thielemann & Yokoi (1984), for type Ia SN. Inspection of Figure 4 shows that in the LMC, the relative number of type Ia SNe was larger than in the Galaxy. However, we emphasize that these curves must be looked "with a grain of salt"; in our Galaxy, the variation of the parameter r (see Freitas Pacheco 1993) with metallicity represents a true temporal evolution; in the LMC case, most of the sampled objects are young (ages ≤ 1-3 Gyr) and the observed spread reflects probably chemical inhomogeneities in the ISM.

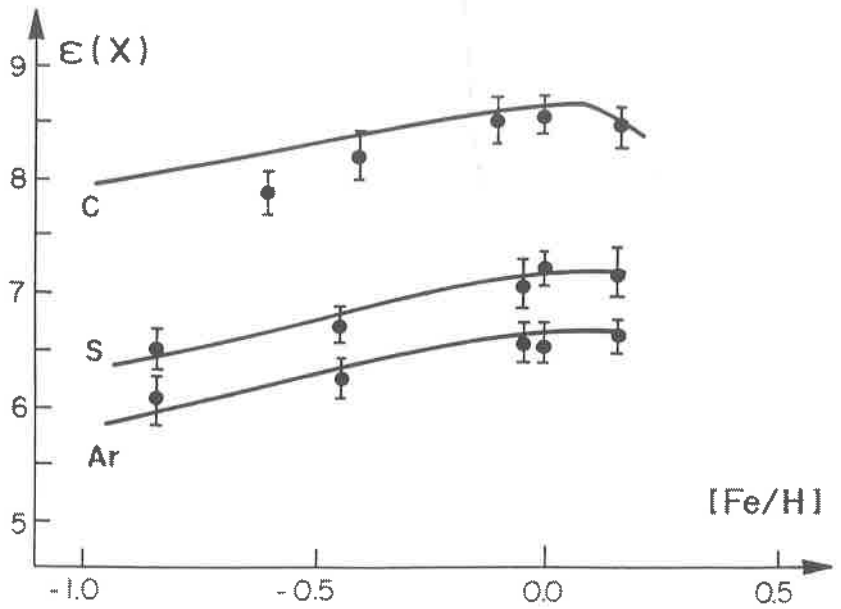

Figure 5 - C, S, Ar vs metallicity for the galactic disk

Figure 5 shows the variation of carbon, sulphur and argon as a function of the metallicity, while Table 1 shows a comparison between predicted elemental ratios and data at the epoch of the solar system formation. The agreement between data and predictions are quite good, but theory seems to predict a slightly higher carbon abundance than observed. In fact, we have to consider that yields for C are still uncertain and contribution from intermediate stars was not included. It is worth mentioning that our computations predicts presently, also a small decrease in the carbon abundance. We emphasize that in the Orion nebula, recent determination of the carbon abundance by Rubin et al. (1993) gives $\varepsilon(C) \approx 8.45$, which is about 0.11 dex lower than the solar value. Again we may argue that the observed C deficiency is due to depletion into grains. However, the stellar data ($\varepsilon(C) \approx 8.39$) by Cunha & Lambert (1994) confirm that both values agree, supporting a small carbon underabundance. A similar picture is found for nitrogen. The B star data by Gies & Lambert (1992) indicate a N/O ratio similar to the sun, suggesting that also N is slightly deficient in the ISM. The CNO deficiency could have effects in the theoretical study of the chemical reactions involving molecules and their computed abundances. Also, it could affect the gas-to-dust ratio, the chemical composition of the grains, and the cooling of the ISM. These are certainly problems which merit further investigations.

Table 1 - α-elements abundance ratios

Ratio	Predicted	Observed
log(Mg/Fe)	+0.01	+0.08
log(Si/Fe)	+0.21	+0.05
log(Ca/Fe)	−1.13	−1.14
log(Ti/Fe)	−2.60	−2.48

4. Conclusions

In this paper we reviewed some particular aspects of tbe evolution of the main structures of the Galaxy.

The metallicity distribution of halo stars can be explained in terms of a simple model, where gas "infall" into the disk is included. The age dispersion of halo objects depends on both the gas conversion into stars and "infall" time scales. The former is about 6.4 Gyr, while the latter is of the order of 1.2 Gyr. The computations of the temporal behaviour of metallicity by Idiart (1994) indicate tbat the onset of type Ia SNe is 2.7 Gyr, considerably longer than usually assumed.

The stellar data on light elements are consistent with the predictions of a hybrid model: most of the lithium isotopes are produced in the ISM, where "alpha-alpha" reactions dominate, while Be and B are produced in a "oxygen-rich" environment existant in the ejecta of type II SNe. The Be and B correlation with metallicity, and the isotopic Li ratio are explained by this model.

If an initial mass function $\xi(m) \propto m^{-3}$ is assumed to be valid in the interval 0.01 to 80 $M_{\odot}$, then the amount of dark matter in the halo, evidentiated by dynamical effects, is consistent with the presence of a large amount of brown dwarfs.

The central bulge requires an efficiency of star formation about 7 times higher than that of the halo, in order to reproduce the metallicity distribution and an age dispersion of about 2 Gyr.

The variation of the (O/Fe) ratio with metallicity in the disk allows the estimate of the relative contribution of both type Ia and II SNe to the chemical enrichment and to predict the evolution of some primary elements with metallicity.

References

Alcock et al. 1993, Nature, 365, 621

Arnett, W.D., 1990, in Chemical and Dynamical Evolution of Galaxies. Eds. Ferrini, F., Franco, J., Matteucci, F. ETS Editrice, Pisa, p. 410

Armandroff, T.E., 1989, AJ, 97, 375

Aubourg et al. 1993, Nature, 365, 623
Barbuy, B., 1988, A&A, 191, 121
Barbuy, B., Erdelyi-Mendes, M., 1989, A&A, 214, 239
Barbuy, B., Freitas Pacheco, J.A. de, Castro, S., 1994, A&A, 283, 32
Boesgard, A.M., King, J.W., 1993, preprint
Borges, A.C.A., Freitas Pacheco, J.A.de 1989, Astrophys. Sp. Sci., 153, 67
Carney, B.W., Latham, D.W., Laird, J.B., 1990, AJ, 99, 572
Carney, B.W., 1993, in Galaxy Evolution: The Milky Way Perspective, ed. S.R. Majewsky, ASP Conf. Ser. 49, p. 83
Catelan, M., Freitas Pacheco, J.A.de, 1993, AJ, 106, 1858
Cunha, K., Lambert, D.L., 1994, ApJ, 426, 170
Deliyannis, C., Malaney, R., 1994, preprint
Duncan, D.K., Lambert, D.L., Lemke, M.,1992, ApJ, 401, 584
Fitzsimmons, A., Brown, P.J.F., Dufton, P.L., Lennon, D.J., 1990, A&A, 232, 437
Freitas Pacheco, J.A.de 1993, ApJ, 403, 673
Freitas Pacheco, J.A.de, Barbuy, B., 1993, in Frontier Objects in Astrophysics and Particle Physics. Eds. Giovanelli, F., Mannocchi, G. Editrice Compositori, Bologna, p. 401
Gies, D.R., Lambert, D.L., 1992, ApJ, 387, 673
Gilmore, G., Gustafsson, B., Edvardsson, B., Nissen, P.E., 1992, Nature, 357, 379
Harmon, R., Gilmore, G., 1988, MNRAS, 234, 1025
Hobbs, L.M., Thorburn, J.A., 1994, ApJ, 428, L25
Hut, P., Djorgovski, S., 1992, Nature, 359, 806
Idiart, T.P., 1994, in preparation
Kraft, R., 1992, Highlights of Astronomy
Kajino, T., Boyd, R.N., 1990, ApJ, 359, 267
Laird, J.B., Rupen, M.P., Carney, B.W., Latham, D.W., 1988, AJ, 96, 1908
Lee, Y.W., 1992, PASP, 104, 798
Luck, R.E, Lambert, D.L., 1985, ApJ, 298, 782
Majewski, S.R, Munn, J.A., Hawley, S.L., 1994, ApJ, 427, L37
McWilliam, A., Rich, R.M., 1994, preprint
Meneguzzi, M., Audouze, J., Reeves, H., 1971, A&A, 15, 337
Nomoto, K., Thielemann, F.-K., Yokoi, K., 1984, ApJ, 286, 644
Norris, J.E., Ryan, S.G., 1989, ApJ, 340, 739
Ortolani, S., Barbuy, B., Bica, E., 1990, A&A, 236, 362
Ortolani, S., Bica, E., Barbuy, B., 1993, A&A, 267, 66
Paczynsky et al. 1994, preprint
Ratag, M.A., 1992, Ph.D. thesis, University of Groningen
Reeves, H., Fowler, W.A., Hoyle, F., 1970, Nature Phys.Sci., 226, 727
Renzini, A., 1994, preprint
Rich, R.M., 1988, AJ, 95, 828
Rubin, R.H., Dufour, R.J., Walter, D.K., 1993, ApJ, 413, 242
Ryan, S.G., Norris, J.E., 1991, AJ, 101, 1865

Schuster, W.J., Nissen, P.E., 1989, A&A, 222, 69
Shaver, P.A., McGee, R.X., Newton, L.M., Danks, A.C., Pottasch, S.R, 1983, MNRAS, 204, 53
Smith, V.V., Lambert, D.L., Nissen, P.E., 1993, ApJ, 408, 262
Spite, M., Spite, F. , 1982, Nature Phys.Sci., 297, 483
Steigman, G., Walker, T.P., 1992, ApJ, 385, L13
Teresawa, N., Sato, K., 1990, ApJ, 362, L47
van den Bergh, S., 1994, DAO preprint
Vangioni-Flam, E., Cassé, M., Audouze, J., Oberto, Y., 1990, ApJ, 364, 568
Walker, T.P., Steigman, G., Schramm, D.N., Olive, K.A., Kang, H.S., 1991, ApJ, 376, 51

Section 4:

EXTRAGALACTIC ASTRONOMY

Mergers of Dissipationless Systems - Clues about the Fundamental Plane *

Hugo V. Capelato
†
Astrophysics Division – INPE

August 1994

1 Introduction

The last decade has witnessed the growing of our understanding of the global properties of galaxies. In particular, the accumulation of high-quality photometric and kinematic data for ellipticals has revealed that these systems form a two-parameter family in the space defined by radius (R), surface brightness (I) and velocity dispersion (σ) ([8, 13, 10]). The relation involving such quantities is called the "Fundamental Plane", FP. The observed FP can be described as R$\sim \sigma^{\rm A}{\rm I}^{\rm B}$, where A$\sim$1.4 and B$\sim -0.9$ ([11]). Assuming homology, for a pure virial theorem we should have R$\sim \sigma^{\rm A}{\rm I}^{\rm B}({\rm M/L})^{-1}$ from which follows (M/L)$\sim{\rm M}^{1/6}$ ([15, 9]). One of the possible consequences of this result is that the formation of elliptical galaxies was partly dissipative, otherwise we should not expect any relation between (M/L) and mass. Other possibilities like the presence of dark matter or varying IMF can also be claimed as reasonable explanations for such dependence [24, 12]. A basic assumption common to all of these analysis is that ellipticals can be understood as homologous systems. However, a more carefull inspection of the major-axis luminosity profiles of early-type galaxies [4], shows that this may not be the case. This poses a serious problem for the study of the FP as a fundamental tool to probe mechanisms of galaxy formation.

In this talk I will discuss the results of a series of numerical experiments of mergers of elliptical galaxies which shed a new light on the question of the origin of the FP correlations [5]. Based on these results I will discuss whether or not the nonhomologous nature of the merger remnants can at least partly explain why the FP deviates from a pure virial theorem. In the next Section I will describe the basic elements of our numerical experiment; Section 3 presents the main results we obtained regarding the properties of the FP. Finally, Section 4 discusses the nonhomologous nature of the remnants of the simulations studied here.

2 Simulations setup

The initial model galaxies used in the experiments reported here are 4096 particle Monte Carlo realizations of a spherical isotropic King model [18] generated with central potential $W_0 = 5$ (concentration $c = \log r_t/r_c = 1.03$,. Although the concentration parameter is too

*Work done in collaboration with Reinaldo R. de Carvalho, Dept. of Astrophysics - ON-CNPq, and Ray G. Carberg, Dept. Of Astronomy, Univ. of Toronto

†Invited talk at the XX Brazilian Astronomical Society Annual Assembly, Campos de Jordão - SP.

low compared to real elliptical galaxies we expect that such a value does not restrict any of our results.

Mass and length units were set as $10^{10}M_{\odot}$ and 1 kpc, respectively; these values, together with $G = 1$, fix our time and velocity units as 4.72 Myr and 207 km s^{-1}, respectively. The initial models have total mass $M = 10$ (which means that the particle mass, m_p, is $\sim$0.00244) and half-mass radius $r_h = 2$ in these units. The σ_* parameter, characteristic of the kinetic temperature of the King models, amounts to 1.086 (225 km s^{-1}). Note that scaling to different values of M and r_h does not change any of our units but does change σ_* by a factor $(M/r_h)^{1/2}$.

The simulations were made using a C translation of the Barnes and Hut TREECODE [1, 20], running on SUN Sparc2 machines. The code parameters were set as: tolerance parameter, $\theta = 0.8$; timestep $\Delta t = 0.025$; potential softening $\epsilon = 0.05$. The force computation includes quadrupole correction terms following Dubinski [14].

We have approximately followed the formulation of Binney and Tremaine [2] to characterize the initial orbital conditions of the encounters. We define the dimensionless energy and angular momentum of the initial orbit as: $\hat{E} = E_{orb}/(1/2)\mu\sigma_*^2$ and $\hat{L} = L_{orb}/\mu r_h \sigma_*$, where $\sigma_* = (\sigma_{*1} \cdot \sigma_{*2})^{1/2}$ and $r_h = (r_{h_1} \cdot r_{h_2})^{1/2}$, the indices staying for each of the initial galaxies; μ is the reduced mass of the system. For initial models other than King's these definitions must be applied by substituting the σ_* parameter by some characteristic internal velocity dispersion of the model.

To fully determine the orbital elements of the encounter, a further dimensionless parameter must be defined:

$$A = \frac{2G(M_1 + M_2)}{r_h \sigma_*^2}$$

Given a set of values of $\hat{E}$, $\hat{L}$ and A, the two-body orbit equation may be straightforwardly obtained by writing the orbital energy and angular momentum as a function of the center-of-mass positions and velocities of the pair, thus allowing the choice of the initial conditions for the encounter. We note in passing that the parameter A depends uniquely upon the internal structure of the initial interacting galaxies. In this paper, we restrain ourselves to the plane defined by $A = 16.96$, given by the initial galaxy model described above.

We have determined the initial separations and velocities for the encounters from a grid of values previously fixed in the $(\hat{E}, \hat{L}, A = 16.96)$ plane. For bound initial orbits these initial conditions were always taken at the apocenter position in order to maximize the dynamical effects of tidal forces between the companions; for unbound orbits the initial conditions were taken such that the separations were about 2 times the tidal radius of the galaxies, which amounts to 10.7 Kpc.

We have runned about 17 different numerical simulations of encounters producing mergers where the initial galaxies were the King model galaxy described in the beginning of this section (the standard model). The remnants of these encounters have been called the "first generation" mergers. However we have also runned four simulations of encounters ocurring among the merger remnants produced by these former experiments, thus producing a "second generation" mergers. Three further simulations using different initial model galaxies were also performed.

Our simulations do not explicitly include a luminous stellar component and an extended dark matter component. There are several arguments for this approach. First, we wish to establish the scaling properties of single component dynamical systems before going on to two component ones. An eventual goal is to do more general simulations with initial conditions drawn from larger scale cosmological simulations. The minimal goal of the simulations discussed here is to establish whether the merging of simple one component systems will destroy any pre-existing FP relation. Second, these one component systems are initiated in

sufficiently close orbits that the physical interpretation is that they have already spiralled through the bulk of their dark halos. Furthermore the effect of dark halos on the visible bodies is, crudely, equivalent to the visible bodies alone but arriving in contact on orbits which have been altered by the dark halos. Consequently, we conclude that investigating the merging of single component systems with "vacuum" exteriors will be a useful guide to the question of how the FP transforms under merging.

3 The Fundamental Plane of the merger remnants

The merger remnants were analyzed so as to reproduce the quantities related to the observed FP of elliptical galaxies. Each remnant was projected in 100 random directions and, for each projection, the barycenter of the distribution was found and quantities like the effective radius r_e (defined as the radius of a circle encompassing half of the particles, $N_p/2$, where $N_p/2$ is the net number of particles after removing the escapers) and the mean surface density inside r_e, $\bar{\Sigma}_e = N_p m_p / 2\pi r_e^2$, were measured. We defined a mean "surface brightness" as $\langle \mu_e \rangle = -2.5 \log \bar{\Sigma}_e + C$, the value of the constant, $C = 29$, is such as to allow this quantity to assume values about the same order as those typically measured in real galaxies. A projected central velocity dispersion, σ_0, was measured inside a square "slit" of side $f \cdot r_e$, as the mean square projected velocity of all particles inside the "slit". The median of these projected quantities (taken from the 100 projections) were then calculated and attributed to the remnant. The corresponding errors are standard deviations based on the quartiles of the distribution of each quantity. The characteristic parameters, $r_e, \sigma_0$and $\langle \mu_e \rangle$ (measured for a slit with $f = 0.2$), for the end-products of the *17 first generation mergers* were then combined in the same way as in Djorgovski and Davis [8] and are shown in Figure 1 as open circles. The factor 0.2 was established by looking at what observers usually take to measure the central velocity dispersion [8, 3]

The solution which optimizes the correlation coefficients and the orthogonal least squares is (dotted line in Figure 1):

$$log\ r_e = (1.36 \pm 0.08)\ [log\ \sigma_0 + 0.2\langle \mu_e \rangle] + C \qquad (1)$$

These coefficients are remarkably similar to those found for real elliptical galaxies in K-band [23]. Our simulations trace the counterpart of the observed elliptical galaxies not significantly affected by dissipative processes as star-formation induced by merging, that is why we compare our results with the infrared fundamental plane. The open square in Figure 1 represents the initial King model for the 17 first generation experiments and it was not included in the fit. We found the solution for the FP slightly dependent on the size of the slit used to measure σ_0. For instance, for a slit with $f = 0.5$ the coefficient 1.36 changes to 1.52 , increasing to 1.95 for a slit covering the whole system. The dependence of this coefficient with the slit size noted before reflects the nonhomologous nature of the velocity dispersion gradient and mass distribution in the central parts of the remnants.

Figure 1 displays the solution in the homologous case as a solid line (pure virial theorem) and it is quite evident that it does not match the FP solution obtained above.

It is important to emphasize that the set of these 17 first generation mergers occupy a region of the $(r_e, \sigma_0, \langle \mu_e \rangle)$ space which corresponds to the locus of the compact galaxies in the observed FP. In other words, the covered portion of the $(\hat{E}, \hat{L})$ plane does not exhaust all the possibilities. In fact, there is a limit to the initial orbital energy of the progenitors, above which there would be no merger within a Hubble time. Therefore, we may not expect to reproduce the observed range of the FP with the initial model galaxy used in this work.

In order to fulfill the observed FP, from compact to giant ellipticals, we have designed three other simulations representing an hierarchical scheme in which some of the

end-products of the former simulations merge with themselves to produce a more massive -"second generation"- object. The representative points of these mergers are shown in Figure 1 as a solid triangle, a solid circle and a solid pentagon, respectively. As can be seen, these secondary mergers are close enough to the solution of the FP obtained using only first generation end-products. This result supports the idea that with such a scheme we might be able to reproduce the global properties of elliptical galaxies.

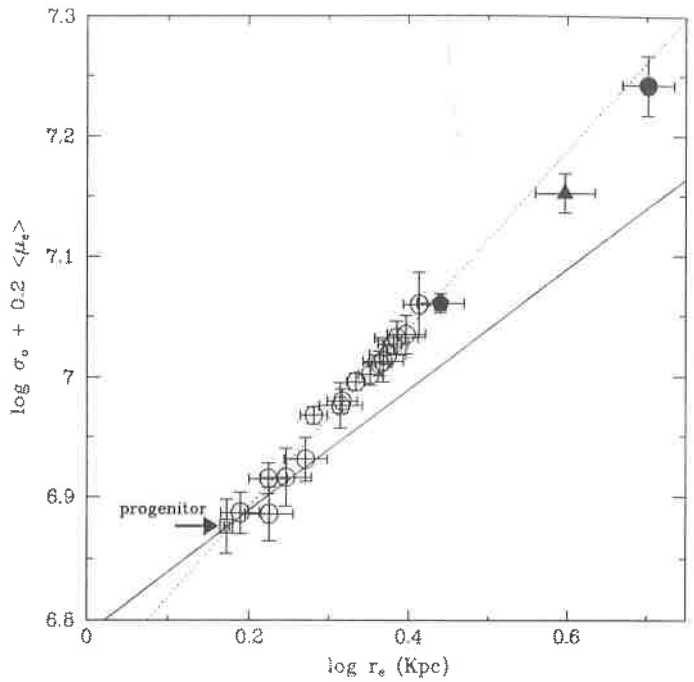

Figure 1: This figure shows the FP of the first generation of mergers remnants. Each remnant is plotted as an open circle; the open square (designated by an arrow marked "progenitor")represents the initial model galaxy for these runs, as described in the text. Second generation remnants are shown with filled symbols (the solid pentagon represents the remnant of a merger between the "standard" King model galaxy ($W_0 = 5$) and one of the first generation merger remnant) The solid line represents the virial relation and the dotted line the best fit line to the points corresponding to the first generation remnants.

As already noted by several authors [11] the observed FP has a remarkable small scatter around it, which is probably associated with some regularity in the process of making elliptical galaxies. Therefore, we should expect that any simulation starting from different initial model galaxies should move by merging to the same FP defined before.

The open triangle in Figure 2 refers to a progenitor which is homologous to our standard initial model but with mass equal to 2M and half radius $2r_h$, which keeps σ_* unchanged . The remnant result by merging this progenitor with itself is displayed in Figure 2 as an open hexagon. The short line which connects these points was taken parallel to the FP solution found before. As can be seen, there is a hint that this progenitor and its remnant in fact define approximately a parallel sequence to the fitted FP.

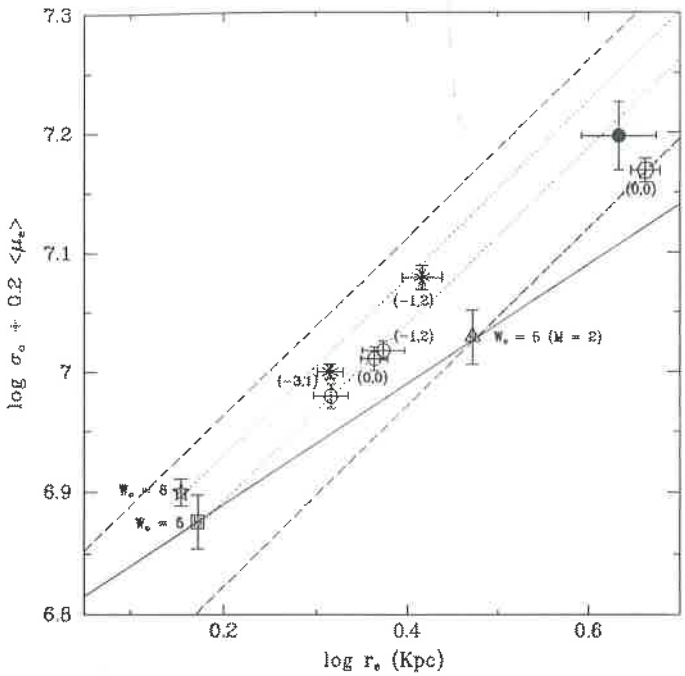

Figure 2: This figure shows the locus of the remnants for the runs starting from different progenitors than the "standard" one (see text). The open triangle represents an homologous progenitor with $W_0 = 5$, but with the mass and half-radius doubled; its remnant is represented by the open hexagon. The open star represents a less compact progenitor with $W_0 = 8$ and mass and half-radius identical to the standard one; its remnants are represented by asterisks a second generation merger is represented by the solid circle. We also plotted the "standard" progenitor (open square) together with some of its remnants having the same initial orbital conditions $(\hat{E}, \hat{L})$ as the other runs represented in this figure. The dotted lines starting from the three progenitors *are parallel* to the FP solution shown in Figure 1. The two dashed lines give the *observed* 1σ upper and lower bounds of the FP, as estimated from the FP solution obtained for cluster sample. The solid line represents the virial relation passing by the "standard" progenitor.

The same seems to be true in the case where the progenitor is non-homologous to our standard one. These are the cases of the two runs displayed in Figure 2 which start from a less concentrated King model with $W_o = 8$, while maintaining the other parameters the same as before (except the σ_* parameter, which in this case values 1.117). Notice that in contrast to our basic model, this initial model may be more realistic when compared to real elliptical galaxies. This model is shown in Figure 2 as an open star whereas its remnants are represented by an asterisk. Also, we can see in this figure the point representing a second-generation merger for this initial model galaxy (solid circle) which exhibits the same trend as seen before (See solid circle in Figure 1). As in the case discussed above, it can be seen that the line joining this progenitor and its remnant also defines a parallel sequence to the fitted FP. It is clear from this figure that the observed fundamental plane has a scatter around it which is roughly twice as big as the scatter we measured in our simulated FP. Such discrepancy could be reflecting the physical constraints on the central potential (W_o) and the mass of the primordial units from which galaxies were formed. Varying W_o and mass we can increase the scatter of the FP and in such case the "observed" scatter restricts the range of variation of these quantities.

Two-body relaxation is a concern in most numerical simulations of gravitational systems and particularly in our case for it acts toward contracting the central parts of the systems and thus goes in the same sense as the deviation shown by the merger remnants relative to the expected virial relation for homologous systems. We have performed various tests and found strong evidence that 2-body relaxation do not play any significant role in the FP correlations discussed before.

That the FP correlations we found are not affected by binary relaxation was further confirmed when we perform the same analysis which was made before at $T_1 = 30 * T_{cr} + T_{per}$, where T_{per} is the time interval before the first pericenter, but now for the mergers taken at $T_2 = 15 * T_{cr} + T_{per}$. Consistently with the discussion above, we find practically no change between the results found at T_2 and T_1: the same tight linear correlation is found, with an angular coefficient of 1.42 ± 0.08 for the $f = 0.2$ slit. It is interesting to note that this result shows that the FP developed well before the completion of the merger. We have also made some robustness tests in order to measure how sensitive our results were to the number of particles in the simulations. We have then re-runned two of the first-generation simulation but with the total number of particles doubled and tripled. We found that the positions of the remnants of these simulations were fully consistent with that obtained before. This shows that the result reached in this work is not an artifact of the low resolution, since real galaxies have a much higher number of particles.

4 On the homology between progenitors and merger products

We found that simple dissipationless merging can partly explain the observed fundamental plane for elliptical galaxies, as we described in the previous section. An important question to be addressed as a natural follow-up of this finding is about the nature of the deviation observed in the FP of elliptical galaxies with respect to the virial theorem and in what way we can use our simulation to learn about it. Indeed, under the dissipationless assumption used here such deviation is clearly associated to the fact that merger remnants are neither not homologous among themselves nor with their progenitors.

This deviation from homology may be more quantitatively stated by writing the scalar virial theorem in terms of the observed quantities σ_o, r_e and $\langle \mu_e \rangle$. We find:

$$r_e = (C_r \cdot C_v)/(2\pi G) \cdot [\sigma_o \cdot \Sigma_e^{-\frac{1}{2}}]^2 \qquad (2)$$

where the coefficients C_r and C_v are defined as

$$C_v \doteq \langle v^2 \rangle / \sigma_o^2 \quad \text{and} \quad C_r \doteq R_G / r_e$$

with $\langle v^2 \rangle^{1/2}$ and R_G being respectively the 3-D velocity dispersion and the gravitational radius of the system.

For a given family of equilibrium models, these two coefficients are constant so that equation (2) defines families of homologous equilibrium systems depending on the product $C_r \cdot C_v$. Note that this equation applies equally to the merger remnants as for their progenitors, since both are found in states of dynamical equilibria. In contrast the observed relation, equation (1), may be written as:

$$r_e = C_{FP} \cdot [\sigma_o \cdot \Sigma_e^{-\frac{1}{2}}]^\alpha \tag{3}$$

where $\alpha \sim 1.6$ and the constant C_{FP} depends on the initial equilibrium models which have been merged.

By taking into account the mass and energy variations of the merger remnants relative to their progenitors it is straightforward to relate the initial and final values of the coefficients C_r and C_v. Figure 3 shows the run of the initial-to-final ratios of the two homology coefficients as a function of $\hat{E}$ and $\hat{L}$, the normalized initial orbital energy and angular momentum of the mergers. The FP variables are also plotted. The first thing to note in this figure is the lack of any obvious dependence of these quantities on $\hat{L}$. This is due to the fact that most of the initial angular orbital momentum of the colliding galaxies is transferred to the outer parts of the merger remnant. Indeed, we found that the remnants of our simulations display negligible rotation velocity in their central regions ($r < r_e$) and that all the angular momentum is carried by the outlying material. This is consistent with results from other merger simulations [17]. We have also verified that there is no significant dependence of these quantities on the structure parameter A, although the small range of variation of this variable in our simulations precludes any firm conclusion on this respect. We are thus forced to conclude that the physical parameter driving the observed values of the coefficients of the FP correlations is the initial orbital energy of the pair.

It is interesting to note that the mass distribution (C_{r_m}/C_{r_p}) seems to follow homology much better than the velocity distribution (C_{v_m}/C_{v_p}). This is even more true for the most bound initial orbits for which the ratio (C_{r_m}/C_{r_p}) $\simeq 1$, as it can be seen in Figure 4. Since it is the combination of these two non-homologies that produces the FP correlation, they somehow reflect how the merger remnants accommodate the input energy in their central parts. In this sense the specific value of α should be viewed as a result of the details in the merging process and we may conjecture that it is also related to the distribution of the $\hat{E}$ at early epochs when the first galaxies started to coalesce to build hierarchically the galaxies we know today.

An independent way to study the homology question is to parameterize the major axis profile of the remnant so that possible correlations between structural parameters and the initial conditions can be investigated. In fact, it has been noted that it is possible to obtain better fits to the major-axis luminosity profiles of elliptical galaxies by using an $r^{1/n}$ law, instead of the ususal $r^{1/4}$ law [4]. The best values for the parameter n for their fits vary from 2 to 20, and are correlated to the effective radius of the galaxies. An important caveat is that such methodology should be applied with some precaution since S0 galaxies ($r^{1/4}$ bulge + an exponential disk) could be fit to an $r^{1/n}$ law with different values of n reflecting probably different disk/bulge ratios instead of nonhomology. However, it is still an important result for it shows that the traditional view by which elliptical galaxies are homologous objects (at least in their luminosity distribution), described by an $r^{1/4}$ law may not be the case. In order to see if a similar effect was present in our merger remnants (and in this case we are not polluted by a disk component) we fit the $r^{1/n}$ law to the mean major-axis mass density

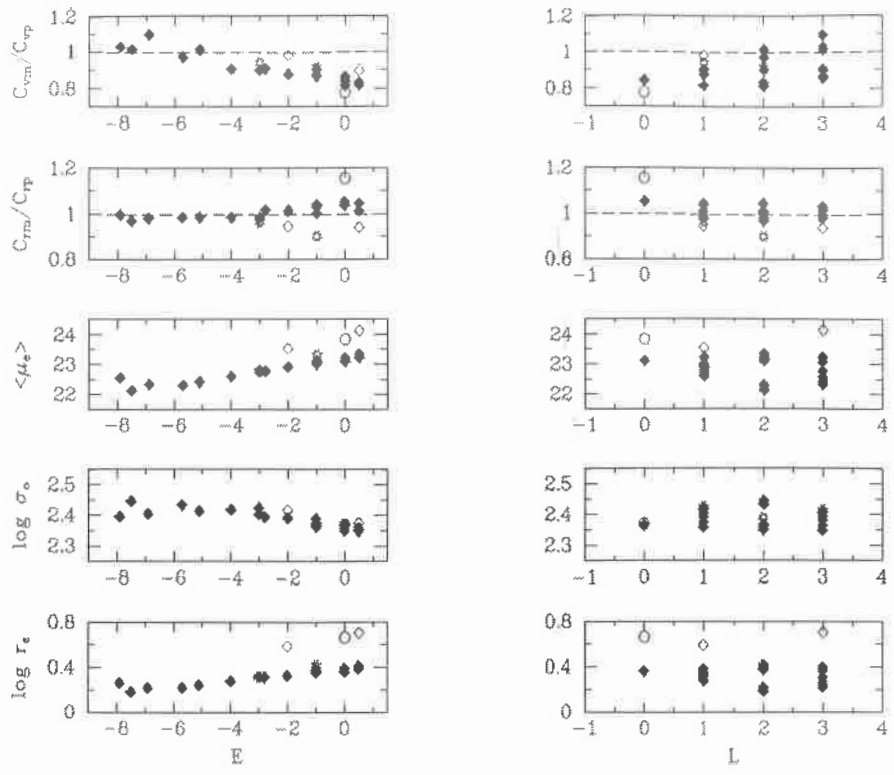

Figure 3: The various projected quantities related to the FP of remnants from equal progenitor mergers plotted as a function of the initial orbital energy (left panels) and the initial orbital angular momenta (right panels). Filled diamonds correspond to first generation mergers coming from the standart model progenitor; asterisks to those first generation coming from the $W_0 = 8$ model. The open diamonds correspond to second generation mergers and the open circle to the merger remnant having an homologous progenitor with $W_0 = 5$, but with the mass and half-radius doubled.

profile. As before this mean profile was obtained from 100 profiles taken from randomly distributed directions. The fitting interval chosen was from 0.5 kpc ($\sim 10\epsilon$) to 1 r_e. The parameter n obtained from these fits varies from 1.2 to 3.4 and it correlates with r_e. In other words, n is correlated to the deviation between the FP and the virial relation in the sense that large deviations correspond to large n. This last result is also consistent with those reported in the litterature [4].

5 Conclusions

In this work we aimed to measure the usual set of quantities which constitute the so called Fundamental Plane (FP) correlations of elliptical galaxies (e.g. r_e, σ_0, $\langle \mu_e \rangle$) for a sample of N-body simulations of mergers of identical galaxies. In doing so we have shown that merger remnants obey a relation which is very close to the observed FP correlation. Actually, by merging remnants of a merging first generation with themselves we found that the FP is still preserved. These results suggest an hierarchical merging scheme, where remnants are merged among themselves to produce successive merger remnants generations, extending

the FP relation over the entire $(r_e, \sigma_0, \langle\mu_e\rangle)$ space of observed elliptical galaxies.

These results indicate that the FP correlations may be originated by pure gravitational processes rather than by dissipative gas processes as is commonly accepted ([15, 9]. Indeed we found that for our dissipationless merger remnants, it is the non-homologous nature of both the velocity and mass distributions in their central region ($r < r_e$) that is responsible for the small departure from the homology prediction, which is characteristic of the observed FP correlation.

We emphasize that it is the central velocity distribution and not the mass (luminosity) distribution that strongest deviates from homology. Thus, although there is some observational evidence (also seen in our simulations) that the *central* luminosity distribution of elliptical galaxies is not homologous [4], it is the observation of their central velocity distribution that may fully reveal this effect. This would be however, a much harder observational task. It is interesting to note that we found no significant homology deviation when we use the global projected dispersion velocity of the merger remnant instead of its central value: this reinforces the view that non-homology effects concern only the central parts of the remnants. Besides, we also find that the non-homologous deviation of a merger remnant from its progenitor is nearly exclusively a function of the initial orbital energy of the pair.

We find that different initial progenitors produce different families of merger remnants, all of them obeying relations similar to the FP correlation but displaced by different amounts. This could be indicative that the central potential and mass of the primordial units did not have a wide distribution, otherwise the scatter of the observed FP would be much larger.

We argue that under the assumptions presented along this paper, elliptical galaxies (or at least those living in clusters of galaxies), could be generated in a dissipationless hierarchical merging scheme. However, it is important to emphasize that although we explain the coefficients involved in the FP definition, the observed scatter in this relation is still not well understood. We could either claim for a constraint on W_o and mass of the first generation galaxies or that dissipation processes contributed to the increasing of the scatter without changing the general trend.

As stressed before, our experiments do not explicitly include any dark matter component. The simulations presented here correspond to galaxies which have already spiralled in through their common dark matter halo, so that at the initial conditions their visible parts are nearly touching. However, as we have shown, the variation of orbits leaves the end-products on the same fundamental plane as they began. It is likely that adding some dark matter at large radii would mainly act to change the effective orbital parameters but in anyway the outcome of the collisions would leave the remnant on the FP. In this sense we are confident that there is indeed no loss of generality in neglecting the effects of any dark matter halo component. We are currently investigating the effect of dark matter on the FP but under different initial conditions and this will be subject for a future contribution.

References

[1] Barnes, J., Hut, P., *Nature*, **324**, 446, 1986

[2] Binney, J., Tremaine, S., "*Galactic Dynamics*", Princeton Univ. Press, Princeton, 1987

[3] Burstein, D., Davies, R.L., Dressler, A., Faber, S.M., Stone, R.P.S., Lynden-Bell, D., Terlevich, R.J., Wegner, G., *Astrophys. J.*, **64**, 601, 1987

[4] Caon, N., Capaccioli, M., D'Onofrio, M.,1993,Mon.Not.R.Ast.Soc.,in press.

[5] Capelato, H.V., de Carvalho, R.R., Carlberg, R.G., 1995, Astrophys. J., in press.

[6] Davies, R.L., Burstein, D., Dressler, A., Faber, S.M., Lynden-Bell, D., Terlevich, R.J., Wegner, G., *Astrophys. J. Suppl.*, **64**, 581, 1987

[7] de Carvalho, R.R., Djorgovski, S.G., *Astrophys. J.*, **389**, L41, 1992

[8] Djorgovski, S.G., Davis, M., *apj*, **313**, 59, 1987

[9] Djorgovski, S.G., *in: Starbursts and Galaxy Evolution - Moriond Astrophysics Workshop*, ed: Thuan, T.X. et al., Gif-sur-Yvette, Eds. Frontières, p.549, 1988

[10] Djorgovski, S.G., de Carvalho, R.R., *in: Windows on Galaxies*, ed: G. Fabbiano et al., Dordrecht: Kluwer p.9, 1990

[11] Djorgovski, S.G., *in: Cosmology and Large-Scale Structure in the Universe - ASP Conference Series No. 24*, ed: R.R. de Carvalho, San Francisco: A.S.P., p.19, 1992

[12] Djorgovski, S.G., Santiago, B.X., *in: Structure, Dynamics and Chemical Evolution of Elliptical Galaxies - ESO Conf. and Workshop Proc. no. 45*, ed: I.J. Danziger, W.W. Zeilinger, K. Kjar, Garching: ESO, p.59, 1993

[13] Dressler, A., Lynden-Bell, D., Burstein, D., Davies, R.L., Faber, S., Terlevich, R.J., Wegner, G., *Astrophys. J.*, **313**, 42, 1987

[14] Dubinski, J., 1988, M. Sc thesis, University of Toronto.

[15] Faber, S., Dressler, A., Davies, R.L., Burstein, D., Lynden-Bell, D., Terlevich, R.J., Wegner, G., *in: Nearly Normal Galaxies*, ed: S. Faber, New York: Springer Verlag, p.175, 1987

[16] Farouki, R.T., Shapiro, S.L., Duncan, M.J., *Astrophys. J.*, **265**, 597 , 1983

[17] Hernquist, L., *Astrophys. J.*, **409**, 548, 1993

[18] King, I.R., *Astron. J.*, **71**, 64, 1966

[19] Miller, R.H., Smith, B.F., *Astrophys. J.*, **227**, 785, 1979

[20] Marinho, E.P., 1991, M. Sc thesis, INPE.

[21] Navarro, J., *Mon.Not.R.Ast.Soc.*, **239**, 257, 1989

[22] Pearce, F.R., Thomas, P.A., and Couchman, H.M.P., *Mon.Not.R.Ast.Soc.*, **264**, 497, 1993

[23] Recillas-Cruz, E., Carrasco, L., Serrano, A., and Cruz-Gonzáles, I., *Astron. & Astrophys*, **249**, 312, 1991

[24] Renzini, A., Ciotti, L., *Astrophys. J. Letters*, **416**, 4, 1993

[25] White, S.D.M., *Mon.Not.R.Ast.Soc.*, **191**, 1p, 1980

DWARF GALAXIES IN TIDAL TAILS: STAR FORMATION HISTORY

Horacio Dottori[1], Felix Mirabel[2] and Pierre-A. Duc[2]

(1) - Instituto de Física – UFRGS, CP 15051,
CEP 91501-970, Porto Alegre, RS, Brasil
(2) - Service d'Astrophysique, Centre d'Etudes de Saclay,
F-F91191 Gif-sur-Yvette, France

Abstract

Spectroscopic observations have been used to probe star formation in tidal tails and to test model predictions on the formation of dwarf galaxies during the interaction of large disk galaxies. Two advanced stage of mergers (NGC7252 and NGC3256) and one younger interaction (UGC4703) have been observed. NGC7252 presents HII region-like emission at the tip of a tidal tail but not at its base. Strong condensations at the base of a tidal tail in NGC3256, do not show any trace of recent star formation. These results favour a scenario where star formation takes place more likely near the tip of tidal tails, contradicting recent numerical results, where star formation should occur on tidal tails preferentially near the merging galaxies. The $\approx$ 0.1 to 0.2 Gyr old interaction of the system UGC 4703 presents similar characteristics than older merges. It shows that star formation at the tip of tidal tails takes place actively from the very beginning of the collision. The mass in stars within the tidal knots is dominated by the stars tidally removed from the colliding disks. The stars formed "in-situ" on a knot in 1 Gyr amount 10-20% of the original knot mass.

keywords: Galaxies: general – merge: NGC 3256, NGC4038/39, NGC7252, UGC4703 – –interstellar matter – dwarf galaxies in tidal tails

Introduction

The study of condensations on tidal tails of merging disk galaxies is a matter of growing interest(van den Bergh, 1993).

The observation that the emitting knots on the tidal tails of antennae-like galaxies become bluer towards the far-end (Schombert, Wallin and Struck-Marcell, 1990; Mirabel, Lutz and Maza, 1991) pointed out that a segregation of stellar population occurs along the tails of interacting galaxies. Van der Hulst (1979) discovered a pool of 10^9 $M_\odot$ of HI, which surround the tip of the southern tail of NGC4038/39. Later on Mirabel, Dottori & Lutz (1992) have shown that a dwarf galaxy have formed at the tip of the southern tail of the *classical antena* (NGC4038/39), where three HII region were detected, which indicates the presence of massive stars, younger than 10 Myr, which demonstrate that star formation occurs actively in the tidally formed knots.

After the pioner work of Toomre and Toomre (1972) many authors faced the problem of galaxies interaction, mainly trying to understand the evolution of the merging galaxies rather than that of the tidal tails. More recently, Barnes and Hernsquist (1992, BH) and Elmegreen, Kaufman & Thomason (1993, EKT) performed numerical simulations of encounters of disks containing stars and gas. EKF models, in which the disk of gas is more extended than the one of stars, reproduce well the accumulation of gas at the tip of tidal tails. BH predicted that more robust dwarf galaxies and a larger activity of star formation should occur at the base than at the tip of t

In the next section we present the observations. In section 3 we discuss the spectrum of tidally formed Knots associated to NGC3256, NGC7252 and UGC4703. In Section 4 we give the onclusions.

The Observations

NGC 7252 has been observed spectroscopically with the EFOSC at the 3.6 mts ESO telescope in June 1991. We have got two one hour spectra with a 1.5 arcsec slit. The weather conditions were below the standard photometric night at ESO.

NGC 3256 and UGC 4703 have been observed spectroscopically and imaged during february 1993 with the EMMI attached to the NTT ESO telescope. We have got 1800 sec spectra under very good weather conditions. A 1.5 arcsec width long slit has been used to perform the spectroscopy in both cases. The spectra have been calibrated through Stones and Baldwin (1985) spectrophotometric standards. Through the discussion all quantities are expressed in terms of the Hubble constant h=H/100.

Results and discussion

NGC 7252

It is one of the 11 Toomre's original candidates to colliding galaxies. Schweizer (1982) proposed that this galaxy will relax into an elliptical galaxy. Borne and Richstone (1991)

simulated the collision event, reproducing the present morphological and kinematical aspects of the galaxy. They obtained an age of 0.8-1.0 Gyr h^{-1} for the age of the interaction. The high surface brightness knots on the tip of the tidal tails of NGC 7252 are excellent candidates to look for HII region like emission to confirm if ionizing stars (stars younger than 1 Myr), are also present in these objects. We have chosen the E tail (Fig. 1) to perform optical spectroscopy. The slit was set along the two high surface brightness condensations, at the tip and at the base of the tidal tail.

We obtained the spectrum of a 700 h^{-1} pc width slice of the small condensation at the tip of the E tail. Although weak, the spectrum shows H_α, [OIII] 5007 Åand [OII] 3727 Åemission. The total H_α luminosity is $h^{-2} L_{H_\alpha} = 1\ 10^{38}$ erg s^{-1}, which is slightly weaker than the weakest region in NGC 4038/39 (Mirabel, Dottori & Lutz 1992). Comparison with galactic HII regions (Kennicutt, 1984), shows that it is $\approx h^{-2}\ L_{NGC\ 224}$. The mass of O-B ionizing stars necessary to fuel the HII region is h^{-2} M(OB)=300 $M_\odot$ and the star formation rate (Kennicutt,1983) is SFR=h^{-2} 8.8 10^{-4} $M_\odot$ yr^{-1}. It is a lower limit for the SFR, since the projected size of the HII region is larger than the slit one (Hibbard et al., 1994). The SFR/area $\geq 5\ 10^{-10}$ $M_\odot$ yr^{-1} pc^{-2}, similar to that of dwarf irregular galaxies (Hunter and Gallagher, 1985). If the rate of star formation at the tip of the E tail of NGC 7252 has been sustained since the beginning of the collision (1 Gyr) it had add 10^6 $M_\odot$ of new formed stars to those already stripped out from the galactic disk. The mass of HI at the tip of the E-tail is h^2 5.4 10^8 M_{odot} (Hibbard et al., 1993), which can sustain the derived SFR.

The *photometric mass* of a slice of 0.7x2.5 kpc of the condensation at the tip of the E-tail is 6.4 10^7 $M_\odot$. The population is well represented by Bica(1988) template S7.

If the HII regions are free of absorption, the ratio [OIII] 5007 Å+ [OII] 3727 Å/ $M_{odot} = 1.7 \pm 0.2$ lead to 12 + log [O/H] = 8.6±0.2. It is 1/2 Solar and twice the LMC. This value is higher than that obtained for the less massive Dwarf galaxies in the Local Group (Skillman et al., 1989) but comparable to similar objects in Hunter and Gallagher's (1985) sample of Irregular galaxies.

The condensation at the base of the E tail do not show line emission. The continuum is too weak to infer on stellar populations.

NGC 3256

NGC 3256 presents a strong activity of star formation within the merging body (Graham et al., 1984, Casoli et al., 1991). NGC 3256 tails look larger and more diffuse than those of NGC 7252. As shown in Figure 2a the strongest condensations on the tidal tails are in an elongated strip, located where the W arm connect tangentially the border of the merging body. The rest of the tails do not show conspicuous condensations. According to BH92 models, candidates like this are more likely to be the more massive bound objects in tidal tails. According to BH92, they might contain up to 25% of the mass in gas, and consequently might present star formation activity.

The spectrum in Figure 2b has been obtained by adding all the light comming from the whole set of knots at the base of the W tail (Figure 2a). No emission lines have been detected in this spectrum. H as well as Na and MgI absorption lines can be distinguished in the spectrum. The S/N is very low to perform a qualitative spectral synthesis. Bica's (1988) template S2 fits reasonably the observed continuum. It is contributed by 85% of old population, 10 to 15% of a 1 to 5 Gyr old one and traces of an even younger population (100 to 500 Myr). Translated into mass content the oldest population contribute 93% to 95% and the intermediate plus the youngest one the rest. So we can conclude that there was not stellar formation at the basis of the W tail of NGC 3256 from the beginning of the merge. This result favours EKT models against BH91 ones.

The Total mass of the h^{-2} 0.4x18 kpc slice covered by the slit was calculated by comparing the absolute flux at 5840Å of the tail base with that of the nose in UGC4703, since both spectra are very similar (Fig. 3b). We obtained a mass of 2.6x10^6 $M_\odot$.

UGC 4703

This system (Figure 3a) is constituted by a couple of galaxies of similar projected diameters, separated by about 4-5 galactic diameters. They are connected by a bridge like structure. The bridge appears constituted by two thin, parallel tails. The northern tail appear connected to the NW galaxy and the southern one to the SE galaxy. Particularly, the northern tail presents at the tip a well dettached bright knot (*Knot* in Fig. 3a) followed by a series of condensations along the tail, towards the NW direction (*cond's* in Fig. 3a). Others structures such as faint loops and ripples appear around both galaxies. Particularly interesting is a elliptical like condensation crowded to the NW galaxy (*Nose* in Fig.3a), whose tidal nature is unclear.

The optical pair is about two magnitudes fainter than NGC 7252 and NGC 3256. Nevertheles, as revealed by the HI data (Gordon and Gottesman, 1981), the relative velocity of both pair members is Δ_{V_R}=320 km/sec, which under equilibrium conditions lead to a total mass of the system of 3 10^{11} $M_\odot$. The total HI mass is $M_{HI} = 1.1\ 10^9\ M_\odot$. Both numbers are of the same order of magnitude as those found for NGC 7252 and NGC 3256. It seems that there is a large amount of hidden mass in UGC 4703.

The redshift of knot and the nose give V_R 3500±300 km/sec and 3700±300 km/sec respectively. Current models (e.g. Barnes 1988) indicate a very young interaction with a high ellipticity orbit, having experienced its first fly-by. If the present one is the largest separation attained by the pair, simple calculation set the interaction time in 0.1-0.2 Gyr, that is 1/10 to 1/5 that of NGC 7252 and NGC 3256.

The knot spectrum shows H lines to the noise level. H_α in emission, H_β, H_γ and H_δ in absorption.

The knot continuum, although bluer, is well represented by B88's S7 template. S7 has strong emission lines. A better fit can be reached by adding a small contribution of HII

region and by increasing that of a 50 myr old population (Y2 in Bica & Alloin's library, 1986).

The contribution of the different stellar populations to the light at 5870Å in the modified B88's S7 template is: trace of HII region like continuum (about 1-2%); ≈33% of 50 Myr old stars; ≈39% of 100-500 Myr old stars (age of the interaction) and ≈ 28% of stars older than 1 Gyr.

Translating the previous figures into mass content ≈ 93% is contributed by stars older than 1 Gyr,≈ 5% by stars as old as the interaction (100 to 500 Myr) and a very small fraction (≈ 0.2%) by stars younger than 50 Myr. So at the present time the largest amount of matter in form of stars within the knot, has been stripped out from the colliding disks by the tidal forces.

Since the SFR derived from the 100-500 Myr old component and that for the stars younger than 50 Myr are much the same, we can conclude that within the Knot, stars are formed at a constant rate after the beginning of the collision. Consequently, in 1 Gyr (present age of NGC 7252 and NGC 3256) it was added about 15-25% of mass to the Knot initial. The new formed stars do not change significantly the mass in stars of the tidally ejected Knot.

The continuum of the Nose was compared to the S2 template. It is constituted by population older than 5 Gyr. The *photometric mass* derived for this dwarf galaxy is 1.1E8 $M_{\odot}$.

The comparison interpolated continua of Knot, Condensations and nose and the disk of the SE component of the colliding pair (Fig. 3b) shows undoubtly that the Knot and the condensations have similar continua. They have a younger stellar population than the disk and the Nose. The similarity between the spectra of Knot and condensations indicates that the SFR/luminosity is similar in both objects. This property is also found in Irregular galaxies (Hunter and Gallagher, 1985).

Using Chiosi's (private communication) new evolutive tracks of a burst of star formation, the nose colors can be explained with a 16 Gyr old population of Z=0.1 $Z_{\odot}$ without absorption or with a ≈ 3 Gyr old one, of Z= $Z_{\odot}$, and A_V=0.66mg. We recall that the Milky Way absorption in the region is A_B=0.13 mag.

The Nose brightness $M_{V\,Nose}$ = -14.3 mg has been compared with that of the galactic globular cluster NGC 6624, ((B-V)=1.1, Harris & Racine, 1979) which has a modern mass determination (M=1.5 10^5 $M_{\odot}$, Grabhorn et al., 1992). The comparison give M_{nose} = 1.1 10^8 $M_{\odot}$.

In order to obtain M_{Knot} we have splited its total brightness in the old, intermediate and young stellar population according to the proportions quoted in the previous paragraph. The brightness of the intermediate and young population were "aged" by applying Chiosi's (1993) fading lines. The reduced *Knot* absolute brightness is M_{vKnot} = -12.4 mg, which lead to M_{Knot} ≈ 2.0 10^7 $M_{\odot}$.

Conclusions

The mass in stars within tidal condensations is dominated by the stars tidally removed from the colliding disks. The stars formed "in-situ" in one of these condensations in one Gyr, amount $\approx$ 20% of the condensation total mass. The brightest condensations reach a mass $\geq 10^8$ $M_\odot$.

Stars formation occurs more likely at the tip of the tidal tails, although large concentrations of mass can also be found at the base of tidal tails.

The triggering of stars formation depend more on the position of the condensation along the tidal tail than on the mass of the condensation.

The SFR in star forming condensations in tidal tails is similar to that of dwarf irregulars . The SFR/Luminosity is constant for condensations of UGC 4703 with large luminosity differences.

The metallicity of condensations in tidal tails is higher than in similar objects of the Local Group but similar to dwarf Irregulars.

References

[1] Barnes, J.E. 1988, ApJ, 331, 699

[2] Barnes, J.E., Hernquist, L.,1992, Nature, 360, 715

[3] Bica, E.L., 1988, A&A, 195, 76

[4] Bica, E.L., Alloin, D., 1986, 162, 21

[5] Borne, K.D., Richstone, D.O. 1991, ApJ, 369, 111

[6] Brinks, E., Klein, U. 1988, MNRAS, 231, 63p

[7] Casoli, F., Dupraz, C., Combes, F., Kazés, I., 1991, A&A, 251, 1

[8] Dottori, H., Mirabel, I.F., Duc, P.A., 1993, ESO/OHP Workshop on Dwarf Galaxies, ESO Conference and Worshop Proceedings No49, Ed. Meylan & Prugniel

[9] Duc,P.-A., & Mirabel,I.F., 1994, A&A, 289, 83

[10] Elmegreen, B.G., Kaufman, M., Thomasson, 1993, ApJ, 412, 90

[11] Gordon, D., Gottesman, S.T., 1988 AJ, 86, 161.

[12] Graham, J.R., Wright, G.S., Meihele, W.P.S., Joseph, R.D., Bode, M.F., 1984, Nature, 310, 213

[13] Grabhorn, R.P., Cohn, H.N., Lugger, P.M., Murphy, B.W., 1992, ApJ, 392, 86

[14] Harris, W.E., Racine, R., 1979, Ann.Rev.A&A, 17, 241

[15] Hernquist, L. 1989, Nat, 340, 687

[16] Hibbard, J.E, Guhatakurta, P., van Gorkom, J.H., Schweizer, F., 1994, ApJ, in press,

[17] Hunter, D.A., Gallagher, J.S, 1985, ApJS, 58, 533

[18] Kennicutt, R.C. jr, 1984, ApJ, 287, 116

[19] Mirabel, I.F., Lutz, D., Maza, J. 1991, A&A, 243, 367

[20] Mirabel, I.F., Dottori, H., Lutz,D. 1992, A&Al, 256, l19

[21] Pastoriza, M.G., Dottori, H., Terlevich, E., Terlevich, R., Diaz, A., 1993, MNRAS, 260, 177

[22] Schombert, J.M., Wallin, J.F., Struck-Marcell, C. 1990, AJ, 99, 497

[23] Schweizer. F. 1982, ApJ, 252, 455

[24] Smith, E.P., Hintzen,., 1991, AJ, 101, 410

[25] Stone, R.P.S., Baldwin, J.A., 1983, MNRAS, 204, 357

[26] Toomre, A., Toomre, J. 1972, ApJ, 178, 623

[27] van den Bergh, S., 1993, Nature, 364, 490

[28] van der Hulst, J.M., 1979, A&A, 71, 131

Figure 1 a) - N top, E right. V image of the eastern tail of NGC 7252, taken with the ESO 3.6m telescope. The tail shows a condensation at the tip and another at the base. b) - Spectrum of the E-tail tip condensation. It shows weak but clear H_α, [OIII]5007Å and [OII]3727Å emission lines.

Figure 2 a) - N top, E left. NTT V images of NGC 3256. The series of knots at the base of the W-tail are by far the brightest feature on the tails, b) - Composed spectrum of the series of knots at the base of the w-tail. Absorption lines appear to the level of noise. The spectrum is compared to B88^2 template S2.

Figure 3 N top, E right. a) - NTT V image of the interacting pair UGC 4703. The slit position is shown trough the disk of the E-component of the interacting pair, the *Knot*, the *condensations* and the *Nose*. b) - Relative continuum of the different features.

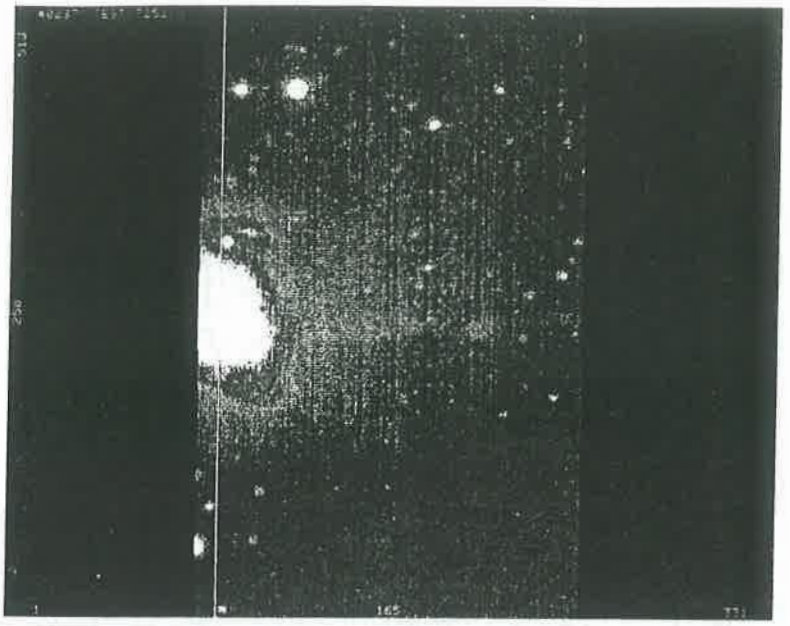

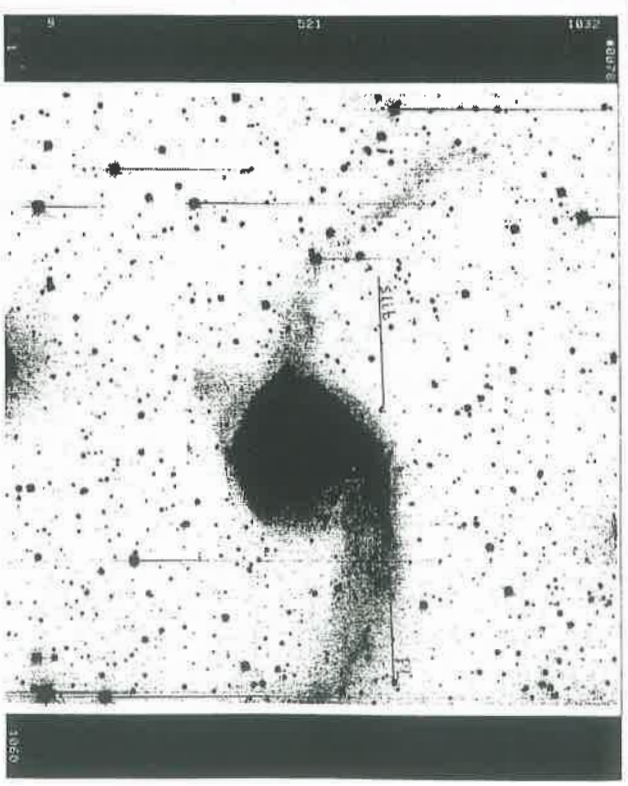

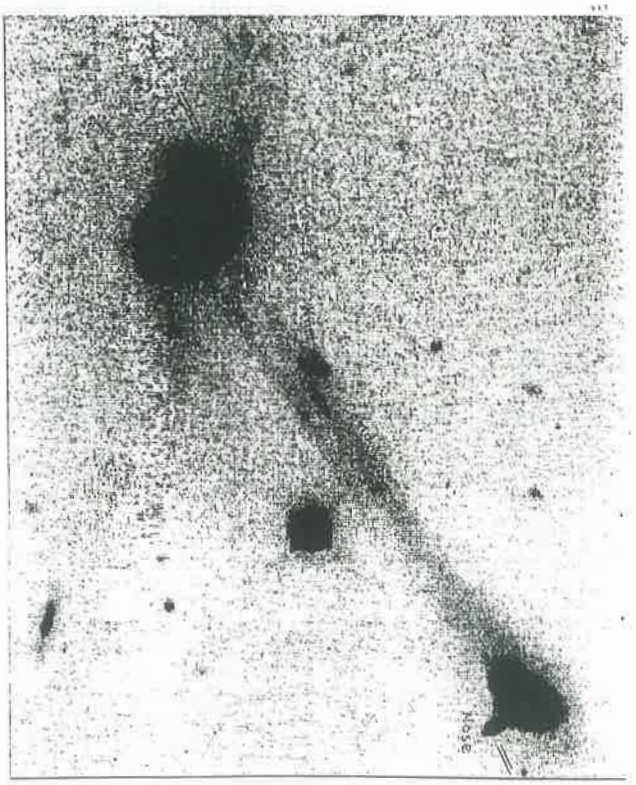

Figures 1a, 2a, 3a - see captions in previous page

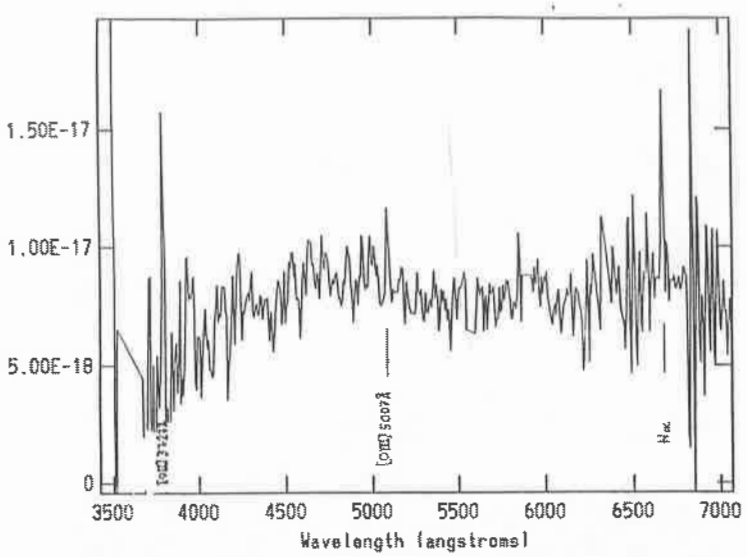

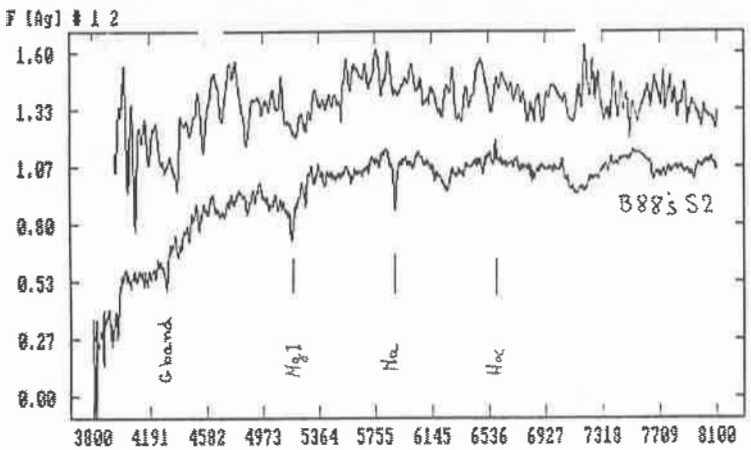

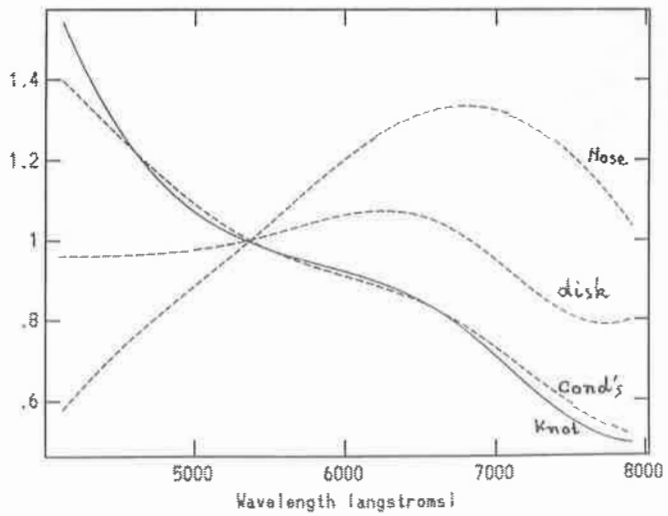

Figures 1b, 2b, 3b - see captions in previous page

Chemical Abundances at High Redshift

Sueli M. Viegas

Instituto Astronômico e Geofísico

Av. Miguel Stefano 4200, 04301- São Paulo, SP, Brazil

Summary

In this paper, a brief review of the nature of the QSO absorption line systems is given in order to discuss results concerning the chemical abundances of young galaxies. The absorbers show undersolar abundances and depending on the location of the gas in the galaxy the values obtained may indicate that we are seeing gas in the outskirts of an evolved galaxy or in the inner parts of a very young galaxy.

1. Introduction

Until recently, data on early time abundances were obtained from halo stars and from low metallicity extragalactic HII regions (see, for instance, Boesgaard & Steigman 1985, Wheeler, Sneden & Truran 1989). A good determinaton of young galaxies elemental abundances is very important both for the study of galactic chemical evolution as well as for the primordial nucleosynthesis and, consequently, for the standard model of the universe. In the last few years, improvements in high resolution observations of the QSO spectra are allowing the determination of the chemical abundances at early epochs from the observed absorption lines (Fan & Tytler 1994, Gruenwald & Viegas 1993, Petini et al. 1994, Petitjean et al. 1994, Steidel 1990, Viegas & Gruenwald 1991).

The absorption line systems, associated with intervening objects, show HI column densities from 10^{12} to 10^{22} cm^{-2}. Those with N(HI) $\leq 10^{17}$ cm^{-2} are optically thin to the Lyman continuum and low ionization absorption lines are weak or inexistent. On the other hand, absorbers with N(HI) $> 10^{20}$ cm^{-2}, which are optically thick, correspond to the so-called damped Lyα systems that show mainly low ionization lines and may be associated with disks of galaxies. Among the absorption line systems, the damped

Lyα systems may provide good determinations of the chemical abundances because the hydrogen is mainly neutral and no corrections must be made to account for unobserved ions. However there are few of them compared to systems with lower HI column densities (Petitjean et al. 1993). Thus, for most of the absorption systems, in order to obtain the chemical abundances ionization correction factors must be calculated. These correction factors are necessary to take into account the ionization states that are present in the gas but show no absorption lines in the observed spectrum. The ionization correction factors depend on the origin of the absorbers since their values rely on the ionizing radiation reaching the absorption line systems.

In this paper, the methods for determining the chemical abundances of the QSO absorption line systems are revised. In §2 , a short review of the nature of the QSO absorbers as well as of the corresponding ionizing radiation field is presented. The chemical abundances are discussed in §3, and the final remarks appear in §4.

2. The Nature of the Absorbers

Following the velocity of the absorption line system, relative to the QSO, Weyman et al. (1979) suggested that systems with $v/c > 0.05$ are associated with intervening galaxies (or proto-galaxies). For many years, the current interpretation for these systems has been that (Sargent et al. 1979, 1980, Wolfe et al. 1986):

(a) Lyman α systems (no metal lines and N(HI) $< 10^{15}$ cm^{-2}) originate from intergalactic clouds;

(b) metal-line systems ($10^{15} <$ N(HI) $< 10^{20}$ cm^{-2}), from galactic haloes; this category includes a sub-set called Lyman limit systems (LLS), for which the optical depth at the Lyman continuum is close to unity,

(c) damped Lyα systems (DLAS, with N(HI) $> 10^{20}$ cm^{-2}), from galactic disks.

Therefore, the ionizing radiation field should be similar to the interstelar radiation field for the damped Ly α systems, while the QSO background radiation should ionize the Ly α systems and metal-line systems. More recently, it has been suggested that the metal systems and the Ly α systems should have the same origin (young intervening galaxies). Metal lines are not seen in Ly α systems probably because the column density of the ions of the heavy elements is too low. It may be do to the fact that these systems

are optically tbin (NHI very low) and/or tbe gas has undersolar abundances. In fact, they have NHI $< 10^{15}$ cm^{-2}; thus, even assuming solar abundances, the column density of a heavy ion is lower than 10^{12} cm^{-2} and the corresponding absorption line is too weak to be detected. Undersolar abundances would make the detection still harder.

More recently, an alternative origin of the metal-line systems has been proposed. Based on the similarities of the absorption line spectrum of gas-rich dwarf irregular galaxies with tbat of QSO absorption line systems, it was suggested that these QSO absorbers are associated with star forming regions (York et al. 1986). In this case, the metal absorption lines are produced in the associated HII region ionized by the hot stars. The study of 20 CIV absorption systems and an equal number of MgII systems favored the star forming region origin (Gruenwald & Viegas 1993, Viegas & Gruenwald 1991).

On the other hand, absorption systems sbowing high column densities of high ionization states of C, N, O as well as of HeI ruled out the ionization by the QSO background radiation (Vogel & Reimers 1993, Reimers & Vogel 1993). It bas been suggested a local origin for the radiation. These systems should be associated with a two-phase halo, where clumps of cold gas are ionized by the radiation from tbe hot gas present in tbe early stages of galactic evolution (Viegas & Friaça 1995). The ionizing radiation has the appropriate sbape to explain the observations.

3. Chemical Abundances

In order to calculate the chemical abundances of the absorbers, the column densities of the ions of a given element must be known and added up. The column densities are obtained from the observed equivalent width of the absorption lines using the curve of growth metbod. Two main difficulties occur: (i) the absorption line may be saturated so that the relation between the equivalent width and the column density depend on the b-parameter; (ii) there are ions present in the gas with no observable lines.

The problem of determining the b-parameter may be solved with high resolution data that are becoming available, allowing different line components to be identified. On the other hand, in order to account for the ions with no observable lines, the sum of the column densities of the ions sbowing absorption lines must be corrected by the so-called

ionization correction factor (icf ≥ 1). The icf can be obtained from photoionization models of the absorbing gas. They depend on the ionizing radiation spectrum, as well as on tbe other input parameters of the photoionization models, i.e., gas density and chemical composition. Adopting an ionizing continuum, the icf for different ions may be obtained from a grid of photoionization models. Thus, for each observed system, the better icf value may be chosen from the grid. Another possible way to overcome the problem of unobserved ions is to model a given absorption system, fitting the observed lines. The best fit determines the best model corresponding to a set of elemental chemical abundances. This method may give better results although it seems more appropriate for the analysis of a small number of absorbers. If one is interested in determine the chemical abundances of a large number of systems, the former method (using the ionization correction factor) is suitable and it is certainly faster.

The DLAS systems are mainly neutral; thus H^+ is negligeable and the correction factor for the N(HI) is practically unity. Thus the chemical abundances depend only on the icf of the ions of the other elements. If these systems are associated with galactic disks, the ionizing radiation must be similar to the UV background of the Galaxy (Draine 1978), and the correction factors for OI, NI, CII, MgII, SiII are also close to unity (Viegas 1995). On the other hand, if the DLAS are ionized by the QSO integrated background radiation, the correction factor of the heavy element ions may be significant.

An important point is the [N/O] abundance ratio. Since N comes from low mass stars and O from high mass stars we expect [N/O] smaller than solar in young galaxies. This is the trend observed in halo stars (Wheeler et al. 1989). In addition, the average [N/O] ratio in metal poor extragalactic HII regions is 4.6 smaller than the solar value. Although the OI and NI resonance lines are in the Lyman α forest (wavelengths shorter than 1216 Å), their detection is now becoming possible (Pettini et al. 1995). A good determination of the abundance ratio will depend on the NI/OI correction factor ratio. This ratio is less than unity for the UV galactic background and is higher than unity for a harder ionizing radiation, as the QSO background radiation or stellar radiation (Viegas 1995).

As pointed out previously, absorbers with lower HI column densities are probably

ionized by a radiation harder than the UV galactic background (i.e, QSO integrated background radiation, hot stellar radiation or hot halo gas radiation), and the ionization correction factors are likely to be important. In this case, the ratio of column densities of ions of the same element is used to determine the intensity of the radiation field. Let us recall that this intensity is generally expressed by the ionization parameter U, relating the density of the ionizing photons to the gas density. With the value of U and NHI obtained from the observations, the icf are determined and then the chemical abundances.

The correction factor method has been used to compute the C, O and Si abundances of some observed absorption systems. For 8 systems with $z \simeq 3$ (Steidel 1990), the U parameter was obtained from the N(CII)/N(CIV) and N(SiII)/N(SiIV) ratios. The results are in the range -2.6 $\leq$ log U $\leq$ -2. The elemental abundances, relative to the solar value, are in the ranges: $10^{-3} \leq$ [C/H] $\leq 10^{-2}$, $10^{-2} \leq$ [O/H] $\leq 10^{-1}$ and $3 \times 10^{-3} \leq$ [Si/H] $\leq 2 \times 10^{-2}$. Using photoionization models to reproduce the observed column densities, Steidel (1990) obtained similar results. In addition, for the absorption system z = 2.318 of the QSO 2116 -358 (Wampler et al. 1993), the abundances obtained using the ionization correction factors are higher: [C/H] is about 0.1 and [Si/H] is about 0.3 of the solar values.

4. Final Remarks

The determination of the elemental abundances at high redshift is a difficult task. Chemical nderabundances in absorbers have been pointed out previously for absorbers with redshift in the range $1.3 < z < 2.7$ from photoionization models assuming the QSO integrated background radiation or a stellar radiation field (Gruenwald & Viegas 1991, Viegas & Gruenwald 1993). In this case the underabundance factor was considered the same for all the elements ($10^{-3} \leq Z/Z_{\odot} \leq 10^{-2}$). Recent observational results for the absorption systems of two QSOs have been fitted using photoionization models where all the chemical abundances also vary by the same factor with respect to the solar abundances (Petijean et al. 1994). Two intervening systems show underabundances of the order of 3×10^{-2} and one of them is probably associated with an HII region. However, these results are only indicative since the chemical enrichment of the gas

depend on the element. Thus, calculating the abundance of each element is a better approach.

The results presented in §3 indicate that metallic absorption systems show very low chemical abundances. These results were obtained for several objects by the empirical method using ionization correction factors. They corroborate the indicative underabundances obtained previously. The absorbers are associated with young galaxies. Evolution models of galaxies indicate that in the central regions solar abundances are reached in less than 1 Gyr whereas in the outer regions it takes longer (Friaça & Terlevich 1994). Thus, metal poor gas may indicate that we are seeing the outskirts of the galaxies (outer shells or halo) of a galaxy or the inner regions of very young galaxies. The analysis of the absorbers abundance and location may provide clues on the galaxy formation and evolution.

Acknowledgements: I am thankful to Ruth Gruenwald and Amâncio Friaça for the friendship, discussions and collaboration.

References

Boesgaard, A. & Steigman, G. 1985, ARAA 23, 319

Draine, B. T. 1978, ApJS 36, 595

Fan, X. M. & Tytler, D. 1994, ApJS (in press)

Friaça, A. C. S. & Terlevich, R. J. 1994, Workshop pn Violent Star Formation from 30 Douradus to QSOs, ed. G. Tenorio-Tagle, CUP:Cambridge, in press.

Gruenwald, R. B. & Viegas, S. M. 1993, ApJ 415, 534

Pettini, M., Lipman, K. & Hunstead, R. W. 1995, (preprint)

Petitjean, P., Rauch, M. & Carswell, R. F. 1994, A&A 291,29

Petitjean, P., Webb, j. K., Rauch, M., Carswell, R. F. & Lanzetta, K. 1993, MNRAS 262, 499

Sargent, W. L. W., Young, P. J., Boksenberg, A., Carswell, R. F. & Whelan, J. A. J. 1979, ApJ 230, 49

Sargent, W. L. W., Young, P. J., Boksenberg, A., & Tytler, D. 1980, ApJS 42, 41

Steidel, C. C. 1990, ApJS 74, 37

Viegas, S. M. & Friaça, A. C. S. 1995, MNRAS 272, L35

Viegas, S. M. & Gruenwald, R. B. 1991, ApJ 377, 39

Viegas, S. M. 1995, MNRAS (in press)

Wampler, E. J., Bergeron, J. and Petitjean, P. 1993, A&A 275, 15

Weyman, R. J., Williams, R. E., Peterson, B. M. & Turnshek, D. A. 1979, ApJ, 234, 33

Wheeler, J. C., Sneden, C. & Truran, J. W. 1989, ARAA 27, 279

Wolfe, A. M., Turnshek, D. A., Smith, H. E., Cohen, R. D. 1986, ApJS 61, 249

PLASMAS IN STARS, GALAXIES AND THE EARLY UNIVERSE

Reuven Opher

Instituto Astronômico e Geofísico, Universidade de São Paulo
Av. Miguel Stéfano, 4200, CEP 04301-904 São Paulo, SP, Brasil

ABSTRACT

Many very interesting problems exist in plasma astrophysics. I started a research group in plasma astrophysics at the University of São Paulo with my students a few years ago and take the opportunity of this 20th anniversary of the Brazilian Astronomical Society to review the results of this research that have been published in the international journals.

---

* Invited talk on the 20th anniversary of the Brazilian Astronomical Society

I. INTRODUCTION

Some major problems in plasma astrophysics are:

1. How do we make a solar wind with the right mass loss rate and terminal velocity, satisfying all the observational data?
2. How do we make solar flare explosions of less then a second duration?
3. How do we produce the MHD structure of the interstellar medium?
4. What is the radiation mechanism of pulsars?
5. How do we produce a supernova II (when a massive star blows itself apart) since the shock produced from the collapse of the iron core has difficulty of blowing off the outer layers of the star?
6. What produces a nova (recurrent explosion of a white dwarf) since we need $\sim 10^{-4}$ $M_\odot$ of accreted matter on the white dwarf to ignite the accreted hydrogen but only $\sim 10^{-6}$ $M_\odot$ is seen in the explosion?
7. How do we produce a supernova I (when a white dwarf blows itself apart) and what differentiates a supernova I from a nova?
8. What produces the highly polarized optical radiation of magnetized white dwarfs (AM Herculis stars)?
9. How do we produce a wind in a hot star (such as a Wolf-Rayet) whose momentum is $\sim$ 4-50 times the radiation field which is supposed to be pushing it?
10. What acceleration mechanism produces the cosmic rays with energy orders of magnitude greater than the highest energy particle accelerator on earth?
11. How do we produce the jets emanating from almost all newly born stars?
12. How do we collimate extragalactic jets which are collimated over five orders of magnitude (e.g., from 1 pc to $> 10^5$ pc) when laboratory supersonic jets are dispersed in one order of magnitude (e.g., a 10 cm radius jet is dispersed in one meter)?
13. How do we produce filaments in extragalactic jets and in the radio lobes at the ends of the jets?
14. How do we produce the superluminal bright radio blobs near galactic nuclei with velocities greater than ten times the velocity of light?
15. How do we produce the extragalactic jets emanating from galactic nuclei?

16. How do we produce the first stars and galaxies starting from density perturbations produced in the primordial universe?
17. What is the physical structure of these first collapsing objects?
18. What produced the enormous voids observed in the universe?
19. What mechanism produced the magnetic fields which observations indicate existed in the early universe?
20. Since fluctuations existed in the hot dense primordial plasma, what are the effects of these fluctuations on primordial nucleosynthesis and the large scale structure of the universe?

I have worked recently on some of the above problems and take the opportunity of the 20th anniversary of the Brazilian Astronomical Society to review in the following sections the results of my research in plasma astrophysics with my students at the University of São Paulo.

II. PLASMAS IN STARS

II.1 The Sun

Alfvén plasma waves can play an important role in driving the solar wind. We have direct evidence for Alfvén waves in the solar wind. Waves are observed in the solar wind with large perturbations in the magnetic field and with negligible density perturbations, indicating the presence of Alfvén waves. Coronal holes are the source of the high speed solar wind stream at the earth's orbit. The observational data on the sun put strong limits on possible flow geometries:

a) solar mass loss rate ~ 2 x 10^{-14} $M_\odot$ /yr;
b) coronal holes occupying an area of ~ 10 - 20% of the solar surface;
c) coronal base pressure (nT) ~ 2 - 4 x 10^{14} cgs ;
d) solar wind passing through a critical point ;
e) coronal hole field ~ 5 - 10 G;
f) velocity at the critical point ≥ 100 km/s ;
g) coronal temperature ≥ 10^6 K ;
h) coronal hole area increasing by a factor 4-8 in a height ~ 1 $R_\odot$; and
i) observed Alfvén wave flux at 0.3 AU.

We found that an Alfvén wave flux ~ 5 x 10^5 ergs cm^{-2} s^{-1} can produce the observational data. We showed that the observational data require a combination of both a slow divergence in a coronal hole in a distance 0.01 - 0.1 $R_\odot$ followed by a rapid divergence up to a height ~ 1 $R_\odot$ (Refs. 1,2).

II.2 Old Stars

Late-type giant and supergiant stars exhibit cool massive winds. We showed that an Alfvén wave flux can explain the observed data (Ref. 3).

II.3 Hot Stars

Hot Wolf-Rayet stars have winds with momentum ~ 4-50 times the radiation fields which are supposed to be pushing them. We can produce a strong hot wind with a photospheric Eddington ratio Γ_{Edd} ~ 0.4 and a Γ_{Edd} that goes up to Γ_{Edd} ~ 0.8 inside the photosphere. However, no theory of stellar interiors produces such Γ_{Edd} values. We showed that a flux of Alfvén waves can solve this "momentum problem" in Wolf-Rayet stars (Refs. 4,5).

II.4 New-Born Stars

Jets emanate from newly born stars. We showed that Alfvén wave can produce these jets (Ref. 6). We showed also that clumps in these jets can be produced by a plasma thermal instability (Ref. 7).

II.5 White Dwarfs

The AM Herculis binaries possess a white dwarf, with a strong magnetic field (> 10^7 Gauss), as one of the stars of the binary. The notable optical properties of these binaries are the very high linear (~ 10%) and circular (~ 35%) polarizations observed. The optical polarization is interpreted as being caused by cyclotron emission in the harmonics ~ 5-20 in a magnetic dipole accretion column. We studied the emission from these objects using cyclotron absorption coefficients which include the effects of collisions and scattering. We reproduced well the observed spectra of a number of AM Herculis binaries (Ref. 8,9). We also reproduced the spectra of DQ Herculis binaries, where the white dwarf possesses a weaker magnetic field (Ref. 10).

III. PLASMAS IN GALAXIES

III.I Jets from Active Galactic Nuclei

Extragalactic jets are not freely expanding and are collimated from ~ 1 pc to > 10^5 pc. The motion of these highly ionized jets in a magnetic field will, in general, excite MHD waves on their borders by the Kelvin-Helmholz instability. We studied the damping of magnetosonic and surface waves in these essentially collisionless plasmas. We showed in general, that transit-time magnetic damping of these low-frequency compressive MHD waves produces appreciable electric currents which can be dynamically important. Typically, for a relativistic electron density n_e, we obtain a current density $J \approx D\ (n_e ec)\ (c/V_{pc})^2\ \xi^3$, where V_{ph} is the phase velocity of the surface or magnetosonic wave, e is the electronic charge, c is the velocity of light, $\xi \equiv |B_{MHD}/B_o|$ with B_{MHD} the magnetic field of the MHD wave, B_o the ambient magnetic field and D a factor ~ 100 for a relativistic power-law distribution. Using indicated values from observations of jets, we obtain $\xi \sim 10^{-5}$ to be necessary to produce a sufficiently strong collimating electric current. The model predicts that a distributed generator acts along the jet

length and avoids problems of previous models requiring a current generator at the galactic nucleus (Ref. 11).

We showed also that kinetic Alfvén waves can produce the electric currents in jets (Refs. 12,13) and that the jets can be produced by Alfvén waves (Refs. 14,15).

III.2 Extended Radio Sources

We investigated whether the filaments observed in extended radio sources (e.g., supernova remnants, jets, radio lobes at the ends of jets) can be produced by a thermal instability. Using luminosities, pressures, and expansion rates indicated by observations of extended radio sources, we made a linear and nonlinear analysis of thermal instability in these sources. We studied a model in which the unknown (as yet) process which creates approximate equipartition in extended radio sources does not act continuously but ceases for time intervals ~ R/V_R where R is the radius of the extended radio source and V_R is the radial expansion velocity. We showed that the maximum value of $q = (V_A/V_S)^2$ under isobaric conditions for thermal instability is $q_{max} = F/G$ where $F = [-2\nu + (3\tau/4)(2\eta-1)]$ and $G = [(2\nu/3) + (2/\tau)]$ with V_A (V_S) the Alfvén (sound) velocity, $\nu = V_R/R$, $\tau = 3P/L_{sc}$, L_{sc} the total synchrotron and inverse Compton losses, $\eta = [1 + 8\pi U_{rad}/B^2]^{-1}$, U_{rad} the energy density of the background radiation, B the magnetic field and P the pressure due to the relativistic electrons. We showed that the filaments observed in extended radio sources can be produced by a thermal instability (Refs. 16, 17, 18). We also showed that the superluminal bright blobs near galactic nuclei with velocities greater than ten times the velocity of light can be produced by a thermal instability (Ref. 19).

III.3 Cosmic Rays

We studied the acceleration of particles in supernova shock waves as a mechanism for producing the observed cosmic rays. The shock structure equation and the corresponding jump conditions were deduced for oblique shock particle acceleration, taking into account wave effects in the

hydrodynamic approximation. Numerical results were obtained for diverse upstream conditions showing the modifications of the shock structure and energetic particle acceleration efficiency due to the wave pressure and the wave energy flux. The effect of wave dissipation was also investigated. The study was based on first order Fermi acceleration near the shock. A particle is scattered by magnetic irregularities across the shock many times between the upstream and downstream regions. The kinetic energy of the background plasma is redistributed in the shock between a thermal and a turbulent component, the latter being dissipated downstream over a much wider region than the shock itself. Energetic particles returning upstream from the downstream region are super Alfvénic and consequently excite Alfvén waves via the streaming instability, generating a turbulent region in front of the shock. Both upstream and downstream regions act as scatterers for energetic particles which are able to cross the shock many times gaining energy in a secular manner due to the relative motion between the upstream and downstream media. In the simplest linear theory for plane shocks and a monoenergetic initial distribution of particles, a power law momentum spectrum is obtained whose spectral index is a function only of the kinematical parameters of the shock. The simple linear theory is in fair agreement with the observational data. For strong shocks, however, the compression ratio tends to 4 and the particle pressure diverges. This indicates the necessity of a nonlinear theory which takes into account the effect of the particle pressure on the background flow. The most remarkable result of the nonlinear treatment is the formation of a precursor of smooth compression followed (or not followed) by an MHD subshock. We studied the case of oblique shocks where all four components - background plasma, magnetic field, energetic particles and waves - are put on an equal footing. We found that: 1) Nonlinear saturation of the waves increases the compression of the shock and decreases the particle acceleration efficiency, η; 2) The efficiency increases with greater far upstream nonthermal fraction of the particle pressure; and 3) The transition between discontinuous (with a subshock) and smooth (without a subshock) solutions moves towards higher M as θ decreases from 90°, where M is the Mach number far upstream with respect to the total sound velocity and θ is the angle between the magnetic field far upstream and the normal to the surface of the shock (Ref. 20). We also studied distributed cosmic ray acceleration by supernova remnants in the Galaxy and showed that observed features of the cosmic ray spectrum can be reproduced (Ref. 21).

III.4 X-Ray Sources

We showed how the X-ray spectrum of Galactic sources can determine the temperature and the density of the source (Ref. 22).

IV. PLASMA IN THE EARLY UNIVERSE

IV.1 Quasars

Quasars are observed to redshifts z ~ 5 which corresponds to less than 10% of the age of the Universe. The high redshifts are identified by the spectra from their broad-line emission clouds, which exist close to the center of the quasar. Since the center of the quasar is a very intense radiation source, the existence of relatively dense emission clouds near the center for a long time is a mystery. We showed that Alfvén waves can create a two-phase region where dense clouds of temperature ~ 10^4 K exist in an ambient hot low dense region of temperature ~ 10^7 K (Ref. 23).

IV.2 Primordial Magnetic Fields

Magnetic fields comparable to the Galactic magnetic field (~ 10^{-6} G) has been identified in the Ly-α forest clouds at redshifts z ~ 2-3. The identification of a mechanism for creating magnetic fields in the early Universe is of great importance. We suggested that the confining electric currents in jets produced by quasars and active galactic nuclei in the early universe were the origin of the magnetic field in the early universe (Ref. 24).

IV.3 The First Objects Formed

Starting from the recombination era ($z \sim 1000$) ($\sim 0.001\%$ the age of the universe), we investigated the cooling and collapse of Population III objects (the first objects that collapsed in the universe, which did not contain heavy elements) for masses $M \geq M_J$, where M_J is the Jeans mass at the beginning of the recombinations era. We took into account not only the internal pressure of the cloud but also photon cooling (from the background radiation), photon drag, photoionization by the background radiation, collisional ionization, a complete set of equations for the formation and destruction of hydrogen molecules, as well as dark matter (Refs. 25, 26, 27, 28, 29). We studied the role of nonspherical collapse and rotation on the epoch of galaxy formation [Ref. 30] as well as collisions of the first clouds [Ref. 31].

V. CONCLUDING COMMENTS

Research was reported in the above sections on only some of the problems discussed in section I. The other problems are presently being investigated and I hope at the 25th silver anniversary of the Brazilian Astronomical Society, I will be able to report results of these investigations.

I would like to thank the organizers for inviting me to give this talk and my colleagues and the University of São Paulo who granted me the conditions for performing the research reported.

ACKNOWLEDGEMENTS

I would like to thank the Brazilian agency CNPq for partial support.

REFERENCES

1. Jatenco-Pereira, V., and Opher, R., Astrophys. J. 344, 513 (1989)
2. Jatenco-Pereira, V., Opher, R., Yamamoto, L.C., Astrophys. J. 432, 409 (1994)
3. Jatenco-Pereira, V., and Opher, R., Astron. and Astrophys. 209, 327 (1989)
4. dos Santos, L.C., Jatenco-Pereira, V., and Opher, R., Astrophys. J. 410, 732 (1993)
5. dos Santos, L.C., Jatenco-Pereira, V., and Opher, R., Astron. and Astrophys. 270, 345 (1993)
6. Jatenco-Pereira, V., and Opher, R., Mon. Not. R. astr. Soc. 236, 1 (1989)
7. Gouveia Dal Pino, E.M., and Opher, R., Astron. and Astrophys. 231, 571 (1990)
8. Canalle, J.B.G., and Opher, R., Astron. and Astrophys. 189, 325 (1988)
9. Canalle, J.B.G., and Opher, R., Astron. and Astrophys. 219, 334 (1989)
10. Canalle, J.B.G., and Opher, R., Astron. and Astrophys. 251, 474 (1991)
11. Jafelice, L.C., Opher, R., Assis, A.S. and Busnardo-Neto, J., Astrophys. J. 348, 61 (1990)
12. Jafelice, L.C., and Opher, R., Astrophys. and Space Sci. 137, 303 (1987)
13. Jafelice, L.C., and Opher, R., Astrophys. and Space Sci. 138, 23 (1987)
14. Opher, R. and Pereira, V., Astrophys. Lett. 25, 107 (1986)
15. Gonçalves, D.R., Jatenco-Pereira, V., and Opher, R., Astron. and Astrophys. 279, 351 (1993)
16. Gouveia Dal Pino, E.M., and Opher, R., Astrophys. J. 342, 686 (1989)
17. Gouveia Dal Pino, E.M., and Opher, R., Mon. Not. R. astr. Soc. 240, 573 (1989)
18. Gouveia Dal Pino, E.M., and Opher, R., Mon. Not. R. astr. Soc. 263, 687 (1993)
19. Gouveia Dal Pino, E.M., and Opher, R., Astron. and Astrophys. 242, 319 (1991)
20. Medina-Tanco, G.A., and Opher, R., Astron. and Astrophys. 240, 178 (1990)
21. Medina-Tanco, G.A., and Opher, R., Astrophys. J. 411, 690 (1993)

23. Gonçalves, D.R., Jatenco-Pereira, V., and Opher, R., Astrophys. J. 414, 57 (1993)
24. Jafelice, L.C., and Opher, R. Mon. Not. R. astr. Soc. 257, 135 (1992)
25. de Araujo, J.C.N., and Opher, R., Mon. Not. R. astr. Soc. 206, 315 (1988)
26. de Araujo, J.C.N., and Opher, R., Mon. Not. R. astr. Soc. 231, 923 (1989)
27. de Araujo, J.C.N., and Opher, R., Astrophys. J. 350, 502 (1990)
28. de Araujo, J.C.N., and Opher, R., Astrophys. J. 379, 461 (1991)
29. de Araujo, J.C.N., and Opher, R., Astrophys. J. 403, 26 (1993)
30. de Araujo, J.C.N., and Opher, R., Astrophys. J. Dec. 10, (1994)
31. de Araujo, J.C.N., and Opher, R., Astrophys. J. Jan. 10, (1995)